

# Printed Inorganic Transistors

**Brent Ridley**

S.B. Chemistry 1996

Massachusetts Institute of Technology

S.M. Media Arts and Sciences 1999

Massachusetts Institute of Technology

Submitted to

the Program in Media Arts and Sciences

School of Architecture and Planning

in partial fulfillment of the requirements

for the degree of

**Doctor of Philosophy**

at the Massachusetts Institute of Technology

September 2003

©2003 Massachusetts Institute of Technology

All rights reserved

Written by **Brent Ridley**

Program in Media Arts and Sciences

August 8, 2003

Certified by **Joseph Jacobson**

Associate Professor

Program in Media Arts and Sciences

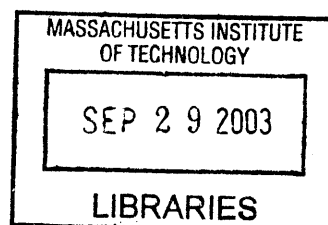
Thesis Supervisor

Accepted by **Andrew Lippman**

Chair of Departmental Committee on Graduate Students

Program in Media Arts and Sciences

  
ROTCH



# Printed Inorganic Transistors

**Brent Ridley**

Submitted to the Program in Media Arts and Sciences  
School of Architecture and Planning  
on August 8, 2003

in partial fulfillment of the requirements  
for the degree of  
**Doctor of Philosophy**

Massachusetts Institute of Technology

## **Abstract**

Forty years of exponential growth of semiconductor technology have been predicated on the miniaturization of the transistors that comprise integrated circuits. While complexity has greatly increased within a given area of processed silicon, the cost per area has not decreased. Current fabrication methods are further hindered by high facility costs and environmentally unfriendly processing. Moving to a new means of semiconductor fabrication may drastically reduce both financial and environmental costs. One such approach is based on the extension of printing techniques to the fabrication of electronic devices. Such printed electronics are envisioned to enable applications in flexible displays and electronic paper, personal fabrication, wearable computing, and disposable medical diagnostics.

This dissertation focuses on the development of printable materials, specifically inorganic semiconductor inks. At the outset of this research, organic semiconductors were the only materials known and pursued as printable semiconductors. The ability to process organic semiconductors in common organic solvents makes them amenable to a wide range of printing technologies, but their electrical performance is fundamentally limited and their utility is confined to applications in which only low speeds are required.

The goal of this thesis was to demonstrate the feasibility of printing inorganic materials, the same materials that are used to fabricate high quality semiconductor devices. Cadmium selenide was studied as a model inorganic semiconductor and silicon was studied because of its commercial dominance. The insolubility and high processing temperatures of inorganic semiconductors, both of which can prevent their use in printed electronics, were overcome through the use of nanoparticle inks. At very small sizes, nanoparticles can be highly soluble in organic solvents and can have a pronounced melting point depression. Leveraging these size-dependent properties, the first semiconductor nanoparticle inks were developed using cadmium selenide and the first all-printed inorganic thin film transistors were demonstrated. Printed active layers in thin film transistors attained a semiconductor mobility of  $1 \text{ cm}^2\text{V}^{-1}\text{s}^{-1}$  and an ON/OFF ratio in excess of  $10^4$ . Further development of inorganic nanoparticle inks and efforts to extend this approach to silicon are described, addressing silicon nanoparticle synthesis, purification, and ink formulation.

**Joseph Jacobson**

Associate Professor

MIT Program in Media Arts and Sciences

Thesis Supervisor

# Printed Inorganic Transistors

**Brent Ridley**

Submitted to  
the Program in Media Arts and Sciences  
School of Architecture and Planning

in partial fulfillment of the requirements  
for the degree of  
**Doctor of Philosophy**  
at the Massachusetts Institute of Technology  
September 2003

**Joseph Jacobson**  
Associate Professor  
MIT Program in Media Arts and Sciences  
Thesis Supervisor

**Akintunde Akinwande**  
ITT Career Development Associate Professor  
MIT Department of Electrical Engineering  
Thesis Reader

**Timothy Swager**  
Professor  
MIT Department of Chemistry  
Thesis Reader

## Table of Contents

7	<b>Introduction</b>
7	Printed Inorganic Electronics at the MIT Media Lab
8	Limitations of Current Commercial Fabrication Technology
8	Printing as a Route to Microelectronics Fabrication
10	Printable Electronic Materials and Processes
11	Printable Organic Materials
15	Printable Inorganic Materials
16	The Nature of Melting in Nanoparticles
18	Polycrystalline Films from Nanoparticle Precursors
19	Nanoparticles for Printed Transistors
22	<b>Synthesis of Cadmium Selenide Nanocrystals</b>
22	Synthesis of CdSe Nanoclusters by Metathesis
30	<b>Device Fabrication with Cadmium Selenide Inks</b>
30	Traditional Fabrication of CdSe TFTs
31	Thin Film Formation and Device Fabrication
41	Conclusions from Experiments with CdSe Nanoparticle Inks
43	<b>Approaches to Printing Silicon</b>
43	Differences in Group IV and II-VI Semiconductors
44	Approaches to Solution Deposited Group IV Semiconductor Thin Films
46	Surface Termination of Printable Group IV Materials
47	Molecular Precursors and Oligosilanes
50	Polysilanes and Network Polysilanes
54	<b>Approaches to Silicon Nanocrystal Synthesis</b>
54	Solution Phase Group IV Synthesis
54	Solution Phase Group IV Synthesis: High Pressure Reduction
56	Solution Phase Group IV Synthesis: Decomposition in Supercritical Fluids
57	Solution Phase Group IV Synthesis: Reduction in Coordinating Solvents
58	Solution Phase Group IV Synthesis: Metathesis
59	Solution Phase Group IV Synthesis: Reduction in Inverse Micelles
64	Solution Phase Group IV Synthesis: Electrochemical Etching
66	Group IV Synthesis Trends
68	<b>Silicon Synthesis by Electrochemical Etching</b>
68	Anticipated Advantages and Limitations of Electrochemical Etching
68	Synthesis by Electrochemical Etching

72	<b>Silicon Synthesis by Metathesis</b>
72	Anticipated Advantages and Limitations Metathesis
72	Synthesis by Metathesis
75	<b>Silicon Synthesis by Reduction in Inverse Micelles</b>
75	Anticipated Advantages and Limitations of Reduction in Inverse Micelles
76	The Role of Surfactants in Reduction in Inverse Micelles
77	Modification of Nonionic Surfactants for Reduction in Inverse Micelles
80	Synthesis According to the Literature: Cationic Surfactants
82	Synthesis According to the Literature: Nonionic Surfactants
90	Synthesis with Modified Nonionic Surfactants: Hydrazine Reductions
98	Synthesis with Modified Nonionic Surfactants: Hydride Reductions
108	<b>Purification and Ink Formulation</b>
108	Purification and Product Tracking: Size Exclusion HPLC
114	Purification and Product Tracking: Reverse Phase HPLC
122	Purification and Product Tracking: Differences from the Literature
125	Ink Formulation and Device Fabrication
137	Limitations Associated with Purification
128	Alternative Means of Purification
130	Nanoparticle Synthesis in Inverse Micelles and Printed Microelectronics
133	<b>Conclusions</b>
133	Printed Inorganic Electronics
137	<b>Experimental Procedures</b>
137	CdSe Synthesis
137	Pyrolysis
138	Metathesis
139	Alkali Metal Selenide Synthesis
139	CdSe Film Formation and Device Fabrication
141	Device Calculations
141	Si Synthesis
142	Nanoparticles from Porous Silicon
142	Metathesis
142	Inverse Micelle Synthesis
143	Surfactant Alkylation
143	Characterization
144	Film Formation and Device Fabrication
145	<b>Acknowledgements</b>
146	<b>References</b>

## Introduction

### Printed Inorganic Electronics at the MIT Media Lab

Over the past five years, research at the MIT Media Lab has focused on printed microelectronics.<sup>1-17</sup> As a part of this effort, the first printable inorganic semiconductors were developed and demonstrated as the active layers in thin film transistors (TFTs) with a semiconductor mobility of  $1 \text{ cm}^2\text{V}^{-1}\text{s}^{-1}$ ,<sup>1,10</sup> to date the highest semiconductor mobility reported for a printed semiconductor. Additionally, liquid embossing was developed as an additive means of rapidly printing sub-micron multilayer inorganic structures.<sup>2-5,11,12</sup> Liquid embossing cadmium selenide semiconductor nanocrystal inks, gold metal nanocrystal inks, and spin-on-glass (SOG) resulted in the fabrication of all-printed inorganic semiconductor devices at plastic compatible temperatures.<sup>2</sup> Additional printing techniques were applied to nanocrystal inks, as well, demonstrating ink jet printing,<sup>6,15</sup> laser and electron beam patterning,<sup>7,13</sup> and even arbitrary patterning of 17 nm dots and 30 nm lines through the development of atomic force microscope transfer techniques.<sup>14</sup>

Printed inorganic electronics are envisioned to leapfrog the 15 year effort in printed organic electronics<sup>18-22</sup> through the superior device performance characteristics available to inorganic materials. Prior to recent developments, these performance advantages had been inaccessible due to the high temperatures and vacuum-based processing schemes associated with traditional microelectronics fabrication. Efforts at the Media Lab sought to combine the performance advantages of inorganic materials with the processing advantages of organic materials through the development of printable inorganic materials<sup>1,10</sup> and complimentary high-resolution and rapid printing processes.<sup>2-7,11-14</sup> This conceptual shift from organic materials to inorganic materials with organic or organic-like processing was supported by subsequent reports from IBM describing TFTs that employed organic-inorganic hybrid materials as the active layer<sup>23-26</sup> and by recent reports of TFT fabrication using chemical bath deposition (CBD) of II-VI semiconductors.<sup>27,28</sup>

## **Limitations of Current Commercial Fabrication Technology**

Current fabrication costs and methods prohibit electronic devices from finding applications where three-dimensional architectures, flexibility, disposability, and extremely large or small unit counts are required. The typical setup cost of a fabrication plant is greater than a billion dollars and electricity alone costs a million dollars a month. Fabrication is expensive, too, as depositing and annealing layers often requires high temperatures and a controlled atmosphere, and patterning and etching these layers generates a large amount of toxic waste.

The high temperatures used in silicon (Si) processing prevent three-dimensional fabrication,<sup>29</sup> large area fabrication,<sup>30</sup> and are incompatible with heat sensitive materials such as organic and biological molecules. High temperatures also prohibit deposition onto low-cost flexible plastics. Today's rigid devices hinder the introduction of electronics into clothing and non-intrusive personal accessories, where a number of medical, information, and communication applications can be envisioned.<sup>8</sup>

## **Printing as a Route to Microelectronics Fabrication**

A seemingly simple technology like printing addresses some of the shortcomings of traditional microelectronics fabrication. A key feature of printing is that it economically deposits materials only where they are needed. Most patterning processes used in semiconductor device fabrication are subtractive and rely on a sacrificial photoresist layer and etching to remove unwanted material that has been deposited over the entire device surface. The waste of such a process is in stark contrast to an additive printing process such as ink jetting,<sup>31</sup> which only deposits material where it is needed. Furthermore, many traditional device processing steps require a flat substrate, while printing can deposit onto surfaces with arbitrary features.<sup>32-34</sup> Although the high temperatures and resolutions used in semiconductor processes are not amenable to standard printing techniques, printing provides a model for the inexpensive and efficient fabrication of both flexible and rigid microelectronic devices.

While additive technologies like printing are attractive because of their efficiency and potentially low cost, considerable hurdles have prevented printing techniques from finding widespread application in semiconductor device fabrication. A major



concern is that the insulators, semiconductors, and conductors used in device fabrication can have melting points well above 1000 °C,<sup>35</sup> preventing their liquid processing. As powders these materials can be printed and then sintered, but this still requires the costly high temperature processing used in current fabrication schemes.<sup>36</sup> The use of a powder also limits the minimum film thickness and the lateral resolution of a printed feature, making it impossible to compete with modern circuitry.<sup>37</sup>

The resolution limits set by powdered materials are insignificant when compared to the resolution limits imposed by traditional printing. “Commercial printing presses achieve a resolution, as defined by the minimal line width of the printed image, on the order of 40 μm,”<sup>38</sup> Offset printing techniques have demonstrated 10 μm resolutions,<sup>39</sup> but even as printing resolutions improve, state-of-the-art electronic devices have feature sizes pushing to 0.10 μm by 2005.<sup>40</sup> “For large area electronic applications, such as light emitting displays, the required resolution is on the order of 20 μm. This feature size can be achieved without photolithography by using contact or noncontact direct patterning methods.”<sup>38</sup> While micron-scale patterning resolution allows the fabrication of respectable devices and may be appropriate for certain large area applications, the ultimate packing density, power consumption, and speed of such devices are limited by the relatively large features. In order for the economy and flexibility offered by printing to compete with current device fabrication, low temperature and high quality printable materials must be developed and the printing process itself must be advanced to allow the deposition of sub-micron features.

A suite of high-resolution printing techniques has recently emerged, promising to address patterning at the sub-micron level.<sup>22,32-34,41-43</sup> The prototypical printing method<sup>44,45</sup> of these various “soft lithographic” techniques, microcontact printing (μCP), employs a micrometer or nanometer-scale patterned elastomeric stamp to transfer a material to a substrate.<sup>44-46</sup> Generally, a self-assembled monolayer is transferred and acts as an etch resist, and as such the process is not an entirely additive technique.<sup>32-34,44-54</sup> Still, μCP and similar methods<sup>2-5,32-34,47-58</sup> provide a route to printed devices.<sup>2,4,5,22,41,42,59-65</sup> Demonstrated resolutions can compete with modern devices and even the next generations of devices, as the patterning of features as small as 35 nm has been reported for “soft” methods<sup>32-34,43</sup> and 25 nm and even 10 nm resolution features have been reported for high pressure nanoimprinting processes.<sup>66-69</sup>

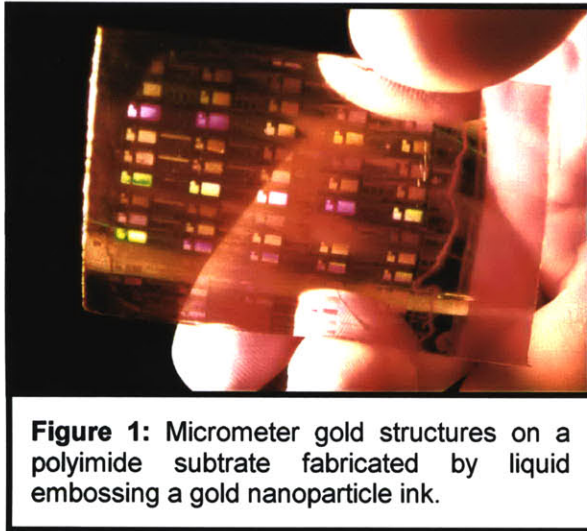


**Figure 1:** Micrometer gold structures on a polyimide substrate fabricated by liquid embossing a gold nanoparticle ink.

Most nonlithographic patterning has been based on microcontact printing<sup>32-34,44-53</sup> or nanoimprinting<sup>66,70,71</sup> a resist that acts as an etch mask. Other approaches include microcontact printing a colloidal or molecular electroplating catalyst,<sup>72,73</sup> molding or imprinting organic light emitters,<sup>74,75</sup> and micromolding organic or sol-gel materials.<sup>58,59,76-78</sup> Of these, the additive techniques rely upon a slow phase change or at best

further chemical treatment, in the form of bath deposition, in order to produce the pattern in the desired material. Liquid embossing addresses each of these shortcomings, differentiating itself from other printing techniques. The first difference is that the patterned material does not undergo a slow phase or chemical change during the printing process. This allows rapid patterning of a diverse materials set, including aqueous biomolecules, polymers, and inorganic nanocrystals in organic solvents.<sup>2,4,5,11,72</sup> The second and critical difference is that the embossing process pushes through the thin liquid film, clearing material away and contacting the substrate beneath. This additive process enables the fabrication of electrically isolated conducting patterns and the direct formation of via structures, both without the etching required for contact-printing<sup>32-34,44-53</sup> and imprint<sup>66,70,71</sup> schemes. Emboss times of less than 10 s, resolutions of 100 nm, and embossed areas exceeding 75 cm<sup>2</sup> have been reported (**Figure 1**).<sup>2,11</sup> Thus, liquid embossing is uniquely enabling for the rapid all-additive printing of electrically active structures through the use of appropriate printable materials.

### Printable Electronic Materials and Processes

A viable printing technology relies on both printable device-quality materials and a printing technique capable of patterning the materials with appropriate resolutions and morphology at great cost savings. There are “four ways in which a new exploratory technology” such as printed electronics “can compete with or supplement a widely used, entrenched technology” such the existing

microelectronics fabrication process, “for which many billions of dollars have already been invested.”<sup>20</sup>

The first of these is the most optimistic, and it is the possibility that printed electronics might improve upon the performance of existing technology. The second is more in-line with the stated goals of many researchers working in the field, and that is to enable an application of the technology by taking advantage of a unique property of the printing process or materials. Flexible and disposable electronics are often thought of as examples of this. The third option is also frequently cited as a goal of printed electronics research, and that is to considerably reduce the manufacturing costs of moderate-performance electronics. The final anticipated mode of disruption from printed electronics is one in which the low cost of the printed product creates a compelling case for devices with performance below that which is readily obtained by traditional fabrication methods, but which come at a considerably higher cost. In any of these four modes, printed electronics could have considerable impact on commercial electronics, especially if new applications are enabled by printing methods and materials.<sup>20</sup>

### **Printable Organic Materials**

To date, printed electronic materials research efforts have focused on organic conductors and semiconductors.<sup>18-22,79-84</sup> Such organic materials do not require high temperature processing and are intrinsically printable if they are designed properly. However, both the semiconducting and conducting properties of organics lag behind the performance of inorganic conductors and semiconductors (**Table 1**).

“There has been tremendous progress in [organic] TFT performance during the last decade,” and “initial product application[s] can be seriously considered.”<sup>20</sup> However, “the most widely used organic semiconductors, such as pentacene, thiophene oligomers, and regioregular polythiophene, seem to have reached ‘maturity’ as far as their performance is concerned.”<sup>20</sup> Organic semiconductors “cannot rival the performance of field-effect transistors based on single-crystalline inorganic semiconductors, such as Si and Ge, which have carrier mobilities about three orders of magnitude higher.”<sup>20</sup> The demonstrated charge

Material	Description	Carrier	Mobility ( $\text{cm}^2\text{V}^{-1}\text{s}^{-1}$ )
<b>Inorganic</b>			
Si	Single crystal <sup>35</sup>	<i>n</i> -type	1000
Si	Liquid solution epitaxy <sup>85</sup>	<i>n</i> -type	540
Si	Laser recrystallized <sup>86</sup>	<i>n</i> -type	450
Si	Metal-induced crystallized <sup>87</sup>	<i>n</i> -type	120
Si	Nanocrystalline <sup>88</sup>	<i>n</i> -type	10
Si	Amorphous <sup>20</sup>	<i>n</i> -type	1
GaAs	Single crystal <sup>35</sup>	<i>n</i> -type	8800
CdSe	Single crystal <sup>35</sup>	<i>n</i> -type	900
CdSe	Vapor deposited <sup>89</sup>	<i>n</i> -type	450
CdSe	Chemical bath deposited <sup>27</sup>	<i>n</i> -type	15
CdSe	Printed nanocrystal ink <sup>1</sup>	<i>n</i> -type	1
<b>Hybrid</b>			
(C <sub>6</sub> H <sub>5</sub> C <sub>2</sub> H <sub>4</sub> NH <sub>3</sub> ) <sub>2</sub> SnI <sub>4</sub>	Melt-processed, laminated <sup>26</sup>	<i>p</i> -type	1.7
(C <sub>6</sub> H <sub>5</sub> C <sub>2</sub> H <sub>4</sub> NH <sub>3</sub> ) <sub>2</sub> SnI <sub>4</sub>	Spin-coated <sup>23,25</sup>	<i>p</i> -type	0.6
[Pt(NH <sub>2</sub> dmoc) <sub>4</sub> ][PtCl <sub>4</sub> ]	Solution-cast <sup>90</sup>	<i>p</i> -type	0.06
<b>Organic</b>			
Carbon nanotube	Polyethylene imine doped <sup>91</sup>	<i>n</i> -type	8000
Pentacene	Vapor deposited <sup>92</sup>	<i>p</i> -type	3
Pentacene	Spin-coated precursor <sup>93</sup>	<i>p</i> -type	0.2
$\alpha$ -Sexithiophene	Vapor deposited <sup>94</sup>	<i>p</i> -type	0.2
Poly-3-hexylthiophene	Spin-coated <sup>95,96</sup>	<i>p</i> -type	0.1
Poly(9,9-dioctylfluorene-co-bithiophene)	Spin-coated <sup>97</sup>	<i>p</i> -type	0.02

**Table 1:** Comparison of semiconductor mobility for inorganic, organic, and hybrid organic-inorganic semiconductors deposited by traditional vapor-based schemes and non-traditional printing and solution methods. Mobility values of  $1 \text{ cm}^2\text{V}^{-1}\text{s}^{-1}$  are useful as the drive TFTs for pixels in displays and other applications that do not require high speed. Row and column driver circuits for displays require higher mobility values of  $\sim 40 \text{ cm}^2\text{V}^{-1}\text{s}^{-1}$ ,<sup>99</sup> and logic applications require even higher mobility values and are best served by single crystal inorganic semiconductors such as Si.

carrier mobilities for such printable semiconductors “can be competitive for existing or novel thin-film-transistor applications requiring large-area coverage, structural flexibility, low-temperature processing, and, especially, low cost.”<sup>20</sup>

Room temperature organic semiconductor charge carrier mobilities as high as  $3 \text{ cm}^2\text{V}^{-1}\text{s}^{-1}$  have been reported in the well-studied vacuum-deposited semiconductor pentacene.<sup>92</sup> Although this mobility compares favorably to that of the amorphous silicon ( $\alpha$ -Si) used in active matrix TFT fabrication for display backplanes,<sup>98</sup> it is near pentacene's upper limit and is not suitable for logic. Additionally, the row and column drivers for an active matrix liquid crystal display (AMLCD) require mobilities of  $40 \text{ cm}^2\text{V}^{-1}\text{s}^{-1}$ ,<sup>99</sup> clearly beyond pentacene's capabilities. Furthermore, pentacene is not directly printable and the best-printed organic semiconductors, poly(3-hexylthiophene) (P3HT) and dihexyl-quinquethiophene,<sup>20,100</sup> have demonstrated a considerably lower mobility of  $0.1 \text{ cm}^2\text{V}^{-1}\text{s}^{-1}$ .<sup>95</sup> Pentacene has been made printable through the use of a soluble but electrically inactive precursor that requires conversion at  $200 \text{ }^\circ\text{C}$  to form the semiconducting pentacene.<sup>93,101</sup> TFT mobilities of nearly  $0.3 \text{ cm}^2\text{V}^{-1}\text{s}^{-1}$  have been achieved with such an approach, the highest obtained from a solution-processed organic semiconductor.<sup>93</sup> It is the solution-processed semiconductor technology "that is believed to have the potential to produce the highest impact on manufacturing costs."<sup>20</sup> Both experiment and theory suggest that organic semiconductors have peak mobilities of  $\sim 1 \text{ cm}^2\text{V}^{-1}\text{s}^{-1}$  or less,<sup>20,21,102-104</sup> and the mobilities that have been practically obtained from solution processed organic TFTs have forced researchers to adopt non-traditional device structures to pass enough current through organic devices to drive display pixels.<sup>104</sup>

Despite the utility of organic materials in low-end applications such as smart cards,<sup>105</sup> tags,<sup>8</sup> and active matrices,<sup>79</sup> they are not suitable for logic and a number of logic intensive applications exist for flexible electronics. In addition to wearable and ubiquitous computing,<sup>8</sup> electronic books<sup>22,41,106,107</sup> depend upon printed electronics. Printed electronics are especially well-suited for this application as the display medium itself can be printable.<sup>107</sup> For a truly paper-like display, pixel resolution will be higher than current displays, requiring pixel transistors with mobilities better than  $\alpha$ -Si.<sup>99</sup> Also, the many displays in a book or newspaper require row and column drivers similar to those in AMLCDs. Such drivers cannot be made with organic materials and even if a traditional fabrication could provide a flexible solution, the cost of 100 pages worth of complex driver circuitry would be cost prohibitive. While organic TFTs have been used to fabricate an active matrix backplane in an electrophoretic display<sup>22,41</sup> – a milestone in the field – the pixel count, resolution, and performance have all been low.

In addition to the limitations associated with the low mobility of organic semiconductors, organic semiconductors have had problems with lifetime, have poor resistance to elevated temperatures, and are constrained in terms of their processing due to their solubility in organic solvents.<sup>20,21</sup> Even pentacene, which is not soluble in organic solvents, is quite “intolerant to exposure to various chemicals used in typical lithographic processes”,<sup>20</sup> requiring new processes to be developed and requiring subsequent deposition steps to avoid the use of chemicals that might degrade the semiconductor’s performance.

Organic semiconductors can have very high mobilities at low temperatures.<sup>20,21</sup> At such temperatures the vibrational energy of the organic molecules is lower than the intermolecular bonding, and as a result phonon scattering is very low. For organic semiconductors the intermolecular Van der Waals energies are usually less than  $10 \text{ kcal mol}^{-1}$ , much less than the covalent bonding energy of Si which is  $76 \text{ kcal mol}^{-1}$ .<sup>20,21</sup> Therefore, one way of greatly improving the mobility of organic semiconductors is to devise a way of increasing the intermolecular bonding energy. Unfortunately, the molecular character of these materials is critical to their processability. Another option is to avoid intermolecular charge transport altogether and to rely upon intramolecular transport only. This is very difficult as the rigidity of the extended  $\pi$ - $\pi$  networks of organic semiconductors prevents them from having high solubilities, as seen with pentacene. This is also difficult because it means that a semiconductor channel has to be of such a small length that it can be spanned by a single organic molecule. Although such processing and nanoscale organization challenges are formidable, a number of advances in molecular electronics<sup>108-121</sup> have been made and carbon nanotubes – essentially extended, rigid organic molecules – have been used to make high mobility TFTs.<sup>122-130</sup> It is in these types of materials that it becomes possible to start discussions about how printed organic electronics might have performance advantages extending beyond state-of-the-art inorganic electronics.<sup>20,21</sup> A number of research efforts are already underway in this area, but such materials are anticipated to become critical only in 2015 when the smallest features in semiconductor devices get to 25 nm, within an order of magnitude of molecular scales.<sup>40</sup>

## Printable Inorganic Materials

Due to the limited applications of organic semiconductors and the outstanding need for printable high-mobility semiconductors, it is desirable to overcome the resolution and high temperature hurdles associated with the printing of inorganic powders. Two broad approaches exist in the printing of inorganic materials. The first is most similar to the printing of organic materials, and it involves the direct printing of an active semiconducting material, most likely a solution-processable organic-inorganic hybrid, although nanowires and even nanoparticles can be envisioned in such applications if the device scale is small enough. The second approach involves printing a precursor, which upon subsequent treatment is transformed into the desired inorganic material. Such an approach could rely on nanoparticle or organometallic inks or could make use of chemical bath deposition, although patterning techniques are somewhat limited for such an approach. Our approach was to devise a method to print materials traditionally used in microelectronics fabrication, with the aggressive goal of the printed material being indistinguishable from that deposited out of vapor in a vacuum process. Our approach was to print nanoparticle inks.

When coupled with advances in soft lithography, inorganic materials can be printed at high resolutions and low temperatures by using a nanoparticle-based ink. Unlike finely ground inorganic particles, which are large enough to retain the properties of the bulk material, nanocrystalline materials display properties somewhere between those of an atom and a bulk crystal.<sup>131</sup> At particle sizes below 5 nm there is a large melting point depression that allows low temperature processing of the nanoparticles into polycrystalline films.<sup>132,133</sup> The reliable feature sizes of such films are only limited to sizes 5 to 7 times the diameter of the deposited nanoparticles,<sup>37</sup> and nanoparticles readily suspend in appropriate solvents,<sup>134</sup> making them ideal candidates for printing.

Nanoparticles, also known as quantum dots or artificial atoms, require ligand stabilizers to prevent particle agglomeration.<sup>135</sup> Such “capping groups” are generally introduced to the particles during their formation, but can be exchanged after synthesis is complete.<sup>131,134</sup> Because of their extremely small size, nanoparticles cannot be formed by grinding, but are instead synthesized by a number of chemical means, including solution-phase chemistry,<sup>136</sup> physical vapor deposition,<sup>137</sup> and etching.<sup>138</sup>

Though conceived independently, the notion of using nanoparticles as precursors for thin films has been proposed by other researchers.<sup>132,139,140</sup> Despite a handful of references in papers<sup>132,139,140</sup> and patents,<sup>141-143</sup> there have been only two studies in which semiconductor nanoparticles were used as precursors for a polycrystalline film in a device.<sup>144-147</sup> In the more successful of those studies, a methanol-based cadmium telluride (CdTe) colloid was spray-deposited onto a hot substrate as a part of solar cell fabrication.<sup>145,146</sup> Device performances were never discussed in the numerous publications from this project,<sup>145,147-150</sup> but related publications mention that a 2,793 cm<sup>2</sup> device has displayed an active area efficiency of 10.5%.<sup>147</sup> While the success of this approach is heartening, spray deposition does not address the differences between the unpatterned thick films of solar cells and the finely patterned thin films required for microelectronics fabrication.

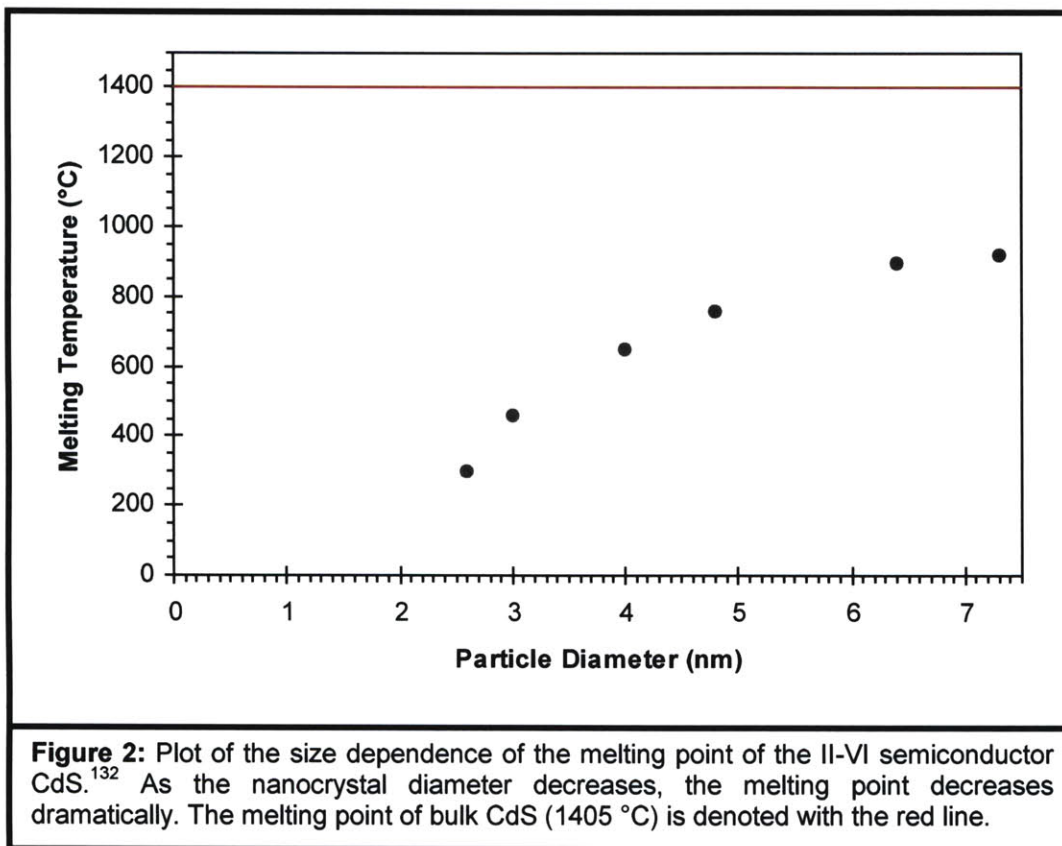
### The Nature of Melting in Nanoparticles

The melting point depression in metal nanoparticles has been known for some time.<sup>133</sup> In 1991 semiconductor melting point depression was demonstrated in the II-VI semiconductor CdS, “indicating that the phenomenon of reduced melting point in small systems is a general one regardless of the type of material.”<sup>135</sup> More recently this behavior has been observed in the semiconductor Si.<sup>37</sup>

Unlike metals, the bonding in semiconductors is “highly directional and covalent.”<sup>132</sup> Despite this difference 25 Å gold (Au) and 25 Å CdS nanoparticles both melt at ~300 °C, well below their bulk melting temperatures of 1063 and 1405 °C, respectively.<sup>132,133</sup> The melting point shows a rough inverse dependence on the particle’s radius,<sup>37</sup> leading to a sharp drop in melting temperature at particle sizes below 5 nm (**Figure 2**).<sup>132</sup> Judging by the melting points of Au and CdS nanoparticles, particles ~25 Å in diameter or less are desirable for keeping processing temperatures plastic-amenable.

Despite observations that “suggest that melting occurs throughout the particle in a narrow range of temperature,”<sup>37</sup> nanoparticles that are in intimate contact with each other are observed to sinter before melting.<sup>135</sup> This is problematic because fine-grained polycrystalline films are formed with domain sizes “comparable to the size of the nanocrystal initially deposited.”<sup>135</sup> This occurs because particles melt at the surface first, forming a “liquid skin”<sup>151</sup> which fuses the particle with its





neighbor. Thus the particle never melts to its core because its effective melting point climbs up the steep melting curve (**Figure 2**)<sup>132</sup> as two particles fuse together. Nanoparticles will fuse at approximately 2/3 of their reduced melting temperature.<sup>37</sup> Recent research has found that the onset temperature of sintering in Au and Pt nanoparticle films is ~200 °C, independent of particle size for the 2-6 nm particles that were studied,<sup>152</sup> but similar studies have found that for particles capped with short, volatile capping groups, sintering of larger particles is actually favored at lower temperatures because of the sintering of the native particle does not limit the coalescence temperature.<sup>153</sup> Instead, nanoparticle fusion is controlled by the loss of the capping ligand,<sup>152,153</sup> and the smaller surface area of larger nanoparticles means there are fewer surface groups to remove prior to nanoparticle coalescence.<sup>153</sup>

Molecular dynamics calculations for Au clusters show that for larger particles, “liquid patches” first develop at the surface and then propagate to the center of the particle, melting it abruptly. However, particles with fewer than ~250 atoms

display no pre-melting effects and the entire particle melts at once.<sup>151</sup> The absence of pre-melting effects at small sizes is important because it suggests that complete melting and subsequent grain growth is possible. Even with surface melting, a rapid thermal or laser treatment might be able to melt the particle throughout, allowing grain growth beyond the dimensions of the nanoparticle.

### **Polycrystalline Films from Nanoparticle Precursors**

A few researchers have used nanoparticle precursors to form semiconductor polycrystalline films. The II-VI semiconductors CdS<sup>139,154</sup> and CdTe<sup>145</sup> have been the most commonly used materials for these studies, mainly because of their use in solar cells. Additionally, CIGS colloids have been prepared and deposited as a part of solar cell fabrication.<sup>147,155</sup> Semiconductor clusters less than 1 nm and as large as 30 nm have been deposited in these studies, requiring fusion temperatures as low as 225 °C and as high as 550 °C.

Sub-nanometer CdS fragments have been deposited and thermally converted to the bulk semiconductor.<sup>139,140</sup> The CdS cluster is bound with an amine and thiophenol, has a precisely known chemical formula,  $(N(CH_3)_4)_4Cd_{10}S_4(SC_6H_5)_{16}$ , and as such is more appropriately characterized as a molecule than as a nanoparticle. When this semiconductor cluster is deposited from pyridine, there are two distinct stages in the transition from molecular solid to bulk semiconductor. The first transformation occurs at 250 °C, and leaves an intermediate species,  $Cd_{10}S_4(SC_6H_5)_{12}$ . At 500 °C this cluster loses the remaining phenyl groups as diphenyl sulfide, and leaves behind a stoichiometric CdS film.<sup>139</sup> Despite the very small size of the cluster, relatively high temperatures are required to form the bulk semiconductor film. This is because the heat treatment does not serve to melt the particle, but instead breaks a formal chemical bond between the cluster and the thiophenol ligand. Such strong inorganic-organic binding interactions are not expected from CdSe-pyridine, as pyridine only weakly caps CdSe particles and has been demonstrated to completely leave the nanoparticle surface under appropriate conditions.<sup>156</sup>

Thiolate-capped CdS nanoparticles ~23 Å in diameter have been reported to fuse at temperatures as low as 200 °C.<sup>157</sup> Formed from the reaction of cadmium acetate with 1-thioglycerol,<sup>157</sup> capping group interactions encourage the particles to form chains when deposited.<sup>154</sup> Fusing these particle chains forms “quantum wires,”

with parallel wires having a 29 Å spacing.<sup>157</sup> Electrical studies of fused CdS films have been limited,<sup>157</sup> but heat treatments of thioglycerol-capped particles synthesized by a similar route leave “traces” of decomposed organic material.<sup>158</sup> The thiolate ligands have been reported to leave between 200 and 300 °C.<sup>157,158</sup> Lower temperature treatments at 200 and 250 °C do not lead to the recovery of bulk optical properties, indicating there is only a partial fusion of the CdS nanoparticles at these lower temperatures.<sup>157</sup>

Nanoparticle-derived CdTe films have successfully been used in the fabrication of solar cells.<sup>147</sup> By spray depositing CdTe colloids onto a hot substrate, films with large grains can be obtained. Nanoparticles 25 to 75 Å in diameter have been found to form grains 60 to 300 Å across at 400 °C, and grain growth is observed at temperatures as low as 240 °C.<sup>145,146</sup> There is no residual nanocrystalline topography in these films. Most importantly these films have been used in the fabrication of high-quality CdTe solar cells, with the best reported cells having a 2,793 cm<sup>2</sup> active area efficiency of 10.5%.<sup>147</sup>

A similar spray-deposition approach has been used to form pure CIGS films, again for solar cell fabrication. The 10 to 30 nm amorphous nanoparticles were deposited at 550 °C and formed porous films. Grain growth was observed, but researchers did not comment on the size of the grains. The best film exhibited a conversion efficiency of 4.6%.<sup>155</sup>

### **Nanoparticles for Printed Transistors**

CdS, CdSe, and Te were used in a number of pioneering TFT efforts in the 1960s and 70s. At the time these materials were used to fabricate the first flexible transistors, deposited onto Mylar, aluminum foil, and even paper, and were used to form a 6×6” active matrix for display addressing in an era when silicon wafers were only 1.5” in size.<sup>159</sup> By 1979, CdSe devices were demonstrated that had been running constantly for a decade.<sup>89,160</sup> Modern CdSe devices have shown mobilities of 450 cm<sup>2</sup>V<sup>-1</sup>s<sup>-1</sup>, ON/OFF ratios of 10<sup>11</sup>, and the ability to switch 500 V.<sup>89</sup>

Despite excellent device performance and some simple aspects of processing, CdSe has not been a popular production material for TFTs. CdSe devices can have hysteresis problems and require complex photolithography.<sup>161</sup> Perhaps the

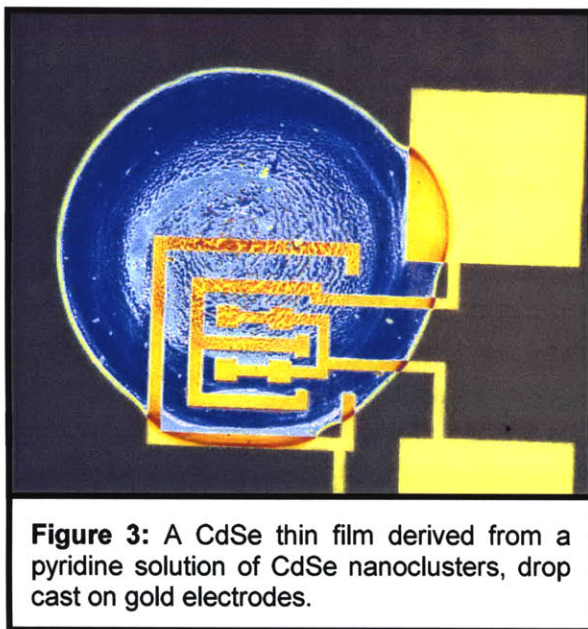


**Figure 3:** A CdSe thin film derived from a pyridine solution of CdSe nanoclusters, drop cast on gold electrodes.

greatest problem is the lack of a high mobility complementary logic.<sup>161</sup> CdSe TFTs are *n*-type, and to complement them *p*-type copper-doped germanium TFTs (Ge:Cu) have been fabricated, but with lower mobilities ( $\sim 10 \text{ cm}^2 \text{V}^{-1} \text{s}^{-1}$ ) and poor ON/OFF ratios.<sup>162,163</sup>

As with the work in the area of organic electronics, our research has focused on developing a printable semiconductor. We chose to first work with the II-VI semiconductor CdSe, in part because of its history in TFT and

active matrix fabrication, and in part because “the best developed semiconductor ‘nanocrystal’ synthesis is that of CdSe.”<sup>136</sup>

Using CdSe nanoparticles we have demonstrated the first printed inorganic semiconductor TFT channels and all-printed inorganic TFTs fabricated by liquid embossing (**Figure 3**).<sup>1,10</sup> Field effect mobilities of  $1 \text{ cm}^2 \text{V}^{-1} \text{s}^{-1}$  are observed and are to our knowledge the highest mobilities ever observed in a printed semiconductor. For such devices ON/OFF ratios of  $3 \times 10^4$  are obtained for a gate sweep of  $-40$  to  $40$  V. Field effect activity is observed in films sintered as low as  $250 \text{ }^\circ\text{C}$ , demonstrating that nanoparticle-based solution deposition can be a plastic-compatible process ( $\leq 400 \text{ }^\circ\text{C}$ ).

Si, which has been the workhorse of commercial microelectronics,<sup>40</sup> was heavily investigated as well. Nanoparticle syntheses of Si are poorly developed when compared to those of CdSe and other binary semiconductors, and the “wet-chemical synthesis” of Si “or any other group IVA element” is “unlikely to produce wafer quality Si.”<sup>164</sup> Still, Si nanoparticles of small size were synthesized by reduction in inverse micelles and in principle were capped with hydrogen,<sup>165</sup> arguably an ideal passivant for Si for application in printed microelectronics.<sup>166</sup> Out of necessity the synthetic chemistry was carried out at low concentration in surfactant-loaded solutions. Purification proved to be difficult, preventing the

successful formulation of nanoparticle Si inks and the fabrication of printed Si TFTs.

Although the difficulties surrounding the synthesis of Si nanoparticles prevented Si ink formulation and the printing of Si TFTs, no fundamental reason preventing the printing of Si was discovered. In fact, hope for the printing of commercially thriving materials such as Si is taken from the successful printing of CdSe TFTs.<sup>1,2,10,11</sup> Such efforts demonstrated for the first time<sup>1</sup> that electronic devices could be printed using inorganic materials. Experimental printing methods such as liquid embossing<sup>2,11</sup> promise rapid printing at high resolutions and printable inorganic materials<sup>1,10</sup> offer an ideal complement for printed microelectronics – both high performance and inexpensive processing.

# Synthesis of Cadmium Selenide Nanocrystals

## Synthesis of CdSe Nanoclusters by Metathesis

We have explored two synthetic methods to produce CdSe nanocrystals below 5 nm in diameter.<sup>1,10</sup> The well-established and more complex pyrolysis<sup>131</sup> scheme allows for tight control of particle size and distribution, but was found to be inappropriate for applications in printed microelectronics due to the persistence of bulky capping ligands at the particle surface.<sup>1,156</sup> In contrast, the simple published metathesis<sup>167,168</sup> route does not provide tight control over particle size, shape, or distribution, but offers high yields, tame reaction conditions, and a reaction medium free of non-volatile surfactants. To overcome the limited size control, a modified metathesis route was developed.

Metathesis has been used to form nanoparticles of a number of chemical species, such as gallium nitride,<sup>169</sup> molybdenum disulfide,<sup>170</sup> and non-binary copper indium gallium diselenide (Cu(In,Ga)Se<sub>2</sub>, CIGS).<sup>147</sup> The synthesis of CdTe by this method was reported in 1992,<sup>167</sup> and only recently have CdSe and the entire family of II-VI compounds been synthesized by this route.<sup>171</sup>



The published reaction is very simple: under an inert atmosphere, methanol (MeOH) solutions of cadmium iodide (CdI<sub>2</sub>) and sodium selenide (Na<sub>2</sub>Se) are mixed together, producing CdSe, and the soluble byproduct, sodium iodide (NaI) (**Equation 1**). The reaction is instantaneous, turning the reaction mixture red and precipitating the nanocluster product. The particles are purified and isolated by repeatedly settling, decanting, and re-suspending the particles, or by repeatedly filtering and washing the particles. The resulting nanoparticles are MeOH capped. Although CdTe nanoparticles have been reported to re-suspend in MeOH,<sup>145</sup> the CdSe nanoparticles synthesized by this method as a part of this work do not. They suspend in pyridine, though, which is known to act as an effective capping group for CdSe nanoparticles.<sup>131</sup>

The published metathesis procedure gives the desired product with essentially quantitative yields<sup>167</sup> and a 1:1 stoichiometry as determined by X-ray photoelectron spectroscopy (XPS),<sup>145</sup> but the synthesis is hindered by a broad size

distribution.<sup>145,168</sup> As an example, metathesis has been reported to produce a distribution of CdTe sizes ranging from 33 to 85 Å, much broader than the 31 to 47 Å range reported for CdTe nanocrystals synthesized by pyrolysis.<sup>145</sup> Still, metathesis has been successfully used to synthesize CdTe nanoparticles for spray deposition for solar cell fabrication. In such a synthesis the nanoparticles were formed at a reduced temperature and are reported to range from 25 to 75 Å in diameter.<sup>145</sup> When forming CdSe particles by this route, however, transmission electron microscopy (TEM) indicates that the majority of particles are ~38 Å in diameter. While TEM is not as sensitive to identifying smaller particles as some other methods,<sup>172</sup> very few particles were observed with diameters below 30 Å. Such relatively large particle sizes are expected to complicate or prevent low temperature, plastic-compatible processing.

Because the majority of CdSe particles produced by metathesis are outside the size regime of interest, we modified the metathesis approach.<sup>1,10</sup> As in pyrolysis reactions,<sup>131</sup> the strategy was to alter the nature of the reaction medium to suppress particle growth relative to nucleation. Pyridine was found to effectively control size and was also useful as a solvent for the nanocluster product.<sup>1,10</sup>

Combining the reagent solutions in pyridine instead of methanol produces a tight distribution of very small particles. The influence of pyridine is immediately seen in the reaction, as instead of yielding a deep red solution, the product solution is yellow. Although the reaction is still instantaneous, pyridine acts to hinder particle growth, yielding smaller particles and a tight size distribution.<sup>1,10</sup> UV-Vis spectra reveal that as the concentration of pyridine increases the average particle size decreases (**Figure 4**). At higher concentrations of pyridine the optical spectra begin to show distinct features, indicating that a narrow distribution of particle sizes is formed. The UV-Vis spectra shift and tighten over the course of 24 hours, turning from a strong yellow solution into a pale yellow solution, with absorption features sharpening and settling at slightly higher wavelengths (**Figure 4**). The optical features match those previously reported for 17 Å CdSe nanoparticles.<sup>134</sup>

Highly monodispersed systems can arise from “bottlenecks” in the growth series. Bottlenecks result from the stability of a complete, closed structural shell and have been observed in CdSe.<sup>131</sup> At small sizes there are fewer available particle geometries and the relatively high surface energies increase the likelihood of observing a bottleneck in the size series. A number of samples formed by different metathesis methods display the same characteristic absorption features

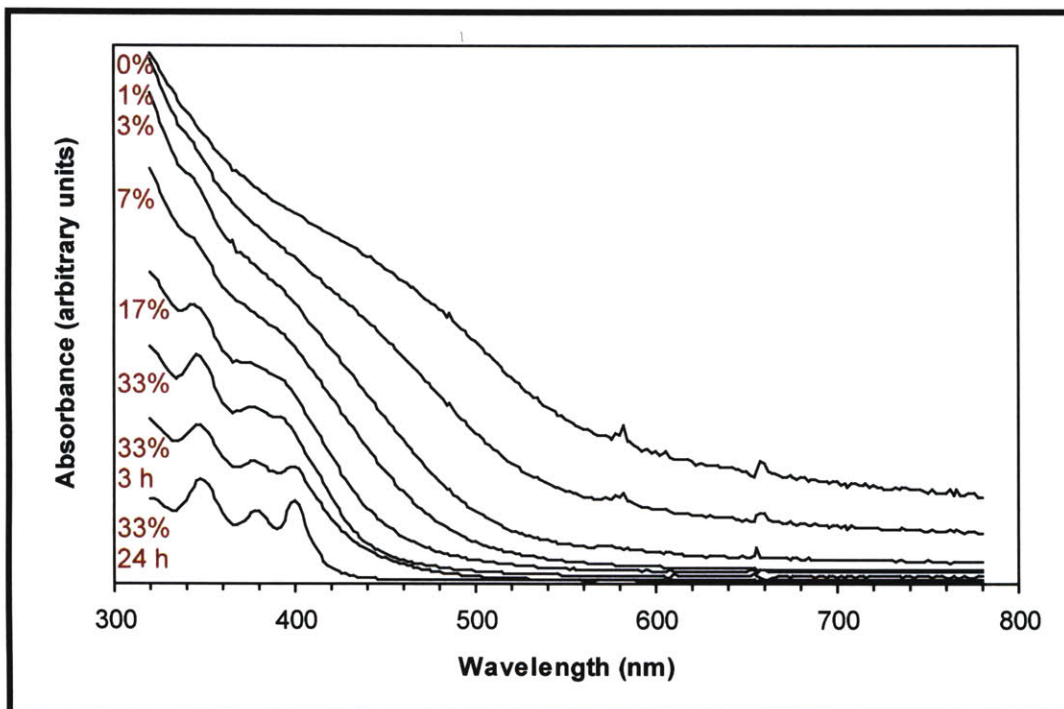


**Figure 4:** Spectra of the UV-Visible region of pyridine solutions of CdSe nanocrystals. As crystallite size decreases, a blue-shift is observed for the absorption onset, and as crystallite size distribution narrows, the spectral features belonging to the dominant crystallite size are more clearly resolved and appear sharper. The series of spectra shown come from a synthetic series showing the influence of pyridine on crystallite growth in metathesis reactions. With 0% pyridine, the methanol reaction solvent is insufficient to tightly control particle size and a dark red product is obtained with broad and featureless UV-Visible absorptions. With even as little as 1% pyridine the average size is observed to decrease, and with increasing pyridine concentration the size distribution is observed to narrow, as well. With 33% pyridine in the reaction solution the yellow product can be ripened for hours or a day and the crystallite size distribution tightened by the room temperature annealing in pyridine, yielding a pale yellow CdSe nanocluster solution.

after sitting for 24 hours. Even particles synthesized in methanol, which initially have a very broad and featureless absorption, develop the same characteristic features of the nanoparticles formed in pyridine and show some additional bottlenecking near 570 nm.<sup>10</sup>

TEM does not resolve the nanoparticles formed in pyridine. EDX indicates that the Cd:Se ratio is 1:1 and XPS of heated samples also indicates that there is an approximately stoichiometric Cd:Se ratio. RBS finds a 1.16:1 Cd:Se ratio, indicating that there is a non-stoichiometric surface layer of Cd.<sup>10</sup> While EDX and



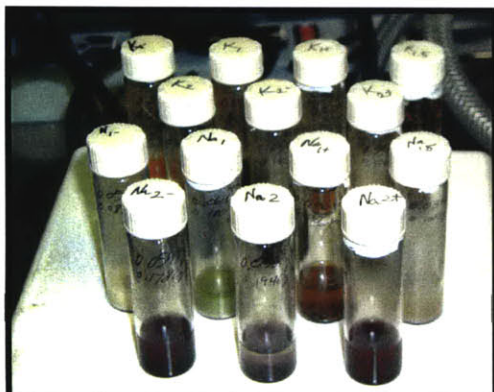


**Figure 5:** Photograph showing a series of potassium and sodium selenides as they are synthesized from the elements in THF with catalytic naphthalene. The violet color of the sodium diselenides are seen in the first row of vials and the color is similar to that obtained from commercial sources as sodium monoselenide.

RBS do not find any I or Na in the samples, these results are in contrast with XPS measurements performed on heated samples that indicate that there is iodine present. The observed I impurity might remain bound to the surface of the nanoparticle if there is an excess of the  $\text{CdI}_2$  reagent in the reaction medium or as a passivating group for a unique surface species on the particle surface.<sup>10</sup>

It has been suggested that the 17 Å particles are discrete molecular species with a precise stoichiometry.<sup>131</sup> These CdSe species have less than 100 atoms and have a tetrahedral structure,<sup>173</sup> and thus are often known not as nanoparticles but as nanoclusters. A number of CdSe clusters have been reported,<sup>174</sup> but they are clearly different

from the species produced by metathesis. Previous reports indicate that there is a large Se excess in CdSe clusters,<sup>174</sup> while the metathesis-formed particles are either stoichiometric or slightly Cd rich. In Se-rich clusters, organic capping groups bind the four Se corners of the tetrahedron. For a Cd-rich cluster produced by metathesis, I might bind to the Cd corners, accounting for the observation of I by XPS. While the stoichiometry of larger nanoparticles produced by metathesis is consistently 1:1, discrete clusters likely will have a stoichiometric imbalance, which may be what is being observed by RBS.

Pyridine's suppression of particle growth was anticipated, but initially there was a concern that adding pyridine to the reaction would hinder the isolation of the product. Pyridine-capped CdSe nanoparticles can be soluble in MeOH,<sup>131,134</sup> and it was feared that the product would not precipitate. However, the presence of 2 equivalents of dissolved NaI seems to shift the polarity of the solvent enough to destabilize the particle suspension. This can be observed by adding NaI dissolved in MeOH to a sample of pyridine capped CdSe nanoparticles formed by pyrolysis; the particles agglomerate and precipitate from the MeOH/pyridine solution.



**Figure 6:** Isolated sodium and potassium mono- and diselenides. Potassium selenides are seen in the back row of vials, and sodium selenides are seen in the front row. From left to right there is an increasing Se:M ratio: 0.95, 1.0, 1.05, 1.5, 1.95, 2.0, and 2.05.

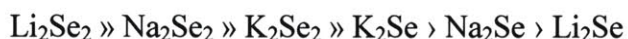
Nanoclusters formed by this modified metathesis route can be isolated as a solid and re-suspended in appropriate solvents. For example, the addition of hexane to a pyridine solution of nanoparticles causes the particles to agglomerate and fall from the solution. The precipitate can then be recovered by centrifuging, decanting, and re-suspending the solids in pyridine.

Over the course of this work it was noticed that approximately one in every four batches of  $\text{Na}_2\text{Se}$  from the vendor was “bad” and would precipitate a black material within minutes of attempting to dissolve the material in MeOH. As a result, the direct synthesis of  $\text{Na}_2\text{Se}$  was

investigated. A simple procedure has been described<sup>175</sup> in which the elements are mixed in the appropriate stoichiometry and refluxed in tetrahydrofuran (THF) in the presence of a catalytic amount of naphthalene (**Equation 2**).



The reaction can even occur at room temperature if an ultrasonic bath is used to drive the reaction. The corresponding potassium and lithium selenides can also be formed in this manner, as well as the so-called “diselenides” such as  $\text{Na}_2\text{Se}_2$ . Both the mono- and diselenides can be produced by simply varying the ratios of the elements to match the desired product stoichiometry. Of direct interest is the report<sup>175</sup> that the monoselenides are colorless, and that the diselenides are heavily colored and that sodium diselenide is a violet color similar to the material that we were receiving and using as the monoselenide. The reactivity toward organic bromides of the various alkali metal selenides is reported<sup>175</sup> as follows:



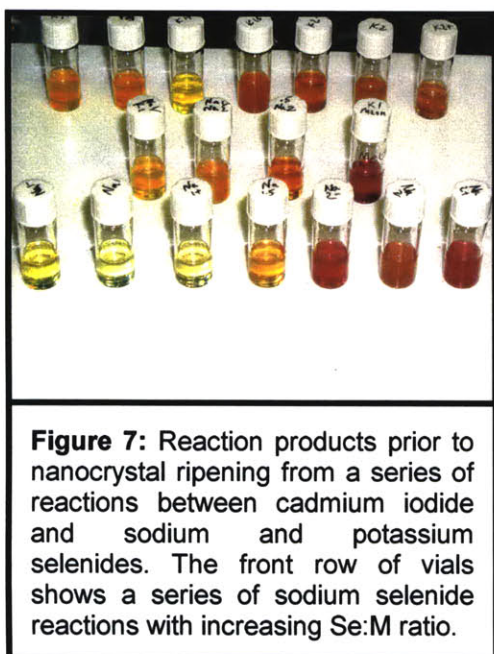


**Figure 7:** Reaction products prior to nanocrystal ripening from a series of reactions between cadmium iodide and sodium and potassium selenides. The front row of vials shows a series of sodium selenide reactions with increasing Se:M ratio.

Seven samples each of the sodium and potassium selenides were synthesized by this route, with stoichiometric ratios of 0.95, 1.0, 1.05, 1.5, 1.95, 2.0, and 2.05. Due to the tendency of the alkali metal and selenium to stick to the vial walls, the precise reaction stoichiometry was compromised slightly as some of the starting material might not participate in the reaction. A variety of colors are seen in the reactions – white, tan, green, orange, red, and violet, as reflected in the reaction products prior to isolation (**Figure 5**). After isolation, white or lightly colored powders (**Figure 6**) are indeed produced for the monoselenides and darkly colored powders are produced

for the diselenides. The dark red color of potassium diselenide is apparently seen as an impurity in potassium monoselenide, giving it a pale orange color.

Both the monoselenide and diselenide readily dissolve in MeOH and form solutions with depth of color comparable to the coloration seen in the powders. Subjecting the various monoselenide and diselenide solutions to reactions with  $\text{CdI}_2$  produced a marked difference in the initial reaction product as the monoselenides give a yellow product and the diselenides give a red product (**Figure 7**). The selenides from reactions of mixed stoichiometry give a deep yellow or orange product. While the initial products vary in color, after ripening in pyridine the same product results, as evidenced by identical UV-Vis signatures.

In the first set of metathesis reactions the product work up consisted of repeatedly washing the precipitated product with MeOH and then re-dissolving the nanocluster precipitates in pyridine, in which the clusters ripen. With excessive washing with MeOH the product was observed to reluctantly disperse in pyridine, suggesting that the MeOH wash removed pyridine from the surface of the precipitated clusters and prevented their re-dissolution. Small amounts of pyridine could be added to the MeOH to address this problem, but there was also the concern that I-bearing byproducts might precipitate with the cluster product and be trapped at cluster surfaces that were inaccessible and deep within an



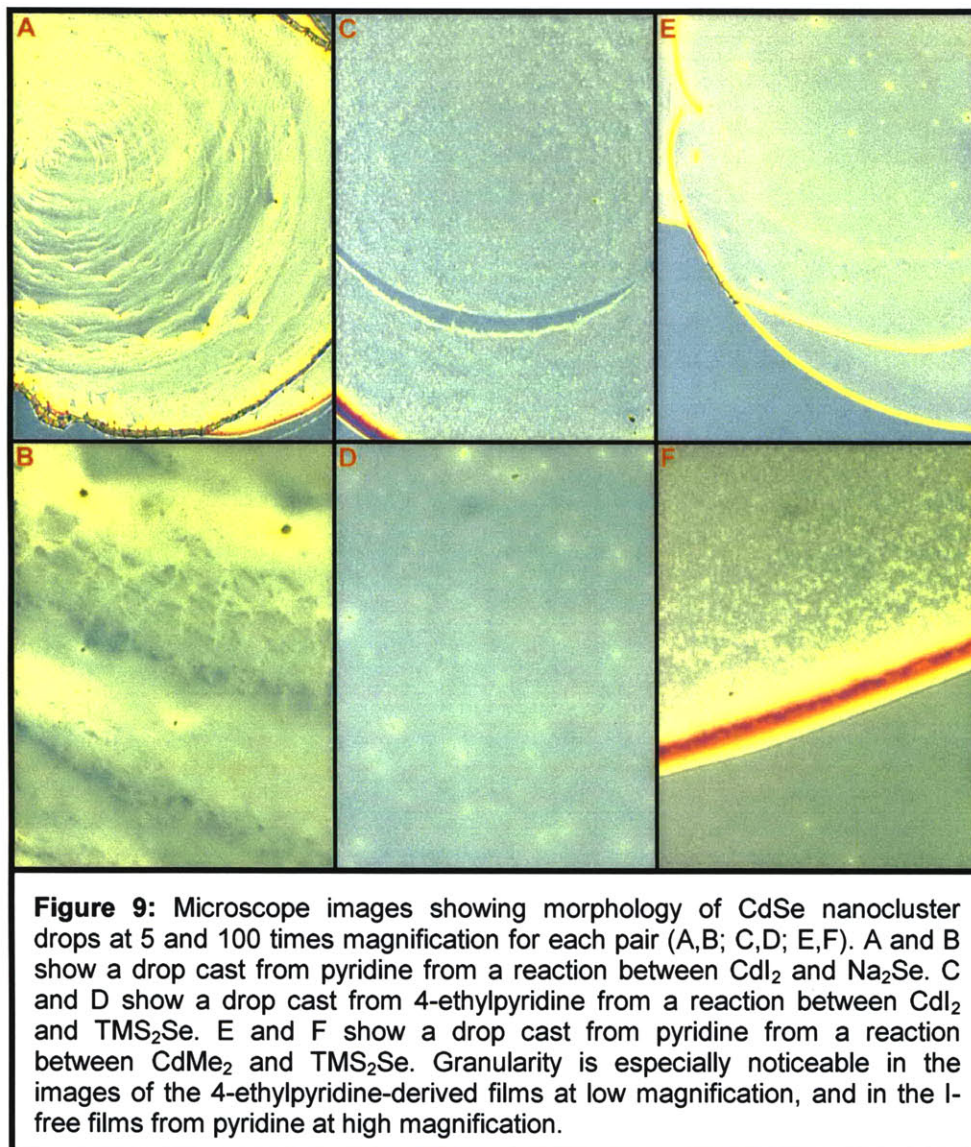
**Figure 8:** CdSe nanocluster solutions after ripening. The pale yellow solutions were ripened in pyridine, the yellow solutions were ripened in methanol, and the red solutions were not ripened and the synthesis was carried out in the absence of pyridine.

agglomerate. In order to minimize such impurities a more rigorous approach was used in which the product was initially re-suspended in pyridine, ripened, and then forced from solution with hexane and subsequently repeatedly suspended, centrifuged, and removed from MeOH. During this residence in MeOH, the ripened clusters further ripened to a slightly larger size. This shift in size was noticeable by eye and was clearly seen in UV-Vis spectra of the MeOH ripened species (**Figure 8**). After such ripening the particles do not revert to their pyridine-ripened size if they are left in pyridine. Thus, two distinct sizes of nanoclusters

can be produced by this method by simply altering the nature of the work up.

In addition to studies with sodium and potassium mono- and diselenides, nanoclusters were synthesized from alternative Se and Cd sources.  $\text{CdMe}_2$  and  $\text{TMS}_2\text{Se}$  have been used successfully in pyrolytic reactions<sup>131,134</sup> and here were reacted at low temperatures in a variety of solvents including pyridine, 4-ethylpyridine, hexylamine, octylamine, nonylamine, decylamine, and dodecylamine. All of these reactions produced an agglomerated product, and most precipitated a yellow solid within minutes of the addition of the second reagent. The yellow color is characteristic of very small CdSe particles ( $\sim 2$  nm), but even the long chained dodecylamine could not prevent particle agglomeration under the conditions employed. Higher temperatures and lower concentrations were found to improve the solubility of the particles, but even those solutions which did not precipitate a product were found to clog 200 nm filters, and thin films from these nanoparticle suspensions were noticeably less smooth than those produced from soluble particles from reactions with  $\text{CdI}_2$  and  $\text{Na}_2\text{Se}$  (**Figure 9**). Reactions between  $\text{CdI}_2$  and  $\text{TMS}_2\text{Se}$  were successful in producing a soluble product, though, suggesting that the I promotes solubility, perhaps as an “impurity” at the surface of the nanocluster that lends stability and solubility through a polar bond to surface-Cd species. Such stabilization is unavailable to the product from  $\text{CdMe}_2$ -derived clusters. Still, it is surprising that the steric stabilization offered

by long chained amines such as decylamine and dodecylamine were not sufficient to stabilize the particles against agglomeration.



## Device Fabrication with Cadmium Selenide Inks

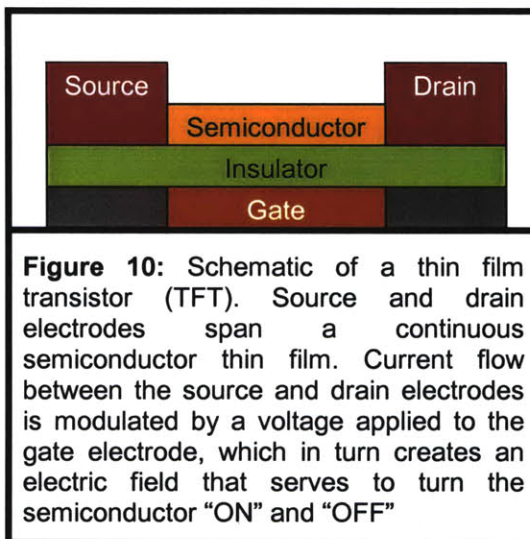
### Traditional Fabrication of CdSe TFTs

In fabricating TFTs (**Figure 10**), CdSe films are usually deposited by evaporation<sup>98</sup> or sputtering.<sup>176</sup> A common criticism of CdSe is that its stoichiometry is not guaranteed.<sup>98</sup> However, the vapor pressure-temperature curves for Cd and Se<sub>2</sub> are very similar<sup>98,177</sup> and the material is very hard to disproportionate.<sup>98</sup> There is a slight excess of Cd present in evaporated films, but the missing Se atoms serve to increase the *n*-type character of the film.<sup>178</sup>

Protecting the semiconductor-insulator boundary is critical to device performance. This is done by sputter cleaning the insulator prior to semiconductor deposition or by depositing the insulator and semiconductor in the same pump-down cycle. In fact, entire CdSe devices have been fabricated during a single vacuum cycle.<sup>179</sup>

One of the attractive features of CdSe is that it requires only a low temperature anneal.<sup>180</sup> The anneal is critical to device performance, though, as without it devices show only a small field effect and have very high OFF currents. Annealing is usually done for 1 to 4 hours at 350 °C<sup>179-181</sup> in a dry air or nitrogen ambient.<sup>182</sup> At such a temperature CdSe grains will grow until they are near the same size as the film thickness. Higher temperatures (400 °C) and longer anneal times (10 hours) can lead to growth of grains larger than the thickness of the film.<sup>183</sup>

It is not only through grain growth that annealing improves device performance. As-deposited films with grain sizes comparable to their thickness do not function well in devices.<sup>180</sup> After the heat treatment the devices perform well, though, as the heat treatment reduces the number of donors and anneals out defects.<sup>180</sup> Se vacancies in the as-deposited film lead to the high donor levels, and so the heat treatment encourages the diffusion of



excess Cd to grain boundaries, lowering the number of Se voids.<sup>184</sup>

Indium (In) and indium selenide ( $\text{In}_2\text{Se}_3$ ) are often used as dopants<sup>179</sup> and have been demonstrated to assist in grain growth during the anneal.<sup>185</sup> For In-doped CdSe, grain growth does not stop when the grain size equals the film thickness. In fact, for similar anneal times, grains in In-doped CdSe films have been observed to grow to twice the size of their undoped counterparts. Even annealing at 200 °C has been observed to grow grains ~50% larger than the thickness of the film.<sup>185</sup>

Cr,<sup>181</sup> Al,<sup>186</sup> and Au<sup>180</sup> have all been used as contact materials for CdSe. Because the metals diffuse into CdSe during the anneal,<sup>180,181,186</sup> an  $n^+$  region is formed near the electrodes and an ohmic contact is created between the metal and semiconductor.<sup>180</sup> Al and Cr have been shown to laterally diffuse into CdSe at room temperature,<sup>187</sup> and Cr has been observed to penetrate up to 20  $\mu\text{m}$  into a TFT channel during a 4 hour anneal at 400 °C.<sup>181</sup> At such temperatures Cr also improves grain growth, producing up to micron-sized grains near contacts. Below 400 °C, though, grain size is found to be uniform across the channel.<sup>181</sup>

Beyond grain growth and forming an ohmic contact, Cr diffusion can have an effect on device performance in two important ways. Channel lengths can be effectively shortened by Cr diffusion, and more importantly, the extent of Cr diffusion can control the semiconductor doping. Al does not diffuse as readily as Cr, but studies have not addressed if Al diffusion and doping can have the large impact on device performance observed for Cr.<sup>181</sup>

### Thin Film Formation and Device Fabrication

In studies of the melting point suppression of semiconductor nanocrystals, CdS particles have been reported to fuse together to form a polycrystalline bulk material with domains no larger than the original particles.<sup>132</sup> The nanocrystal surface has a lower melting point than its interior, and sintering is generally observed at approximately two-thirds of the size-reduced melting temperature.<sup>37</sup> In the work described here, the crystal domains that initially form during particle sintering may be the same size as the nanocrystals, but the 30- to 60-min heat treatment serves as both a sintering and an annealing step. Transmission electron microscopy (TEM) finds that the heating yields crystalline areas up to 15 nm across (**Figure 11**), which are comparable to grain sizes reported for vapor-

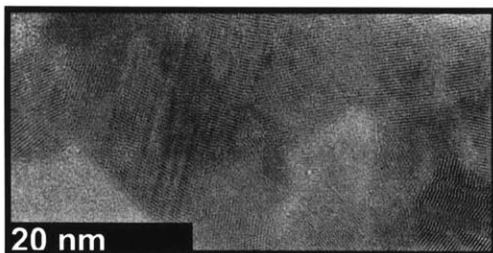


**Figure 11:** TEM image of a CdSe thin film from CdSe nanocrystals sintered at 350 °C for 30 minutes. Crystalline grains larger than 15 nm across are seen, derived from 100s of <2 nm nanocrystals. A ribbon-like texture can be seen in some of the grains, suggesting anisotropic fusion as a growth mechanism. Similar behavior has been reported in solution for Si nanocrystals.<sup>254</sup>

deposited CdSe TFTs.<sup>180</sup> TEM images are markedly different from images of unheated nanocrystals, as unheated nanocrystals have extremely small sizes that are near the detection limit of the electron microscope.

Bulk thin films were formed by drop casting a pyridine solution of CdSe nanoclusters and heating the dried thin film to 350 °C. Such CdSe thin films were used as the active layer in thin film transistors and demonstrated field effect mobilities as high as  $1 \text{ cm}^2\text{V}^{-1}\text{s}^{-1}$  and ON/OFF ratios in excess of  $10^4$  for a gate swing of  $-40$  to  $40 \text{ V}$  (**Figure 12**).<sup>1</sup> In

addition to being the first demonstration of a printed inorganic semiconductor device, to our knowledge, the observed mobilities are the highest reported in a printed semiconductor, although recently melt-processed laminated organic-inorganic hybrid semiconductor TFTs<sup>26</sup> have attained a mobility of  $1.7 \text{ cm}^2\text{V}^{-1}\text{s}^{-1}$  and chemical bath deposition followed by a 400 °C anneal has been used to fabricate solution processed CdSe TFTs<sup>27</sup> with mobilities of  $15 \text{ cm}^2\text{V}^{-1}\text{s}^{-1}$ .

Hysteresis has been reported for CdSe TFTs,<sup>161,188</sup> but the origin of the hysteresis (**Figure 12**) in printed CdSe TFTs is not known. The hysteresis might be related to the decreasing currents found at increasing drain voltages, which might be the result of carrier scattering off of accumulated charges in the semiconductor film or at interfaces, or might be the result of localized heating in the film due to non-uniform current passing through the nanocluster-derived film.

In our initial studies, TFTs were formed by solution casting the printable semiconductor as the active layer in a device otherwise fabricated in a clean room using standard semiconductor processing techniques to fabricate a semiconductor-free TFT structure with a global doped-Si gate electrode, a thermal gate oxide, and Cr/Au source and drain electrodes. Here we describe similar devices in which Au source and drain electrodes with a  $0.8 \mu\text{m}$  channel length were printed using liquid embossing. CdSe TFTs fabricated with embossed electrodes had a field effect mobility of  $0.1 \text{ cm}^2\text{V}^{-1}\text{s}^{-1}$  and an ON/OFF ratio of  $10^3$  (**Figure 13**),<sup>2</sup> both



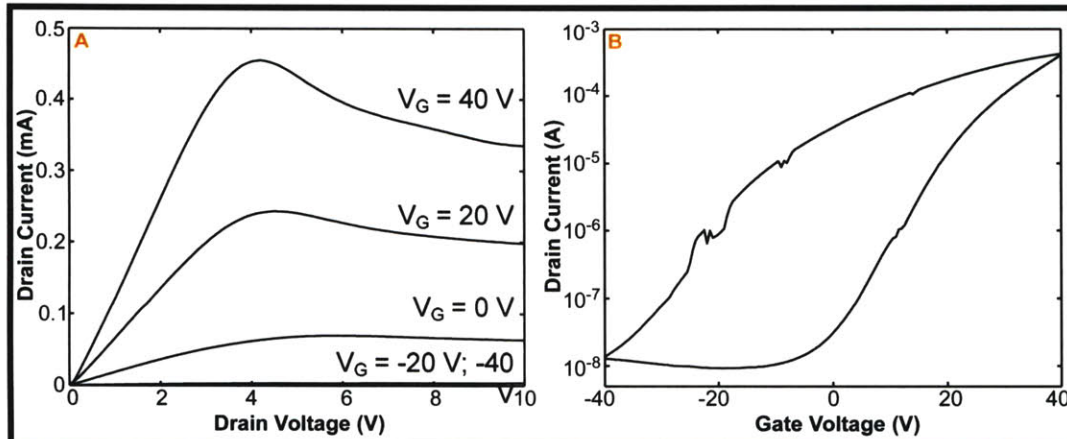


**Figure 12:** Drain current versus drain voltage (A) and drain current versus gate voltage (B) for a TFT fabricated with a CdSe nanocrystal-derived semiconductor channel. A 350 °C anneal was employed to convert the semiconductor particles to the bulk material. The TFT test structure was a coplanar inverted TFT (Figure 10) with a global n+ Si gate electrode, 100 nm dry thermal SiO<sub>2</sub> gate insulator, and Cr/Au (10 nm/100 nm) source and drain contacts deposited by electron beam evaporation. The channel had a length (L) of 8 μm and a width (W) of 293 μm. (A) Drain current versus drain voltage with a gate voltage sweep from -40 V to 40 V in 20 V steps. (B) Logarithm of drain current versus gate voltage indicates an ON/OFF ratio of  $3 \times 10^4$  for a gate sweep of from -40 V to 40 V at a drain-source voltage of 2.5 V. The subthreshold slope is ~7 to 10 V per decade and the hysteresis is clockwise. A linear regime mobility ( $\mu$ ) of  $1 \text{ cm}^2\text{V}^{-1}\text{s}^{-1}$  is extracted by equating the slope of the plot to  $(W/L)\mu C_{\text{ox}}V_{\text{DS}}$  at  $V_{\text{DS}} = 2.5$  V, where  $C_{\text{ox}}$  is the capacitance of the insulating gate oxide. A threshold voltage of 6.7 V is extracted from the  $V_G$  intercept of the  $I_D$ - $V_G$  plot.

within an order of magnitude of the results obtained for devices fabricated with vapor-deposited electrodes.<sup>1</sup> The reduced device performance might be the result of impurities from the printed Au disturbing the metal-semiconductor interface or the semiconductor-insulator interface. The differences might also result from the absence of Cr, which is the metal interfacing the source and drain electrodes and the printed semiconductor channel in the devices with the best mobilities and ON/OFF ratios. Cr is known to enhance the channel conductivity near the contact between the metal and CdSe.<sup>189</sup>

Additionally, all-printed inorganic TFTs were fabricated by using a printed Au layer as a global gate electrode and a layer of spin-on glass as the gate dielectric (Figure 14).<sup>2</sup> The best of these all-printed inorganic TFTs had an ON/OFF ratio of  $10^3$ .<sup>27</sup> Compared with the TFT formed on a thermal oxide, the ON current was two orders of magnitude lower in the all-printed device, indicating that the mobility was two orders of magnitude lower for the all-printed TFT. The poor

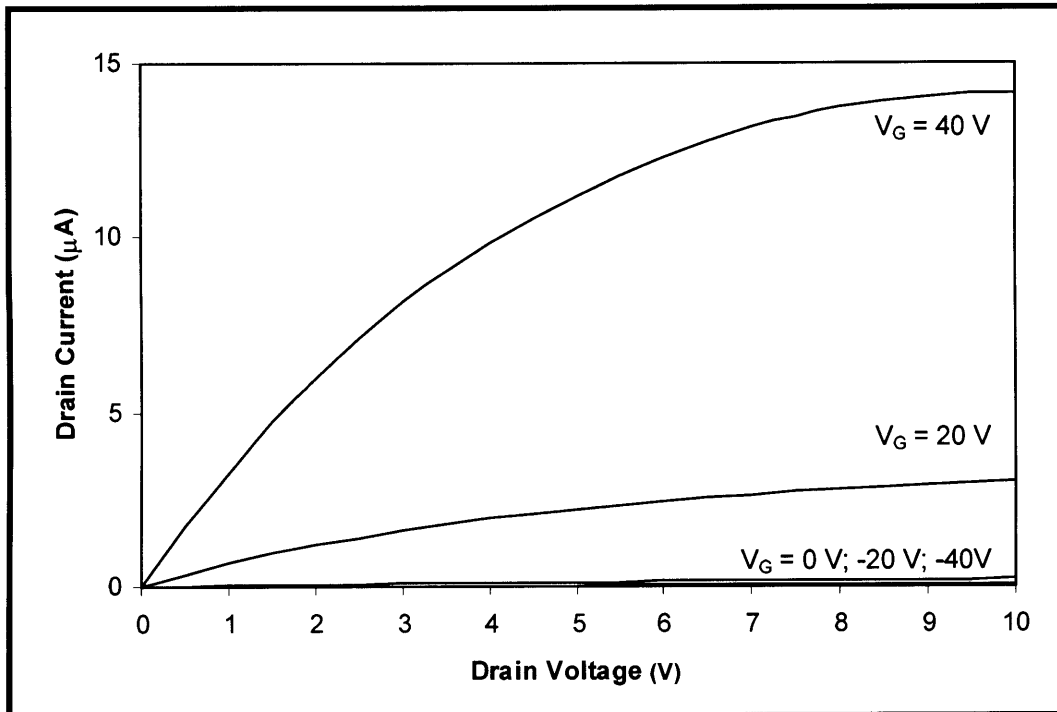


**Figure 13:** Drain current versus drain voltage at varying gate voltages for a TFT fabricated by liquid embossing an Au nanoparticle ink to form the source and drain electrodes and by printing a pyridine solution of CdSe nanocrystals to form the semiconductor channel. A 350 °C anneal was employed to convert the semiconductor particles to the bulk material. An electron mobility of  $0.1 \text{ cm}^2\text{V}^{-1}\text{s}^{-1}$  was observed with an ON/OFF ratio  $>10^3$ , a threshold voltage of 15 V and a subthreshold slope of 17 V/decade.

mobility is likely the result of traps at the interface between the printed insulator and semiconductor. In all-printed organic TFTs, the use of a printed insulator has been observed to have a negative effect on the ON/OFF ratio.<sup>82</sup> The semiconductor-insulator interface has not been directly investigated in our studies and even for the devices fabricated on thermal oxide insulators it is possible that the absence of a surface clean immediately prior to device fabrication leads to sub-optimal device performance.

CdSe semiconductor inks have been printed with liquid embossing, but for simplicity, the half-printed and all-printed devices were fabricated by solution casting the semiconductor. Due to the high volatility of the ink solvent, pyridine, thin liquid films were not formed prior to embossing, but instead the approach of

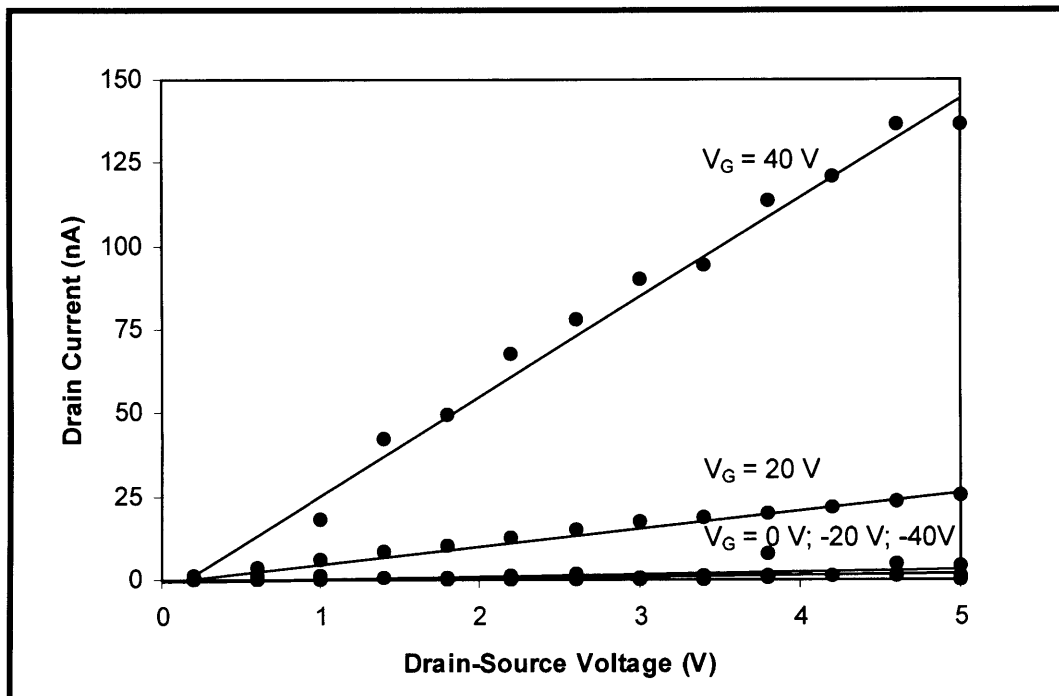


**Figure 14:** Drain current vs. drain voltage at varying gate voltages for an all-printed inorganic TFT. A CdSe nanocrystal solution was used as a precursor for the semiconductor channel and an Au nanoparticle ink was deposited and liquid embossed to form the gate, drain, and source electrodes. A 350 °C anneal was employed to convert the semiconductor particles to the bulk material. A spin-on glass was used as the gate insulator. The electron mobility is poor,  $\sim 10^{-3}$  cm<sup>2</sup>V<sup>-1</sup>s<sup>-1</sup> with a respectable ON/OFF ratio of 10<sup>3</sup>. The untreated, uncleaned semiconductor-insulator interface may be responsible for the low mobility. The lines in the figure are shown to guide the eye.

the elastomeric stamp was used to force the semiconductor ink into a thin film immediately prior to the embossing.

The first batch of CdSe ink produced in our lab was used in the initial TFT fabrication studies repeatedly and consistently over the course of many months. However, subsequent CdSe nanocluster syntheses and ink formulations yielded TFTs with drastically reduced electrical performances. Reagent purity, solvent purity, and reaction work-up conditions were varied in an attempt to reproduce the first ink, but none of the investigated parameters were found to be responsible for the difference in ink quality. After rigorous nanocluster work up and TFT fabrication, it was noticed that the CdSe thin film appeared noticeably thinner than it had in previous fabrication attempts and so thicker films were fabricated

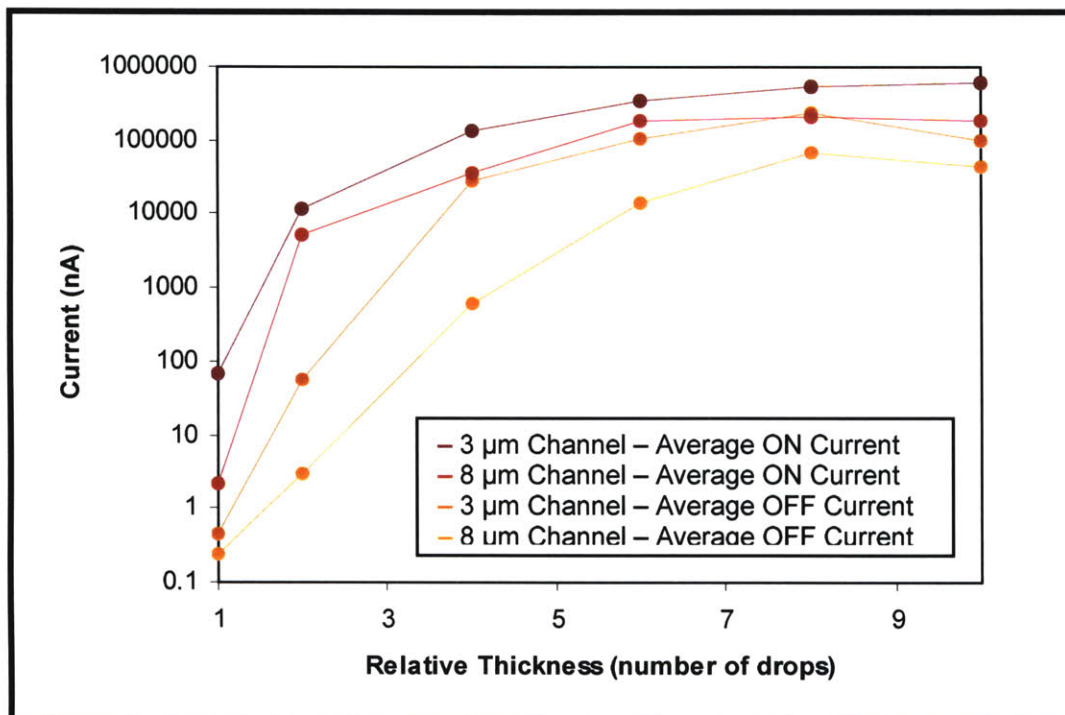


**Figure 15:** Plot of the average ON and OFF currents observed in TFTs with printed CdSe semiconductor channels according to varying semiconductor thickness. A single layer results from a single drop cast onto the surface. Single layers ranged from 12 to 16 nm thick. The highest ON/OFF ratios are found when the semiconductor is 24-32 nm thick.

by multiple depositions. Electrical measurements of these TFTs found the performance to be nonlinearly dependent on the thickness of the semiconductor thin film (**Figure 15**). The thickness of the semiconductor layer had been overlooked as a possible cause of the inconsistency in the printed devices because it had been studied with the first ink batch: with a thickness greater than that produced by a single drop from a micropipette there had only been reduced device performance, raising the OFF current appreciably while having only minimal effect on the ON current. The thickness-dependent data presented here confirms these results, but also indicates that films that are too thin are incapable of high quality device performance. Presumably, the imprecise work up conditions employed yielded inks of reduced concentration compared to the initial work, especially as more aggressive work up conditions were employed in attempt to improve purity, even at the cost of yield. As a result of the reduced ink concentration, the semiconductor films were too thin for optimal performance.

For both 3 and 8  $\mu\text{m}$  channel printed CdSe TFTs, the ON current, which is proportional to the semiconductor mobility, and the OFF current as well, increase exponentially with increasing thickness (**Figure 15**). Below a critical size, this behavior is expected for the ON current, but the OFF current is expected to rise linearly with semiconductor thickness. A difference of  $10^5$  in the OFF current is seen between semiconductor layers differing by only a factor of 5 in their thickness. The non-linearity suggests that dopants accumulate at an interface in the semiconductor channel as the device gets thicker. This is possible if impurities or non-stoichiometric Se or Cd atoms diffuse to or collect at an interface, doping the channel and making it much more conductive with increasing thickness.

X-ray photoelectron spectroscopy (XPS) (**Table 2**) data indicate that excess Se or residual iodine<sup>1</sup> might act as such a dopant, although either might leave as a volatile material or byproduct upon annealing, especially Se which is known to leave as Se and  $\text{SeO}_2$ , as well as possibly  $\text{H}_2\text{Se}$ .<sup>190</sup> I seems to be a likely source of doping, as  $\text{CdI}_2$  has been reported as a flux for promoting low temperature crystallinity and grain growth in Cd II-VI semiconductor thin films, and the “flux represents a source of doping impurities which are easily incorporated in the crystal growth process.”<sup>191</sup> Na is not detected, indicating that the I is not carried through the nanoparticle synthesis work up as the byproduct salt, but is instead associated with the particle itself, perhaps as a surface group capping Cd dangling bonds. XPS also indicates a slight increase in the concentration of I with increased semiconductor thickness, which would be expected if I were accumulating at the surface. Thicker CdSe films should have more I available to concentrate at the surface, doping the channel at the surface to produce a more conductive path between source and drain electrodes, thereby increasing OFF currents.

Thickness	Cd	Se	I
1	1	1.11	0.26
2	1	1.16	0.27
6	1	1.15	0.33

**Table 2:** Ratios of Cd, Se, and I detected by XPS in nanocrystal-derived CdSe thin-films of varying thickness. The thickness measurement represents the number of layers. Each layer is 12-16 nm thick.

Consistent with the accumulation of dopants at an interface are the results of secondary-ion mass spectrometry (SIMS) (**Figure 16**), which find I at the surface and the concentration dropping off at greater depths within the semiconductor channel. Interestingly, C is consistently found at higher concentrations in thinner samples, suggesting that the C impurities are introduced primarily at

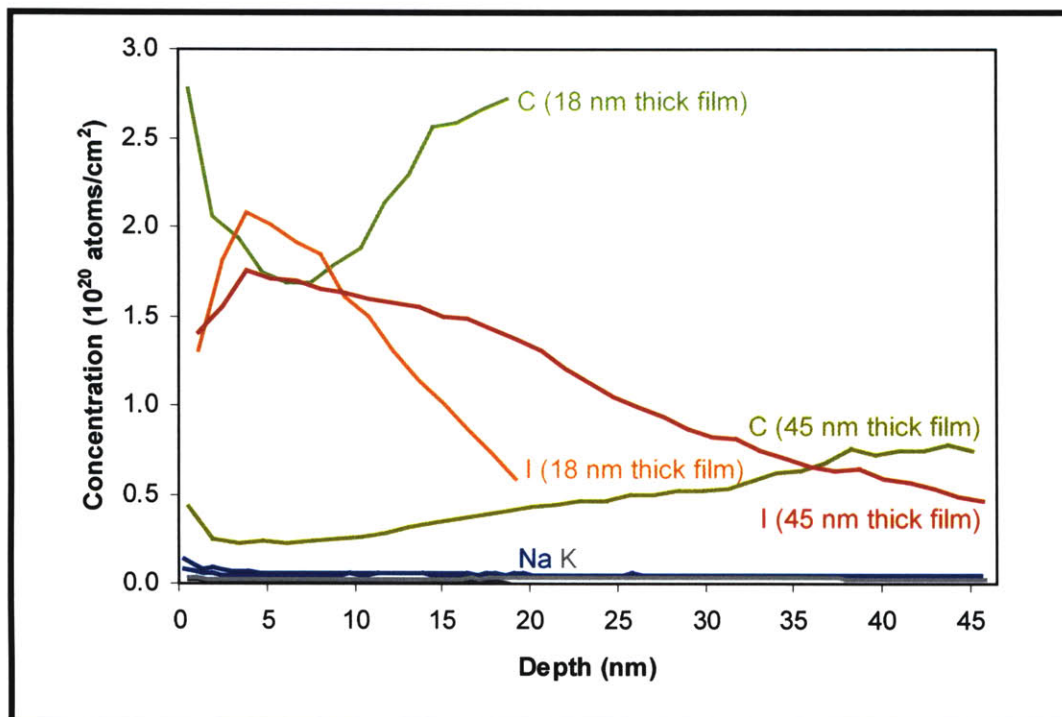


**Figure 16:** SIMS data for I, C, Na and K impurities in CdSe thin films derived from nanocrystals. The nanocrystals were produced by the metathetic reaction between  $\text{CdI}_2$  and  $\text{Na}_2\text{Se}$  in methanol:pyridine (2:1). Although the surface concentration of I is not found to be higher in the thicker sample, I is consistently found in higher concentrations at the surface of the film when compared to the interior. Na levels are more than an order of magnitude lower than those of I, indicating that the I is not carried through the synthetic workup as  $\text{NaI}$ . K levels are 2-5 times lower than those of Na. There was no known source of K in the nanocrystal synthesis or ink formulation.

the surface of the wafer and are not the result of residual organic content from the CdSe ink solvent, pyridine. With thicker films, this C content diffuses throughout the channel, leading to a lower concentration in the film. Na is detected at levels more than an order of magnitude less than I. It is not possible to determine if the Na is from the synthesis or from reaction or ink solvents or reagent impurities. These are the only possible sources of K, and K is detected, although at levels 2-5 times lower than Na. Still, these levels are not drastically different than those observed for Na, suggesting solvent or reagent impurities are possible sources of the Na detected in thin films.

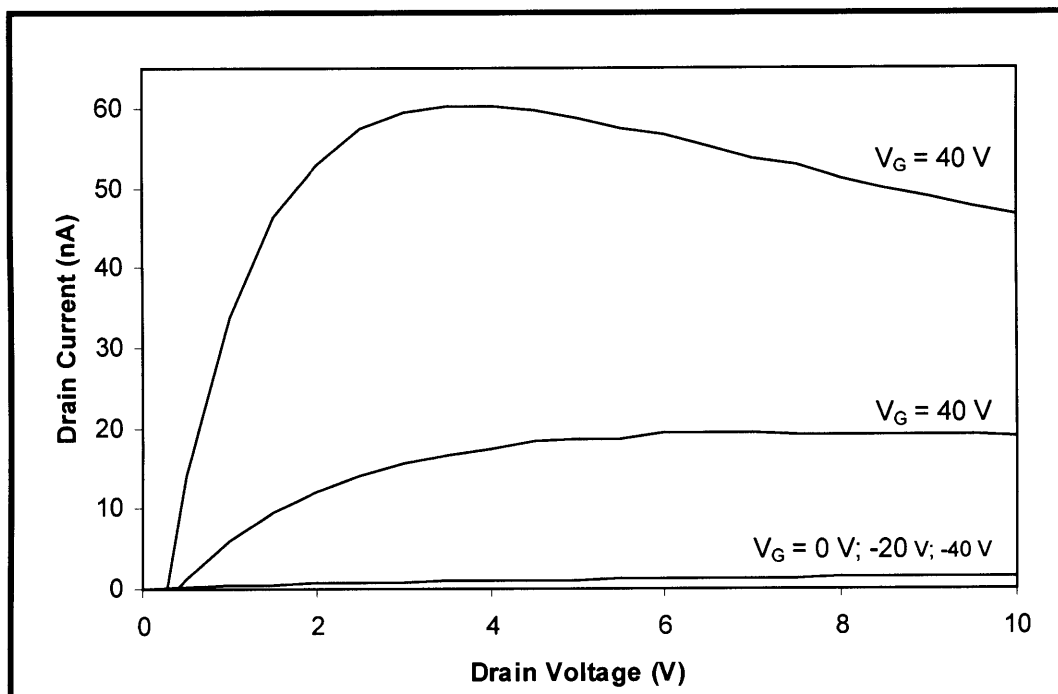


**Figure 17:** Drain current versus drain voltage characteristics of a TFT with a semiconductor channel derived from a suspension of I-free CdSe nanoparticles in pyridine. An ON/OFF ratio of  $1.9 \times 10^3$  is observed for a gate sweep of  $V_{GS} = \pm 40$  V in 20 V steps at  $V_D = 5$  V. The mobility is  $\sim 10^{-4} \text{ cm}^2 \text{ V}^{-1} \text{ s}^{-1}$ , the threshold voltage is 20 V, and the subthreshold slope is 17 V/decade.

In an attempt to determine if I impurities were responsible for the non-linear thickness-dependence of the OFF currents, I-free syntheses were investigated. CdMe<sub>2</sub> and TMS<sub>2</sub>Se had been used successfully in pyrolytic reactions<sup>131</sup> and here were reacted at low temperatures in a variety of solvents including pyridine, 4-ethylpyridine, and a number of straight-chained alkylamines. Although UV-Vis data indicate that the CdSe product is of similar size to the nanoclusters produced from the inorganic metathesis reaction, the product was more heavily agglomerated and thin films from these nanoparticle suspensions were noticeably less smooth than those produced from soluble particles with residual I (**Figure 9**).

TFTs made from inks with nanoparticles produced by the reaction of CdMe<sub>2</sub> and TMS<sub>2</sub>Se were very poor (**Figure 17**), with ON currents 4 orders of magnitude lower than those previously reported.<sup>1</sup> Among these low-quality devices it was found that films produced from pyridine solutions gave the best results. Nanoparticles from reactions in 4-ethylpyridine, for example, although they

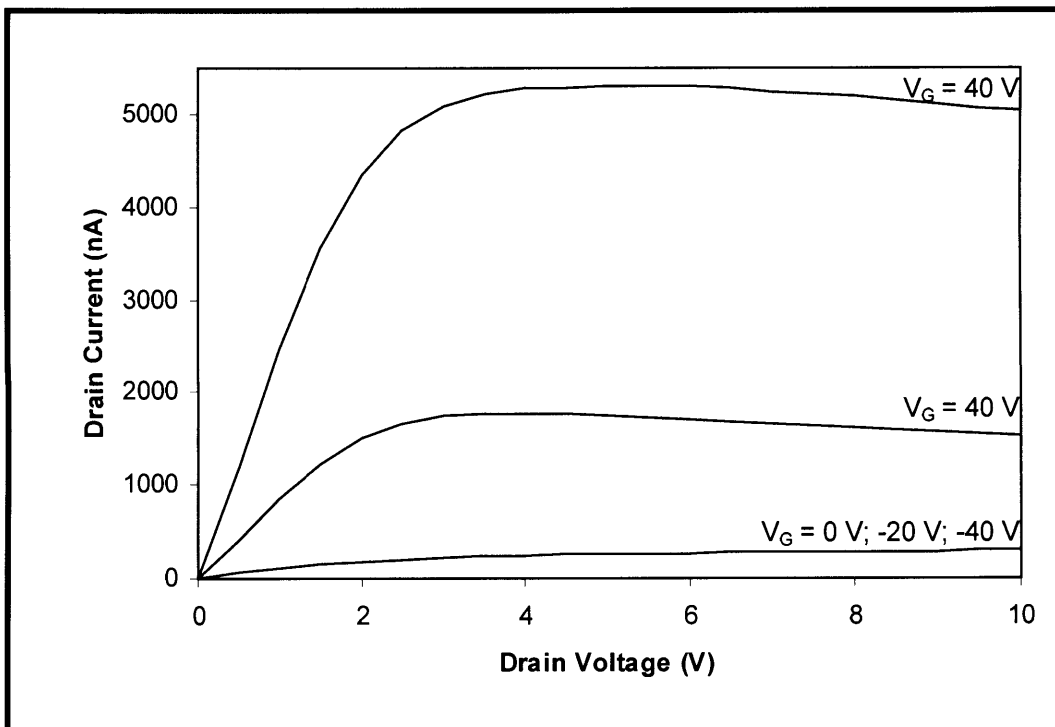


**Figure 18:** Drain current versus drain voltage characteristics of a TFT with a semiconductor channel derived from a pyridine solution of CdSe nanocrystals synthesized from  $\text{CdI}_2$  and  $(\text{TMS})_2\text{Se}$ . An ON/OFF ratio of  $3.9 \times 10^3$  is observed for a gate sweep of  $V_G = -/+ 40$  V in 20 V steps at  $V_D = 5$  V. The mobility is  $\sim 10^{-2} \text{ cm}^2 \text{ V}^{-1} \text{ s}^{-1}$ , the threshold voltage is 8 V, and the subthreshold slope is 9 V/decade.

yielded a comparable product in terms of cluster size and apparent solubility, did not yield any operable TFTs. These poor results could come from morphological defects, seen in films cast from 4-ethylpyridine (**Figure 9**), and water or other chemical impurities associated with the solvent.

The product from a reaction of  $\text{CdI}_2$  and  $\text{TMS}_2\text{Se}$  in pyridine gave reasonably good TFT results (**Figure 18**), with ON currents 5  $\mu\text{A}$  and above, suggesting that I plays a critical role in the fabrication of these printed TFTs. The I may act to increase the ON currents through doping or through improving the thin film morphology. The same nanoparticle product was dissolved in 4-ethylpyridine and the resulting TFTs had only sub-nA ON currents (**Figure 19**). In this case, the presence of I does very little to improve the performance of the TFT, suggesting that the influence of the I is largely masked by poor morphology, residual C, or oxidation from dissolved water resulting from the use of 4-ethylpyridine as the



solvent. Due to the fairly low boiling point of 4-ethylpyridine (168 °C), it seems unlikely that the solvent persists in the thin films. Poor morphology, resulting from the use of the more hydrophobic substituted pyridine, seems a more likely cause of the degradation of the transport properties, as thin films appear peppered with large agglomerates (**Figure 9**). The beneficial role apparently played by I may simply be in enabling the product to dissolve in pyridine and to subsequently produce a film with favorable morphology. Pure CdSe nanoparticles in pyridine precipitate from solution due to the inability of pyridine to provide a sufficiently large repulsive force to screen the interparticle van der Waals interactions.<sup>131</sup> The precipitation of CdSe particles from pyridine is readily seen in the CdMe<sub>2</sub>/TMS<sub>2</sub>Se reactions. Thus, the high solubility of nanoparticles from reactions carried out with CdI<sub>2</sub> suggests that the residual I impurities are located at the particle surface where they can play an important role in solubilizing the nanoparticles. A direct comparison of the printed devices (**Table 3**) indicates that other morphological and chemical effects contribute to the overall landscape of CdSe nanocrystal ink formulation and device fabrication, as well.

Cd Source	Se Source	Reaction Solvent	Ink Solvent	Mobility (cm <sup>2</sup> V <sup>-1</sup> s <sup>-1</sup> )	ON/OFF
CdI <sub>2</sub>	Na <sub>2</sub> Se	Pyridine	Pyridine	1	10 <sup>4</sup>
CdI <sub>2</sub>	TMS <sub>2</sub> Se	Pyridine	Pyridine	10 <sup>-2</sup>	10 <sup>3</sup>
Cd(CH <sub>3</sub> ) <sub>2</sub>	TMS <sub>2</sub> Se	Pyridine	Pyridine	10 <sup>-4</sup>	10 <sup>2</sup>
CdI <sub>2</sub>	TMS <sub>2</sub> Se	Pyridine	4-Ethylpyridine	10 <sup>-6</sup>	10
CdI <sub>2</sub>	TMS <sub>2</sub> Se	4-Ethylpyridine	4-Ethylpyridine	No Field Effect	

**Table 3:** Comparison of mobility and ON/OFF ratio for TFTs fabricated from CdSe inks synthesized with differing Cd and Se sources as well as differing synthesis and ink solvents. For all devices the curing and annealing conditions were the same (350 °C for 30 min in the N<sub>2</sub> atmosphere of a glove box).

### Conclusions from Experiments with CdSe Nanoparticle Inks

The high solubility and low-melting of nanoparticles makes them suitable precursors for the printing of inorganic thin films. CdSe TFTs with active semiconductors derived from nanoparticle inks are found to vary with the thickness of the semiconductor channel and the solvent used as a carrier for the nanoparticles. If impurities in the semiconductor collect at an interface to create a highly doped channel it would explain the observed non-linear thickness-

dependent OFF current. Appropriate impurity candidates are non-stoichiometric Se or residual I impurities, which are observed to collect at the semiconductor surface. I may play another role in the success of TFT, as nanoparticle solutions without any I impurities are not very soluble and film morphology suffers. At the same time, TFTs made from nanoparticles with and without I impurities are found to be sensitive to the solvent used to cast the thin films, with pyridine producing the best results of the solvents studied. Most likely the solvent influences the TFT performance through the semiconductor morphology, an influence that is known in organic semiconductors. Taken together, these results show that impurities, solubility, and the choice of solvent can be interrelated and can heavily influence thin film structure and TFT performance. These should all be simultaneously considered in order to optimize TFT performance for all-printed low-cost large area applications.

## Approaches to Printing Silicon

### Differences in Group IV and II-VI Semiconductors

Although CdSe has excellent properties in thin film transistors,<sup>89,98,160</sup> its widespread application is limited because of problems with complimentary logic due to its low *p*-type semiconductor mobility.<sup>163</sup> Furthermore, concerns with the toxicity of Cd have been a source of controversy for more than 40 years.<sup>89,98,160,161</sup> As a result, CdSe and II-VI semiconductors have not been adopted in many commercial applications. Instead, Si has dominated the existing microelectronics marketplace<sup>40</sup> with its high electron and hole mobilities, abundance, and low cost. Even though the commercial success of the microelectronics industry has been driven by the use of silicon, “a major bottleneck in developing a low-temperature TFT process is the deposition of the silicon film.”<sup>86</sup>

Beyond differences in their adoption in commercial microelectronics, CdSe and Si have a number of chemical differences that suggest that fewer technical hurdles exist for the application of CdSe in printed electronics. Amongst these hurdles are the bulk annealing temperature of the semiconductor, which is considerably lower for CdSe, and of more primary concern, the extent of knowledge regarding nanoparticle synthesis, which for CdSe is the most developed of any semiconductor.<sup>136</sup> In fact, the synthesis of Si nanoparticles is rather poorly understood and developed, and to date researchers have been unable to convincingly demonstrate the production of oxygen-free Si nanoparticles at ~3 nm or less that would be desired for printing Si thin films. Particles have been formed by relatively impractical methods such as pyrolysis<sup>192</sup> and laser ablation,<sup>193</sup> as well as solution phase reduction<sup>164,165,194-196</sup> and electrochemical dissolution of bulk Si.<sup>138,197,198</sup> Reductive methods suffer from the possibility of salt impurities and a “wet-chemical synthesis” of Si “or any other group IVA element” is “unlikely to produce wafer quality Si,” although it “could have many advantages.”<sup>164</sup> In contrast, most etch methods tend to produce particles with large size distributions. To complicate matters further, the exclusion of oxygen during work-up is an issue that faces both methods of particle formation.

“Synthetic methods for II-VI quantum crystallites typically exploit the relative ease with which II-VI materials anneal into crystals—a requirement for further characterization. Ease in crystallization is due to the relatively weak, partially

ionic bonds of these materials, and the use of strongly coordinating solvents which facilitate structural rearrangement. However, in the covalent, strongly bonded diamond lattice Si system, [it is anticipated] that a quite high temperature will be required to anneal an aggregate of  $10^2$ - $10^4$  atoms into the most thermodynamic isomer.”<sup>192</sup> Traditional anneal temperatures of bulk Si are much higher than those for CdSe. However, the expectation that nanometer-sized Si particles will require high temperatures is inconsistent with experimental observations of Si melting as low as 200 °C for small crystalline Si nanoparticles formed by electrochemical dissolution.<sup>37</sup> Of course, a particle is expected to anneal at a temperature lower than its melting point, indicating that for particles in the size regime of interest, high temperature synthetic conditions are not required, though they may still be advantageous.

### **Approaches to Solution Deposited Group IV Semiconductor Thin Films**

Although printed TFTs have been demonstrated using II-VI nanoparticle inks,<sup>1,2,10</sup> the differences in II-VI and group IV semiconductor chemistry urge a re-evaluation of the approach and the options for solution processed Si TFTs. While it is easy to describe the characteristics of an ideal Si precursor for printed microelectronics, it is not simple to identify what material would best provide those characteristics, and it is even less clear how to make that material. Ideally, the material should convert to bulk amorphous or polycrystalline Si at a temperature of 300 °C or lower. The material should be of semiconductor purity, readily processed and printable, and any solvents or surfactants should not leave behind residue when the precursor is converted to the bulk material. In general, there are four options – molecular precursors, oligomeric and polymeric precursors, network polymeric precursors, and nanoparticle precursors.

Molecular precursors offer the simplest purification through routine recrystallization or distillation. At the same time they bring with them the maximum amount of material that needs to be removed as every bond to the Si atom must be cleaved to leave behind clean Si. It is worth mentioning that a molecular precursor such as SiH<sub>4</sub> only has 4 “impurity” atoms to remove per Si atom. Although 4 bonds need to be cleaved, the amount of material that has to be removed is still small. For comparison, a nanoparticle precursor may only have a single bond to cleave for every 2-4 Si atoms, but each of those cleavages might correspond to a number of atoms, perhaps 8 atoms in the case of an octyl group at

the surface. Especially for Si, which has fairly strong bonds to H and C, molecular precursors might not be desirable because of the large number of bonds that must be broken to produce a clean film.

Short linear polymers are somewhat similar to molecular precursors, but they have a reduced number of groups to remove during the conversion to the bulk thin film and can have reduced conversion temperatures due to delocalization.<sup>199</sup> Short hydrogenated polysilanes might act as a convenient bridge between the molecules, polymers and thin films, because they might be purified by distillation or recrystallization, and might have low conversion temperatures (below 300 °C).

Longer hydrogenated linear polymers have not been studied because they are intractable.<sup>200</sup> As such, the majority of polysilane syntheses have not focused on hydrogenated Si polymers, but have instead focused on alkyl-bearing Si polymers.<sup>201,202</sup> These polymers are generally not considered as precursors for Si deposition because they readily “extrude stable di(organo)silylene fragments”<sup>203</sup> due to their 1:2 Si:alkyl-aryl ratio. Their facile decomposition has led to these polymers being considered as e-beam resists.<sup>202,204</sup>

Network polymers, or polysilynes,<sup>203-208</sup> have a 1:1 Si:alkyl-aryl ratio and do not decompose into volatile Si-fragments.<sup>203</sup> The polymers are heavily branched, sheet polymers with a two-dimensional structure. Again, a hydrogenated polymer would be intractable and is not an option, but soluble alkyl and aryl polysilynes have been made.<sup>203-208</sup> They are generally produced by the Kipping<sup>203-209</sup> reaction of trichloro-organosilanes with sodium metal in hot toluene.<sup>204,206-208</sup>



These reactions, like those used to make poly(alkylsilanes), are plagued with impurities.<sup>203</sup> Removal of the salt byproduct is difficult, most likely more difficult than with nanoparticle products because the linear or branched polymer is flexible and can wrap around impurities or can create a pocket in which impurities can reside through the washing sequences that are a part of the product work up. Similarly, the polymer chain itself has regions that become inaccessible to the reagents, carrying Cl through the workup or leading to oxidation at sites where unreacted Cl remained. During heat treatment the polymers may also trap impurities or volatile groups trying to escape, while a nanoparticle might provide a more direct route for mass transfer out of the film.

Transitioning from a two-dimensional sheet polymer to a three-dimensional network, researchers have reported on Si and Ge clusters<sup>194,210-216</sup> and their role as precursors to solution deposited group IV films. Ideally, the three-dimensionality of nanocrystals offers pre-existing nucleation sites and crystallinity, and the thin film derived from the precursor is anticipated to be nanocrystalline. The electronic delocalization throughout the particle should lead to a minimal cleavage temperature for surface groups and the particles should be easier to purify as any impurities should present themselves at the surface of the particle. Additionally, nanoparticles offer minimal geometric constraints with regard to the retention of impurities and favorable ratios of Si to surface groups. In general nanoparticles also offer the possibility to use non-covalently bound surface groups to stabilize nanoparticle inks.

The numerous advantages of nanoparticles make them the most attractive choice as a solution processable precursor to Si thin films, but hydrogenated oligomeric species also have some promise, as they may be readily purified, have low conversion temperatures, possess hydrogen as a relatively innocuous surface group, and can remain processable if small enough. Larger polymers, whether linear or branched, have been largely disappointing. They can become intractable without appropriate side chains and most importantly are plagued with a number of impurities.

### **Surface Termination of Printable Group IV Materials**

The question of surface termination is relevant for all of these methods of printing group IV semiconductors. While “surface” termination is most obviously an issue of concern for nanoparticles, polymeric species have similar side chains or groups that bind to the polymer backbone and even molecular species have groups that sit at the periphery of the molecular skeleton. In general, H-passivation is preferred to alkyl or C-passivation<sup>166</sup> because of the small size, ideal electrical passivating characteristics of hydrogen, and limited options for undesirable and uncontrollable side reactions. Although a H-passivated Si surface is not highly resistant to oxidation, the surface is much more stable than an exposed, unpassivated Si surface and the Si-H bonds on crystalline surfaces are not observed to cleave appreciably below 400 °C.<sup>217</sup> Perhaps more important than the positive characteristics of H-passivation are the negative aspects of C passivation,

primarily the persistence of the Si-C bond and the inability to entirely remove alkyl surface layers by purely thermal means.<sup>217,218</sup> The difficulty of cleaving Si-C bonds has been observed on crystalline Si surfaces<sup>217,218</sup> as well as in Si polymers.<sup>208</sup> Additionally, alkyl termination of Si nanoparticles is unable to passivate all of the Si sites due to steric constraints,<sup>217,218</sup> meaning there must always be a secondary capping group, although there has been an isolated report of a complete alkylation of Si nanoparticles.<sup>219</sup> Si-C or alkyl passivation does offer some advantages, though, most notably an expected increase in solubility and a resistance to oxidation.<sup>218</sup>

### **Molecular Precursors and Oligosilanes**

Recently, researchers at Showa Denko K.K. in Japan have described a production-scale apparatus for producing “higher silanes” – Si<sub>3</sub>H<sub>8</sub>, Si<sub>4</sub>H<sub>10</sub>, Si<sub>5</sub>H<sub>12</sub>, Si<sub>6</sub>H<sub>14</sub>, Si<sub>7</sub>H<sub>16</sub>, Si<sub>8</sub>H<sub>18</sub>, and Si<sub>9</sub>H<sub>20</sub>.<sup>199</sup> The yield of higher silanes is in excess of 75% and the production rate exceeds 0.5 kg/min. The continuous zone reactor they describe relies on the reaction of the monosilane, SiH<sub>4</sub>, with itself via disproportionation to form disilane, Si<sub>2</sub>H<sub>6</sub>, and the subsequent reaction of disilane and monosilane to form trisilane and so forth to produce other higher silanes. The silane feed is first diluted to between 20 and 60% in an inert gas and fed into the first reaction zone at a moderately high pressure of 0.9 MPa. The residence time in the first reaction zone is brief (10 s) because the first reaction zone’s temperature is the highest of the zones, generally 400-500 °C – hot enough to react the silane but not so hot that the reaction is uncontrolled and Si is deposited. Subsequent zones are not as hot because they are designed to react with and grow higher silanes, which does not require the high temperatures required to react the monosilane. The higher silane products from the first reaction zone are condensed by cooling and then introduced to the second reaction zone at 375 °C for 20 s. The products from the second zone are then condensed by cooling and separated by distillation – 40% Si<sub>3</sub>H<sub>8</sub>, 30% Si<sub>4</sub>H<sub>10</sub>, 16% Si<sub>5</sub>H<sub>12</sub>, 8% Si<sub>6</sub>H<sub>14</sub>, 4% Si<sub>7</sub>H<sub>16</sub>, 2% Si<sub>8</sub>H<sub>18</sub>, and <1% Si<sub>9</sub>H<sub>20</sub>. The volatile products (mono and disilane) from both the first and second zones are recycled back into the first zone for reaction.<sup>199</sup>

The simplicity, high yield and high production rate of the zone reactor suggest that this technique is ideal for industrial-scale production of higher silanes. Although the yields of silanes larger than tetrasilane are not large, a third zone could be introduced to increase the yield of the larger silanes. As described, the

zone reactor is only suited for the production of higher silanes that are liquid at ambient pressures. Above a certain size (heptasilane), some isomers of the higher silanes are expected to be solids and cannot be handled by the zone reactor operating in continuous fashion.

These solid higher silanes might be the most desirable for printed microelectronics applications. Higher silanes decompose at lower temperatures, and some solid higher silanes have been found to slowly lose H<sub>2</sub> at room temperature.<sup>220</sup> Of the higher silanes the smaller silanes, especially trisilane, have been used in the fabrication of Si thin films through chemical vapor deposition,<sup>221,222</sup> photochemical deposition,<sup>223,224</sup> and direct-writing with lasers,<sup>225</sup> all techniques dependent on the trisilane vapor and not the trisilane liquid. For printed microelectronics, there is some concern with the low boiling points of low molecular weight liquid silanes, such as trisilane and tetrasilane (bp <110 °C), which are well below their decomposition temperatures.<sup>226,227</sup> Practically, this means that very little Si deposition can be expected from a simple liquid-based deposition or printing process. Without a highly pressurized environment, the silane will simply evaporate before decomposing. For printed microelectronics applications, the ideal silane precursor would be a liquid under ambient conditions and would decompose before evaporating. Unless spray deposition is to be used, the requirement that the silane decompose before evaporating is critical. Solid silanes have demonstrated that decomposition can occur before evaporation, but it is not clear that this can occur in a liquid silane. Solid higher silanes may be required, which would complicate the patterning process because the higher silanes may not be soluble and therefore would have to be melt processed. However, these silanes might decompose upon melting. Thus, there very well may be an uneasy crossover point in these materials as they shift from liquids to solids and from precursors that decompose in the gas phase to those that decompose in the liquid phase.

The zone reaction scheme<sup>199</sup> is well-suited to industrial production of low molecular weight liquid silanes, and it may be possible to extend the reaction scheme to the production of solid silanes if the reactor is modified to carry out late-stage reactions sequentially and not continuously. Still, the method of production requires considerable infrastructure and is inappropriate for a small research laboratory environment. Furthermore, it is somewhat lacking in chemical elegance as it does not offer a route to specific isomeric silanes or to specific sizes

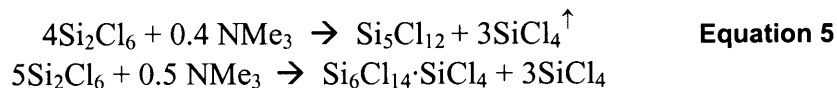


of silanes except through repeated purification and re-reaction of the smaller byproducts.

Synthesis of the corresponding chlorosilanes can be more straightforward, though, and can be carried out in a standard research laboratory.<sup>220</sup> Chlorosilanes can be converted to the corresponding silanes with high yield by reacting the chlorosilane with LiAlH<sub>4</sub> in ethers (**Equation 4**).<sup>209,226</sup>

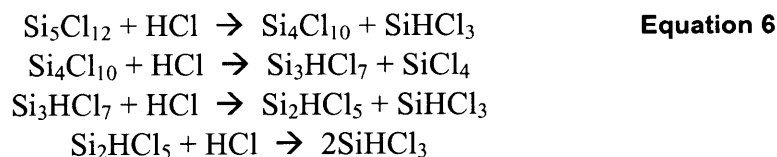


Synthesis of higher chlorosilanes can be carried out using hexachlorodisilane as a precursor. With 0.1% trimethylamine higher chlorosilanes can form (**Equation 5**).<sup>220</sup> If conditions are employed such that the byproduct tetrachlorosilane (SiCl<sub>4</sub>) is removed during the reaction, dodecachloropentasilane (Si<sub>5</sub>Cl<sub>12</sub>) is produced. If the byproduct SiCl<sub>4</sub> is not removed during the reaction, it complexes to the product, tetradecachlorohexasilane (Si<sub>6</sub>Cl<sub>14</sub>).



In both reactions the product precipitates. The Si<sub>6</sub>Cl<sub>14</sub> is readily freed from the SiCl<sub>4</sub> complexed to it by treating it *in vacuo* at room temperature. Both crystalline products can be purified by sublimation.

On treatment with hydrochloric acid, the higher chlorosilanes decompose to form lesser silanes (**Equation 6**).<sup>220</sup>



Although the products have not been individually isolated, it should be possible to do so, and the hydrogenated forms of the chlorosilanes should also be able to be isolated. However, for printed microelectronics it is probably undesirable to induce decomposition to lesser silanes, as the higher silanes are anticipated to be better Si precursors.

A promising alternative to the use of linear oligomeric hydrogenated silanes is the use of hydrogenated cyclosilanes. In the patent literature, the same researchers at Showa Denko K.K. that describe the continuous flow reactor for the production of linear silanes describe the use of cyclic hydrogenated silanes as precursors for the production of Si thin films.<sup>227</sup> A wide range of cyclosilanes have been described in the patent literature<sup>166,228,229</sup> by researchers at Japanese Synthetic Rubber with the expressed purpose of using them as liquid-phase precursors for printed microelectronics.<sup>166,229-231</sup> In general, these materials would be expected to face the same limitations of the linear oligosilanes, balancing the reduced decomposition temperature, reduced solubility and increased boiling point with increasing molecular weight, although there may be some favorable reduction in conversion temperature due to ring strain or some favorable increase in boiling point due to the cyclic structure. However, some cyclosilanes are reported which undergo ring opening metathesis polymerization (ROMP) at low temperatures,<sup>166</sup> presumably below their boiling point, which leads to the *in situ* production of high molecular weight hydrogenated linear polysilanes in thin films of the precursor. The polymerization creates a continuous thin film and the polymerized material subsequently decomposes to yield amorphous Si. Temperatures as low as 300 °C are reported, but 400-500 °C is preferred.<sup>166</sup> Although there are patents that relate to the fabrication of electrical devices using these precursors, electrical device data are not presented.<sup>229-232</sup>

## Polysilanes and Network Polysilanes

Cyclosilanes are generally produced by a alkali metal reduction of a substituted organohalosilane.<sup>166,228,229,233</sup> Similar reducing chemistry is used for the production of higher molecular weight polymers and network polymers,<sup>200-203,205-208</sup> and even for producing crystalline nanoparticles.<sup>164,165,195,196,234-236</sup> The extent of polymerization and cross-linking is controlled through the specific reaction conditions and the choice of the silane or substituted silane precursor.

In 1997, researchers at Tohoku University in Japan published a paper on the synthesis of Si “nanoclusters”.<sup>194</sup> The group was following the natural progression of their work with Si polymers from 1 to 2 dimensions and finally to 3 dimensions.<sup>237</sup> The group had been synthesizing polysilynes, which are network polysilanes.<sup>204,207,208,238</sup> Within their work they were investigating a number of “organometallic polymer[s] with a Si-Si main chain and an organic side chain.”<sup>207</sup>

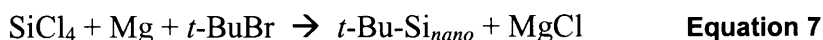
Such polysilanes have been studied as novel electronic materials, and the related network polymers, polysilynes, have been studied for their use as UV-sensitive photoresists.<sup>202,203,205</sup> Additionally, polyalkylsilanes have been used as precursors to SiC fibers via conversion to a polycarbosilane intermediate.<sup>204,206</sup>

The researchers at Tohoku were initially interested in using polysilynes as single step precursors to SiC thin films.<sup>204</sup> Due to their 1:2 Si:alkyl or aryl ratios, polysilanes “extrude stable di[organo]silylene fragments” and so the polymers readily form volatile fragments and decompose on heating. Polysilynes have a 1:1 Si:alkyl or aryl ratio, and therefore will not decompose into volatile byproducts upon heating. The Tohoku researchers found that when poly(phenylsilyne) is heated above 600 °C, a SiC film is formed.<sup>204</sup> They also realized that they could exploit the UV sensitivity of the polymer and produce patterned thin SiC films by exposing the precursor film to UV radiation through a mask.<sup>204</sup> If the film is exposed in air, the polymer backbone is photooxidized and upon heating to 300 °C *in vacuo* the oxidized polymer forms a SiO<sub>2</sub> film.<sup>204,210</sup>

In addition to SiC and SiO<sub>2</sub> films, the researchers found that poly(alkylsilyne) precursors yield  $\alpha$ -Si films upon heating above 300 °C.<sup>207,208</sup> Of the few precursors they examined, the best was poly(*n*-propylsilyne).<sup>208</sup> The remaining Si-Cl bonds of the polymer were reacted with butyl groups to prevent Cl impurities. At 300 °C there was evidence of  $\alpha$ -Si formation, but it was not until 400 °C that the propyl group completely left.<sup>208</sup> The choice of butyl groups to tie up the remaining reactive Cl sites is confusing, as they noted that the isobutyl groups of poly(butylsilyne) are only partially removed at 400 °C. A heat treatment at 500 °C for one hour *in vacuo* yields silver solid with no detectable C at the surface. However, upon etching, 9% of the Si atoms are reported to be bound to C. It is unclear if this C remains from the butyl groups or from propyl groups trapped by the Si network.<sup>208</sup> No morphological or electrical characterization was made.

Although the Tohoku researchers not reported the use of their polymer-derived films in devices, it was a goal<sup>206</sup> of their work to form a “soluble organic polysilane... precursor [that] makes it possible to form a large-area semiconducting film.”<sup>207</sup> The “nanocluster” synthesis that they subsequently developed was designed with such applications in mind, despite the group’s apparent lack of interest in the size-dependent melting of the particles. “The organosilicon nanocluster is expected to be used as a new precursor for semiconductor and inorganic materials, such as  $\alpha$ -Si and SiO<sub>2</sub>, because of its

solubility in common organic solvents and its processibility.”<sup>194</sup> The procedure developed at Tohoku University is very similar to what researchers at IBM had published 5 years earlier,<sup>164</sup> but the reduction is mild, there is no crystallization step, and only one Si reagent used.



The reaction is carried out in THF, which had been found to be necessary for complete reduction of the Si-Cl bonds,<sup>203</sup> something that the IBM preparation had overlooked. After sonicating at 0 °C, the particles are insoluble and Cl capped. By treating the insoluble brown substance with *t*-BuBr at 50 °C, via a Grignard intermediate the butyl group reacts with the chlorinated Si surface to cap the cluster with the bulky alkyl group.<sup>194</sup>

The choice of a sterically hindered capping group is strange, because it will not pack tightly on the particle surface, leaving some unreacted Si-Cl bonds that will react with MeOH during the synthetic workup. Methoxy groups are problematic because they will activate the Si atom they are bound to and encourage further reaction and oxidation of the Si.<sup>209</sup> Unless the particles continue to grow without a bulky capping group, a smaller capping group might better serve the particle by reducing the population of OMe groups. The *t*-Bu group used by researchers at Tohoku gave a ratio of Si:Bu:O of 1:0.30:0.07. Although some of the oxygen may come from adventitious oxidation, they attribute all of the oxygen to OMe groups, correlating their elemental analysis with <sup>1</sup>H-NMR data.<sup>194</sup> Analogous Ge nanomaterials are reported to have a much larger amount of organic substituent, as the smaller *i*-Pr group is used and the Ge:propyl ratio is 1:1.45.<sup>214</sup> When the Si “nanoclusters” are used as precursors to Si films, propyl groups are used for surface treatment and the Si:propyl ratios are not reported.<sup>211,216</sup> When the Si “nanoclusters” are used as precursors to SiO<sub>2</sub> the *t*-butyl termination is used,<sup>210</sup> which might be beneficial in that the bulky butyl-termination covers less of the surface and more Si-Cl or Si-O surface species are carried through to the product and can participate in film formation.

Size selective precipitation can narrow the size distribution of the particles by using THF as the solvent and MeOH or H<sub>2</sub>O as a precipitant.<sup>194</sup> Although they report no TEM or XRD data to confirm the particle size, size exclusion chromatography found the particles to be 1-2 nm in diameter.<sup>194</sup> For vapor-phase nanoparticle reactions to form oxide-coated Si nanoparticles, TEM and

chromatography data have been shown to be well-correlated.<sup>192</sup> The optical band gap values reported by the Tohoku researchers are higher than those previously reported, which is consistent with their smaller particle sizes.<sup>194</sup> Still, questions about the true nature of the “cluster” precursors remain, as the researchers’ claims are not backed by TEM or XRD data and the network polymer poly(*n*-propylsilylene) has a band gap of 2.9 eV,<sup>207</sup> which compares favorably to the 2.8 eV reported for the smallest “nanoclusters”.<sup>194</sup> Additionally, the reported ratios of semiconductor to surface group range from numbers that are consistent with a cluster product for bulky surface groups<sup>194</sup> to values that are consistent with a network polymer for less sterically bulky surface groups.<sup>211,214,216</sup> Since these two products come from the same type of reaction and the surface group is merely a reflection of the unmodified surface area, these results suggest that there is too much surface area in these materials for them to be clusters and that they are instead network polymers. NMR results suggest a cluster product,<sup>238</sup> but in either case, cluster or network, the retention of impurities and subsequent Si-O bond formation during workup indicates that the product has a number of inaccessible sites, resulting in films of compromised quality. For example, Ge films derived from such Ge clusters are found to undergo a huge swing in conductivity ( $>10^8$ ) when heated to 1000 °C instead of 400 °C, as C impurities are driven out of the Ge at the higher temperatures.<sup>214</sup>

Researchers developing network polysilanes for photoresist applications published a number of practical methods for improving the quality of the synthetic product.<sup>203,205</sup> They found that washing the product with water is ineffective for removing inorganic salt byproducts. Dissolution in THF, followed by sequential precipitation with water, methanol, and ethanol works much better, as demonstrated by 2 precipitations reducing the salt content from 1% to 0.1%. Also, they found that incomplete reduction leads to excess Cl content in the polymer, and that a polar solvent like THF is necessary to ensure the complete reduction of the Si reagent.<sup>203</sup> The group at Tohoku university was aware of the synthetic methods developed for polysilanes, and included these approaches in their work. However, these synthetic methods apparently have not been known to a number of other research efforts to produce group IV nanomaterials and a number of improvements might be had by combining knowledge from the areas of polysilane and nanoparticle synthesis.

## Approaches to Silicon Nanocrystal Synthesis

### Solution Phase Group IV Synthesis

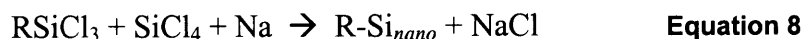
A number of routes have been published for the solution-phase synthesis of Si and Ge nanoparticles.<sup>164,165,195,196,234-236,239-253</sup> Although the most common approach relies on reductive chemistry similar to that employed in the synthesis of polysilanes, metathesis,<sup>242-248</sup> decomposition,<sup>239-241,250</sup> and recently oxidation<sup>249</sup> routes have also been reported. Unlike molecular and polymeric precursors to Si, which have been reported to make bulk thin films (even if electrical characterization has not been reported), there has not been a clear demonstration of Si nanoparticles as low temperature precursors to bulk thin films and the only reports of solution-based production of semiconductor thin films from nanoparticle precursors have been reported for II-VI materials.<sup>1-5,10,145,146,148-150</sup> However, *n*-butyl capped Si nanoparticles have been observed to fuse when heated in solution, first fusing selectively along the (111) crystal facets, forming dimers and then ribbons, and then undergoing lateral fusion at higher temperatures to form single crystal Si plates and larger sheets.<sup>254</sup> Although the fusion of these particles in solution might result from defects in the butyl-passivation of the surfaces<sup>254</sup> or might rely upon solvent-dependent mechanisms that are not available in nanoparticle thin films, the observation of grain growth and particle fusion offers hope for low temperature grain growth and suggests that group IV nanoparticles might make suitable low-temperature semiconductor inks.

### Solution Phase Group IV Synthesis: High Pressure Reduction

The first bench chemical preparation of Si nanoparticles was reported in 1992.<sup>164</sup> At the time, researchers at IBM were trying to develop the first syntheses of Si and Ge nanoparticles. Most of their work focused on Ge because it has a lower melting point, thus requiring a lower reaction temperature to anneal or crystallize the semiconductor dot.<sup>235,236,255</sup>

As with the pioneering work done on the preparation of CdSe, the syntheses of Si and Ge nanoparticles were designed to separate the nucleation and growth events.<sup>164,235</sup> Nucleation proceeds by reducing the reagents SiCl<sub>4</sub> and RSiCl<sub>3</sub> with Na or a Na/K alloy in a nonpolar solvent. The reaction mixture is then transferred

to a bomb and crystallized by heating the particles above 300 °C at 100 atm for a few days (**Equation 8**).



Theoretically, the ratio of surface Si atoms to interior Si atoms will be controlled by the initial ratio of  $\text{RSiCl}_3$  to  $\text{SiCl}_4$ .<sup>164</sup> This is demonstrated in the synthesis of MeSi-capped Ge nanoparticles. A Ge core is formed from the reduction of  $\text{GeCl}_4$ , while  $\text{MeSiCl}_3$  in the reaction pot proceeds to form an alkyl-terminated Si overcoat.<sup>236</sup> There is no evidence of alloying in such particles, indicating that the group IV element with the R group does indeed passivate the surface.

Although the ratio of  $\text{RSiCl}_3$  to  $\text{SiCl}_4$  influences particle size,<sup>164</sup> the size distribution of particles produced by this method does not approach those reported around the same time for II-VI nanoparticles.<sup>131</sup> For R = octyl, Si nanoparticles are reported to average  $5.5 \text{ nm} \pm 2.5 \text{ nm}$ .<sup>164</sup> Such a large distribution of particles and such a relatively large size prohibits this synthesis from being appropriate for the desired application. When R = H, the high crystallization temperatures prevent the H from being an effective passivant, and the particles grow to sizes up to  $3 \text{ }\mu\text{m}$ .<sup>164</sup> Interestingly, for R groups larger than Me,  $\beta$ -hydride elimination occurs and although the alkyl group controls particle size, the particles are found to be primarily H-passivated.<sup>164</sup> Similarly, in the synthesis of Ge nanoparticles, R = phenyl is observed to eliminate from the surface of the particle at the elevated growth temperature, 270 °C.<sup>235</sup>

Altering the growth conditions or the initial ratio of  $\text{RSiCl}_3$  to  $\text{SiCl}_4$  might improve the size control, but the synthesis has other drawbacks. In addition to the nanoparticles, the Si synthesis yields a large amount of amorphous material,<sup>164</sup> although no amorphous material is observed for the Ge synthesis.<sup>235</sup> This is attributed to Ge's lower melting and annealing temperatures. Most notably, though, ~1% of the byproduct NaCl is found to be present in the product.<sup>164</sup> Although the original Si synthesis did not take into account synthetic methods shown to reduce salt content,<sup>203</sup> it is clear that the authors became aware of this work after their initial publication. Subsequent published Ge synthetic papers<sup>235,236</sup> did utilize some of these established methods, but still found residual Cl in the nanoparticle product.

## Solution Phase Group IV Synthesis: Decomposition in Supercritical Fluids

The vast majority of reported wet chemical syntheses of group IV nanoparticles use a group IV halide as the nanoparticle precursor.<sup>164,165,194-196,214,234-236,251,255</sup> In part this is due to the low cost and ready availability of SiCl<sub>4</sub>, but this is also in part due to the considerable thermal stability of the Si-C bond. Organometallic precursors have been used in a number of nanoparticle syntheses, both in the prototypical semiconductor synthesis, CdSe,<sup>131</sup> and in the synthesis of Si's neighbor on the periodic table, Al.<sup>256</sup> However, the Si-C bond is not removed until ~350 °C,<sup>164,217</sup> well above the boiling point of most organic solvents, thus preventing the use of standard bench chemistry techniques unless the organosilane is decomposed photochemically.<sup>250</sup> In order to access high decomposition temperatures, researchers have turned to decomposition in supercritical fluids.<sup>239-241,257</sup> Using this technique, nanoparticles of metals such as Ag<sup>258</sup> and Cu<sup>259</sup> have been synthesized, as well as the group IV semiconductors Si and Ge.<sup>239-241,257</sup>

In the synthesis of 1.5-4 nm Si nanoparticles,<sup>239,240</sup> supercritical octanol is used as the solvent and is diluted with hexane to form particles with larger diameters. The reaction is carried out at 500 °C and 345 bar, well above the supercritical point for either of the solvents. Diphenylsilane is injected into the supercritical solvent and decomposed at the high temperature, yielding a Si radical that acts as the initiation of nanoparticle growth. If pure hexane is used as the solvent, or if a non-sterically inhibiting alcohol like ethanol is used as the solvent, then particle growth is uncontrolled and large particles precipitate from the reaction. However, if Au nanoparticles are introduced into the reaction, they serve as nucleation sites for the growth of Si (or Ge) nanowires.<sup>241,257</sup>

The size control of the supercritical synthesis is good, and the smallest nanoparticles that are produced are smaller than those of any of the other wet chemical syntheses.<sup>239,240</sup> For luminescence applications the synthesis is ideal, as the quantum efficiencies are high (23%).<sup>239,240</sup> Initially, the synthesis was low yielding (<5%) and throughput was a problem. However, recent advances have enabled the daily production of gram quantities of Si nanoparticles and for nanowire synthesis the yields approach 100%.<sup>260</sup>

The major disadvantage of the synthesis is the surface passivation. For nanowire synthesis, in which a non-coordinating solvent is used, oxide-terminated nanowires are produced. For nanoparticle synthesis, octanol is used and the



particles are alkoxy-capped, making their surface termination inappropriate for printed microelectronics applications.<sup>239-241</sup>

### **Solution Phase Group IV Synthesis: Reduction in Coordinating Solvents**

Two recent reports have described the synthesis of Si nanoparticles<sup>196</sup> and nanotetrahedra<sup>195</sup> by the solution-phase reduction of SiCl<sub>4</sub> in glyme. The reported reaction conditions for the synthesis of nanoparticles ranging from 2-10 nm and for the formation of 40-130 nm nanotetrahedra are the same. To date, the researchers do not understand how to control the reaction to produce particles or tetrahedra, as the reaction can yield both products.

The reaction was designed to produce Si nanoparticles. Conceptually, the particle size is controlled by the ratio of the reducing agent to the Si source, and the sub-stoichiometric amount of the reducing agent yields a Cl-passivated surface (**Equation 9**).<sup>195,196</sup>



The residual Si-Cl bonds at the surface of the particle or tetrahedra are then further reacted with an alkylating agent<sup>195</sup> or octanol<sup>196</sup> to cap the surface.

The first reactions described in the literature use sodium naphthalenide as the reducing agent.<sup>195,196</sup> More recently, magnesium anthracenide has been used,<sup>261</sup> and early results indicate improved size control relative to the 5.2 +/- 1.9 nm seen in the sodium naphthalenide reductions. The conceptual means of size control and the use of non-hydride reducing agents have given only alkyl and alkoxy terminated products, which are anticipated to be undesirable or inappropriate for printed microelectronics applications.

Compared to syntheses that rely on metathesis<sup>242,244-247</sup> and reduction in inverse micelles<sup>165,234</sup> to form group IV nanoparticles, these reductions promise improved yields and/or improved throughput. Although it may be possible to introduce more favorable surface termination, to date, attempts at H-termination have failed.<sup>261</sup>

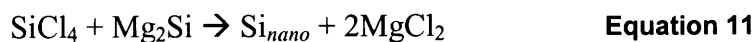
For printed microelectronics, surface termination is an area of concern with this route, especially considering the apparent oxidation of tetrahedral surfaces.<sup>195</sup> These reductive routes are still in the early phases of development and understanding is limited, as evidenced by the uncontrolled production of both nanoparticles and nanotetrahedra.<sup>195,196</sup> However, understanding the synthetic origins of such relatively large tetrahedral structures might come soon, as similar nanotetrahedra have also been observed<sup>262</sup> in oxidative syntheses carried out at similar concentrations in glyme (**Equation 10**).<sup>249</sup>



Research into these oxidative routes have just been initiated and they appear almost as promising as the reductive routes.<sup>262</sup>

### Solution Phase Group IV Synthesis: Metathesis

Metathesis routes to group IV nanoparticles have been pursued for almost 10 years,<sup>242,244-247</sup> but have very recently been abandoned in favor of oxidation<sup>249,262</sup> and reduction<sup>195,196,261</sup> routes to Si and Ge nanoparticles. In essence, the metathesis reaction combines the Si-bearing reagents from these oxidation and reduction routes and pairs them together (**Equation 11**).<sup>246</sup>



Metathesis reactions are carried out with an excess of the halosilane or germane and a nanoparticle product with a halogenated surface is presumably produced. This surface is then reacted with a Grignard reagent or an alkyllithium reagent in order to alkylate the particle surface, producing a material that is both soluble in organic materials and is somewhat resilient to oxidation, enabling purification through standard organic-aqueous extraction.<sup>242,244-247</sup>

The reaction is low yielding (<40%),<sup>246</sup> although very recently a higher yielding (>50%) synthesis of Ge was reported,<sup>248</sup> and the reaction produces a product with particles averaging 4 nm in diameter and ranging from 1 to 10 nm. Although the average particle size is slightly larger than the anticipated ideal size for substantial melting point reduction in a silicon nanoparticle ink, the synthesis has more pressing problems facing it. The use of a halogenated surface as a precursor for

alkylation introduces problems because the steric diameter of the alkyl group that is to be grafted to the surface occupies more space than is allowed if the alkylation is to completely consume the halogen surface termination.<sup>217,218</sup> This means that the nanoparticle product is bound to have halogen residue at the surface unless a hydrogenation procedure is developed or the silicon halogen bond is oxidized with a sterically unhindered oxidant like methanol or water, which can occur during the reaction work up. Very recently the first hydrogenation procedure was reported for halogenated particles,<sup>249</sup> but the extent of surface coverage is unknown and oxygen and organic groups still dominate the IR spectra of the partially-hydrogenated samples. Such difficulties related to surface termination affect not only the metathesis reaction but also oxidation and reduction routes for the production of nanoparticles and network polymers and these difficulties strongly suggest that new surface modifications and combinations of surface modifications need to be introduced to produce halogen-free nanoparticles by these routes.

In addition to  $Mg_2Si$ , the more reactive silicides  $NaSi$  and  $KSi$  have been used in these reactions.<sup>242,247</sup> Although the increased reactivity leads to smaller nanoparticles (average size 2-3 nm), addressing one concern with the metathesis route, there are still problems with the surface termination and yield. Additionally, the use of these more reactive silicides leads to the production of amorphous material.

The yield problems with the metathesis approach may originate with the poor solubility of the metal silicide. Under the conditions that are described, the silicide compounds are not soluble. For Si,  $Mg_2Si$  residue remains even after the reaction has proceeded to "completion",<sup>246</sup> although for Ge the  $Mg_2Ge$  completely reacts.<sup>244,247,248</sup> Even with the increased reactivity of  $NaSi$  and  $KSi$  the silicide is not consumed during the reaction,<sup>242</sup> which lasts for days at elevated temperatures. The heterogeneous reaction conditions are undesirable, as nucleation and growth are not separated and the particle size distribution is expected to suffer.

### **Solution Phase Group IV Synthesis: Reduction in Inverse Micelles**

At the outset of this work, the only published wet chemical synthesis of Si and Ge nanoparticles to offer H-passivation, instead of alkyl or alkoxy passivation, was

the reduction of Si or Ge salts in inverse micelles.<sup>165,234,263-265</sup> The primary reason for this is the use of hydride reducing agents in the synthesis, and in principle these reducing agents could be extended to other reduction routes, though to date, there has only been one published attempt.<sup>249</sup>

The anhydrous reduction of inorganic salts in the hydrophilic interior of inverse micelles has been used for over a decade<sup>266-269</sup> to form nanoparticles of a large number of metals and semiconductors including Au,<sup>266-268,270-272</sup> Ag,<sup>272</sup> Pt,<sup>273</sup> Ir,<sup>269</sup> Fe,<sup>274</sup> Si,<sup>165,263-265</sup> and Ge.<sup>234,264</sup> Through the use of a complimentary reagent instead of a reducing agent, binary semiconductor and sulfide nanoparticles have been synthesized by this method, most notably CdS,<sup>267</sup> MoS<sub>2</sub>,<sup>275</sup> FeS<sub>2</sub>.<sup>276</sup>

In general, reductions in inverse micelles consist of the same basic steps.<sup>267</sup> First an inverse micelle solution is formed, usually at 10% surfactant by weight. The reported surfactants come from two broad categories, cationic and nonionic. The cationic surfactants are alkylammonium halide surfactants such as tetraoctylammonium bromide and they are typically dissolved in toluene. The nonionic surfactants are aliphatic polyethers of the C<sub>*i*</sub>E<sub>*j*</sub> family, consisting of an alkyl chain *i* units long and *j* number of ethyl ether units, terminating with an -OH group. The most commonly used surfactant is C<sub>12</sub>E<sub>5</sub>, CH<sub>3</sub>(CH<sub>2</sub>)<sub>11</sub>(OCH<sub>2</sub>CH<sub>2</sub>)<sub>5</sub>OH. These nonionic surfactants are dissolved in “anhydrous oils” such as the alkanes octane or decane. Once the surfactants fully dissolve, an inorganic salt is dissolved into the surfactant solution.

Although the inverse micelle solution consists predominantly of a hydrophobic alkane or aromatic solvent, polar inorganic solids can dissolve up to a level of ~0.2 M, as they effectively are “hydrated” by the polar groups of the surfactants.<sup>267</sup> These polar groups phase separate in the hydrophobic medium, creating a polar interior at the center of the inverse surfactant micelles that form. In theory, it is in this polar interior, a nanocompartment within the hydrophobic solution, that nanoparticle formation takes place. The resulting nanoparticles are stabilized by the surfactants. If the nonionic surfactant is too hydrophilic (*i* is large) or too hydrophobic (*j* is large), the colloids are not found to be very stable and suffer from agglomeration.<sup>268</sup> Hydrophobic surfactants and their reaction products are best stabilized with hydrophobic solvents (such as hexadecane instead of hexane). In general, C<sub>12</sub>E<sub>5</sub> balances the hydrophobic and hydrophilic constraints and is common to many of reported inverse micelle reactions. The choice of surfactant has a small influence over nanoparticle product size, with

more hydrophobic surfactants yielding particles of smaller size than surfactants with more hydrophilic character.

Once the inorganic salt is dissolved in the surfactant solution, a reducing agent is added to the surfactant solution, reducing the inorganic salt to the base metal or semiconductor and producing nanoparticles. "In pure inverse micelle systems the average number of metal ions per micelle controls the final colloid size. When a reducing agent, [such as] hydrazine, is added, the many metal ions become quickly reduced to neutral metal. Nucleation sites then exist uniformly throughout the solution wherever a micelle contains one or more metals atoms. Aggregation occurs when two micelles collide and exchange contents, with the larger clusters growing at the expense of the smaller ones, until all the available metal is used up. The colloidal particles are then stabilized by the absorbed surfactant."<sup>267</sup> Although there is transfer of the contents of micelles, the surfactant solution retards particle growth and contributes to the control of the resulting particles' sizes. With smaller amounts of surfactant, the inverse micelles are larger and as a result, average particle size increases.<sup>267</sup>

In addition to the amount of surfactant used, the inorganic precursor, the precursor concentration, and the choice of reducing agent can influence particle size. Of these, the strength of the reducing agent might have the largest influence on particle size. As an example, in the synthesis of Au nanoparticles, the use of a weak reducing agent, hydrazine, yields 16 nm particles, and a "more rapid initial reduction and nucleation" is observed with the use of strong reducing agents such as  $\text{LiAlH}_4$ , producing 2 nm particles.<sup>268</sup>

With the use of stronger reducing agents come concerns regarding the compatibility of the reducing agent with the surfactants. This is primarily a problem facing the nonionic surfactants, which have an alcohol terminating their polar end. Strong reducing agents such as LAH and Na metal react vigorously with alcohols, setting up a situation in which there is a competition between the reaction between the reducing agent and the inorganic salt and the reducing agent and the surfactant. This problem is exaggerated by the high surfactant concentration compared to the inorganic salt, as there can be  $10^3$  times more surfactant molecules than inorganic precursor molecules. Although the published procedures utilize aggressive reducing agents such as LAH and Na,<sup>165,234,267,268</sup> they do so without understanding what the actual reaction stoichiometry is due to

the competition for the reducing agent between the inorganic precursor and the surfactant alcohol.

Beyond the questions regarding the compatibility of specific reducing agents with certain surfactants, the role of the surfactant in stabilizing the nanoparticle product is not completely clear from the literature. Cationic surfactants are reported to irreversibly bind to nanoparticle surfaces,<sup>267</sup> although uncontrolled nanoparticle growth and film formation has been reported for the product from syntheses with cationic surfactants,<sup>277</sup> indicating that there is some access to the particle surface. Still, the aggressive cationic surfactant interaction with the particle surface is consistent with the small sizes generally observed from syntheses that employ these surfactants.<sup>267</sup> While cationic surfactants are anticipated to tightly bind to Si and Ge surfaces, the nonionic surfactants might also bind to the particle surfaces through the surfactant alcohol, forming a stable Si-O bond. In either case, the surfactant-capped product would make a poor nanoparticle ink due to the low volatility of the surfactant and the tight binding to the particle surface. Although the published report describing the synthesis of Si<sup>165</sup> comments that HPLC purification removes surfactants, no specific data is presented and the type of surfactant employed in the synthesis is not mentioned.

General trends regarding nanoparticle synthesis in inverse micelles are described in the literature,<sup>267,268</sup> but specific details for synthesis of Si nanoparticles are not provided,<sup>165</sup> and the suggested reaction concentrations span three orders of magnitude, from  $10^{-5}$  to  $10^{-2}$  M.<sup>267</sup> Furthermore, reaction stoichiometry is not directly addressed in the papers that deal with Si or Ge synthesis, although a few papers describing the synthesis of metal particles report the use of a fourfold excess of the reducing agent.<sup>270,271,273</sup> While the possibility of a H-capped Si nanoparticle product is enticing, the conditions to realize this product are not clear from the published literature and the reaction conditions required to produce a specific size of particle are not well described for any of the systems.

Only recently have precise reaction conditions been described for nanoparticle synthesis in inverse micelles,<sup>270,271,273</sup> and in all cases the synthesis is for the production of metal nanoparticles. The metal salt concentration in the 10% nonionic surfactant solution (C<sub>12</sub>E<sub>4.8</sub>) is reported as 10 mM, with 4 equivalents of Superhydride, LiBH<sub>4</sub>, or LAH as the reducing agent. When we began synthesis of Si nanoparticles in inverse micelles, we did not know common values for reagent

concentration and reducing agent stoichiometry, and the absence of practical experimental numbers was a source of concern.

Outside of concerns with the reaction conditions, there were concerns with the purification and surface termination of the nanoparticles produced from reductions in inverse micelles. Separation of the product from the surfactants by HPLC is described,<sup>165,234,265,272</sup> but specific HPLC conditions are not fully described and the issue of residual surfactant remaining at particle surfaces is not directly addressed. HPLC is a convenient tool for separation and purification and can also provide analytical information, but the technique uses 100-1000 times more solvent than the volume of the sample that is to be purified and any impurities, such as residual water, dissolved oxygen, or organic peroxides, are therefore present in undesirable amounts and might oxidize Si nanoparticle surfaces.

Alternative purification means have been reported for separating metal particles from surfactant solutions.<sup>270</sup> The use of solid phase extraction is most similar to HPLC, as the reaction product solution is passed through an extraction cartridge that contains a packing material similar to the size exclusion or reverse phase material in an HPLC column. For reactions in nonionic surfactant solutions, extraction is commonly used to purify metal particles. After capping the nanoparticles with alkanethiols, to render the particle surface hydrophobic, ionic byproducts and the surfactant are extracted into an immiscible organic solvent like NMF (or DMF, acetonitrile, etc.). The partitioning ratios are most favorable for NMF, then DMF, and are not very favorable for any of the other solvents studied. Some NMF remains in the alkane with the nanoparticles, and can be removed with a subsequent aqueous extraction. Precipitation is another option for separating nanoparticles from the large excess of surfactant that remains from the reaction. For cationic surfactants the addition of an alkane forces the surfactant to precipitate from the solution, while the nanoparticles remain in solution, although it is believed that this is due to the polar head of the surfactants tightly associating with the particle and the hydrophobic alkyl groups providing a measure of solubility in the alkane and aromatic solvents. For nonionic surfactant solutions, the excess surfactant can be forced from the solution by reducing the temperature and thereby reducing the solubility of the surfactant in the alkane solvent. Precipitation of the nanoparticles themselves is another option, but it is reported to be difficult and low yielding, and it is not recommended for nanoparticles in inverse micelle solutions.<sup>270</sup>

In spite of the hazy details of the inverse micelle chemistry – what surfactant, what reducing agent, what concentration, what stoichiometry, what type of chromatography was used – nanoparticle production in inverse micelles was anticipated to be advantageous because of its proven applicability to a wide range of materials,<sup>165,234,267,268,273,275,276</sup> the likelihood of hydrogen passivation,<sup>165</sup> and possibility of producing HPLC-grade Si nanoparticles.<sup>165</sup>

### **Solution Phase Group IV Synthesis: Electrochemical Etching**

In addition to more traditional chemical routes to nanoparticles in which start with Si salts or molecular compounds, an opposite route has been explored in which a single-crystal Si wafer is etched down to produce nanoscale features which are then ultrasonically fractured and freed from the crystalline substrate into a carrier solvent.<sup>138</sup>

The first step of the process is the production of a porous-Si surface, which is brought about through an electrochemical etching of a Si wafer in an HF etch bath.<sup>138,278</sup> The wafer acts as one electrode and Pt as the counterelectrode. Although bath compositions vary, in general a fairly concentrated HF solution is used in which 49% HF (aqueous) is mixed in equal portions with methanol or ethanol. Electrical conditions also vary, but prototypical conditions described for the preparation of Si colloids are 0.1-5 mA/cm<sup>2</sup> and 0.6-1.6 V for p-type wafers and 0 V under illumination with a tungsten lamp for n-type wafer etching. The resulting wafer has a nano-porous structure at the surface and is highly photoluminescent. A luminescent Si colloid is formed by sonicating the wafer in an organic solvent under N<sub>2</sub>. As expected for a Si surface freshly removed from an HF bath, prior to sonication the porous Si wafer displays strong Si-H signals in its IR spectra and no “discernable peaks [are observed] for surface Si-O”.<sup>138</sup>

A primary problem with this method of forming Si nanoparticles is the size control, which is limited and has been reported to produce particles ranging from 10-300 nm for concentrated HF baths (49%)<sup>279</sup> and 2-40 nm for diluted HF baths (20%).<sup>280,281</sup> However, on closer examination, the large particles that are seen in these colloids were found to be composed of smaller nanocrystals, 2-20 nm.<sup>280,281</sup> The agglomerates are certainly not ideal, but it is possible that the constituent



nanocrystals would have a size-suppressed melting point and could be useful as a printable semiconductor.

Size control in porous Si etching has been reported by introducing hydrogen peroxide as an additive to the etching solution and slowly dipping the Si substrate into the bath,<sup>282</sup> as the etching rates are highest at the meniscus where the current is most concentrated.<sup>283</sup> The porous Si wafer, prior to sonication, is dominated by monohydride surface species as evidenced by IR spectroscopy. The features associated with dihydrides and defect monohydrides are not detected in these samples like they are in traditional porous Si etch baths that do not contain hydrogen peroxide. These monohydride terminated Si surfaces have “ideal” passivation and an “ideal” ultrasmall nanoporous structure.<sup>283</sup> Additionally, “ideal anodization” provides much smaller nanoparticles when the porous substrate is sonicated in an organic solvent.<sup>198</sup> In fact, discretely sized nanoparticles have been reported from this preparation.<sup>197</sup> At the smallest, “ultrasmall” 1 nm particles are produced,<sup>198</sup> for which a surface reconstructed  $\text{Si}_{29}\text{H}_{24}$  structure has been proposed.<sup>197,284</sup> Although the initial description of these nanoparticles claimed that “the particles are composed of silicon with no oxygen present,”<sup>198</sup> reports later indicated that “the particles are composed of Si with less than 10% oxygen.”<sup>285</sup> IR spectra demonstrate the presence of oxygen, and most likely the initial statement of that there was “no oxygen present” was based on the observation that the porous silicon wafer, prior to sonication, was hydrogen terminated without detectable oxygen.<sup>283</sup>

“It is probable that Si-O and Si-OH bonds are formed by the combination of very small concentrations of  $\text{O}_2$  and  $\text{H}_2\text{O}$  present in the solvent plus the high temperature produced in ultrasonication.”<sup>281</sup> “The chemical effects of ultrasound (sonochemistry) arise from acoustic cavitation, that is, the formation, growth, and implosive collapse of bubbles in liquid... [This] generates localized hot spots... with transient temperatures of  $\sim 5000$  K, pressures of 1800 atm, and cooling rates in excess of  $10^{10}$  K/s.”<sup>252</sup> It seems quite possible that such extreme conditions could lead to oxidation of Si surfaces during the ultrasonic fracture of porous silicon wafers. Because of the fracturing in an organic solvent, the resulting colloid will always be produced with a non-hydrogenated surface that was the particle’s bonding site to the porous structure. When the particle is cleaved from the porous network, the dangling bonds that are produced are highly reactive and subject to oxidation or surface rearrangement. Even by using a glove box, careful attempts to limit  $\text{O}_2$  and  $\text{H}_2\text{O}$  exposure to porous silicon wafers were not able to

prevent oxidation of the colloid.<sup>279-281</sup> In fact, as-etched wafers, which were found to be exclusively H-passivated by IR spectroscopy, were observed to attract hydrocarbons even under solvent free conditions, and colloids produced from such wafers were found to be devoid of IR Si-H features and dominated by organic and Si-O features.<sup>280,281</sup> The long sonication times (7 days) might account for the complete lack of Si-H features, but a weak ultrasonic bath was used for the suspension and anaerobic conditions were used and complete oxidation was still observed.<sup>280,281</sup> The shorter sonication times or improved stability of the ideally passivated Si surface might account for the apparent resilience of Si colloids from “ideal anodization” experiments,<sup>197,198,283-285</sup> which have less than 10% oxygen at the surface. It is possible that this is the limit for samples prepared in this way, as the extremity of sonication and the high reactivity of fractured Si surfaces might ensure some oxidation occurs at the surface of the Si nanoparticles.

#### Group IV Synthesis Trends

Consistency, surface termination, and yield have been or remain an issue for Si nanoparticles formed by reduction,<sup>164,165,195,196,253</sup> oxidation,<sup>262</sup> decomposition,<sup>239,240,250</sup> and electrochemical etching.<sup>138,197,198,279-281,283-285</sup> Even the UV-visible spectra of these samples has been inconsistent and varied (**Figure 20**) without explanation or meaningful correlation with particle size, surface, or crystallinity.

At the initiation of our research in this area, the only wet chemical synthesis to offer H-passivation was reduction in inverse micelles,<sup>165</sup> although reductions, oxidations, and metathesis reactions could offer such a surface with further development, and recent efforts toward that end have demonstrated only imperfect surfaces that require more research.<sup>249</sup> Even though the inverse micelle synthesis offers a H-passivated surface, it was not anticipated to be an ideal synthesis, as the synthetic details are lacking from the published literature,<sup>165</sup> reaction concentrations are assumed to be low and surfactant concentrations are very high, the interaction of the surfactant at the particle surface is unclear, purification details are limited and purification is anticipated to be difficult. Alternatively, the electrochemical etching of bulk Si to produce porous Si and, subsequently, Si nanoparticles was known to yield a H-terminated Si nanoparticle product,<sup>197,198,285</sup> although it, too, suffered from low concentrations, a lack of

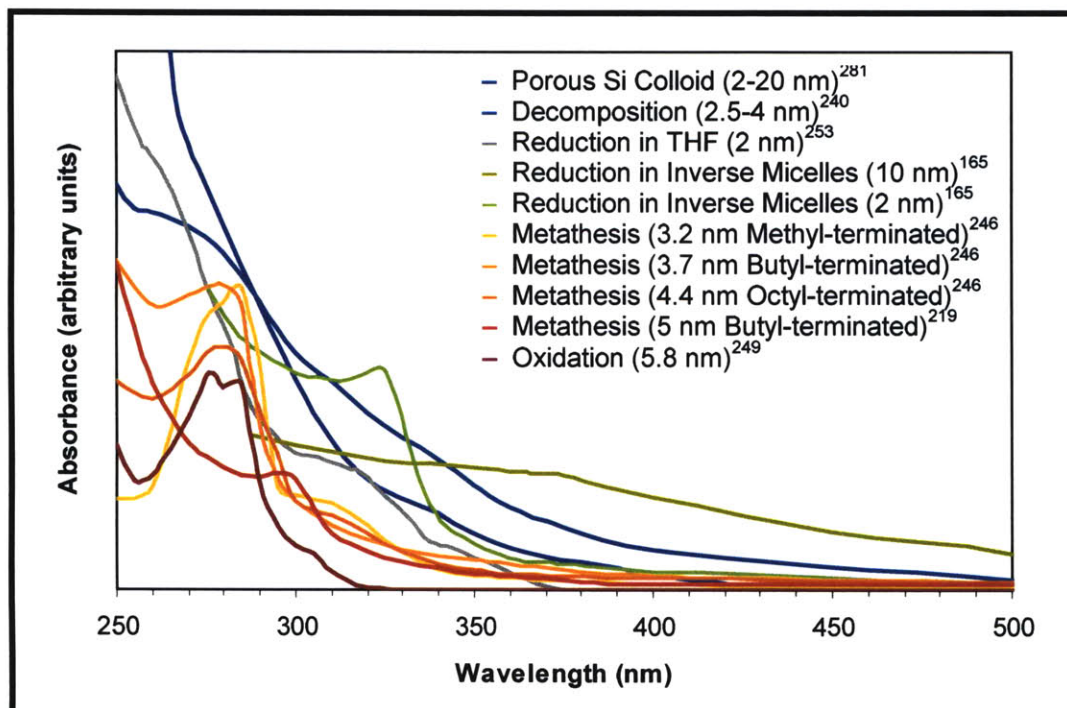


**Figure 20:** Comparison of the UV-Vis spectra of 2-10 nm Si nanoparticles reported in the literature. Literature reports do not agree on UV-Vis spectral characteristics for Si nanocrystals, placing the absorption onset between 280 and 370 nm. Even within a specific synthetic approach, such as metathesis using  $Mg_2Si$  and  $SiCl_4$ ,<sup>219,246</sup> differing UV-Vis features have been reported. While this variability makes product identification by UV-Vis spectroscopy difficult, Si nanocrystals should still be identifiable with their absorptions between 280 and 370 nm.

specific, well described published experimental details, and well-documented problems with oxygen impurities.<sup>280,281</sup>

# Silicon Synthesis by Electrochemical Etching

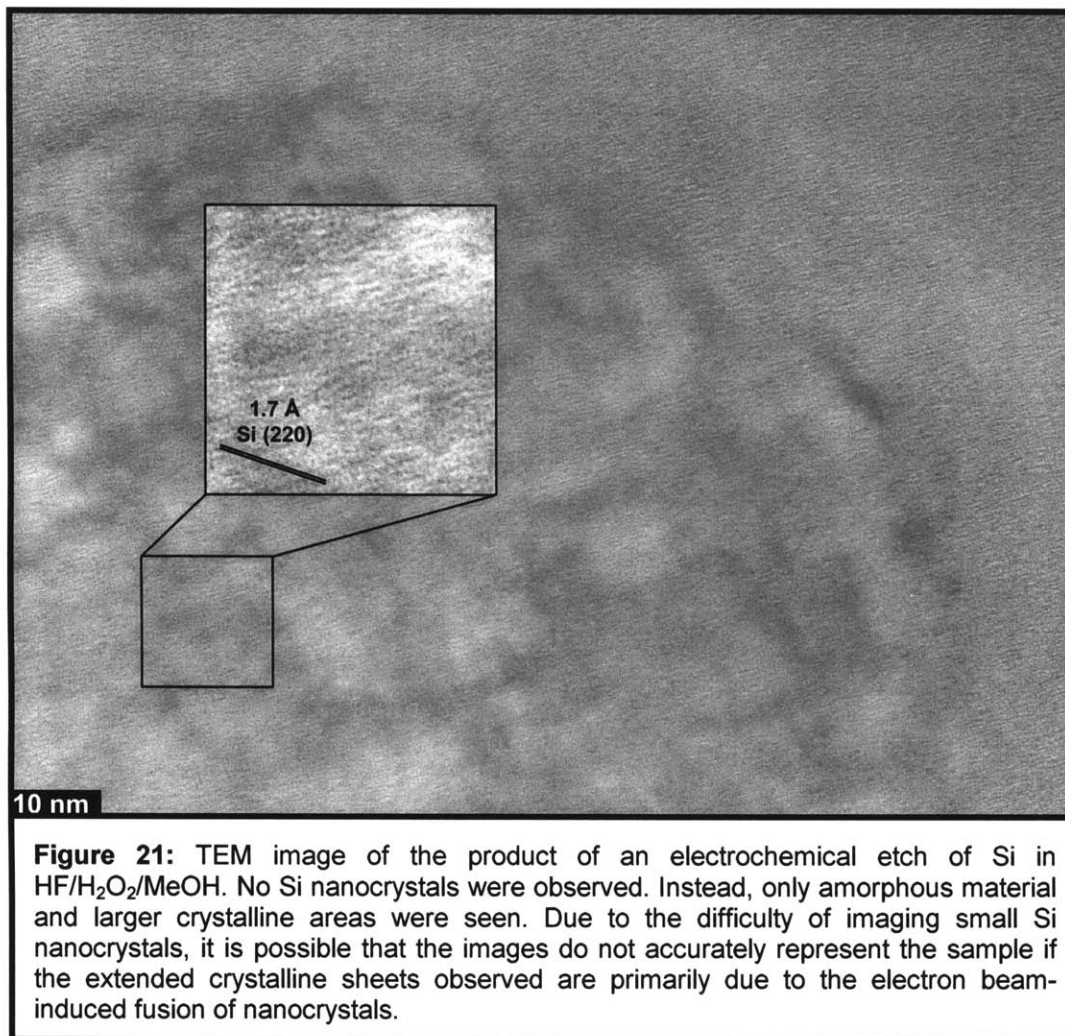
## Anticipated Advantages and Limitations of Electrochemical Etching

Electrochemical etching of doped Si wafers to form a nanoscale porous network has a number of advantages when compared to wet chemical syntheses. The purity of the Si is of the highest quality, as a semiconductor grade wafer is used as the substrate for etching. Additionally, all of the chemicals used in the process are used in the semiconductor industry and so their compatibility with semiconductor processing is well established. It is also conceivable that the use of wafers with different doping levels would provide control over the doping level within the resulting nanoparticle ink, although etch conditions would most likely have to be different for wafers of different doping levels.

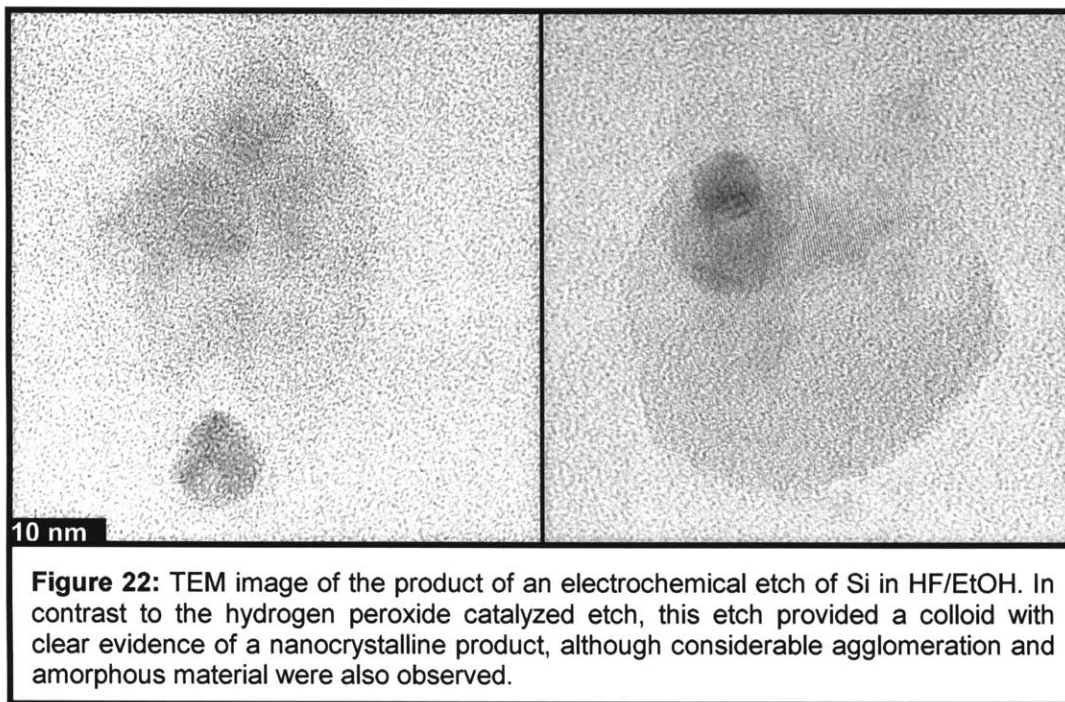
There are also a few disadvantages to electrochemical etching. Chief amongst them is the absence of a clear demonstration of an unoxidized product.<sup>197,198,279-281,285</sup> In fact, careful studies of the product have been carried out with the expressed purpose of producing an oxygen-free surface, and have failed.<sup>279-281</sup> Size control remains an issue, although lateral anodization and “catalysis” through the use of hydrogen peroxide have made it possible to isolate <5 nm particles.<sup>197,198</sup> The yield of the process is also an issue, arguably not at production scale, in which a number of etches might be done in parallel to make up for any yield shortcomings, but at the research scale where analysis is made on the products of single etches.

## Synthesis by Electrochemical Etching

Two electrochemical etching procedures were investigated as a part of this work.<sup>17</sup> The simpler of the two used an ethanol and aqueous HF bath as the etchant and a low etch current. The procedure has been described to yield a luminescent Si colloid with particles <50 nm in size.<sup>138,280,281</sup> The other etch that was experimented with uses higher electrical currents and a bath consisting of methanol and aqueous HF with hydrogen peroxide as an added “catalyst.”<sup>198</sup> Also, the wafer is slowly advanced into the electrochemical etch bath to create a wide meniscus region, as the etching is greatest at the meniscus, the interface between the bath solution, wafer, and air.<sup>283</sup>



While the use of lateral anodization and hydrogen peroxide has been reported to produce <5 nm Si nanoparticles,<sup>197,198</sup> experiments carried out as a part of this thesis research did not find this to be the case. The product of such etches – using aqueous HF, methanol, and hydrogen peroxide – was difficult to resolve by TEM, often finding what appeared to be amorphous material. TEM also found larger crystallites, sheets, or agglomerates, and clearly detected crystalline areas much larger than 5 nm (**Figure 21**). One area where there could be considerable difference between the reported etches and those described here could be in the settling of the product. Although the early published experimental procedures did not mention it,<sup>198</sup> later reports describe a settling out of larger crystallites from the product solution,<sup>197,285</sup> leaving only the smallest particles suspended in the



solvent. There is no description of the settling and it is possible that there was a critical difference in the procedures. Also, the amount of solvent is not mentioned, and concentration could influence the effectiveness of the TEM imaging.

One area where a conscious change was made to the procedure was in the choice of the product solvent. Glyme was used instead of acetone, which probably contained some residual water in the published reports,<sup>198</sup> likely oxidizing the product surface. Glyme was chosen for its ability to complex to the Si surface while avoiding the possibility of it formally bonding to the particle surface. Glyme had also been reported as a solvent for the synthesis of Si nanoparticles by metathesis.<sup>242-244,246,247</sup>

Although literature reports claim discretely sized Si nanocrystals result from the catalyzed lateral anodization of Si,<sup>197</sup> the experiments described here were found to yield a larger crystalline product (**Figure 21**). Published TEM images<sup>197</sup> are clearly different from those reported here, but in addition to the Si particles of discrete sizes, published images show some agglomeration and larger materials such as a 6.6 nm prolate particle and a 4.5 nm spherical particle, both of which fall out of the “magic” size regime. In addition to questions regarding the size control of the catalyzed etch, there was concern with that the use of an oxidant,

H<sub>2</sub>O<sub>2</sub>, would compromise the ideal hydride-surface termination of the etch. Because of this, a more established and peroxide-free etch solution was investigated.<sup>138</sup>

The reported size control for particles produced from uncatalyzed porous silicon etching is not great, as the product is dominated by 20-50 nm agglomerates of smaller Si nanoparticles.<sup>138,279-281</sup> Colloids derived from porous Si were used in a study of the melting point depression effects in a wide range of nanosized Si, and particles above 20 nm are produced alongside the desired 2-3 nm particles.<sup>37</sup> In our lab at MIT we found the major product of an etch using aqueous HF and ethanol was 10 nm agglomerates consisting of smaller grains (**Figure 22**). Some single crystal areas were seen at this size scale, as well, but a number of particles were found to consist of smaller particles that had agglomerated or fused during the production. The extreme conditions of sonication may induce particle fusion,<sup>252</sup> but it is promising and of interest that a number of 2-4 nm nanocrystals are produced, even if they are not easily isolated without agglomeration.

The nanoparticle agglomeration or fusing observed in the etch products might also result from the highly reactive surface that is created during the sonication-induced crumbling and cleavage of the porous silicon material. While the surface of the porous Si that has been exposed to the etchant is expected to be stabilized by a hydrogen monolayer, the cleaved Si surface that results from the sonication may be highly reactive and any “dangling bonds” might be very quick to oxidize in the absence of a medium that is able to provide H passivation. Similarly, the reactive surface resulting from the ultrasonic fracture of porous silicon in an organic solvent might be responsible for the observed particle fusing. Porous silicon wafers have been reported to have perfect hydrogen terminated surfaces with no detectable oxidation in spite of the high surface area.<sup>218</sup> However, oxygen free particles have not been reported, even though rigorous attempts were made.<sup>280,281</sup> While the extreme conditions of the sonication<sup>252</sup> might be directly responsible for some particle oxidation from residual water or dissolved oxygen, it seems likely that the primary cause is the creation of highly reactive dangling bonds during the sonication-induced mechanical wafer crumbling. Although these issues might be addressed in the future, such unwanted oxidation and the difficulties encountered with the control of the product’s size distribution made porous silicon an unattractive route to Si nanoparticle production for applications in printed microelectronics.

## Silicon Synthesis by Metathesis

### Anticipated Advantages and Limitations of Metathesis

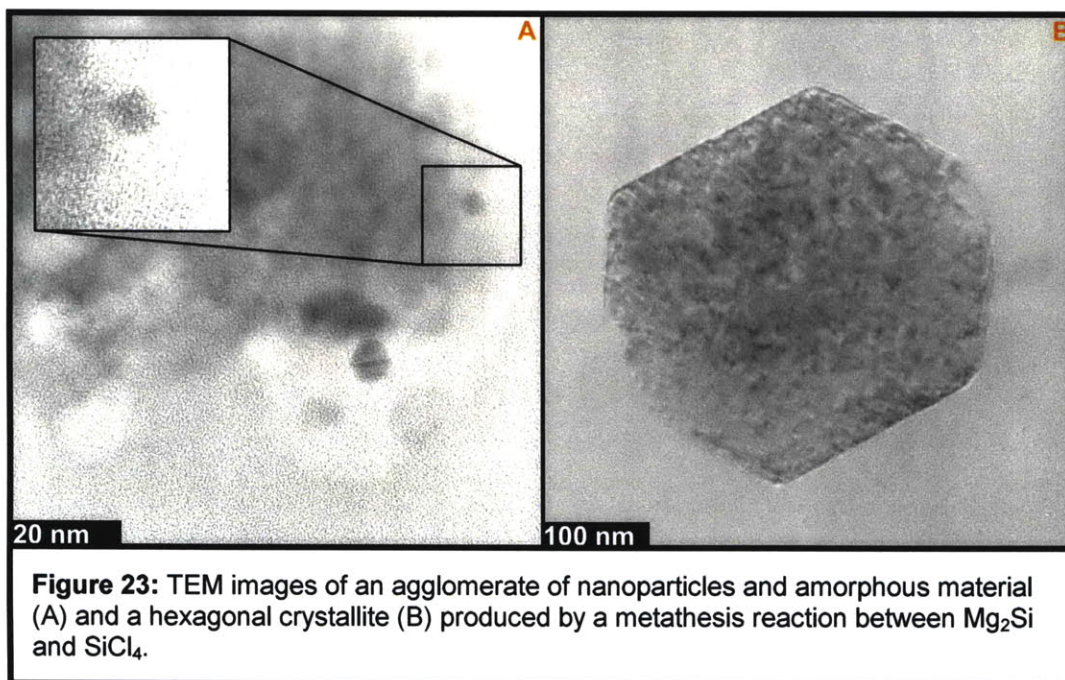
The metathesis reactions that have been reported for the synthesis of Si nanoparticles employ low-boiling solvents such as glyme and diglyme.<sup>242,246</sup> The lack of a high-boiling surfactant makes the reaction attractive, because removing heavy surfactants would be necessary for nanoparticle ink formulation and such purifications might be difficult. While the reaction solvent is attractive, the solvent is not able to dissolve the silicide and so the reaction proceeds slowly and the heterogeneity was anticipated to compromise the resulting particle size distribution. Surface termination was also anticipated to be a problem, as the reported alkyl termination did not provide a great deal of flexibility and was believed to incompletely passivate the surface.

### Synthesis by Metathesis

The metathesis chemistry is simple to carry out. An excess of  $\text{SiCl}_4$  is added to a silicide such as  $\text{KSi}^{242}$  or the commercially available  $\text{Mg}_2\text{Si}^{246}$  in glyme or diglyme and the reaction mixture is refluxed for 1-2 days. The volatile components of the reaction are removed under vacuum, glyme is reintroduced to the reaction vessel, and the assumed Si-Cl terminated particle surface is derivatized with an alkylating Grignard reagent. The product is then isolated by aqueous extractions.

Unlike the literature reports of Si nanoparticle synthesis in inverse micelles,<sup>165</sup> the metathesis reaction conditions are precisely described in the literature. However, in the work reported here the reaction results differed from those that have been reported.<sup>246</sup> Most notably, the reaction product (**Figure 23**) was found to greatly vary in size, with only a few isolated small nanoparticles seen, a larger number of agglomerates and larger crystalline areas, and even a hexagonal crystallite >200 nm on a side, similar to the product seen from early reduction syntheses.<sup>164</sup> The particles were often found to be crystalline, but there was no apparent size control. It is possible that the extended crystalline sheet areas were the result of the e-beam fusing of small nanocrystals or polymeric species in the TEM, but





even discounting these materials, there was a great deal of variability in the size of the product.

The published reports do not describe any means of controlling size in the metathesis reactions, and so an adoption of this technique would require extensive study of the reaction.<sup>242,246,247</sup> Additionally, the reaction might be fundamentally flawed, as it is a heterogeneous reaction, intrinsically troubled when it comes to size control. Beyond size control, the metathesis reaction was found to provide a poorly terminated surface. Residual Cl was routinely detected at a few percent level by EDX, and sometimes Mg was carried through the reaction work up as well. The Cl was surprising because the product is exposed to methanol and water and these should react with the Si-Cl bonds that remain from incomplete surface passivation. However, the incomplete surface derivatization comes about primarily from steric reasons, as some Si-Cl sites become inaccessible and effectively trapped between alkylated sites. The observation of Cl in the metathesis product indicates that some of the Si-Cl species also become inaccessible to methanol and water during the product work up. In fact, similar Si-Cl species have been reported for these reactions,<sup>254</sup> although there has been a report describing complete surface alkylation through a week-long alkylation under reflux.<sup>219</sup>

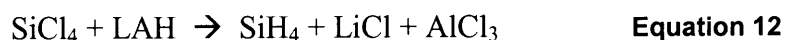
Beyond the considerable problems with size control and surface termination, the metathesis reaction, as reported, provides a poor reaction yield.<sup>246</sup> This, as well as the poor size control, has been attributed to the heterogeneity of the reaction.<sup>246</sup> An attempt to utilize this synthetic chemistry for the demonstration of a Si nanoparticle ink was deemed likely to fail due to the number of improvements that would need to be brought to the synthesis and its work up. Thus, metathesis was not considered for further development.

## Silicon Synthesis by Reduction in Inverse Micelles

### Anticipated Advantages and Limitations of Reduction in Inverse Micelles

In the early stages of this project, the metathesis synthesis was anticipated to provide a product more appropriate for ink formulation than the inverse micelle synthesis. In part this was due to the greater number of papers describing the metathetic route, the conceptual ease and elegance of the metathesis reaction, and the specific data regarding size, but it was also due to the difficulties anticipated with the inverse micelle synthesis. Synthetic details relating directly to the synthesis of Si using inverse micelles as nanoreaction compartments are limited<sup>165,234,263-265</sup> and it was and is unclear how much experimental detail translates directly from the more studied metal systems,<sup>266-268,270-274</sup> to semiconductors, especially the covalently bonded group IV elements.

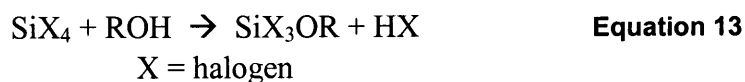
The likelihood of success with the inverse micelle synthesis method was also questioned because of concerns regarding surface termination. No surface data has been directly reported, although H-termination was suggested as a likely termination,<sup>165</sup> and is certainly possible given that the production of silane has historically come from the reaction of the halosilane SiCl<sub>4</sub> with LAH (**Equation 12**).<sup>226</sup>



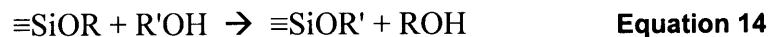
Silane gas is highly explosive and reacts with water and oxygen,<sup>226</sup> so even if a hydrogen terminated particle were the product from the inverse micellar synthesis, the lifetime of the Si-H bond was considered a possible problem, as was the stability of a solution of these H-passivated particles without capping groups or ligands to prevent agglomeration and precipitation from solution. This aggregation might not be a problem when in the reaction medium, but in order to be useful as a semiconductor ink the bulky organic surfactants need to be removed from Si product, and in the absence of any such stabilizer the product was feared to irreversibly form large insoluble agglomerates. At the same time, if H-capped Si nanoparticles could remain in solution and be protected from oxidation they might serve as an ideal Si ink due to low conversion temperatures and intrinsic passivation of dangling bonds and defects in the resulting thin film.

## The Role of Surfactants in Reduction in Inverse Micelles

Related to this concern with surface termination was the role and choice of surfactants. Two general classes of surfactants were explored for this reaction – cationic and non-ionic. Cationic surfactants such as tetraoctylammonium bromide and dimethyldodecylammonium bromide are known to aggressively bind to metal nanoparticle surfaces.<sup>267</sup> In contrast, the non-ionic surfactants of the  $C_iE_j$  family, have been shown to be much more likely to be removed from nanocrystal surfaces.<sup>271</sup> However, these surfactants bear an alcohol functionality at their polar terminus, and this alcohol can react with both halosilane precursors<sup>209</sup> and some of the stronger reducing agents employed.<sup>286</sup> This complicates the reaction as the surfactant can interact with both of the reactants in the synthesis, and could also bind a large surfactant to the particle surface (**Equation 13**).<sup>209</sup>



These types of reactions are reversible, as swamping the reaction with another alcohol and driving the undesired alcohol from the reaction by boiling it off can effectively swap alkoxy ligands from a Si center (**Equation 14**).<sup>209</sup>



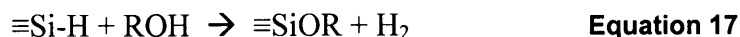
In fact, the dynamic nature of this reaction (**Equation 14**) might enable the alcohol to act as an effective capping group, retarding growth, stabilizing and solubilizing the particle, thereby playing a critical role in the mechanism of the particle synthesis. Furthermore, the direct reduction of orthosilicates with the strong reducing agent LAH is known (**Equation 15**).<sup>209</sup>



Also, alkoxy-capped Si nanoparticle networks have been reported from a sonicated reaction between sodium metal and tetraethylorthosilicate (**Equation 16**).<sup>252</sup>



So, while the alcohol bearing  $C_iE_j$  surfactant is expected to react with the precursor halosilane (**Equation 14**), the bond is expected to be dynamic and reversible (**Equation 15**), and there is the possibility of a favorable direct reduction with LAH (**Equation 16**), as well. Even the Si-H bond can react with an alcohol, although usually at slightly elevated temperatures (**Equation 17**),<sup>287,288</sup> and so the suitability of the non-ionic surfactant family  $C_iE_j$  was still thought to be questionable.



### Modification of Nonionic Surfactants for Reduction in Inverse Micelles

Given the purity constraints of a semiconductor ink, neither the cationic or non-ionic surfactants reported in the literature seemed to be ideal for the synthesis of Si nanoparticles for ink formulation. The cationic surfactants have been reported to non-specifically bind to nanoparticle surfaces<sup>267</sup> and the nonionic surfactants could possibly bind directly to the surface and promised to interact with both the Si precursors and reducing agents employed in the reaction. If the alcohol terminus of the non-ionic surfactant could be alkylated, though, the resulting “capped” surfactant would avoid the concerns regarding the surfactant influence in surface chemistry and particle growth. The modified surfactant would still have a high molecular weight and would have to be removed for Si ink formulation, but it might provide a more straightforward route to understanding the reaction chemistry and might be the only way to produce a nanoparticle product that is free of surface-bound surfactant.

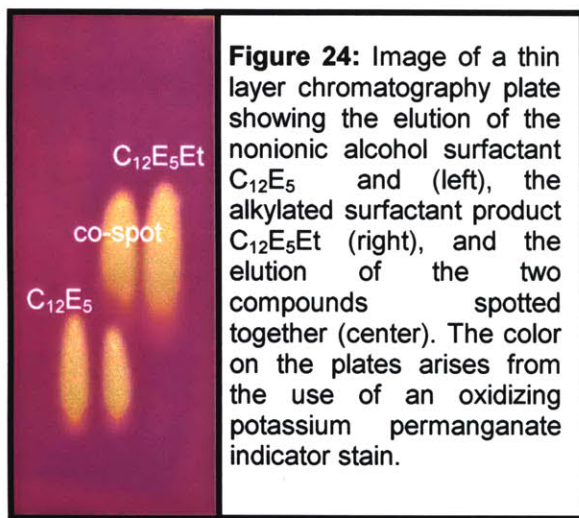
A number of procedures are known for alkylating alcohols. One such reaction takes place in a polar aprotic solvent such as dimethyl sulfoxide (DMSO) and occurs between an alcohol and an alkyl halide in the presence of a strong base such as KOH (**Equation 18**).<sup>289</sup>



DMSO can be difficult to remove from reaction products because of its high boiling point. The reaction was attempted as a neat reaction, free of DMSO, because the polarity of the ether groups belonging to both the starting material surfactant and the desired product were anticipated to create a sufficiently polar environment for the KOH to be involved in the reaction (**Equation 19**).



Although KOH did not appreciably dissolve, the KOH pellets in the reaction did not remain as pellets and became a white powder or paste at the bottom of the reaction vessel.

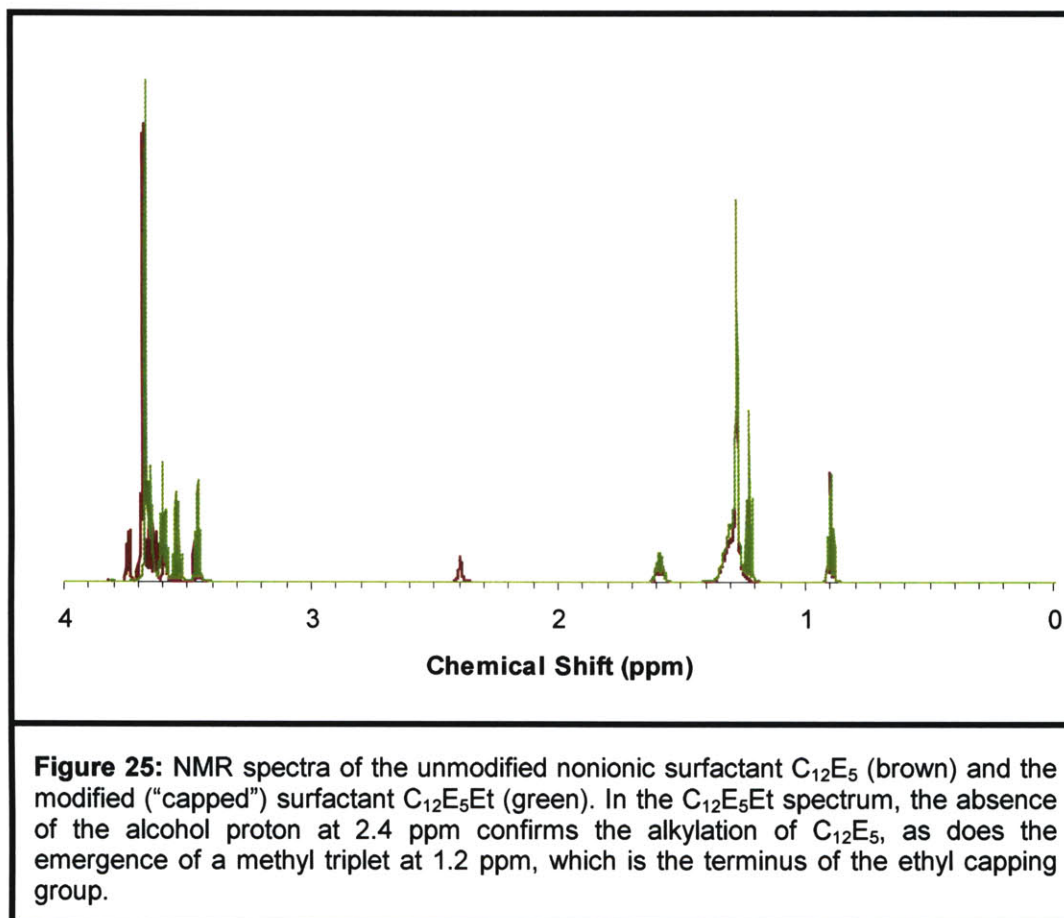


Small, gram-scale reactions were monitored by thin layer chromatography (TLC) using 25% acetonitrile and 75% toluene as the mobile phase and a potassium permanganate stain to visualize the optically inactive surfactants, and the reaction was found to run to completion overnight. Larger-scale reactions (25g) were found to take more time and were left to run for 3 to 7 days. TLC confirmed the disappearance of the starting material spot and the

emergence of the product spot, which ran higher on the TLC plate due to its decreased polarity and reduced interaction with the polar stationary phase (**Figure 24**).

Column chromatography was used to purify the modified surfactant. Pure toluene was used as the eluent initially, and gradually acetonitrile was introduced to bring the amount of acetonitrile up to 25% by volume. The collected fractions were concentrated under high vacuum and the resulting capped surfactant was thereafter handled just like the unmodified  $C_iE_j$  surfactant.

In limited trial runs the best results were obtained using ethyl bromide as the alkyl halide, and so it was used in the large-scale alkylations.  $C_{12}E_5$  was used as a



substrate, as it seems to be the most versatile non-ionic surfactant used in metal nanoparticle synthesis.<sup>267,268,270-273</sup>

Nuclear magnetic resonance was used to determine the success of the surfactant alkylation reaction (**Figure 25**). The peak associated with the alcohol proton can be seen to completely disappear and new alkyl peaks are seen at low ppm values, corresponding to the protons introduced by the ethyl group. Further illustrating the success of the alkylation is the observation that the unmodified surfactant C<sub>12</sub>E<sub>5</sub> bubbles vigorously when in the presence of LAH, but the capped surfactant C<sub>12</sub>E<sub>5</sub>Et has no apparent reaction. This qualitative test is particularly relevant because one of the primary concerns with using the unmodified surfactant is its reactivity with reducing agents such as LAH, and how that might influence reactant progress and stoichiometry.

After establishing the success of the surfactant modification, there was still a question of the ability of the modified surfactant to form inverse micelles in the alkanes used in this work (octane and hexane) and of the extension of the surfactant system to the synthesis of Si nanoparticles. Looking beyond this primary concern, the capped surfactant system offered more variability in the synthesis of Si nanoparticles by enabling surface modification with alcohol sensitive reagents such as Grignard reagents.

### Synthesis According to the Literature: Cationic Surfactants

A broad range of reaction conditions has been reported for inverse micelle

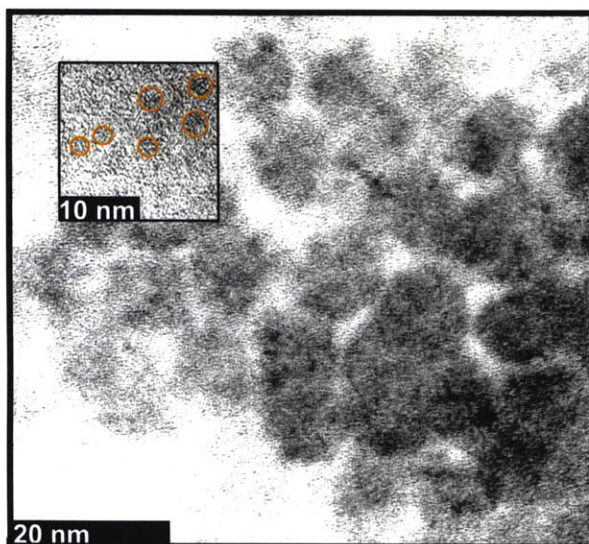


**Figure 26:** TEM image of the product of a reduction of  $\text{SiI}_4$  with 5 equivalents of  $\text{N}_2\text{H}_4$  in a toluene solution of the cationic surfactant DDAB. The inset highlights the smaller particles (average size 2.4 nm with a standard deviation of 0.5 nm), which are only clearly visible with exaggerated contrast ratios. The larger particles (average size 10.0 nm with a standard deviation of 1.6 nm) are found to be highly agglomerated and crystalline, suggesting that the smaller particles might be crystalline as well, although their very small size prevents clear imaging of the crystal lattice.

reactions, but there has been no experimental procedure published specifically for Si or the similar group IV element, Ge. The “generic process” procedures cited for the synthesis of both Si and Ge are from a patent<sup>267</sup> and a paper<sup>268</sup> from the early 1990s and they deal primarily with the synthesis of Au and other metals. In these publications, reaction concentrations are reported to range from  $1 \times 10^{-5}$  to  $5 \times 10^{-2}$  M, the role of reactant stoichiometry in particle growth, surface termination, and product purification is not addressed, a wide range of reducing agents are suggested for use, and a number of methods of purification are given. When considered alongside the choices of the Si precursor and the surfactant, these variables make for a very large and complicated space for synthetic exploration. Some



general trends are described, for example, average nanoparticle size is expected to decrease with increased reducing power, nanoparticle size is expected to decrease with the aggressiveness of the surfactant, and nanoparticle size is expected to decrease with decreasing reaction concentration. However, these trends are reported for Au, and their relevance to group IV materials has not been established.

Si and Ge nanoparticle synthesis by reduction in inverse micelles is discussed in five papers<sup>165,234,263-265</sup> without disclosing information or data mentioning any specific surfactant other than the polyether C<sub>12</sub>E<sub>5</sub>, and C<sub>12</sub>E<sub>5</sub> is seen only in HPLC data from a Si synthesis.<sup>265</sup> Although the use of cationic surfactants is broadly described in the primary paper on Si nanoparticle synthesis,<sup>165</sup> it incorrectly describes the reaction solvent as a “water-free oil” such as “octane or decane”, when cationic surfactants are poorly soluble in alkanes and toluene is typically used to form inverse micelle solutions with cationic surfactants.<sup>267</sup> The paper also inaccurately describes tetrahalide silicon precursors as “completely insoluble” in alkanes.<sup>165</sup> Researchers have noted that silicon tetrachloride is very soluble in octane and have questioned the role of micellization in the production of Si nanoparticles by reduction.<sup>195</sup> Unlike SiCl<sub>4</sub>, silicon tetraiodide is a solid at room temperature and solubility experiments found it only partially soluble in octane. However, toluene is used to dissolve cationic surfactants like DDAB,<sup>267</sup> and SiI<sub>4</sub> is soluble at 3% by weight in toluene at room temperature.<sup>290</sup> So, the role of micellization in cationic surfactant reactions is unclear, especially given that cationic surfactants are more aggressive in their binding to nanoparticle surfaces and might be used as a more traditional surface group to solubilize nanoparticles.

Using a solution of DDAB in toluene at 10% by weight, 2 mM SiI<sub>4</sub> was reduced with 5 equivalents of hydrazine (1 M in THF). The reaction product was purified by high performance liquid chromatography (HPLC) with a size exclusion chromatography (SEC) column and the size distribution of the resulting nanoparticles was bimodal, with a number of large and sometimes interconnected nanoparticles (average size 10.0 nm with a standard deviation of 1.6 nm) mixed with small nanoparticles (average size 2.4 nm with a standard deviation of 0.5 nm) (**Figure 26**).

A similar reaction in which 2 mM SiI<sub>4</sub> was reduced with 4.5 equivalents of Super Hydride in an inverse micellar solution of DDAB in toluene at 10% by weight gave similar results. The reaction product was purified by HPLC with a size

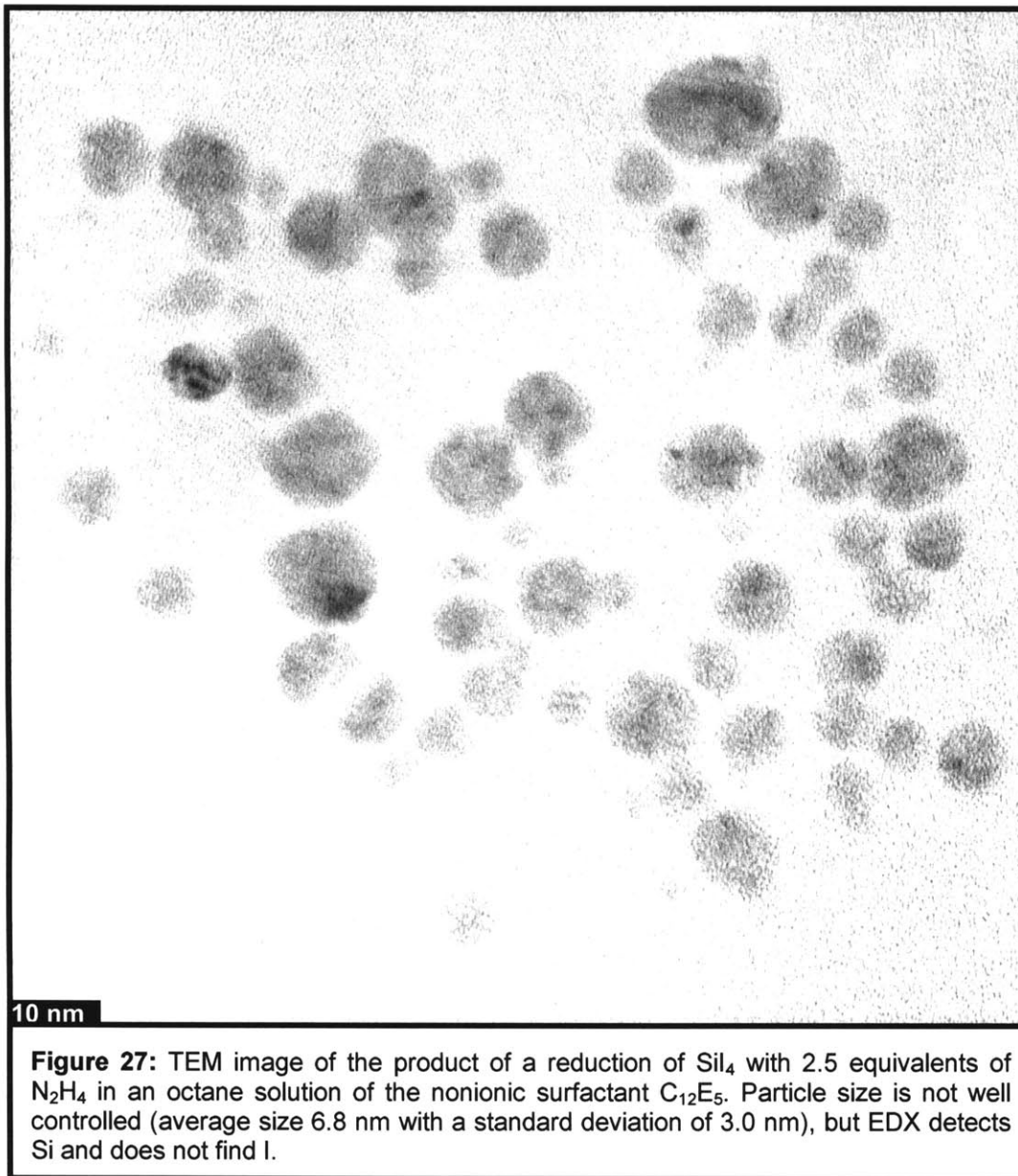
exclusion chromatography (SEC) column and two fractions were taken back-to-back from the HPLC run. No nanoparticles were seen in the early fraction by TEM. Only larger crystallites were seen, which is consistent with the early elution time, as larger particles cannot interact with the smallest pores of the column and pass through the column unimpeded. The second fraction from the HPLC contained Si nanoparticles with an average size of 4.3 nm and a standard deviation of 1.3 nm, as seen and measured by TEM. Energy dispersive X-ray spectroscopy (EDX) detected a considerable amount of Br, suggesting that the cationic surfactant either eluted at the same time as the product particles or that the surfactant was bound to the particle surface.

TEM does not sample the entire product, and so the amount of larger, crystalline material might be quite small and non-problematic. Still, given the broad range in particle size and the likelihood of the surfactant binding to the particle surface, it was decided to focus on reactions with nonionic surfactants instead of cationic surfactants like DDAB.

### **Synthesis According to the Literature: Nonionic Surfactants**

Although there is very little experimental detail in the five published reports that deal with Si and Ge nanoparticle synthesis,<sup>165,234,263-265</sup> in one paper there is a chromatogram from an HPLC run that has a peak labeled “C<sub>12</sub>E<sub>5</sub>”.<sup>265</sup> The nonionic surfactant C<sub>12</sub>E<sub>5</sub> is commonly used in metal nanoparticle synthesis and is somewhat of an all-purpose surfactant because of its balance between hydrophobicity and hydrophilicity.<sup>267,268,270-273</sup> A number of other surfactants have been reported as well, with more or fewer ether units and longer or shorter alkyl chains, but C<sub>12</sub>E<sub>5</sub> is the most common surfactant used and was the primary focus in the work described here.

There has been some controversy in the scientific literature regarding the synthesis of Si particles by inverse micellization because it is unclear if alkane-soluble Si precursor compounds are confined to the interior of the micelles.<sup>195</sup> There is another level of ambiguity in the synthetic mechanism in that the more aggressive cationic surfactants used for inverse micelle formation, the cationic surfactants DDAB and TOAB, might act to retard particle growth and any micellization might be irrelevant to the central mechanism of particle growth and size control. Due to the specific chemical interaction between the alcohol bearing

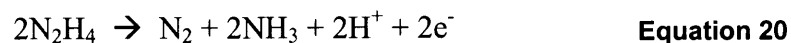


nonionic polyether surfactants and silicon tetrahalides, these nonionic surfactants might also act to retard particle growth, and any micellization in the system might be incidental.

In the research described here, the first promising results with the inverse micelle synthesis of Si nanoparticles came from a reduction of 1 mM  $\text{SiI}_4$  in a  $\text{C}_{12}\text{E}_5$  stock

solution in octane, using 2.5 H-equivalents (that is, 2.5 H from N<sub>2</sub>H<sub>4</sub> per 1 I from SiI<sub>4</sub>) of 1 M hydrazine in THF as the reducing agent. The reaction product was extracted into acetonitrile and further purified by HPLC using an SEC column and THF as the mobile phase. TEM found the Si product consisted of nanoparticles (**Figure 27**) with inconsistent shape and an average size of 6.8 nm and a standard deviation of 3.0 nm. EDX confirmed the presence of Si without detecting I.

The product from a similar reaction in which only 1 H-equivalent of hydrazine was used as the reducing agent appeared to have poor control over particle size and shape. In this reaction there is less than half of the amount of hydrazine used previously, and to fully reduce the tetrahalide silicon precursor perhaps another 3 or more equivalents would need to be added. This is because the reducing power of hydrazine is such that there may be only a single electron donated per molecule, not a single electron per H (**Equation 20**).<sup>291</sup>



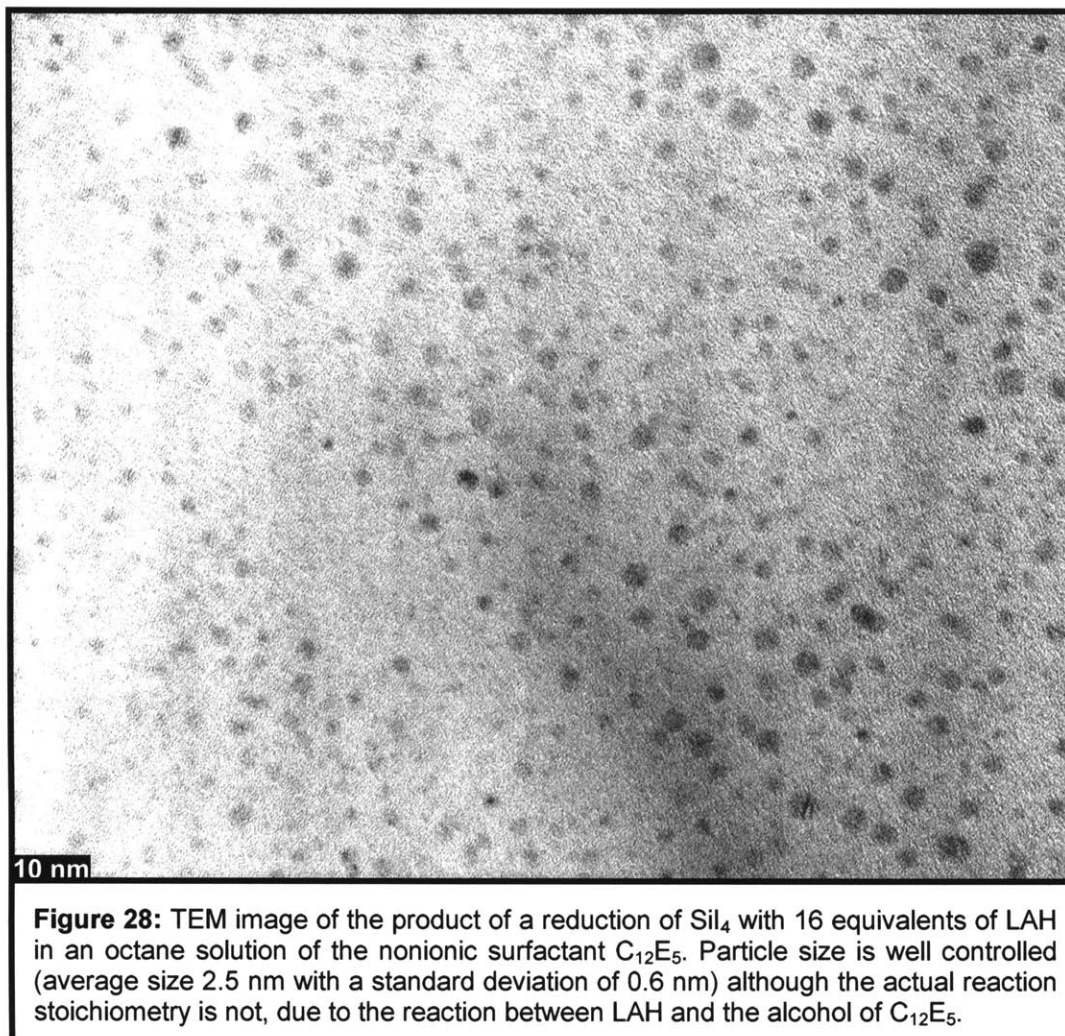
Under a variety of conditions, 1, 2, and 4 electrons can be gleaned from a single hydrazine molecule,<sup>291</sup> but in these reductions, with a haloacid as a byproduct, it might be expected that only 1 or 2 electrons of reducing power are obtained and that the acid forms complexes with the ammonia side product. When heavily substoichiometric, the reaction product had a broad range of sizes and shape control was poor, but even the promising 6.8 nm particles were the product of a substoichiometric reaction. In spite of this incomplete reduction, no I was detected, suggesting EDX was not sensitive enough due to low product concentration, there was separation of the product into I-rich and I-free materials or phases, or there was some additional reaction beyond that intended in the reaction. SiI<sub>4</sub> is photosensitive, readily liberating iodine (I<sub>2</sub>), and the Si-I bond could also be attacked by oxygen, water, or something else in the ambient prior to the TEM and EDX analysis.

Due to the reactivity of the unmodified surfactant's alcohol terminus with hydride reducing agents, a wide range of stoichiometries were investigated. In a reduction of 2 mM SiI<sub>4</sub> in a stock solution of C<sub>12</sub>E<sub>5</sub>, a large excess of the reducing agent LAH was used to ensure complete reduction, using 16 equivalents, or 4 equivalents under the assumption that only a single electron of reducing power is available from the reducing agent. A vigorous reaction between the surfactant and the reducing agent was seen on adding the LAH, as H<sub>2</sub> was released and bubbled

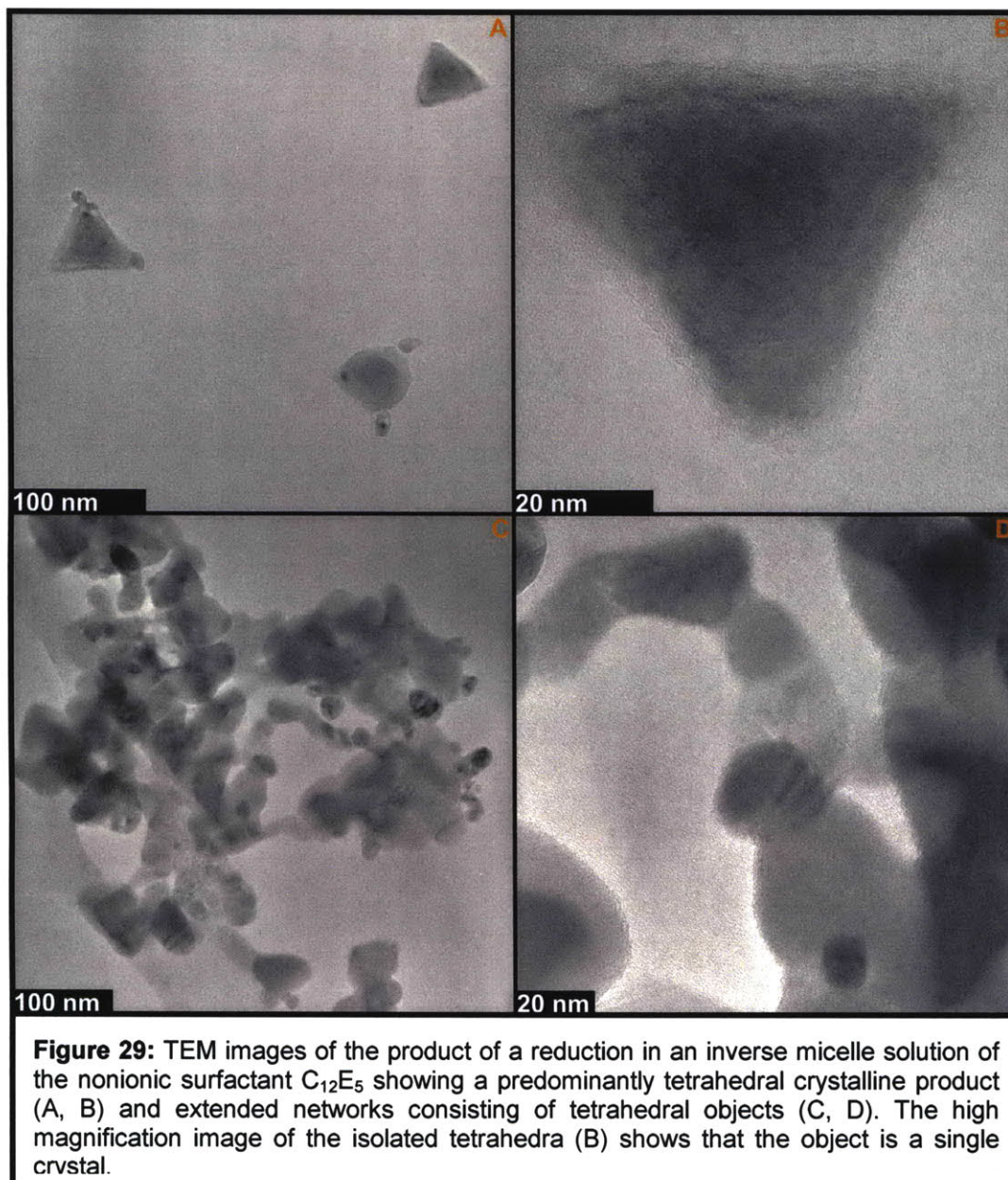
out of the reaction mixture, illustrating why an excess of the reducing agent was necessary. After reacting for 30 minutes and purifying by reverse phase HPLC, TEM (**Figure 28**) found the product to consist small, size monodisperse nanoparticles (average size 2.5 nm with a standard deviation of 0.6 nm). Unlike a number of the reactions carried out under substoichiometric reduction conditions, there was not a population of larger particles detected. While the TEM images obtained do not reveal crystallinity, lattice fringes were observed on the CRT monitor during TEM use. It is impossible to rule out the option that the majority of the particles seen on the TEM negative are amorphous, but much larger Si crystalline areas have been seen over the course of this work by TEM and lattice fringes were seen during TEM use, and so the absence of lattice fringes on the photographic negatives can most likely be attributed to the difficulty of imaging particles at the ~2 nm size scale.

Studies of the inverse micelle reaction were further extended to alternate Si precursors and reaction concentrations. Using  $\text{SiCl}_4$  as a precursor and increasing the concentration to 100mM, a reaction was carried out using 1.25 equivalents of LAH in THF at 1 M. The reaction conditions are within the bounds of the chemistry described in the limited publications on group IV materials and the more extensive publications on metal synthesis via reduction in inverse micelles, and it is assumed that the majority of the data published on Si nanoparticles synthesized in inverse micelles comes from reactions in which LAH was used as the reductant, as a handful of papers allude to its use, even if they do not clearly state that the presented data is from reactions using LAH. Also, private communications with the author revealed that LAH was most commonly used as the reducing agent.<sup>292</sup>

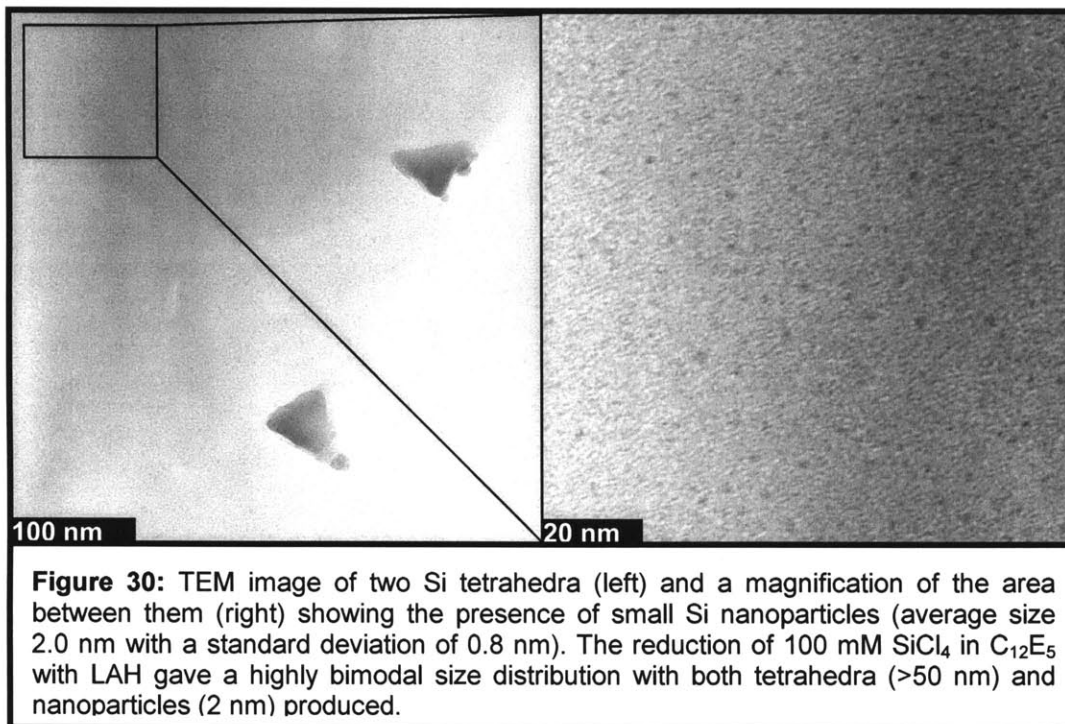
The largest difference between the reactions previously described and this reaction between  $\text{SiCl}_4$  and LAH is the increase in reactant concentration by two orders of magnitude. At this concentration the more reactive precursor  $\text{SiI}_4$  is not stable in the  $\text{C}_{12}\text{E}_5$  surfactant solutions, growing dark red in color and precipitating solids as the Si precursor decomposes. The  $\text{SiCl}_4$  solution is apparently stable, though, and the reaction proceeds like reactions carried out at lower concentrations. After purifying by HPLC, collecting the late fractions from a reverse phase column, the product was analyzed by TEM. The product was found to be highly bimodal, consisting of large tetrahedra and networks of tetrahedral growths (**Figure 29**), as well as small nanoparticles (**Figure 30** – average size 2.0 nm with a standard deviation of 0.8 nm). Single crystal tetrahedra



are observed, with sizes ranging from 50-80 nm and clear single crystallinity seen across a single tetrahedra with a base edge 64 nm across (**Figure 29 B**). The uniformity of these tetrahedra is noteworthy (average size 64 nm with a standard deviation of 9 nm), as no isolated tetrahedra are seen below 50 nm in size. There are, however, a number of smaller tetrahedra that appear to nucleate at the vertices of existing tetrahedra. While it is possible that these smaller tetrahedra grow in an isolated fashion and then self assemble and organize with the larger tetrahedra, this seems unlikely as the interaction between tetrahedra is not maximized in the arrangement and no self-organization was observed between larger tetrahedra. Usually, mixed systems self-segregate and systems of mixed nanoparticles organize into size-homogenous populations.



Tetrahedra have been reported in the literature from the reaction between  $SiCl_4$  and sodium naphthalenide in THF.<sup>195</sup> In an attempt to control growth by leaving an unreacted Cl-terminated surface, the reported reaction is carried out with a 20% deficiency of the reducing agent. The remaining unpassivated surface sites are further reacted with an alkylating agent. The product is found to consist of



tetrahedra of a similar size to those reported here. The major differences in the reaction conditions reported here and that reported in the literature is the use of a hydride reducing agent and the use of a nonionic surfactant solution as the reaction medium. The reaction product differs in that the product is highly bimodal and that in addition to the isolated tetrahedra there are extended crystalline Si networks, often with tetrahedral subunits.

The effective stoichiometry of the reaction is difficult to determine because of the reactivity between the reducing agent and the surfactant itself. So, although a slight excess of the reducing agent was used, the actual amount of LAH available to react with SiCl<sub>4</sub> might be less than stoichiometric, and might approximate the stoichiometry of the published tetrahedral formation reaction.<sup>195</sup> At the same time, the surfactant, which is expected to react with the Si precursor, SiCl<sub>4</sub>, might react with and effectively cap any remaining Si-Cl bonds at the tetrahedra surface, allowing for product's hydrophobicity, reflected in the late retention times on the reverse phase column used for purification.

Further complicating the reaction is the presence of a large volume of THF. For a 1 mL reaction at 100 mM, 125 μL of 1 M LAH in THF are added. While THF is



miscible with the octane surfactant solution used and might be expected to swell inverse micelles with unknown effects on nanoparticle growth, the presence of ionic reactants and byproducts induces a phase separation. In the absence of agitation, the reaction mixture separates into a polar lower layer and a nonpolar upper layer. Consistent with THF constituting the majority of the lower layer is the ratio of the layer volumes, which is approximately 1:10. Presumably, the precursor and the reducing agent can be found in both layers during the reaction, and perhaps two distinct reactions can occur: one in the interior of inverse micelles in the upper layer, and the other in THF in the lower layer. Each of these reactions could produce distinct materials, leading to the bimodal size distribution and the observation of both small nanoparticles and large tetrahedra.

The relationship between the possible reactions in the inverse micelle solution and in THF is unclear. It is possible that there is exchange between the inverse micelle layer and the THF layer and that some nanoparticles from the micellar solution are consumed in the growth of the tetrahedra. Although most of the tetrahedra have smooth and straight edges, there are some with a more scalloped appearance where it appears that nanoparticles may have stuck to the surface or been incorporated as a part of the growth process. Further exploration of these two competing growth processes and their relations should be useful not only for reactions at high concentrations where the separation into a polar and nonpolar phase is obvious, but also for lower concentration reactions where there may be similar phase separation or substantial inverse micelle swelling. Also of question is the surface termination for both the published product and the tetrahedra reported here, as both products appear to have an oxide at the surface, but the tetrahedra reported here clearly retain at least some crystallinity at the tetrahedra surface.

Synthesis in surfactant solutions of the unmodified surfactant  $C_{12}E_5$  were found to produce nanoparticles (**Table 4**), but the possibility of the surfactant alcohol group reacting with the halosilane precursor, the nanoparticle product surface, and hydride reducing agents made the reaction undesirable. However, the observation that nanoparticles could be produced by reduction with both hydrazine and LAH was promising as it suggested a range of reducing agents might be selected in order to tune the product size or to aid in product work up or yield. If the reaction could be extended to capped surfactants, then there was the possibility that this synthetic chemistry might be used for the formation of Si nanocrystal inks.

Precursor	Concentration	Reductant	Stoichiometry	Average Size	Standard Deviation
SiI <sub>4</sub>	2 mM	N <sub>2</sub> H <sub>4</sub>	1 eq.	Uncontrolled	N/A
SiI <sub>4</sub>	1 mM	N <sub>2</sub> H <sub>4</sub>	2.5 eq.	6.8 nm	3.0 nm
SiI <sub>4</sub>	2 mM	LAH	16 eq.	2.5 nm	0.6 nm
SiCl <sub>4</sub>	100 mM	LAH	1.25 eq.	64 nm	2.0 nm

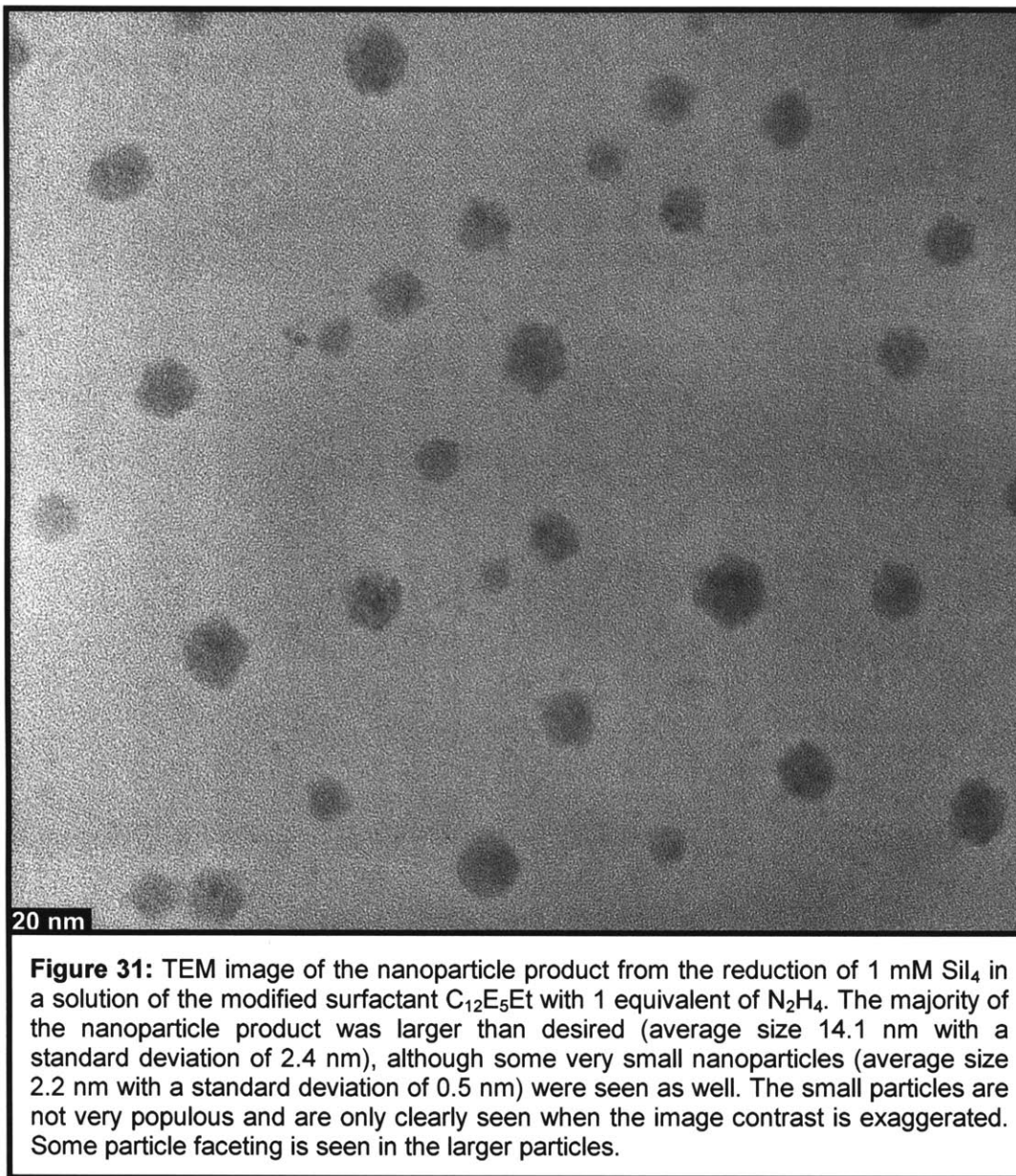
**Table 4:** Comparison of reaction products from reductions in the inverse micelle solutions of the unmodified nonionic surfactant C<sub>12</sub>E<sub>5</sub>. Low concentrations (2 mM) and a stoichiometric excess of the reducing agent were found to provide the smallest nanoparticles (shown in red).

### Synthesis with Modified Nonionic Surfactants: Hydrazine Reductions

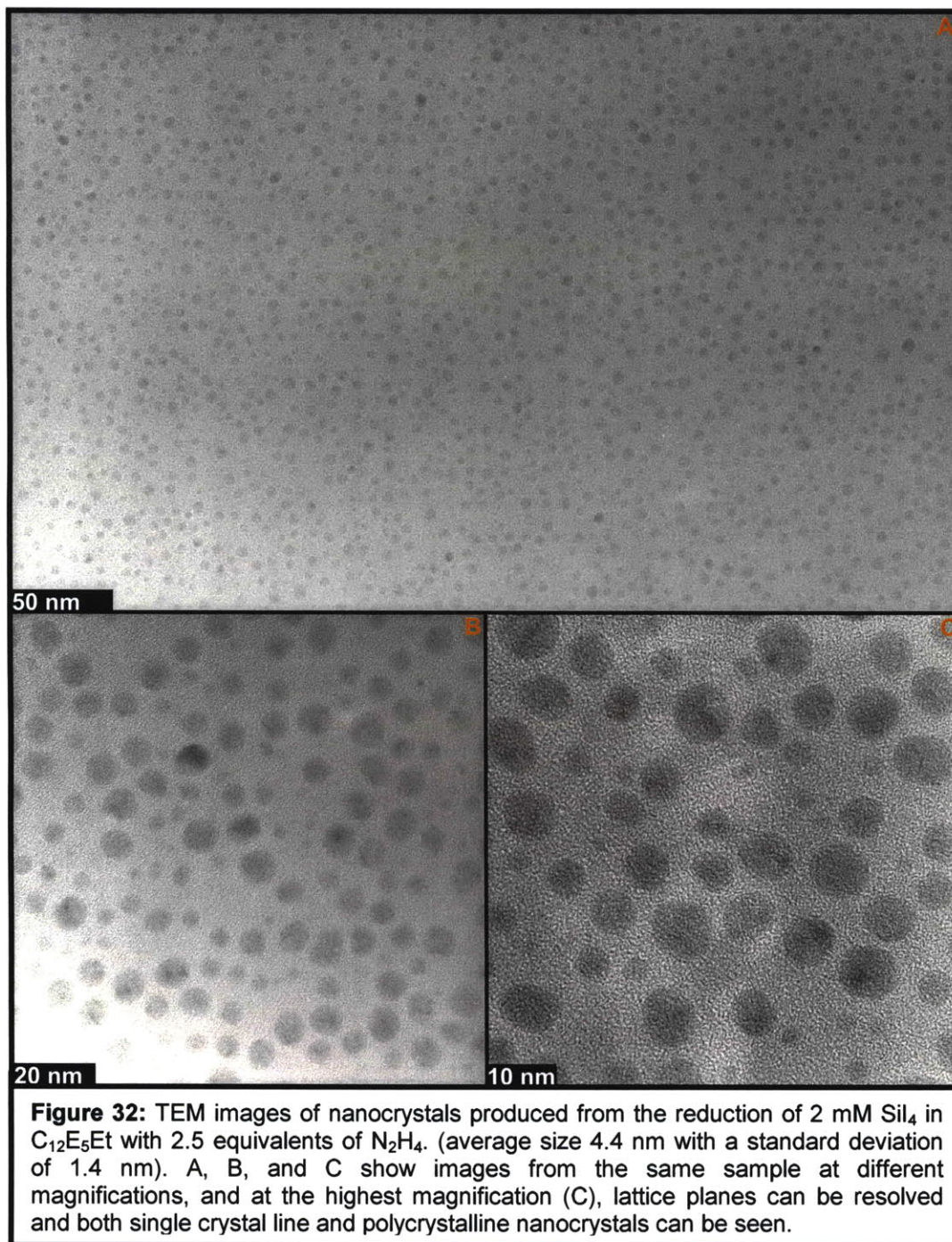
The majority of the work done as a part of this thesis project was carried out using the modified surfactant CH<sub>3</sub>C<sub>11</sub>H<sub>22</sub>(OCH<sub>2</sub>CH<sub>2</sub>)<sub>5</sub>OCH<sub>2</sub>CH<sub>3</sub> (C<sub>12</sub>E<sub>5</sub>Et), an analog of the nonionic surfactant C<sub>12</sub>E<sub>5</sub> that was used in the Si nanoparticle and tetrahedra syntheses previously described. In addition to sidestepping concerns with the surface termination from reactions using cationic surfactants and traditional nonionic surfactants, capped nonionic surfactants allow further modification of surface chemistry and can provide insight into the somewhat controversial synthetic mechanism. The capped surfactant helps in elucidating the mechanism by ruling out pathways that rely upon direct chemical reactivity between the surfactant and precursor and the surfactant and reducing agent.

At low concentrations (1-10 mM), solutions of SiI<sub>4</sub> appeared to be similar in both C<sub>12</sub>E<sub>5</sub> and C<sub>12</sub>E<sub>5</sub>Et. The SiI<sub>4</sub> readily dissolved over a few minutes and formed a pale to moderate yellow colored solution. Over the course of a few days, however, the C<sub>12</sub>E<sub>5</sub>Et solution invariably became unstable, becoming first orange and then red in color and precipitating solids. The C<sub>12</sub>E<sub>5</sub> solutions appeared to be stable at these lower concentrations, though, suggesting that the surfactant might have reacted with the precursor, producing a more stable precursor (**Equation 19**).

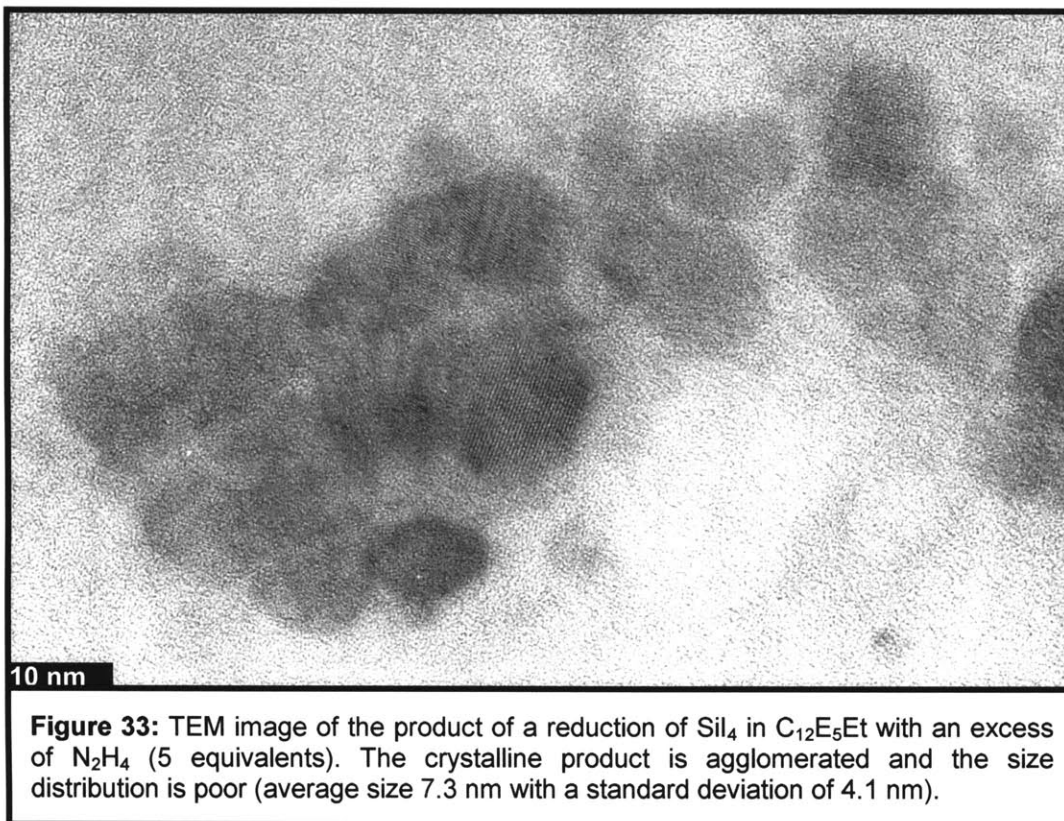
However, at high concentrations, such as those used in the 100 mM SiCl<sub>4</sub> reactions that yielded a bimodal distribution of nanoparticles and tetrahedra, C<sub>12</sub>E<sub>5</sub> solutions of SiI<sub>4</sub> were not stable enough to dissolve the precursor at the desired concentration and the solution rapidly degraded into a dark red solution



with a sludgy precipitate. Highly concentrated solutions of  $\text{SiI}_4$  were readily made in  $\text{C}_{12}\text{E}_5\text{Et}$ , though. Like their low concentration analogs, these  $\text{C}_{12}\text{E}_5\text{Et}$  solutions degraded over the course of a few days, but they were stable enough to carry out a series of reactions.

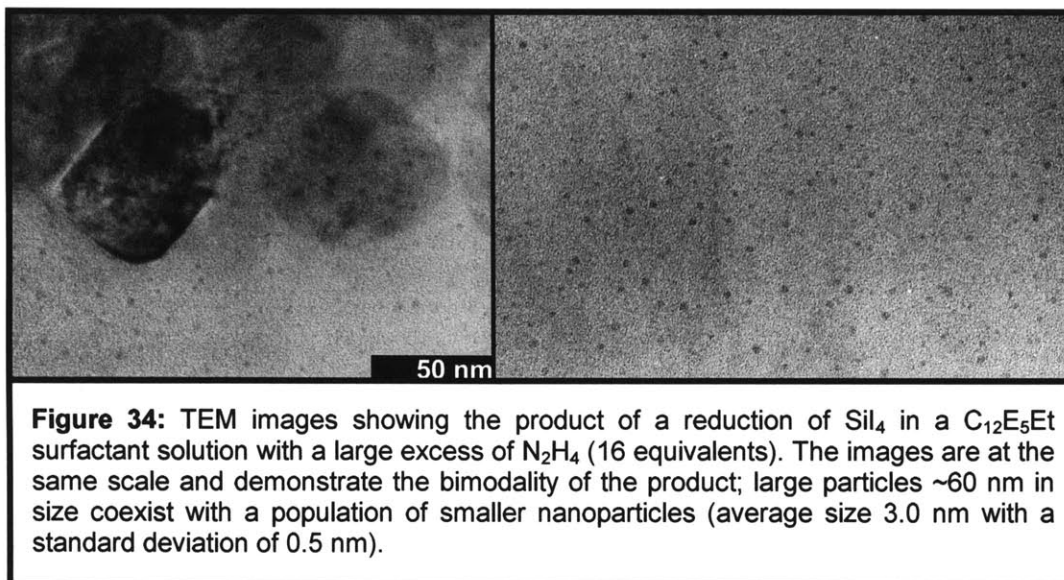


The first reductions carried out in the capped surfactant  $\text{C}_{12}\text{E}_5\text{Et}$  were done with a low concentration of  $\text{SiI}_4$  and only 1 H-equivalent of 1 M hydrazine in THF,



which, as described previously for the analogous reaction in  $\text{C}_{12}\text{E}_5$ , is a substoichiometric amount of hydrazine, as each hydrazine molecule has the reducing power of only a single electron. Similar to the results seen in  $\text{C}_{12}\text{E}_5$  for such substoichiometric conditions, the bulk of the nanoparticle product was larger than desired (**Figure 31** – average size 14.1 nm with a standard deviation of 2.4 nm). However, very small nanoparticles (average size 2.2 nm with a standard deviation of 0.5 nm) were faintly seen in the reaction product mixture as well. In addition to these small particles, the larger particles were faceted, showing a tendency to have a hexagonal shape. The faceting and small particle populations are easily seen when the image contrast is heavily exaggerated.

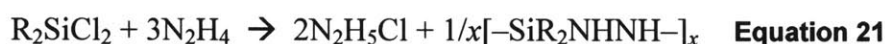
At a slightly higher concentration and under more stoichiometric reaction conditions, the reaction product appears to be more consistent, mirroring the trend seen with the analogous  $\text{C}_{12}\text{E}_5$  reaction. Using 2.5 H-equivalents hydrazine (1 M in THF) to reduce a 2 mM solution of  $\text{SiI}_4$  in a  $\text{C}_{12}\text{E}_5\text{Et}$ /octane stock solution results in a reaction product with a more uniform size distribution and a tighter size control of the larger particles (**Figure 32** – average size 4.4 nm with a standard



deviation of 1.4 nm). Even though nanoparticle fields can be seen extending over very large areas, areas of lower coverage were found in which a smaller particle population dominates (average size 2.4 nm with a standard deviation of 0.4 nm), faintly seen surrounding the sparse population of larger particles. So, TEM might not provide a representative or accurate view of the product, even in cases where the sampled population is large and the consistency appears to be very good. At the same time, the wide fields of nanoparticles (**Figure 32**) also indicate that there is a bimodal distribution, with populations centered around 2 and 4-5 nm. Similar to the possibility of reduction in a second polar phase and within the alkane micelle solution producing two types of materials in the reduction that yielded both  $>50$  nm tetrahedra and 2 nm nanoparticles, reduction in the interior of micelles and in the free alkane solution might lead to two different particle size populations like the 2 and 4-5 nm sizes seen here (**Figure 32**).

EDX of this reaction product found no trace of I, similar to the analogous reaction in  $\text{C}_{12}\text{E}_5$ , even though a substoichiometric amount of hydrazine was used in the reduction. This is not wholly surprising as the unreacted Si-I bonds that are expected to remain might be removed as molecular byproducts or unreacted starting material during HPLC purification, they might go undetected if the concentration is low or if there is self-segregation in the material or phase separation, or remaining Si-I bonds might degrade due to the presence of oxygen, water, or ambient light.

Reactions in  $C_{12}E_5Et$  surfactant solutions without a deficiency of hydrazine yielded a multi-modal and partially agglomerated product similar to the analogous reactions in the cationic surfactant DDAB. Compared to the substoichiometric reactions with hydrazine, using 5 H-equivalents of the reducing agent yielded a larger agglomerated product with a broad size distribution (**Figure 33** – average size 7.3 nm with a standard deviation of 4.1 nm). While LAH is known to produce silane ( $SiH_4$ ) from  $SiCl_4$  (**Equation 12**), no such H-termination is known with hydrazine reductions. In fact, polymeric Si-N complexes have been reported for the reaction between alkylchlorosilanes and hydrazine (**Equation 21**).<sup>293,294</sup>



In substoichiometric reactions with hydrazine, both the surfactant solution and halide might act as caps, controlling nanoparticle growth. Similarly, in reactions with LAH, H-capped surfaces might retard particle growth. However, if the Si-H surface termination is inaccessible to reactions that use hydrazine as a reducing agent, stoichiometric reactions might remove a critical component of the size control mechanism (Si-Y) and would not introduce a substitute (Si-H), inducing undesirable growth and agglomeration.

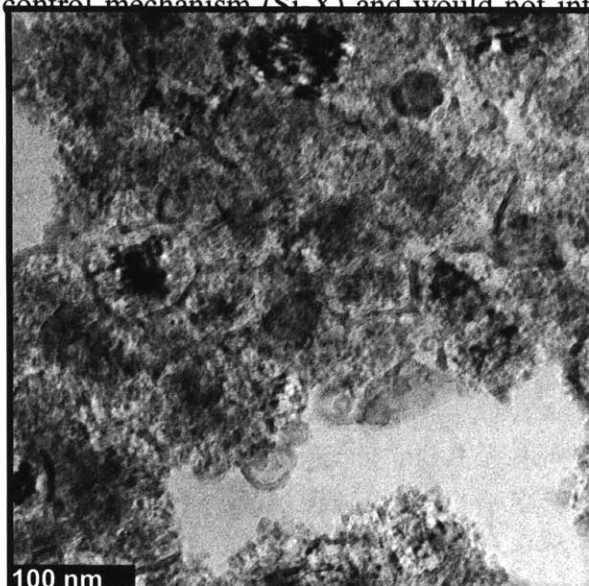
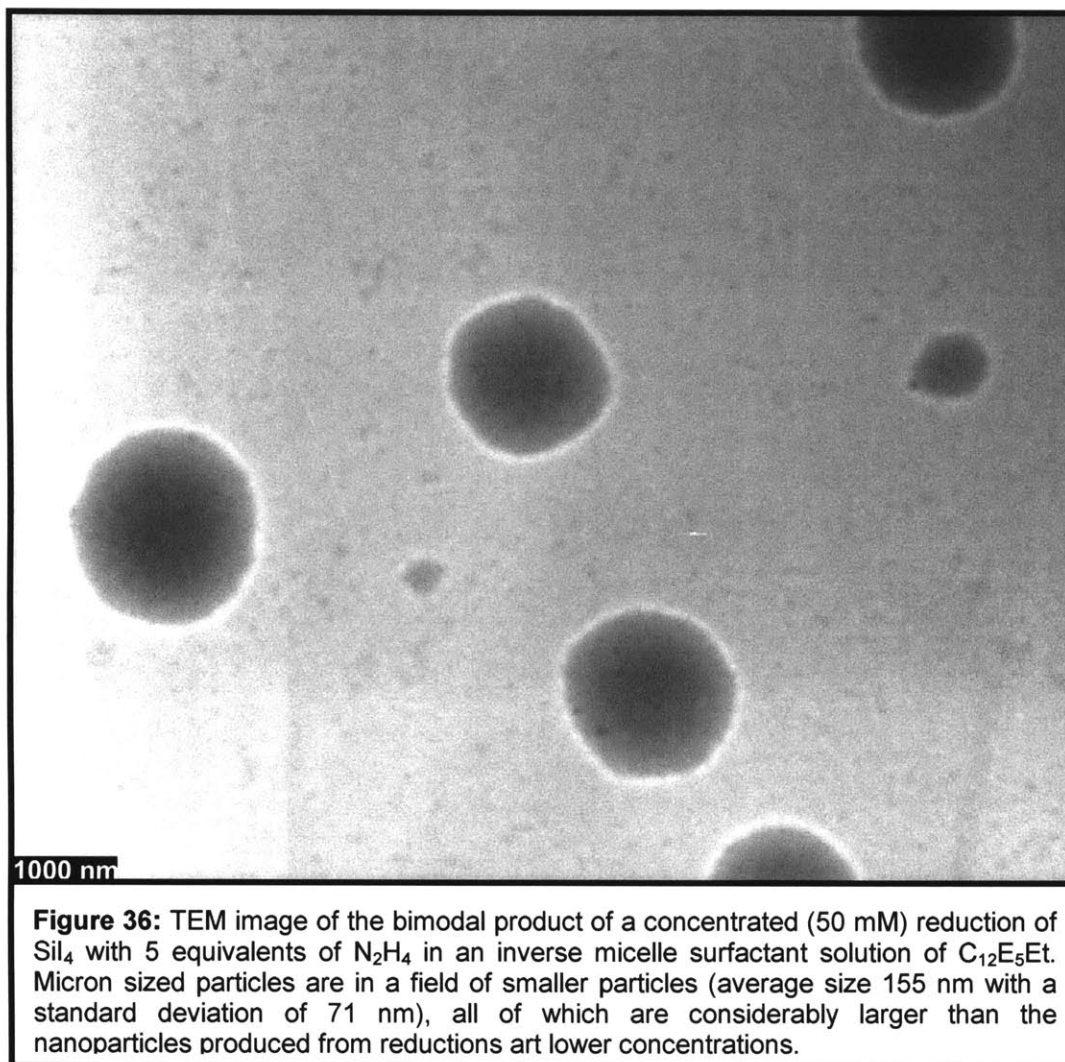


**Figure 35:** TEM image of the product of a 16 equivalent hydrazine reduction of a 10 mM solution of  $SiCl_4$  in  $C_{12}E_5Et$ /octane. The product is highly agglomerated and consists of both small nanoparticles (~5 nm) and larger structures.

Upon increasing the amount of hydrazine to 16 eq., a partially agglomerated bimodal product is seen (**Figure 34**). The larger particles in the agglomerates are ~60 nm in size, but there is also a smaller population of nanoparticles throughout (average size 3.0 nm with a standard deviation of 0.5 nm).

A similar reaction with 16 eq. hydrazine at a slightly higher reaction concentration (10 mM) yields a highly agglomerated product (**Figure 35**). Although no individually isolated



nanoparticles are detected, a number of the agglomerates clearly consist of small, ~5 nm particles.

Moving to considerably higher reaction concentrations, a reaction at 50 mM  $\text{SiI}_4$  in  $\text{C}_{12}\text{E}_5\text{Et}$  with 5 H-eq. hydrazine yielded a large bimodal product (**Figure 36**). Micron sized particles were seen amid a field of smaller particles (average size 155 nm with a standard deviation of 71 nm). Both sizes of the product are much larger than the product from any of the reactions carried out at lower concentrations. The large size of both populations is unique, as most of the reactions yield smaller material ranging from 2-4 nm. At the magnification of the image showing the large nanoparticles and microparticles it would not be possible



to see such small particles, but no particles are seen anywhere near 10nm, as the smallest particles are more than 80 nm in diameter. It seems that at higher concentrations considerably larger than 10 mM, Si growth is not well controlled and the dominant product is outside of the range of sizes over which strong size dependent melting effects have been reported.<sup>37</sup>

Hydrazine reductions in inverse micelle solutions of the unmodified surfactant C<sub>12</sub>E<sub>5</sub>Et were found to produce nanoparticles ranging from ~2 nm to agglomerations and particles in excess of 1 μm (Table 5). The reaction became uncontrolled when substoichiometric hydrazine was used (1 eq.), when a large excess of hydrazine was used (16 eq.), and when the Si concentration was too high (10 mM and above). It was encouraging that Si nanocrystals were seen from these reductions, even if the range of synthetic conditions was fairly narrow, due to the possibility of obtaining Si-N polymers, instead (Equation 21). Hydride reducing agents seemed to hold more promise, as the likelihood of hydrogen termination (Equation 12) seemed high and the increased reducing strength might lead to smaller particles<sup>267,268</sup> (Table 4) better suited to nanocrystal ink formulation.

Precursor	Concentration	Reductant	Stoichiometry	Average Size	Standard Deviation
Si <sub>4</sub>	1 mM	N <sub>2</sub> H <sub>4</sub>	1 eq.	14.1 nm 2.2 nm	2.4 nm 0.5 nm
Si <sub>4</sub>	2 mM	N <sub>2</sub> H <sub>4</sub>	2.5 eq.	4.4 nm	1.4 nm
Si <sub>4</sub>	2 mM	N <sub>2</sub> H <sub>4</sub>	16 eq.	>50 nm 3.0 nm	N/A 0.5 nm
Si <sub>4</sub>	10 mM	N <sub>2</sub> H <sub>4</sub>	16 eq.	>5 nm	Agglomerated
Si <sub>4</sub>	50 mM	N <sub>2</sub> H <sub>4</sub>	5 eq.	>1 μm 155 nm	N/A 71 nm

**Table 5:** Comparison of reaction products from hydrazine reductions in inverse micelle solutions of the modified nonionic surfactant C<sub>12</sub>E<sub>5</sub>Et. Low concentrations (2 mM) and a moderate stoichiometric excess of the reducing agent were found to provide the smallest nanoparticles (shown in red).

## Synthesis with Modified Nonionic Surfactants: Hydride Reductions

Although hydrazine was initially investigated as a reducing agent for these Si nanoparticle reactions, the possibility of the use of hydrazine yielding polymeric Si-N materials and the concern regarding surface termination led to the investigation of other reducing agents. Hydride reducing agents were the most attractive because of the increased likelihood of forming hydrogen-capped Si nanoparticles. Due to their reactivity with water, these hydride reducing agents ensure a water-free reaction environment, but they can also react with any uncapped alcohols in the surfactant. It has been reported that particle size is inversely proportional to the strength of the reducing agent used,<sup>267,268</sup> and for the hydride reducing agents, the strongest reducer is LAH, which may have reactive byproducts that tend to form gels and that are difficult to remove from the reaction mixture. Also, LAH has 4 hydrogen atoms available for reaction, but the reactivity of the four are not the same, complicating the mechanistic understanding of the reaction. Reducing agents such as superhydride have only a single hydrogen atom available for reaction and offer more attractive byproducts, but they do not provide the same reducing power. The three hydride reducing agents that were primarily examined were LAH, Red-Al, and superhydride.

Of the hydride reducing agents used in this work, Red-Al is unique in that it has two reactive hydrogens and is commercially available as a solution in toluene, not in THF. The solubility in toluene and the miscibility of toluene with alkanes suggests that reduction of the silicon tetrahalide precursor might occur outside of the interior of the inverse micelle, instead occurring in the alkane phase. Since the silicon precursor has some solubility in both the polar interior of the inverse micelles and the nonpolar continuous oil medium, in reactions with more polar reducing agents the localization of the reduction within the confines of the inverse micelles might be the result of the solubility of the reducing agents in the micellar interior. In fact, the polarity of the THF-soluble reducing agents LAH, superhydride, and hydrazine might be largely responsible for confining particle growth to the interior of the inverse micellar solution. If all or some of the reaction between Red-Al and silicon tetrahalide occurs outside of the interior of the inverse micelles, unique growth could be expected.

A 2 mM solution of SiI<sub>4</sub> in a C<sub>12</sub>E<sub>5</sub>Et/octane stock solution was reduced with 2 H-equivalents of Red-Al in toluene. After purifying with HPLC (using both SEC and reverse phase columns), TEM found a nanoparticle Si product with a broad

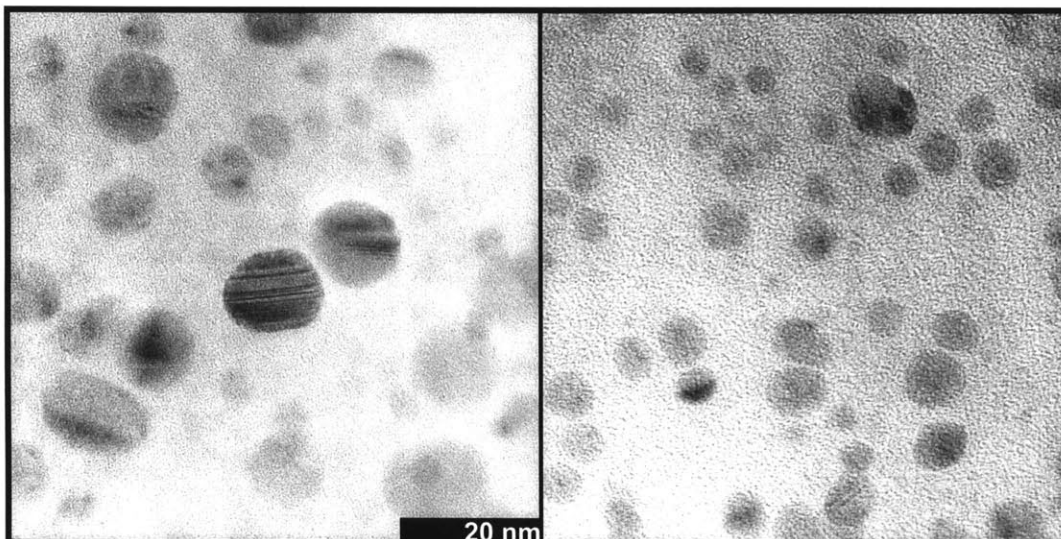
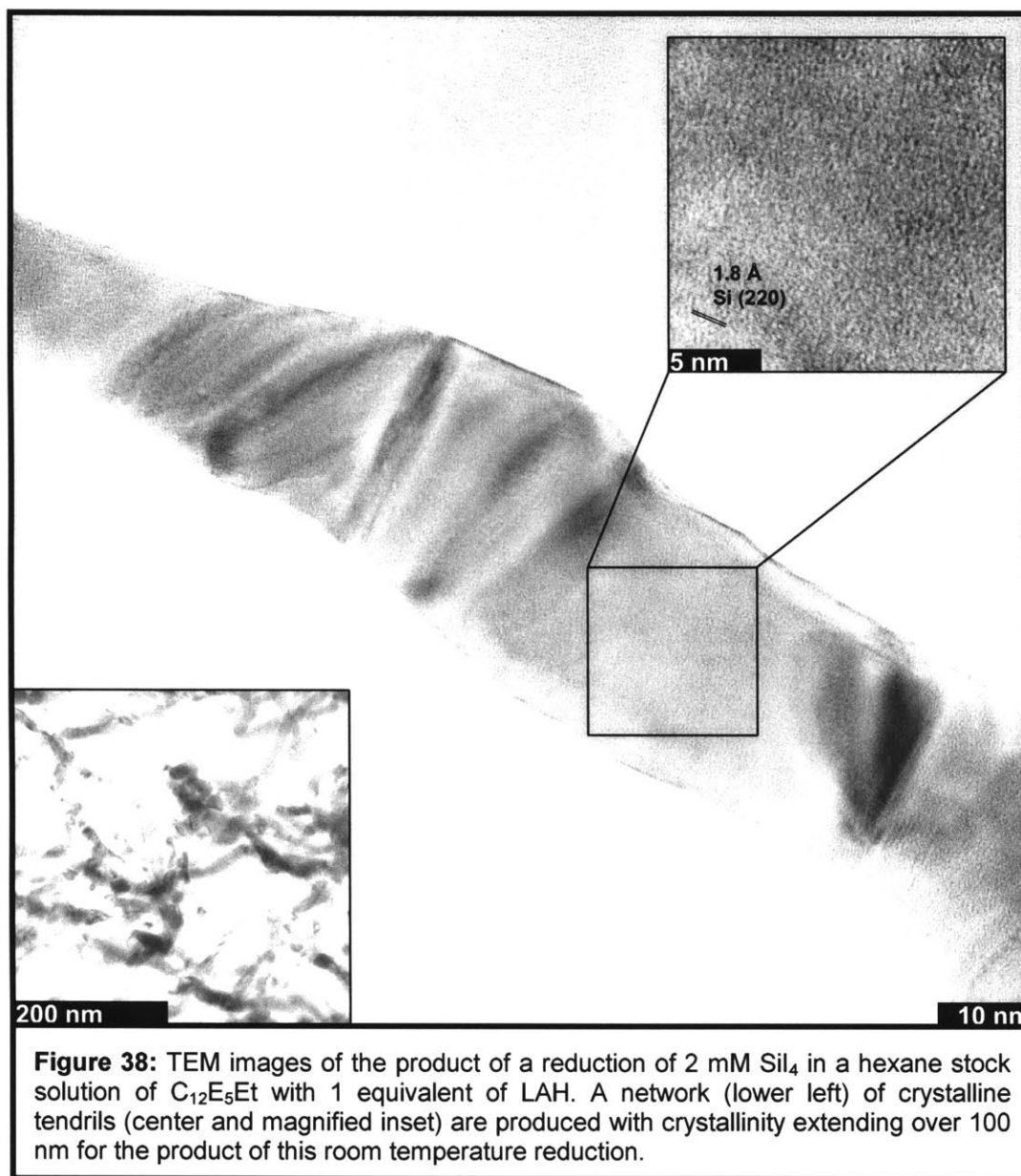


**Figure 37:** TEM images showing the product from the reduction of 2 mM  $\text{SiI}_4$  with an excess of Red-Al. The larger particles ((average size 13.0 nm with a standard deviation of 3.0 nm, left) were observed to have self-segregated from the smaller particles (average size 5.4 nm with a standard deviation of 1.8 nm, right) on the TEM grid. For similar reaction conditions, Red-Al produced larger nanoparticles than reactions employing  $\text{N}_2\text{H}_4$  or LAH as the reducing agent.

size distribution and oblong and round shape (**Figure 37**). Size segregation was seen on the TEM grid, with larger particles sitting closer to the grid bars (average size 13.0 nm with a standard deviation of 3.0 nm) and smaller particles sitting further toward the middle of the amorphous-C grid (average size 5.4 nm with a standard deviation of 1.8 nm). Both populations are considerably larger than the analogous populations that result from reactions with hydrazine and from the more monodisperse product from reactions with LAH. The shape of the particles is also unique, as the majority of particles are round and larger particles tend to have a slightly oblate, pill shape. Some of these larger particles show crystal facets and in one case a tetrahedral core is seen at the center of a round particle.

The larger size and unique shape of the Red-Al product suggest that there is a difference in the control of particle growth when Red-Al is used as a reducing agent. It seems likely that the larger sizes and oblate shapes are the result of unconfined reduction occurring outside of inverse micelles, similar to the tetrahedral particles seen in high concentration reactions in  $\text{C}_{12}\text{E}_5$  that seem likely to result from reduction outside of inverse micelles and in the separated THF layer. Growth outside of the inverse micelle interior would be expected to be



uncontrolled if there is an absence of either steric or chemical retardation of particle growth; the continuous oil medium of the surfactant solution is an example of such a non-interacting solution.

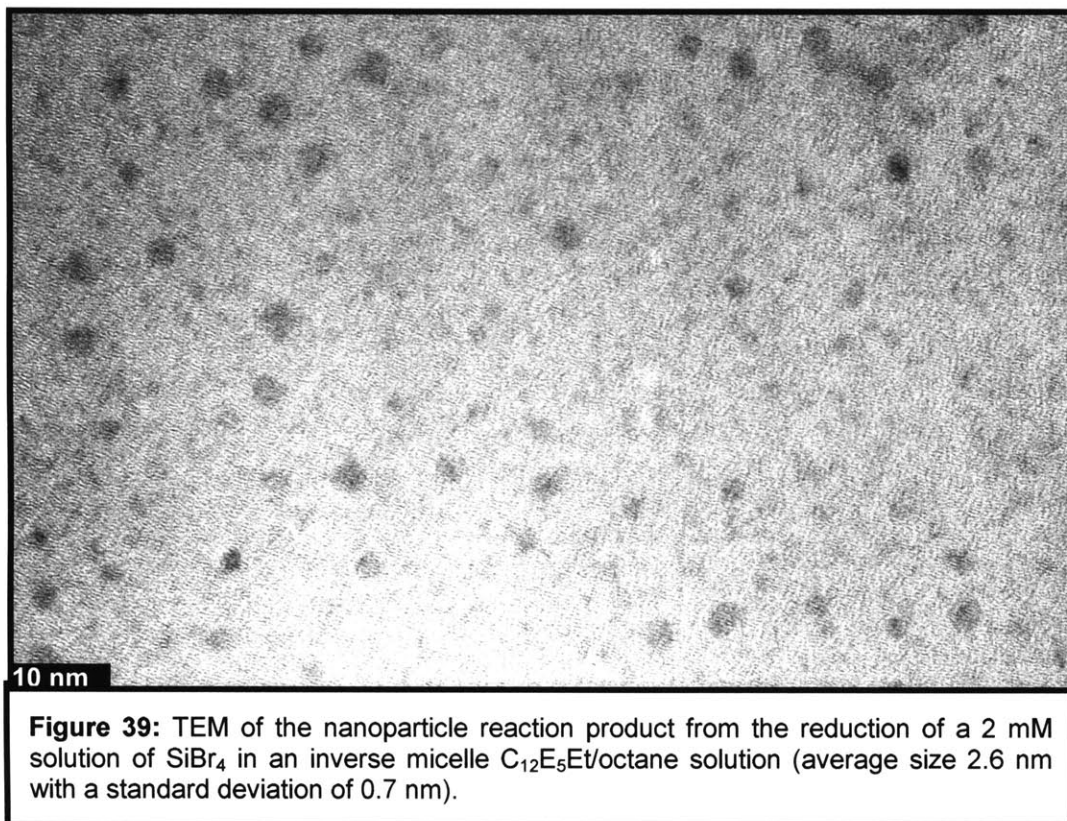
At high concentrations like those employed to synthesize Si tetrahedra in  $\text{C}_{12}\text{E}_5$ , the dissolution of ionic materials in THF induces a phase separation. By using

Red-Al in toluene, there is no polar solvent present to phase separate. However, a very small amount of a colorless, oily separated layer can be seen at the bottom of the reaction vessel when Red-Al is used. It is assumed that this layer consists predominantly of surfactant and dissolved ionic byproducts. Phase separation in inverse micelle solutions have been reported for both inorganic salt solutions at high concentrations and product/byproduct solutions.<sup>267,268</sup>

The majority of reactions carried out with hydride reducing agents used a 1 M solution of LAH in THF. A broad range of reaction stoichiometries were investigated in order to assess the role of stoichiometry in particle size distribution and surface termination. The stoichiometry in LAH reductions in  $C_{12}E_5$  was complicated by the reaction of LAH with the surfactant's alcohol terminus, but no alcohols are free with the capped  $C_{12}E_5Et$  surfactant. Still, the difference in the reducing power of each of the four hydrides of LAH allows for an unclear situation and stoichiometry might control particle size, if not shape and surface termination.

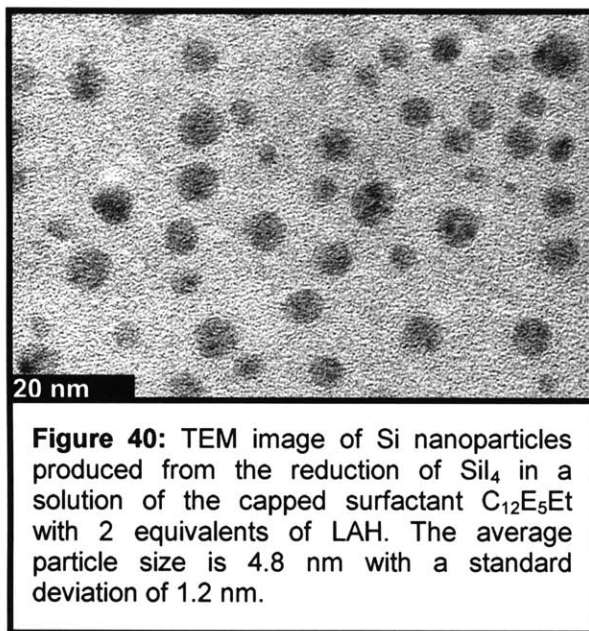
Similar to substoichiometric reactions with hydrazine in both  $C_{12}E_5$  and  $C_{12}E_5Et$ , a single equivalent of LAH led to uncontrolled Si growth in 2 mM  $SiI_4$  in a hexane stock solution of  $C_{12}E_5Et$ . Although the growth was uncontrolled, the nature of the growth was unique in that a network of Si wires and tendrils was produced (**Figure 38**). Additionally, the reaction was different from those using hydrazine in that it was intended to be stoichiometric – any substoichiometry was minimal and was due to human or equipment error in the solution preparation or handling or due to the low reducing power of the partially spent LAH. The crystallinity seen in the product from this reaction is remarkable. Similar to the synthesis of tetrahedra, the reaction produces single crystal wires and networks with single crystalline tendrils stretching over 100 nm in length.

Using a slight stoichiometric excess of 1.25 eq. LAH, small nanoparticles were seen as the only product in a reduction of 2 mM  $SiBr_4$  in a  $C_{12}E_5Et$  stock solution in octane (**Figure 39**). Unlike the multi-modal reaction products from reduction with a comparable excess of hydrazine, the HPLC-purified nanoparticle product from this LAH reaction is not bimodal and no particles are detected larger than 4.5 nm. Although the reactivity of  $SiBr_4$  is lower than that of  $SiI_4$ , perhaps leading to the expectation that a larger particle product should result from the use of  $SiBr_4$  when compared to  $SiI_4$ , the product from the reduction of  $SiBr_4$  is found to be very small (average size 2.6 nm with a standard deviation of 0.7 nm), suggesting



that for  $\text{SiBr}_4$  and  $\text{SiI}_4$ , the reactivity of the reducing agent controls the product size more than the Si precursor. This seems to be the case even though the ratio of the most active hydrogen of LAH to reactive Si-halogen bonds is 0.3:1, requiring the reaction of less-reactive hydrides to afford complete reduction of the Si precursor.

Imaging the product of the reduction of  $\text{SiBr}_4$  with 1.25 eq. LAH was very difficult, as the field of nanoparticles captured by the photographic negative of the TEM was not seen on the monitor during TEM use. Instead, only a single, monocrystalline nanoparticle was seen. The particle passed from the field of view of the instrument's monitor due to stage movement, and after settling, an image was taken in the area, with the hope that the particle and any other undetected particles in the vicinity might fall within the larger field of view of the negative. In fact, hundreds of particles were imaged by the negative, and the fact that they could go undetected at the time of use suggests that there can be error in TEM measurements, especially when imaging smaller nanoparticles or when the user is unaware of smaller nanoparticles. With TEM it is always possible to overlook a

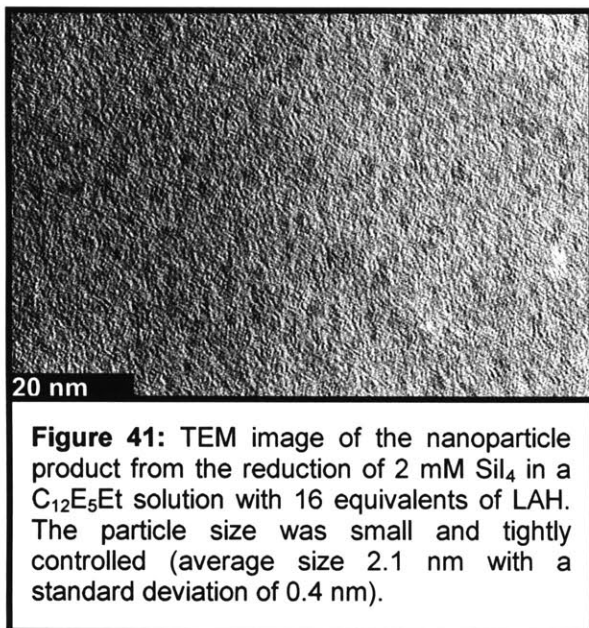


segment of the product population due to phase separation and sampling only sub-populations, but it is also possible to be unable (or unaware of the ability) to detect Si nanoparticles because of their small size, the poor contrast of Si, or the possibility of amorphous particles. In this sample, the product is believed to be crystalline, even though the image does not show any crystal lattice fringes. At the time of the measurement, only a single particle was detected, and lattice fringes were observed for the

nanoparticle. These fringes are not seen on the negative, and it is possible that the focusing and TEM operation were not able capture the nanoparticle lattice fringes for such a small and low contrast sample. Furthermore, much larger Si crystalline areas from similar reactions have been routinely imaged throughout this work and it seems unlikely that the largest particles are crystalline and the smallest particles are amorphous.

The alkane-solubility of  $\text{SiBr}_4$  and  $\text{SiCl}_4$ , both liquids at room temperature, is higher than for  $\text{SiI}_4$ , a solid. If reduction were able to occur in the continuous oil medium of the surfactant solution instead of the inverse micelle interior, a difference in product size might be expected from the use of  $\text{SiI}_4$  and  $\text{SiBr}_4$ , as the  $\text{SiBr}_4$  would be more susceptible to reduction in the nonpolar medium. The  $\text{SiBr}_4$  might be expected to appear similar to the product seen from the Red-Al reactions, in which the use of the toluene-soluble reducing agent leads to a larger distribution of particle sizes and particle shapes. The fact that this is not seen suggests that the reduction occurs in the micelle interior and that at low concentrations the reduction with LAH is fairly insensitive to the alkane-solubility of the Si tetrahalide.

By increasing the amount of LAH used in the reduction of 2 mM  $\text{SiI}_4$  in  $\text{C}_{12}\text{E}_5\text{Et}$  to 2 eq. of the reducing agent, there is enough reducing agent to reduce half of the

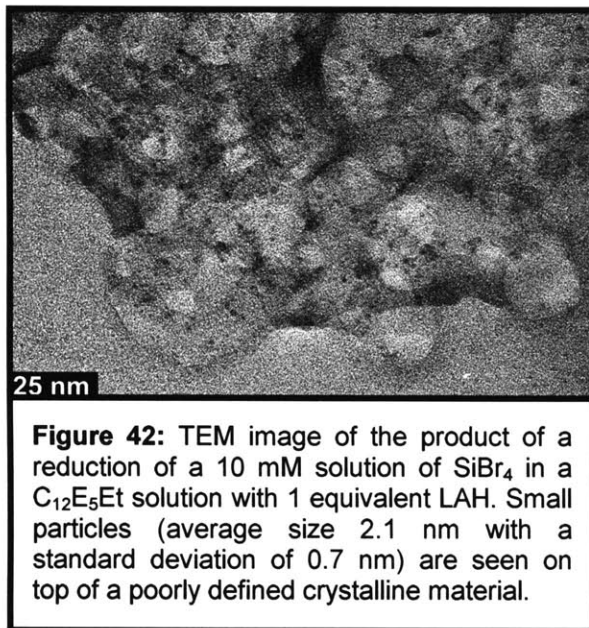


Si-halogen bonds with the most reactive hydride of LAH. Surprisingly, this reaction leads to an increase in nanoparticle size (**Figure 40** – average size 4.8 nm with a standard deviation of 1.2 nm) when compared to the reaction between  $\text{SiBr}_4$  and only 1.25 eq. LAH. This is unexpected because the increased amount of reducing agent should yield a smaller nanoparticle product. At the same time,  $\text{SiI}_4$  might be more inclined to give a larger nanoparticle product than  $\text{SiBr}_4$  due to its greater reactivity and a

greater growth rate. In comparing reactivity rates between silicon tetrahalides, it is important to remember that there are at least two distinct processes involved in nanoparticle formation: nucleation and growth. If the growth rate increases faster than the nucleation rate when the reactivity of the tetrahalosilane increases, then there would be an expected increase in particle size when using  $\text{SiI}_4$  instead of  $\text{SiBr}_4$  for reactions of similar concentration and stoichiometry. It is possible that this is seen in this comparison between  $\text{SiI}_4$  and  $\text{SiBr}_4$  with LAH and that the difference in silane reactivity dominates over the 60% increase in reductant stoichiometry. It is also possible that the TEM images do not fully represent either sample, especially given that the  $\text{SiBr}_4$  sample was very difficult to image due to the small particle size. A similar grouping of ~2 nm nanoparticles in the  $\text{SiI}_4$  sample (or any other Si nanoparticle sample) would be easy to pass over when operating the TEM due to the poor contrast of Si, the small size of the nanoparticles, and the sensitivity of the instrumentation.

The reactivity of the alcohol terminus of the unmodified  $\text{C}_i\text{E}_j$  surfactant family led to reactions with a large excess of the hydride reducing agent. This was done in an attempt to ensure that there was complete reduction of the silicon tetrahalide and that the consumption of the reducing agent by the surfactant did not lead to a stoichiometric deficiency. Although the modified surfactant is unreactive toward hydride reducing agents, similar reaction conditions were employed, where 16 eq.



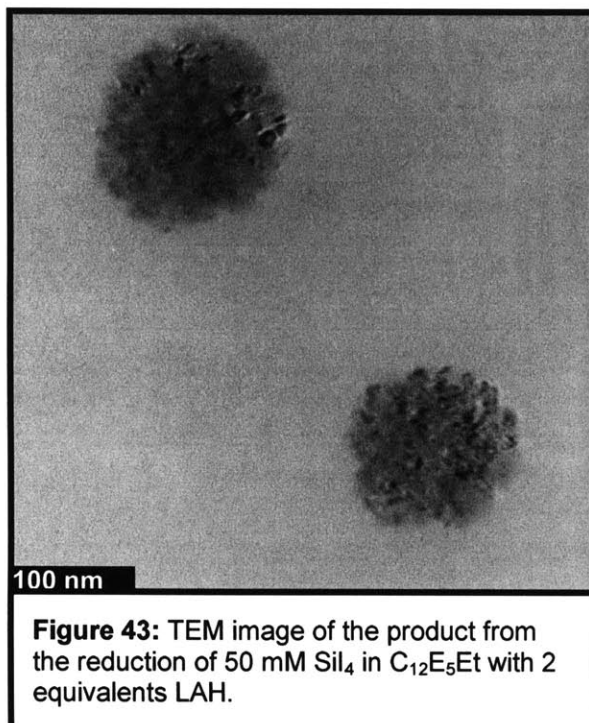


LAH were used to reduce a 2 mM  $\text{SiI}_4$  solution in a  $\text{C}_{12}\text{E}_5\text{Et}$  stock solution. The choice of 16 eq. was based on a four-fold excess of LAH assuming that only the most reactive hydrogen of the reducing agent would participate in the reduction of the tetrahalosilane. Similar to the reaction carried out in a  $\text{C}_{12}\text{E}_5$  stock solution (**Figure 28** – average size 2.5 nm with a standard deviation of 0.6 nm), after purifying with reverse phase HPLC, the reaction product from a reduction in a  $\text{C}_{12}\text{E}_5\text{Et}$  stock solution yielded

very small and uniform nanoparticles (**Figure 41** – average size 2.1 nm with a standard deviation of 0.4 nm). Like the small,  $\sim 2$  nm nanoparticles seen from other reactions, lattice fringes were not seen for these particles. However, the images are somewhat astigmatic and the small size and low contrast of Si increase the difficulty of imaging the nanoparticles.

At Si concentrations above 2 mM in  $\text{C}_{12}\text{E}_5\text{Et}$  stock solutions, inverse micelle-based reductions were found to yield a wide range of products and were generally found to be inappropriate for providing a high yield, size-controlled nanoparticle product. The best results came from the reduction of a 10 mM solution of  $\text{SiBr}_4$  with 1.25 eq. LAH. After purification the product was found to be bimodal. The nanoparticle product was promising, with small size and a small size distribution (**Figure 42** – average size 2.1 nm with a standard deviation of 0.7 nm). However, the nanoparticles were dispersed within or on top of a larger, ill-defined crystalline Si network more than 100 nm in size. At 10 mM, a solution of  $\text{SiI}_4$  in  $\text{C}_{12}\text{E}_5\text{Et}$  reduced with 16 eq. of LAH was found to be similar, with an agglomerated nanoparticle product ( $\sim 5$  nm) coexisting with a network product.

At even higher concentrations no nanoparticle product was detected at all. After reduction of 50mM  $\text{SiI}_4$  in  $\text{C}_{12}\text{E}_5\text{Et}$  with LAH, 100 nm agglomerates are seen in the TEM (**Figure 43**). The scalloped edges of the particles appear to result from



smaller particles growing or sticking together, but at higher magnification it is clear that the agglomerate consists of only a few crystalline grains. This might result from a few grains coming together or might result from smaller particles growing together selectively on certain crystal faces so as to preserve the single crystallinity of the particle. Such growth has been observed at moderately elevated temperatures,<sup>254</sup> but all of these reactions were carried out at room temperature. The presence of agglomerates is not surprising, but the reaction product is dissimilar from the high

concentration reactions carried out with hydrazine in  $\text{C}_{12}\text{E}_5$ Et and with LAH in the unmodified surfactant  $\text{C}_{12}\text{E}_5$ . Both of these reactions gave a bimodal product, although they were quite different. Reducing  $\text{SiI}_4$  in  $\text{C}_{12}\text{E}_5$ Et with hydrazine produced micron-sized spherical agglomerates and a population of  $\sim 150$  nm particles, while the reduction of  $\text{SiCl}_4$  in  $\text{C}_{12}\text{E}_5$  with LAH produced  $\sim 65$  nm tetrahedra, crystalline networks that included tetrahedral growths, and a substantial population of  $\sim 2$  nm nanoparticles. A bimodal population might be expected from all of these reactions because of the possibility of nucleation and growth in both the inverse micelle solution and in the separate polar phase that comes about from the introduction of a considerable volume of THF when the reducing agent is added.

Of these high concentration reductions, the reaction in the unmodified  $\text{C}_{12}\text{E}_5$  is unique in that the stoichiometry is not firmly established due to some consumption of the reducing agent by the surfactant alcohol. Thus, the reaction is to some unknown extent substoichiometric, similar to the reaction conditions reported in the literature for the production of Si tetrahedra.<sup>195</sup>

Hydride reductions in inverse micelle solutions of the unmodified surfactant C<sub>12</sub>E<sub>5</sub>Et were found to be the best suited to producing nanoparticles <5 nm (**Table 6**). Unlike similar reactions in unmodified surfactants, as reported in the literature,<sup>165</sup> these hydride reductions in C<sub>12</sub>E<sub>5</sub>Et are of known stoichiometry thanks to the inert character of the alcohol-free surfactant. The reaction became uncontrolled when nearly-substoichiometric LAH was used (1 eq.) and when the Si concentration was too high (50 mM), but in comparison with hydrazine reductions the range of reaction conditions was more forgiving and the distinct possibility of H-termination termination (**Equation 12**) made these reductions the preferred route to Si nanocrystals. The primary limitations of this synthetic approach are the low Si concentration and the large excess of surfactant that must be removed from the nanocrystal product. However, through the extension of the technique of reduction in inverse micelles to alcohol-free nonionic surfactants, the major uncertainty of this synthetic chemistry was removed and nanocrystal solutions were prepared for purification and analysis by HPLC.

Precursor	Concentration	Reductant	Stoichiometry	Average Size	Standard Deviation
SiI <sub>4</sub>	2 mM	LAH	1 eq.	Uncontrolled	N/A
SiBr <sub>4</sub>	2 mM	LAH	1.25 eq.	2.6 nm	0.7 nm
SiI <sub>4</sub>	2 mM	LAH	2 eq.	4.8 nm	1.2 nm
SiI <sub>4</sub>	2 mM	LAH	16 eq.	2.1 nm	0.4 nm
SiI <sub>4</sub>	50 mM	LAH	2 eq.	>100 nm	N/A

**Table 6:** Comparison of reaction products from hydride reductions in inverse micelle solutions of the modified nonionic surfactant C<sub>12</sub>E<sub>5</sub>Et. Low concentrations (2 mM) and a stoichiometric excess of the reducing agent were found to provide the smallest nanoparticles (shown in red).

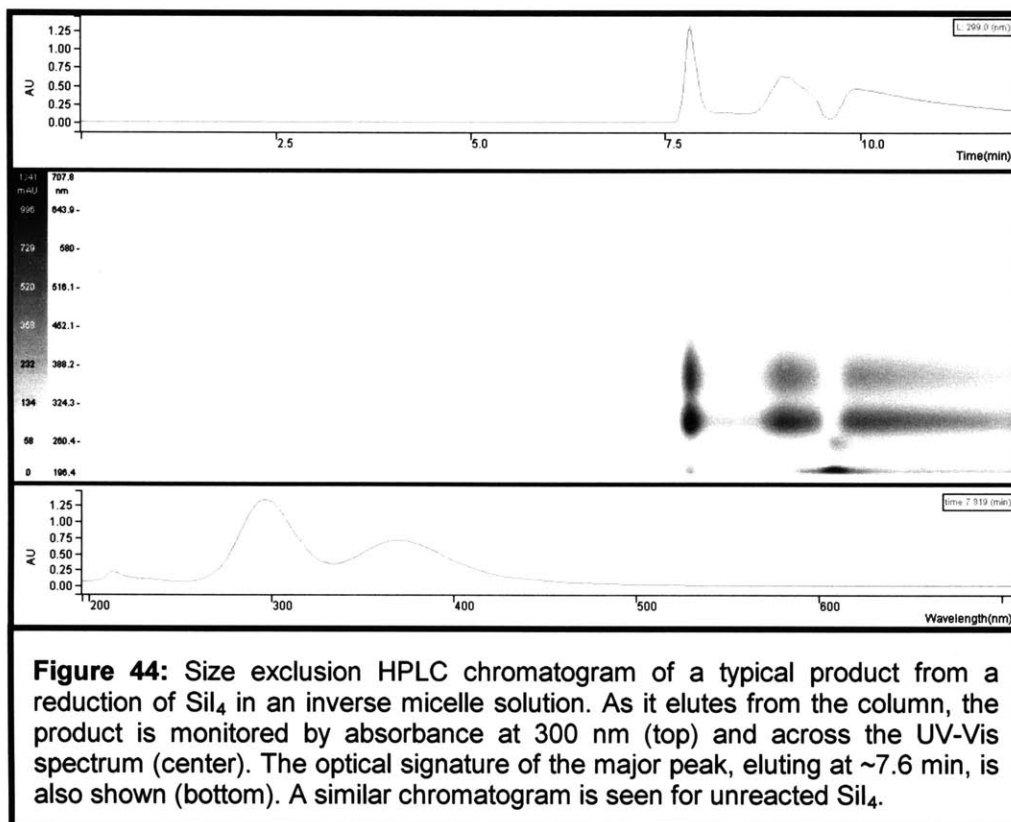
## Purification and Ink Formulation

### Purification and Product Tracking: Size Exclusion HPLC

In the five published papers dealing with Si nanoparticles produced from reduction in inverse micelles, HPLC is used to purify the product, removing both inorganic byproducts and the organic surfactant from the nanoparticle product.<sup>165,234,263-265</sup> Reverse phase HPLC is described as providing nanoclusters that are free of both inorganic impurities and residual organic surfactants, providing a solution of the nanoclusters in the HPLC mobile phase, usually acetonitrile. Acetonitrile “is an electron donating solvent that passivates the surfaces” of similarly-synthesized Ge nanocrystals “and prevents unwanted aggregation” and presumably acts in a similar fashion with the related Si nanoparticles, as acetonitrile is known to bind to Si wafer surfaces.<sup>234</sup> Other methods of purification have been published for inverse micelle reactions, including extraction and precipitation,<sup>270,271</sup> but neither has been reported for group IV materials.

Although considerable success has been reported for the HPLC purification of Si and Ge nanoparticles, in this work HPLC was found to introduce or expose a number of complications with the inverse micelle chemistry. In general, problems can arise from the use of HPLC if the mobile phase contains dissolved water or oxygen that attacks the nanoparticle product, if the column contains reactive sites that can degrade the product through oxidation, or if the column retains reduction byproducts or surfactants and these elute off the column with subsequent nanoparticle purifications.

The majority of the reductions of  $\text{SiI}_4$  yield a similar HPLC chromatogram when an SEC column is used (**Figure 44**), independent of reaction concentration and stoichiometry, even though concentration and stoichiometry are known to greatly influence the outcome of the reaction, as evidenced by TEM of the HPLC-purified products. Published chromatograms<sup>165,234,265</sup> generally do not identify byproducts or surfactants, suggesting that the published data is actually for a sample that was previously purified and the data is from the second HPLC purification.<sup>165,234</sup> When byproducts and surfactants are identified,<sup>265</sup> the byproducts are observed to elute early from a reverse phase column, and the surfactant and alkane solvent are observed to elute late off the column. The



nanoparticle product elutes in between, with some selectivity between sizes claimed in the reports.<sup>165,234,265</sup> These sizes are analyzed by TEM and UV-Vis spectrophotometry, allowing for a correlation between particle size and optical characteristics. Combined with the experimental results from other Si nanoparticle syntheses, the optical properties can be seen to be complicated and somewhat inconsistent or poorly understood (**Figure 20**). These inconsistent optical characteristics, considered alongside our initial observation that Au nanoparticles from a biphasic reduction<sup>295</sup> eluted between 7.0 and 7.4 min on an SEC column under identical HPLC conditions (compared to 7.6 min for the Si sample), allowed for the initial assignment of the early eluting UV-active peak to Si nanoparticles (**Figure 44**). And in fact, the collected fraction corresponding to this peak contained Si nanoparticles, as seen in TEM studies. However, there was the concern that similar optical features eluted at later times, perhaps suggesting a second, considerably smaller nanoparticle population with very similar optical characteristics. In control runs, however, these peaks were observed in unreacted  $\text{SiI}_4$  solutions. Initially, this was thought to be the result of the Si-I bond at both nanoparticle surfaces for the early-eluting peak and unreacted  $\text{SiI}_4$  or similar

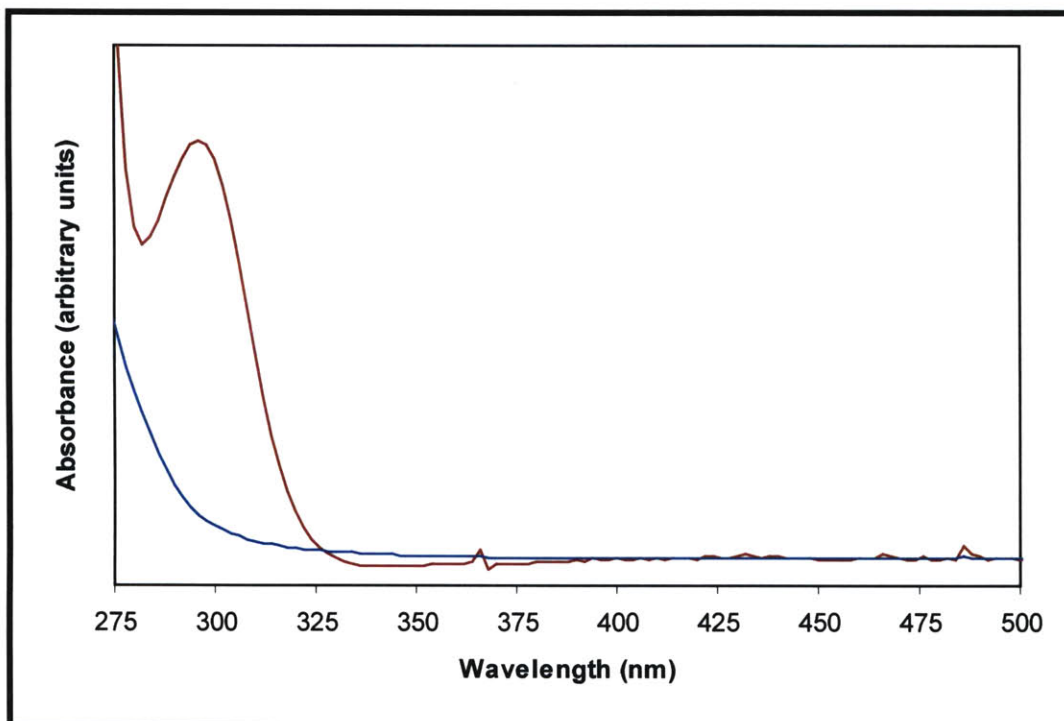
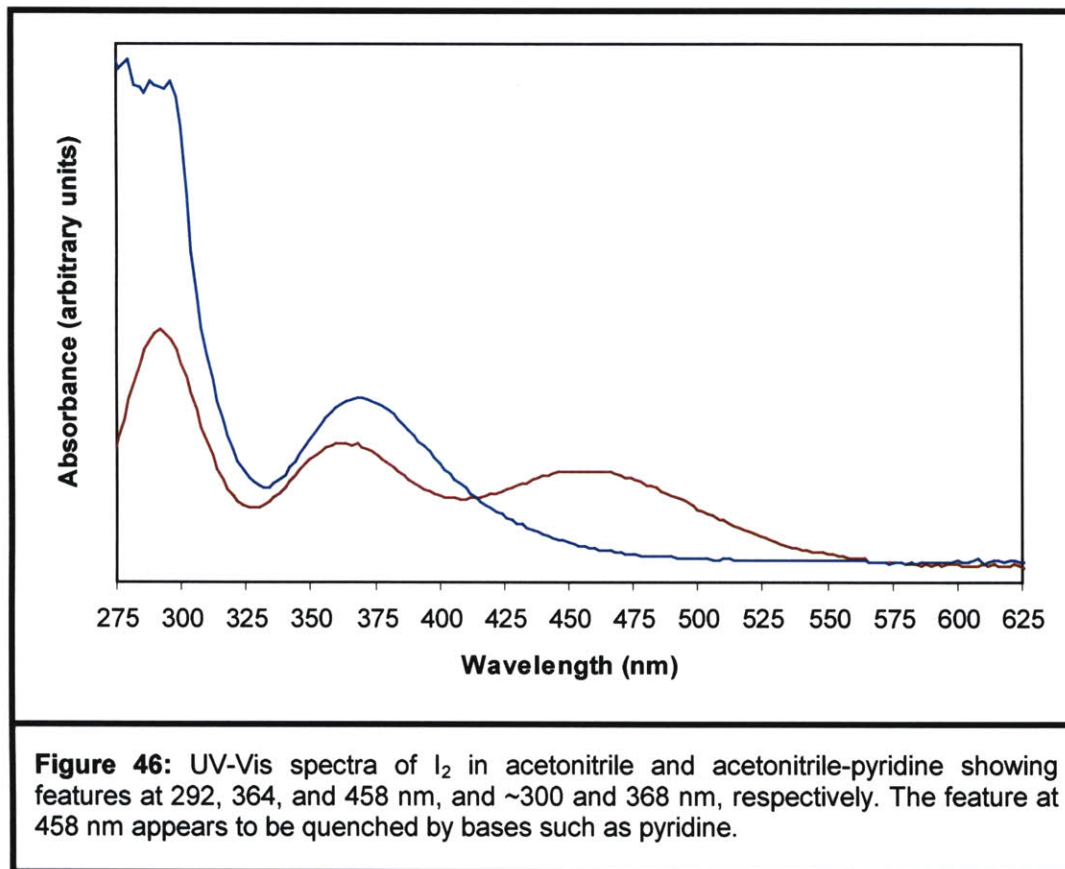


**Figure 45:** UV-Vis spectra of typical  $\text{SiI}_4$  reduction products in inverse micelle solutions. The feature centered around 296 nm was observed for a reduction in  $\text{C}_{12}\text{E}_5\text{Et}$  using 2 equivalents of LAH to reduce  $\text{SiI}_4$ . Although such features were sometimes observed, the majority of reaction products were optically featureless like the spectra shown for the reduction of  $\text{SiI}_4$  in  $\text{C}_{12}\text{E}_5\text{Et}$  with 8 equivalents of  $\text{N}_2\text{H}_4$ .

molecular species in the late-eluting peaks. But even the early eluting peak at 7.6 min was observed in control runs with unreacted  $\text{SiI}_4$ , suggesting that  $\text{SiI}_4$  was responsible for the optical features and that it was co-eluting with the nanoparticle product that was found by TEM in these product fractions.

The dominant optical features of the peak seen eluting off of an HPLC SEC column were at 320 and 370 nm, leading to a yellow color when the material is concentrated enough. This yellow color is not seen in the reaction product prior to HPLC purification, and in fact the optical characteristics of the crude reaction products (**Figure 45**) are different than those seen eluting from the HPLC (**Figure 44**). The product solution was also observed to yellow on standing outside of the glove box where oxygen and moisture might seep into the product vial, and also upon introduction of solvents that might carry with them some dissolved oxygen or water. The yellowing emerged very quickly, though, when uninhibited THF



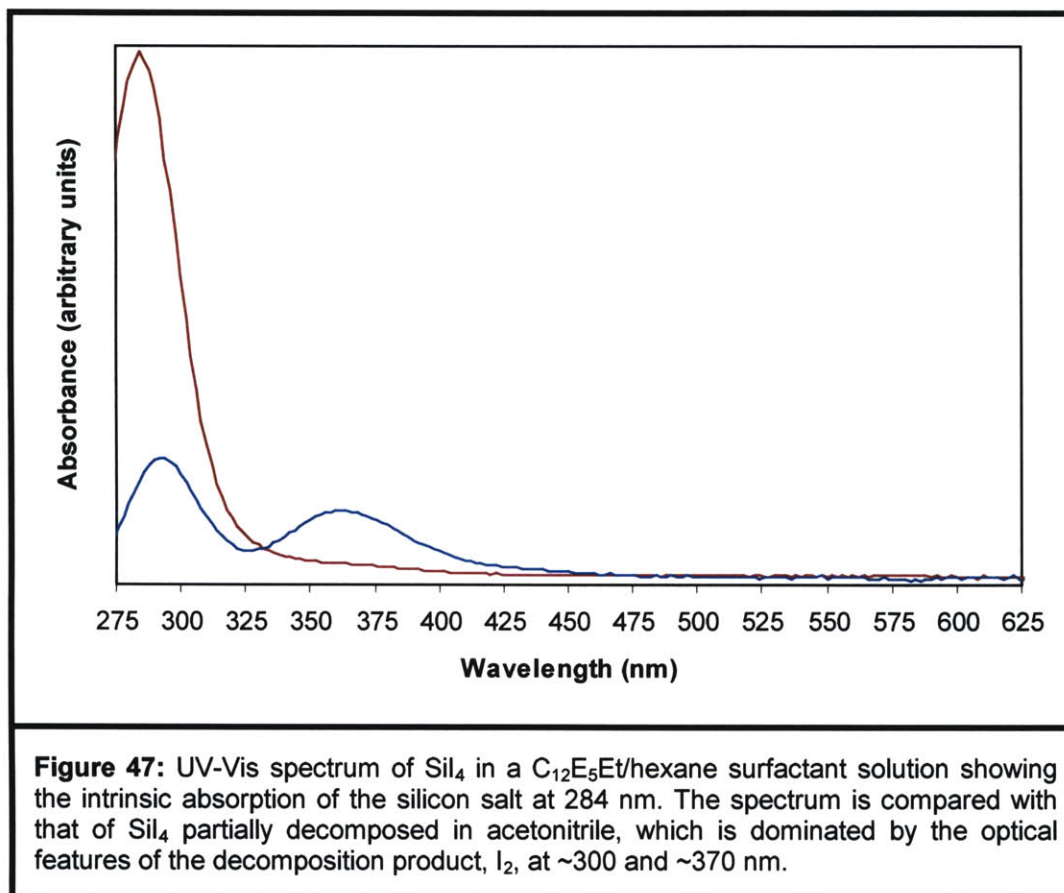
was added to the product solution. The increased peroxides levels in the uninhibited THF apparently drive the reaction forward, causing the yellowing.

Although there is a reference in the published literature that mentions Si nanoparticle solutions yellowing on exposure to air and attributes this to surface oxidation,<sup>165</sup> oxidation is not the source of coloration here. Iodine was initially considered a source of this coloration through Si-I bonding, but the onset of coloration that was seen with exposure to peroxides suggests another source, as peroxides would not be expected to induce halogenation. Slight coloration was noticed when making some  $SiI_4$  stock solutions, but heavy coloration was seen when highly concentrated stock solutions were attempted with  $C_{12}E_5$  in octane. In these solutions, a very dark red color emerged and some precipitate formed. Given the photosensitivity of  $SiI_4$  and the anticipated byproducts of its photochemical decomposition, it was assumed that this coloration came from the liberation of  $I_2$  from the silicon tetrahalide. Subsequent to that realization it

became clear that  $I_2$  might also be liberated from either the nanoparticle product surface or from iodine-containing byproducts when the materials were exposed to peroxides or perhaps to water, oxygen, and/or light. UV-Vis spectra of iodine in acetonitrile/THF found that it had distinct peaks very similar to those seen in the HPLC chromatograms (**Figure 46**), although there was an optical feature missing. This peak, centered at 458 nm, as well as the peaks at ~300 and 370 nm, may result not only from free  $I_2$ , but also from triiodide species resulting from complex of HI and  $I_2$ .<sup>296</sup> In fact, the 458 nm feature can be quenched when a base such as pyridine is added to iodine solutions (**Figure 46**). This HI-free iodine spectrum appears to be the same as that seen in the HPLC chromatograms of both  $SiI_4$  and Si nanoparticles (**Figure 44**). HPLC runs of an iodine stock solution confirm this and also show that iodine elutes from the column at multiple times, including at 7.6 min, a retention time at which nanoparticles and similarly sized molecules might be expected to elute from the SEC column, and a time at which Si nanoparticles were observed to elute from the column.

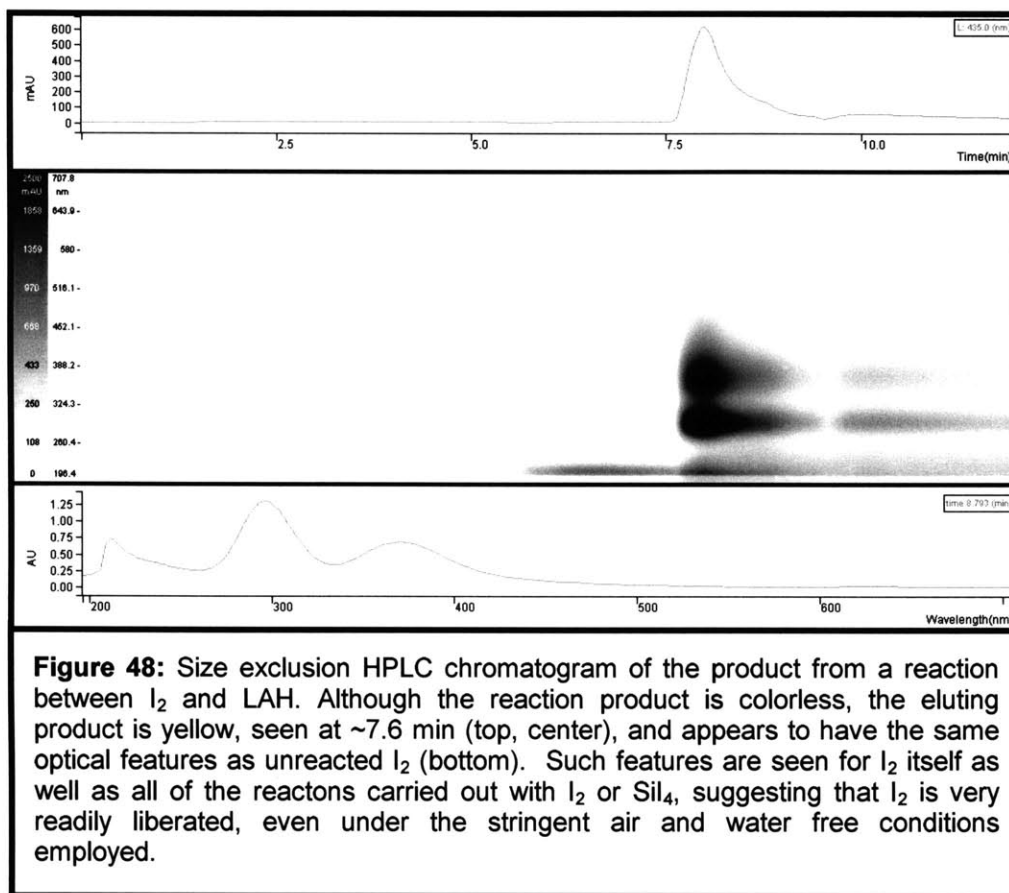
Having identified iodine as the dominant source of optical features detected during HPLC purification of these reductions in inverse micelles, the question remained as to the source of the iodine. The  $SiI_4$  that was used in the majority of these reactions was from Aldrich and solutions of the photosensitive yellow solid found that the absorptions of iodine dominated. High purity  $SiI_4$  from Alfa Aesar was white, though, and UV-Vis characterization did not identify peaks associated with iodine, instead detecting a unique absorption centered at 284 nm (**Figure 47**). In the reaction product the liberation of  $I_2$  might occur from unreacted  $SiI_4$ , from residual Si-I bonds at the surface of nanoparticles or Si-based polymers, or from the iodine containing byproducts. It seems unlikely that  $SiI_4$  remains unreacted considering the stoichiometric excess of reducing agent that was sometimes employed in these reductions. For similar reasons it seems unlikely that a considerable population of Si-I bonds remain at particle surfaces, although there may be an equilibrium population that acts as an effective source of iodine. It is clear, though, that the byproducts from the reaction can act as a source for the liberation of iodine. Control reactions in which  $I_2$  is dissolved in a surfactant stock solution and an excess of reducing agent is introduced, yielding a colorless product solution, were found to contain  $I_2$  when purified by HPLC (**Figure 48**). While it cannot be ruled out that the liberated iodine in part comes from the surface of the nanoparticle product, or that it comes from unreacted starting material, some or all of the iodine that is liberated by the HPLC comes from reaction byproducts. The HPLC could induce this liberation through trace solvent





impurities such as peroxides, or perhaps through traces of dissolved oxygen or water. Solvents were always flushed with nitrogen, and even when anhydrous solvents were used this problem was observed, suggesting that the iodine source is very sensitive to these influences, if they are, in fact, responsible for the liberation of iodine.

In non-coordinating solvents such as toluene the spectral features of iodine are different and do not match those seen in the reverse phase HPLC data. Just as the optical features shift in coordinating and non-coordinating solvents, the retention time of the iodine is very different and iodine is observed to elute broadly from the column at late retention times when toluene is used as a mobile phase, indicating that the iodine is to some extent sticking to the column, even though the SEC column is designed to have non-chemically specific interactions with the eluent and sample. With toluene as the mobile phase the Si product should not be masked by the co-elution of  $\text{I}_2$  unless the nanoparticles stick to the column like  $\text{I}_2$



does. At the same time, the absorption of toluene blocks out any absorption data below 300 nm, and so optical detection is dependent on the weaker absorptions in the nanoparticle product. Although  $I_2$  elutes much later than the expected range of a nanoparticle product eluting on the size-exclusion column when toluene is used as the mobile phase, no Si nanoparticles were detected.

### Purification and Product Tracking: Reverse Phase HPLC

All of the published data regarding Si and Ge nanoparticle purification by HPLC discuss the use of reverse phase HPLC,<sup>165,234,265</sup> not size exclusion HPLC. SEC columns have been described in the purification of other nanoparticle materials<sup>271</sup> and were investigated in this work for their extension to Si because of the possibility of extracting information about the average particle size and size distribution. This was anticipated as being important since the inverse micelle

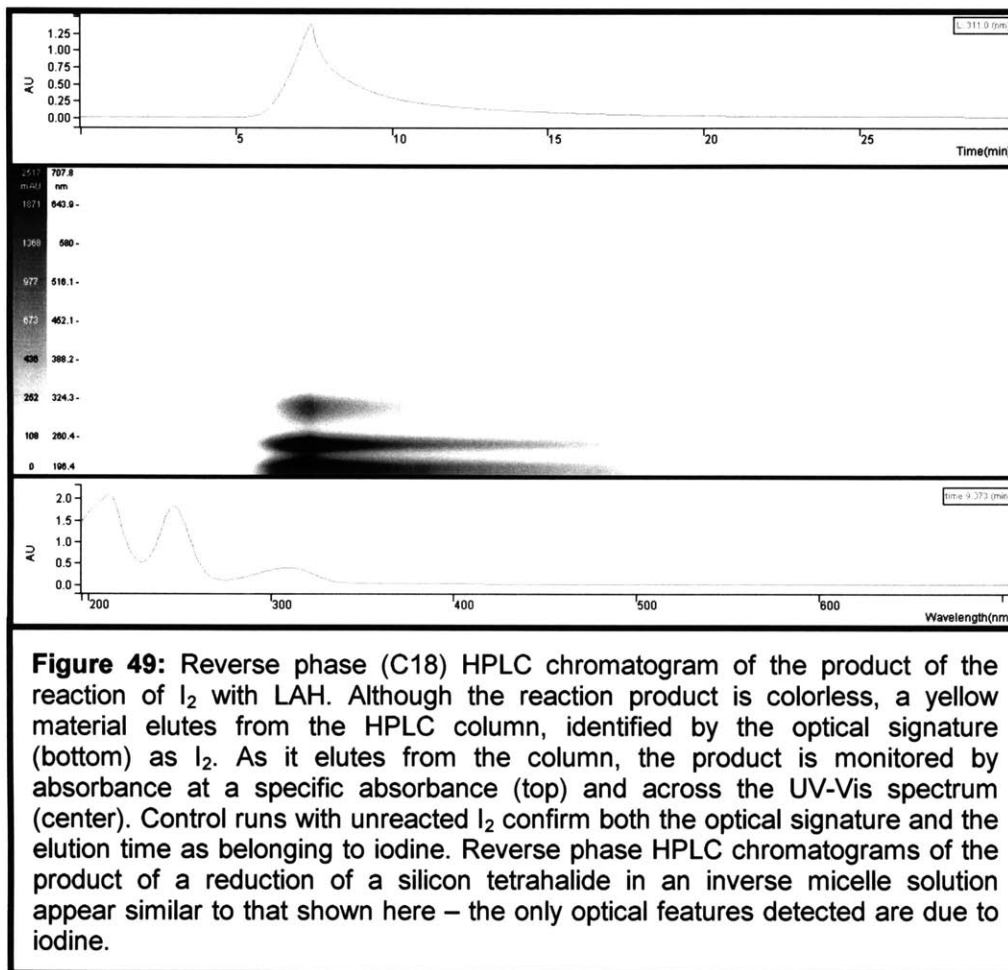


**Figure 49:** Reverse phase (C18) HPLC chromatogram of the product of the reaction of  $I_2$  with LAH. Although the reaction product is colorless, a yellow material elutes from the HPLC column, identified by the optical signature (bottom) as  $I_2$ . As it elutes from the column, the product is monitored by absorbance at a specific absorbance (top) and across the UV-Vis spectrum (center). Control runs with unreacted  $I_2$  confirm both the optical signature and the elution time as belonging to iodine. Reverse phase HPLC chromatograms of the product of a reduction of a silicon tetrahalide in an inverse micelle solution appear similar to that shown here – the only optical features detected are due to iodine.

synthesis was claimed to produce nanoparticles from 2-10 nm and size control and separation might be critical to successful ink formulation. However, identification of the product was difficult because of the co-elution of iodine (Figures 44 and 48). Even when the elution time of iodine was shifted by moving to an alternate mobile phase such as toluene, the nanoparticle product was not identified, suggesting it, too, shifted, or that the optical signal was very small.

To determine if these problems with the identification of the nanoparticle Si product were unique to size exclusion chromatography, reverse phase separation was investigated using acetonitrile as a mobile phase. Two types of reverse phase columns were investigated, and both gave similar results. A traditional octadecylsilanized silica gel column (Varian) was primarily used, but a polymeric reverse phase column (Polymer Labs) was used as well. This column had the

same packing material as the SEC columns but had different swell characteristics, giving rise to the alternate mode of operation. Seeing as the results were similar with the two columns, the surface modified silica gel column was used most of the time, as published results describe these columns specifically.<sup>234,265,271</sup>

An I<sub>2</sub> solution analyzed by reverse phase HPLC found the iodine eluting early from the column, near the solvent front where polar materials would be expected to elute. Control reactions between iodine in a surfactant stock solution and a reducing agent appeared very similar to reactions in which SiI<sub>4</sub> was reduced with a similar amount of a reducing agent, and I<sub>2</sub> was detected in both (**Figure 49**). Despite the I<sub>2</sub> or SiI<sub>4</sub> having reacted with the reducing agent, I<sub>2</sub> is liberated on the column and runs close to the solvent front.

According to published data, Si nanoparticles from reduction in inverse micelles should elute in the middle of a reverse phase HPLC run, after the polar reaction byproducts but before the surfactant and the non-polar alkane solvent.<sup>265</sup> While the surfactant could not be detected very well with a photodiode array spectrophotometer, by collecting fractions from a purification of a surfactant stock solution and concentrating and weighing them, the elution time of the surfactant could be determined, and it was found to come near the end of the run. Optically, there were no peaks unique to the silicon tetrahalide reductions that were detected eluting before the surfactant.

Prior to the identification of the strong optical features detected by HPLC as belonging to I<sub>2</sub>, they were considered to belong to Si nanoparticles. As such, the fraction correlating to the elution of I<sub>2</sub> was collected in early attempts to purify the nanoparticles. This was usually done after an initial SEC purification, as the SEC was feared to only partially remove the surfactant due to the considerable bulk of the surfactant and the column's discrimination based on size. In these collected fractions Si nanoparticles were detected and successfully imaged by TEM, sometimes without detecting any iodine by EDX measurements. At the time, it seemed surprising that the nanoparticles would elute so quickly from a reverse phase column, as this suggests that the particles are quite polar and perhaps that there are polar groups at the surface of the particles, perhaps Si-I bonds, although the Si-I bond is not very polar,<sup>209</sup> or perhaps Si-O bonds. In these early reactions the presence of Si-I bonds at the surface seemed likely, as substoichiometric amounts of hydrazine had been used in the syntheses. However, similar results

were seen with a stoichiometric excess of LAH, indicating that the particles eluting near the solvent front were not likely to be Si-I terminated.

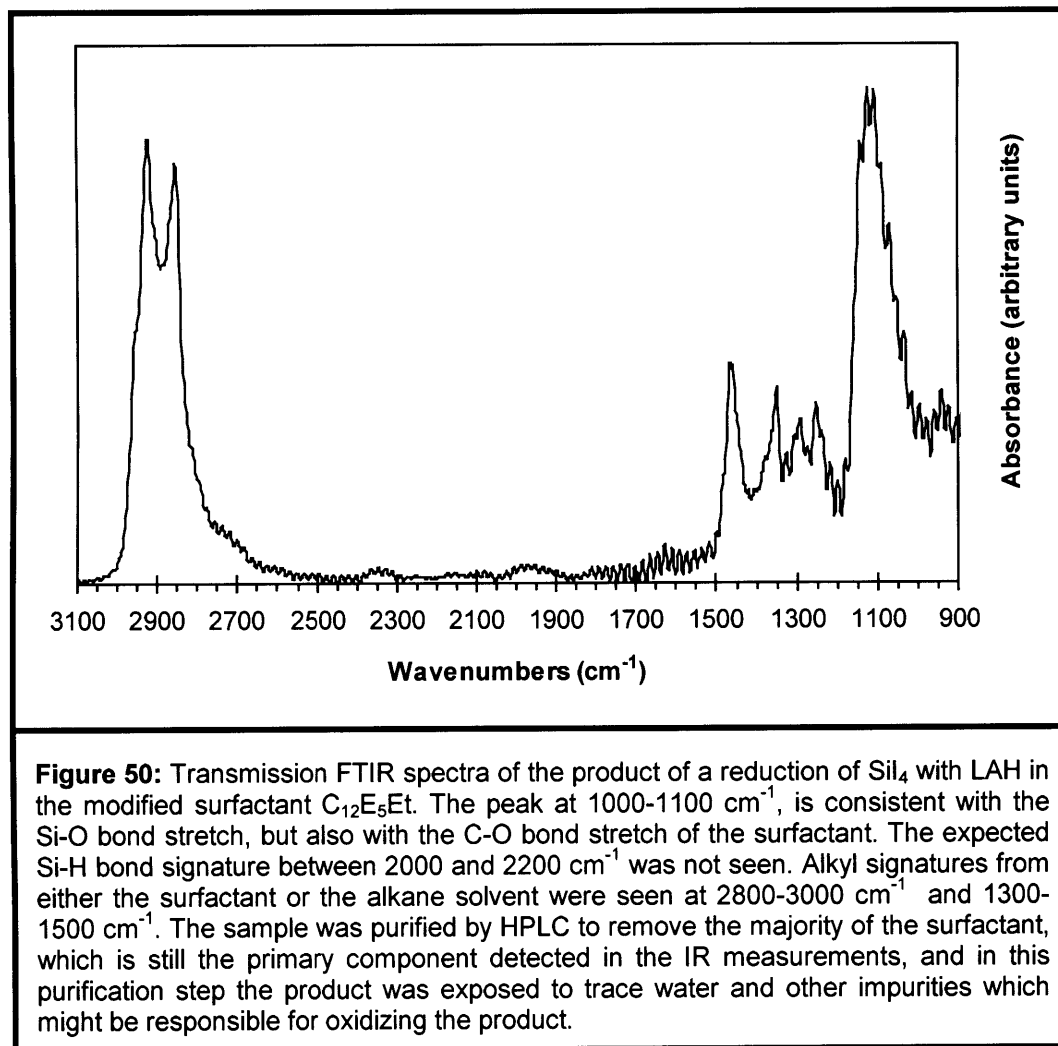
A 3.3 mM solution of  $\text{SiI}_4$  in a  $\text{C}_{12}\text{E}_5$ Et stock solution was reduced with 2 eq. 1 M LAH in THF. After reacting, octylamine was added as a stabilizer and a quench for the remaining unreacted LAH. The reaction product was analyzed by preparative scale reverse phase HPLC and four fractions were collected and analyzed by EDX. The collected fractions were all of comparable volume and covered 50% of the run, from the onset of the elution of iodine until the onset of the elution of the surfactant. The first fraction contained the majority of the iodine peak, the second fraction contained the trailing edge of the iodine peak and an unidentified deep UV feature, and the remaining two fractions contained no detectable peaks. Despite this, Si was detected in each of the fractions. The first fraction, which contained the iodine peak, was dominated by Si, although there was some I as well. The second fraction found Si and I in almost equal amounts, but the third and fourth fractions detected Si without I. Al was also detected in the fourth fraction, although it might not come from LAH as Ge, Cl, Br, Na, K, Mg, Fe, and Cr were detected in small amounts in some of these fractions and were unexplainably detected in samples apparently at random across this research project. It should be noted that trioctylphosphine oxide was added to each of the fractions in a controlled manner in attempt to provide a quantitative reference (P) for comparison of the EDX measurements. In only one of the fractions was P detected, though, suggesting that there was phase segregation, and also further suggesting that EDX measurements cannot be relied upon in an entirely quantitative way, as they may not fully represent the sample.

A fraction of the above reaction was set aside and extracted with acetonitrile. Both the polar acetonitrile phase and the non-polar octane phase were characterized by EDX. Similar to the HPLC fractions from the reaction, Si was detected in both phases. Also, I was detected in both the polar and non-polar layers. The ratio of Si:I in the polar phase was 95:5 and in the non-polar phase was 82:18. It is somewhat surprising that there was any I detected in the non-polar phase, but the polarity of the Si-I bond is not that great,<sup>209</sup> and  $\text{SiI}_4$  clearly has a reasonable solubility in a surfactant solution in octane.

So, even when a stoichiometric excess of LAH is used in the synthesis of Si nanoparticles, Si is found to partition between the nonpolar and polar phases of an extraction and is observed to elute broadly across a reverse phase HPLC column.

Although it seems unlikely given the excess of LAH used in the synthesis, the data suggests that there is a variety of surface termination that results in the particles exhibiting a large range of solubility and polarity. The 2 eq. of LAH might be substoichiometric if only a single electron of reducing power is available from the LAH, but LAH has been used in similar ratios for the complete hydrogenation of less reactive Si-Cl compounds<sup>166</sup> and SiCl<sub>4</sub> (Equation 12).<sup>209,226</sup> Unlike reactions with unmodified nonionic surfactants, there is no loss of LAH due to a reaction with the capped surfactant. Still, it is possible that there are some residual Si-I bonds at equilibrium or that some Si-I bonds are trapped in internal sites of poorly formed particles, agglomerates, or Si polymers. While this would explain the detection of iodine in a number of these samples, it would not explain the range of surface chemistry observed in the HPLC analysis of these product solutions, as Si-I bonds would need to present themselves at the surface of the particle to augment surface chemistry, polarity, and reverse phase retention time. If the Si-I bond were available at the surface for such interaction, it would also be available for further reduction with LAH and would most likely be removed from the nanoparticle product. Any equilibrium population of Si-I bonds would be anticipated to be such a small population that it would not be expected to make a large difference in particle polarity and would not lead to product elution over the entire range of the HPLC run.

If some of the nanoparticle Si product had a single Si-I bond, other particles had 2 Si-I bonds, and so forth, a broad surface distribution could exist and the product might wash over the entire HPLC run. To address the possibility that diverse surface termination caused the broad range of Si product HPLC elution times, a large excess of LAH was used to ensure complete reduction and a substoichiometric reduction was followed with a Grignard reaction to alkylate the halide-terminated Si product. A considerable excess of a reducing agent (16 eq. of LAH, 1 M in THF) was used to reduce a 2 mM SiI<sub>4</sub> solution in a stock solution of C<sub>12</sub>E<sub>5</sub>Et. The reverse phase HPLC chromatogram showed the same type of trace that was seen for substoichiometric and stoichiometric reactions. In an alternate scheme to control surface termination, by intentionally using a substoichiometric amount of superhydride or hydrazine, a halide-capped product was presumably produced and subsequently alkylated. An excess of butylmagnesium chloride was introduced to alkylate the Si-I surface sites and hopefully create a highly alkane-soluble and hydrophobic Si product. Similar chemistry has been published for the surface derivatization of Si nanomaterials produced by metathesis,<sup>242,246</sup> but has been inaccessible to inverse micelle chemistry due to the reactive alcohol of the



unmodified nonionic surfactants employed. Unfortunately, there is no apparent difference in the HPLC trace of the product after the alkylation. Neither the use of an excess of the reducing agent, in an attempt to force Si-H bond formation, or the use of Grignard alkylation, in an attempt to create a hydrophobic surface termination, were able to produce a particle surface of sufficient chemical uniformity to elute in a controlled and detectable fashion with reverse phase HPLC.

The failure to observe these surface modifications by HPLC does not necessarily indicate that they were not successful, and it may be that the product surface is quite uniform without such treatments. The inability of the HPLC to recognize a

Si product peak might result from differences in the surface character of the product, but might also relate to the low concentration of the product. This seems possible, but iodine is readily identified by the HPLC detector at these low concentrations and HPLC runs at higher concentrations do not detect any new peaks. The reaction could be low yielding, but the published account claims an 80% yield.<sup>165</sup> Of course, the same accounts also claim an identifiable peak when characterizing with reverse phase HPLC, and this is not seen, and so it is possible that there is a considerable difference between the published account and our experience with similar reactions. It is possible that the product oxidizes on the column and that the ongoing *in situ* oxidation of the product dynamically changes its retention time, leading to the broadened elution time(s) and the effective loss of any Si signal due to dilution across the entire HPLC run. This also seems unlikely, not only because the HPLC solvents are dried over molecular sieves and are flushed with nitrogen, but also because the alkylated product should be fairly immune not only to such oxidation,<sup>218,297</sup> but also immune to any drastic change in the elution time if any of the alkylated product is oxidized. The extent of alkylation was not investigated, though, and it remains possible that oxidation would influence retention time. There is some evidence of surface oxidation, though, as FTIR measurements did not detect appreciable Si-H bonding but instead detected Si-O bonding (**Figure 50**). The signature Si-O bond stretch between 1000 and 1100  $\text{cm}^{-1}$  is complicated by the surfactant C-O stretch, which is seen and likely constitutes the majority of the peak at  $\sim 1100 \text{ cm}^{-1}$ . In either case – Si-O or C-O detection – there is a problem to be overcome, as both oxidation and incomplete surfactant removal are a problem for HPLC purification. Oxidation could occur during sample handling, although efforts were made to protect the sample from air throughout the sample handling and measurement, and oxidation from such exposure would have to be very rapid and inconsistent with experiments with H-terminated porous Si.<sup>218</sup> If oxidation occurs during the HPLC purification, it might also remove nanoparticles from the eluent by inducing particle agglomeration and precipitation. It is also possible that the column does not distinguish well between the nanoparticles or that they tend to stick on the column, removing the Si product from the eluting solvent. The column media was not developed with nanoparticle separations in mind, but it seems unlikely that the column material would artificially broaden the elution times of the Si product. It also seems unlikely that the particles stick to the column, as reactive sites on the column are capped with reactive and sterically unhindered silanes such as trimethylchlorosilane as a part of the column media manufacturing process. This analysis does not leave many options, but the fact that there is no detectable signal



with either SEC or reverse phase HPLC suggests that the problem is not with the column media but instead relates to either the sample itself or to impurities in the HPLC lines or solvents. Low yield and concentration would seem to be the likely failure modes for the sample, and oxidation or agglomeration seem to be the likely failure modes for the solvent system. Unfortunately, none of these seem to be particularly likely, and none are easily addressed.

One way of addressing the shortcomings of the HPLC is to use an alternate means of purification. Although precipitation with cold isopropanol and acetone has been reported for metal reductions in inverse micelles,<sup>270,271</sup> it has not been reported for Si or Ge and was not investigated here because the H-terminated product was anticipated to have difficulty re-dissolving after precipitation and unwanted surface oxidation was expected from trace water introduced by the polar antisolvent. Beyond precipitation, extraction has been reported for the purification of nanoparticles synthesized in inverse micelles. The general approach has been to add a stabilizer, such as a long-chained alkane thiol to a metal such as gold or silver, and then extract the polar byproducts and the surfactant into an immiscible polar phase such as acetonitrile.<sup>270</sup> While the surfactant does not exclusively prefer the polar phase, depending on the ratio of the polar and non-polar regions of the surfactant the partitioning ratio can heavily favor the acetonitrile layer. With a few extractions the vast majority of the surfactant can be removed.<sup>270</sup> Of course, the protective alkane surface layer aids in maintaining the nanoparticle's solubility in the non-polar phase while the reaction surfactant is repeatedly extracted into the polar phase. With Si nanoparticles there isn't an alkanethiol analog; there isn't a readily reversible surface termination that offers both stabilization with volatility. With a stabilizer such as octylamine the Si product partitions between both the non-polar octane layer and the polar acetonitrile layer of the extraction, and so some loss of the product might be expected from the extraction. If this partitioning is due to halogenated or oxidized surface sites, though, removal by extraction into acetonitrile could be desirable. Of course, iodine was still detected in the octane layer of the studies to address this, so extraction alone is clearly not a solution. After purification by SEC HPLC using THF as the mobile phase and concentrating the collected fractions in acetonitrile, the acetonitrile layer can be washed with repeated octane washes to remove the surfactant. The SEC column presumably removes all of the polar molecular materials from the reaction product, leaving a nanoparticle product and any surfactant impurities. The modified C<sub>12</sub>E<sub>5</sub>Et surfactant is considerably less polar than the unmodified

alcohol surfactants described in the literature. In fact, by studying the weights of the surfactants  $C_{12}E_5$  and  $C_{12}E_5Et$  after partitioning into equal volumes of octane and acetonitrile, it was determined that the capped surfactant favors the octane 50-fold over the unmodified surfactant. Using an alkane volume twice that of the acetonitrile, 5 washings with octane removed 98% of the surfactant, as monitored by NMR. And so the majority of the remaining surfactant can be removed by extraction. This has been applied with moderate success, as nanoparticles were clearly imaged after this method of purification, suggesting that the product did not partition very evenly between the two layers and that the majority of it remained in the acetonitrile layer across the 5 extractions. While this technique may be a valuable way of removing surfactant from the product, it does not address the iodine impurities that are routinely detected during HPLC purification.

### **Purification and Product Tracking: Differences from the Literature**

Silicon nanoparticles can be recovered by reverse phase HPLC from fractions collected early in the run, late in the run, and in between. There are not any detectable peaks associated with the particles in these fractions, though, suggesting that the particle concentration is low due to poor reaction yield, product agglomeration, or surface oxidation and varied elution. Alternatives to chromatography like precipitation and extraction introduce undesirable opportunities for oxidation or loss of product.

The concentration of the reductions carried out as a part of this work were two orders of magnitude lower than the highest concentrations reported for reductions of metal salts in inverse micelles. The literature that deals with Si and Ge directly<sup>165,234</sup> does not disclose the actual concentrations used in the group IV reactions, and it is possible that the data reported in those papers was for reactions carried out at concentrations higher than those routinely employed in this thesis research. Still, as a part of this thesis, reactions were carried out at these elevated concentrations, and no consistent differences were seen in the HPLC chromatograms of these results. Additionally, reactions at these concentrations were found to produce large particles, agglomerates, and networks, suggesting that they were not the concentrations used in the literature reports. After speaking to one of the authors of the Si nanoparticle literature reports, we found that a reaction concentration of 10 mM was commonly used<sup>292</sup> in the work that the

published reports were based on,<sup>165</sup> about 5× what was routinely used in the reactions reported here. Even the concentrated products from the 2 mM reactions described here, where the majority of the reaction solvent was stripped to yield a concentration nearly 10× that of the initial reaction, were not found to have any distinct Si peaks in either reverse phase or size exclusion HPLC runs.

A standard benchtop laboratory spectrophotometer with a 1 cm path length has a path length 20 times that of the in-line photodiode array spectrophotometer of the HPLC, and this might allow for more sensitivity toward the Si nanoparticle product and would also enable analysis prior to exposure to HPLC solvents and column media. Although the optical features of Si nanoparticles reported in the literature vary from report to report (**Figure 20**), the majority of the results describe a Si nanoparticle product with an absorption at 300 nm. Analysis with a benchtop UV-Vis spectrophotometer of the reaction products from the reductions described in this thesis found a wide range of results. There were some reactions in which the optical features were consistent with a nanoparticle product (**Figure 45**), with both featureless and featured absorptions at 300 nm. These absorptions could be seen in both the acetonitrile and octane layers of an extraction of the product, suggesting that any nanoparticle product responsible for the optical features was partitioning between the two. But there were similar reactions in which there were no optical features detected at 300 nm, and those in which the acetonitrile and octane layers of an extraction appeared very differently. Complicating the results further was the observation that the HPLC chromatograms of the same samples did not detect the critical spectral features at 300 nm that were seen with the UV-Vis spectrophotometer, suggesting that the photodiode array detector was not sensitive enough or that the HPLC was suffering from broad elution times or from lost product.

The inconsistent optical features detected from reaction to reaction by the UV-Vis spectrophotometer suggests that there might be some variability in the synthesis, and given the broad range of synthetic parameters described in the papers dealing with the synthesis of Si nanoparticles via reduction in inverse micelles, there might be some critical differences in the chemistry as implemented in this report and as implemented in the published literature.<sup>165,234</sup> The reaction concentrations, which were considered as a possible explanation for the absence of distinct Si peaks in HPLC chromatograms, were found to be fairly similar to those employed in the research that the published literature was based off.<sup>165,234,292</sup> Stoichiometry and the duration of the reaction were two other possibly critical parameters that

were not directly dealt with in the published literature. The average reaction carried out in this work used only a stoichiometric amount of a reducing agent and the reaction was allowed to run for 1-4 hours. In speaking with one of the authors of the papers reporting the synthesis of Si nanoparticles by reduction in inverse micelles, it was learned that the average reaction described in that work used a large excess of the reducing agent LAH and that the reaction time was more than 24 hours.<sup>292</sup> In those reactions, the unmodified, alcohol-bearing surfactant C<sub>12</sub>E<sub>5</sub> was used in the inverse micellization, and so an excess of the reducing agent was necessary to overcome the competing consumption of the reducing agent by the surfactant. Still, four or more equivalents were used assuming that only a single H was active from the 4 available H of LAH. The reactions were allowed to proceed for a long time, sometimes more than a week, because the product, as immediately produced, was found to be “optically dead.”<sup>292</sup> The synthesis takes place at room temperature and is very different than the more established high temperature nanoparticle synthesis routes that take place at 200 °C or more,<sup>131,298</sup> where annealing of the particle is intrinsic in the growth process, due to the high temperatures. The *in situ* aging, then, was primarily to anneal the particle at room temperature and to improve the photoluminescence characteristics. As initially formed, the product was non-luminescent, but after a week the product became quite luminescent.<sup>292</sup> In the chemistry described in this thesis, such aging experiments were conducted, but no shift in optical properties was seen after 4 or 7 days, and no consistent or repeatable onset of luminescence was seen, either. The use of a large excess of a reducing agent was successful in producing Si nanoparticles, but it did not lead to the emergence of any peaks in HPLC chromatograms and did not make a notable difference in the product as seen by TEM.

The chromatography columns used for purifying Si nanoparticles that are mentioned in literature reports are not always clearly identified.<sup>165,234,265</sup> Size exclusion columns are not reported on at all, but for reverse phase columns only one of at least two types are clearly defined, and that column is only described in the isolation of Ge nanoparticles.<sup>234</sup> In conversing with one of the authors of this report, it was still not clear who manufactured the unidentified octadecylsilanized reverse phase columns.<sup>292</sup> But even with the column that was clearly defined, a DeltaPak reverse phase column, octadecylsilanized with 300 Å porous separation medium, the purification the nanoparticles described in this thesis did not yield results similar to those that were reported in the literature. Other than the column itself, there are a few chromatography conditions that might be different from the

literature reports. The lifetime of the column might be relevant if there are a number of defect sites on the column that interact with the particles. As mentioned earlier, this seems unlikely, though, as the nanoparticles are quite large compared to the reactive silanizing agents that are used to cap the separation medium. In the literature reports the solvents used in the HPLC purification were anhydrous solvents.<sup>292</sup> Although the work described here did not always employ anhydrous-grade solvents, molecular sieves were used to dry the solvents and nitrogen was used to flush the solvents, and in some cases anhydrous solvents were used, with no apparent change. The researchers responsible for the literature reports of HPLC purification of nanoparticles have been working in that area for more than five years, and have a more advanced HPLC system than what was available at MIT. The differences that might be responsible for the chromatographic differences seen in the work reported here and that reported in the literature are that the literature reports were based on a system with improved nitrogen flushing of the solvents and an inline solvent degassing system that might aid in removing any dissolved oxygen that remains after the nitrogen flushing.<sup>292</sup>

It remains possible that subtle differences in the chromatography or synthetic conditions lead to the observed differences in the HPLC purification of the Si nanoparticles produced as a part of this thesis research and those reported in the literature. Differences between the two are not as problematic as is the absence of a peak associated with Si nanoparticles that can be detected and followed by HPLC. This absence might result from oxidation during HPLC purification, low reaction yield, unknown aspects in the aging of nanoparticles, or unanticipated agglomeration. It is also possible that the literature reports<sup>165,234,265</sup> wrongly ascribe the peaks to Si nanoparticles, as Si nanoparticles have been observed to have a wide range of elution times in the work described here. This seems unlikely, though, as the optical features compare favorably with other literature reports of Si nanoparticles, and photoluminescence studies were performed on the purified product.

### **Ink Formulation and Device Fabrication**

Ink formulation and device fabrication were difficult because the reaction yield and surface termination were unknown. For the routine preparative scale HPLC purifications of 2 mM reactions, the theoretical yield was only 0.028 mg.

Assuming the published synthetic yield, 80%, was obtained in spite of the failure to track a peak associated with Si in the HPLC chromatogram, 45 purifications would have to be run to obtain 1 mg of product. Because of this, the HPLC solutions were used as inks without any ink formulation other than removal of solvent to increase the concentration. Repeated deposition was employed to build up layers of appreciable thickness.

In the purified reaction product, FTIR spectroscopy did not find evidence of Si-H bonding, but did find some evidence of Si-O bonding, complicated by the surfactant C-O stretch which sits in the same spectral region, and found no evidence of Si-H bonding (**Figure 50**). Unfortunately, it was not possible to identify when any oxidation occurred, and the measurements were very difficult to make, given the small amounts of material that were available. The nature of the oxide is also unknown, although OH groups were not detected by FTIR, suggesting that any reaction between the SiH surface and water falls below the detection limit of the FTIR for such dilute samples. Surface OH groups will insert into Si-Si bonds and act as nucleation sites for further oxidation<sup>299</sup> if they are not removed. Attempts to demonstrate by FTIR the removal of surface oxides with an aqueous HF etch while the product was retained in a nonpolar phase were due the difficulty of obtaining enough material for analysis.

Oxidation could occur during the reduction, but this seems very unlikely given that an excess of LAH was used and LAH is highly reactive with both water and oxygen. Oxidation could more likely occur during the handling of the product solution prior to HPLC or during the purification of the product by HPLC. After quenching any excess LAH, the product is briefly exposed to air before it is injected onto the HPLC, and throughout the HPLC run there are opportunities for oxidation if there is any dissolved oxygen or water. The HPLC might be the likely place for oxidation because the product is separated from the surfactant, which up to that point might act as protective layer, by either retarding oxygen or water diffusion to the particle surface or by stabilizing the surface through coordination. Assuming that any residual water in the solvent reacts with the nanoparticles purified by HPLC, and assuming that 50% of the Si is at the particle surface and reacts, only 4  $\mu\text{M}$   $\text{H}_2\text{O}$ , or 0.00001% by weight  $\text{H}_2\text{O}$  in the HPLC mobile phase is needed to completely oxidize the nanoparticle surface. In general, commercial anhydrous-grade solvents are not anhydrous to this extent, especially for polar solvents that are useful for reverse phase HPLC. For example, the anhydrous acetonitrile used in this work was <0.001%  $\text{H}_2\text{O}$ . Given that  $\text{I}_2$  is liberated from

the product solution during the HPLC run, it is clear that some chemical reaction is occurring during the HPLC run, possibly with reaction byproducts and possibly with the product itself. It is also possible that the nanoparticles are oxidized prior to FTIR analysis while in transit to the facility or during measurement. However, liquid cells were used to ensure that the product was minimally exposed to air, and H-terminated Si surfaces are known to be moderately resilient to oxidation.<sup>218</sup> While the cells do not leak liquid, it cannot be ruled out that some air seeps in and oxidizes the dry nanoparticle product.

After concentration, the HPLC-purified Si nanoparticle samples were used in device fabrication, despite their apparent surface oxidation. The inks were deposited over Al electrodes and subjected to a 400 °C treatment in Ar on a hot plate. Due to the low concentration of the inks, a large number of drops were deposited to ensure adequate coverage and thickness. This was also necessary because the product preferred to wet the Al electrodes, oftentimes dewetting and pulling away from the SiO<sub>2</sub> gate oxide surface. By careful drop placement and drying between each deposited layer, continuous thin films were cast in 1, 3, and 5 μm channels of TFT structures. Unfortunately, none of the fabricated devices were operable transistors, as no field effect activity was observed.

### **Limitations Associated with Purification**

Printed Si thin film transistor fabrication was unsuccessful, the result of a cascade started with the inability to identify and track a Si nanoparticle product by HPLC. It is possible that another problem sits behind this one – *in situ* oxidation, poor reaction yield, loss of material to defect sites on the column – but the heart of the problem can be found in the difficulties with the purification of the reaction product. This work established that reduction in inverse micelles, at very least at concentrations from 1-3 mM, can yield a nanoparticle Si product with a small average particle size and good size control. Yield and surface chemistry remain concerns, primarily because problems with purification prevented an assessment of yield and hindered any attempts to modify and analyze surface chemistry.

The problems with the purification of the group IV nanoparticle product are perplexing in large part because of the apparent success with similar purification efforts described in the literature.<sup>265,270,271</sup> Although it remains possible that the literature reports of HPLC purification were based on considerably more

concentrated samples, private communications with one of the authors indicated that the sample concentrations were not much higher than those routinely used in our work.<sup>292</sup> Additionally, as previously described, higher reaction concentrations were investigated as well as higher product concentrations, and no improvement was found with HPLC analysis. Residual water in HPLC solvents might oxidize the reaction product and lead to its varied elution or precipitation, but similar problems would be expected for the published reports unless dissolved oxygen is the primary agent of oxidation and the solvent degas unit used in the published work is able to remove reactive dissolved oxygen. It is also possible that the reaction conditions were different between the work pursued as a part of this thesis and the work that has been published. There are few experimental details in the literature and the described reaction conditions are very broad. Still, conversations with one of the authors of the published reports confirmed that the publications were based on the same Si precursor ( $\text{SiI}_4$ ), the same reducing agent (LAH), the same surfactant ( $\text{C}_{12}\text{E}_5$ ), the same reaction concentration (10 mM), the same stoichiometry (4 eq. LAH, assuming only the most active hydride is involved in the reduction), and the same duration of reaction (days) as were explored in this thesis.<sup>292</sup> Additionally, this thesis explored alternative precursors, reducing agents, surfactants, concentrations, stoichiometries, and reaction durations and none of these were found to elucidate or simplify the purification problems. These contrasting results seem to indicate that there must be differences between the experimental details of the published reports and those described here, but for both the synthesis and purification there are no obvious differences that explain the stark differences seen in the HPLC results. Identifying these differences would enable an assessment of the reproducibility of synthesis in inverse micelles and would enable a thorough study of surface termination in the products from these reactions. After conversations with one of the authors of the published reports,<sup>292</sup> the largest difference between the published work and that described here is with the HPLC itself, which in the published reports had been used extensively for nanoparticle purification and had an inline solvent degasser and may have had improved inert gas purging of the solvents.

### **Alternative Means of Purification**

Purification is critical to the larger aims of this project, and if the product cannot be purified by HPLC, or if the purified product has an oxidized surface, further treatments or alternative purification techniques need to be investigated.



Alternative syntheses are also worth consideration, but the synthesis of Si nanoparticles in inverse micelles remains the best option available in the open chemical literature because of the possibility of superior size and surface control. While the low concentration of inverse micellar syntheses is undesirable, yields have been reported to be high<sup>165</sup> and there are ways to concentrate the product prior to and during purification. One option is to freeze out the surfactant from the reaction solution.<sup>267</sup> The solubility of  $C_iE_j$  surfactants can be sensitive to temperature and the 10% solutions used in these syntheses are close to saturation. Difficulties arise with this technique because the surfactant can be flocculent when it crashes from the solution, and there is a lot of it, making separation difficult. Furthermore, the temperature must be kept low at all times in order to ensure that the surfactant is not redissolving during centrifugation or filtration. The cationic surfactant DDAB can similarly be forced from toluene solutions by adding an alkane.<sup>267</sup> Experimentation with this system found that the large amount of precipitated surfactant made it difficult to isolate the solution. After removing the majority of the surfactant through precipitation, the product could be concentrated and further purified by HPLC or extraction, either of which might be inappropriate for purification of the crude reaction product due to concentration or efficiency, but which might be well suited for this proposed later-stage purification.

The most difficult aspect of purification with these inverse micellar reactions is the removal of the surfactant, because 10% of the reaction mixture is surfactant. For reactions run at 2 mM, for every nanoparticle produced there are ~1,000,000 surfactant molecules. While the removal of iodine may prove difficult as well, and while there are 4 iodine atoms per Si atom, there are still 200× more surfactant molecules than iodine atoms in the reaction mixture, and each surfactant molecule is a high molecular weight oligomer. Any purification that separated the nanoparticle product from the majority of the surfactant would enable concentrated purification by HPLC and extraction.

To address the HPLC Si tracking problem, more elaborate experiments could be run. Alternative means of HPLC detection such as total ion count mass spectrometry (TIC MS) might offer insight into the relative amounts of Si eluting at different times during the purification, and MS might additionally offer information about particle size or surface termination. Alternatively, a number of purifications might be tried to determine whether the product is lost on the column due to precipitation or sticking or if the product is not detected simply due

to low concentration or dilution across the HPLC run. One of these brute force experiments would include a large number of purifications and the collection of all of the material eluting before the elution of the surfactant. Perhaps 50 or 100 separate injections would have to be made and the products from these purifications combined, concentrated, and weighed. In combination with analysis to determine how much iodine and oxygen was in each fraction, by directly monitoring the mass, this experiment would indicate if material were lost to the column. Such a difficult experiment, requiring 50 to 100 separate purifications, illustrates the limitation of synthesis in inverse micelles at the low concentrations that were found necessary to control Si particle size. Still, even the most recent literature reports<sup>248,249,262</sup> do not offer consistent or direct routes to H-capped Si nanoparticles.

The most straightforward way to reconcile the differences between the experimental results described here and those that have been published would be to work directly with the authors of the published reports to carry out a detailed and controlled study with variation of a wide range of synthetic parameters and careful attention paid to HPLC purification techniques. As a part of this, alternative means of purifying the sample might be investigated and more careful mechanistic studies might be carried out to settle the controversy in the literature.<sup>195</sup> If the experiments were successful and the surface well characterized and in fact found to bear an abundance of Si-H bonds, the nanoparticle Si product would be ripe for ink formulation and evaluation as a low temperature precursor for Si thin films in microelectronic devices.

### **Nanoparticle Synthesis in Inverse Micelles and Printed Microelectronics**

The vision of this thesis work was to establish that Si nanoparticles could be used in the low temperature fabrication of microelectronic devices, in a similar fashion to work that is described in this thesis that we had done with the II-VI semiconductor CdSe.<sup>1-5,10</sup> The synthesis of Si nanoparticles was known to be difficult, and there was not an accepted synthetic procedure as there was with CdSe<sup>131</sup> and similar binary semiconductors. However, these established synthetic routes had been found to be inappropriate for the preparation of II-VI semiconductor inks, and so a modified synthetic procedure was developed.<sup>1,10</sup> In the case of Si, a similar situation was anticipated: the published synthetic procedure for producing Si nanoparticles in inverse micelles would be

appropriate, except that surfactant modifications would need to be introduced in order to prevent bulky surfactants from formally binding to the particle surface and introducing large amounts of C and O impurities into the anticipated semiconductor thin films. Surfactant modification was anticipated as being enabling, and in fact might be enabling, if the product can be purified without oxidation.

Despite critical problems with Si nanoparticle purification, a number of synthetic advances were made as a part of this work. Chief among them was the successful use of a modified nonionic surfactant, preventing the nanoparticle product from formally bonding to the nanoparticle surface and possibly enabling the production of a high quality nanoparticle ink by this synthetic route. Without this advance, it is possible that there would be no chance for this synthetic technique to be successful in the production of semiconductor inks, as the reported cationic surfactants lead to tight binding at nanoparticle surfaces<sup>267</sup> and the reported nonionic surfactants can bind through their alcohol terminus to nanoparticle surfaces, both introducing large amounts of undesirable and critical impurities.

The use of a capped surfactant also provides some insight into the mechanism of nanoparticle formation in inverse micelles. The possibility of intimate binding of both cationic surfactants and non-modified nonionic surfactants to the Si precursors used in the reduction could be used to explain the nanoparticle growth. Although the literature describes the particle size control as arising from the dissolution of the Si precursor in the interior of the inverse micelle, there is some controversy<sup>195</sup> regarding the mechanism and it was possible that the size control came from the use of aggressive surfactants. As described here, a capped surfactant should not formally bind to the precursor, the growing nanoparticle, or the product surface. Presumably, electron density donation from the numerous ether oxygens helps to stabilize the growing particle and the product, and also helps to dissolve the precursor, as SiI<sub>4</sub> was not found to be highly soluble in alkanes without the use of the surfactant. The published inverse micellization mechanism is not proven by these results, but these results show that the reaction of the surfactant with the Si tetrahalide to form an intermediate is not critical to the reaction mechanism. These results also implicate the surfactant in the reaction, which has been questioned, as SiI<sub>4</sub> is only soluble in alkanes with some surfactant or a more polar co-solvent such as diglyme. The fact that diglyme also acts as an effective co-solvent with alkanes for the dissolution of SiI<sub>4</sub> indicates that there is not a requirement for micellization for the solid halosilane to dissolve, though that

in no way rules out the possibility that micellization is critical to the reaction mechanism. Although reactions with the capped surfactant were able to rule out a mechanistic path that relies on tight binding between the surfactant and the growing particle and intermediates, at a mechanistic level a clear picture of particle size control is still needed. A number of experiments could be carried out to address these mechanistic issues, including reductions in mixtures of alkanes and diglyme, glyme, and THF, as well as reactions run without any alkane, of which there are two recent reports,<sup>195,196</sup> both lacking a clear picture of how size is controlled in the polar medium.

Further glimpses into the reaction mechanism were seen in the breadth of reactions that were carried out as a part of this project. For example, the reducing agent Red-Al produced the largest particles for reactions at a given concentration. Used as a solution in toluene, Red-Al is the most nonpolar of the investigated reducing agents and might be more inclined to reduce silicon precursors outside of the polar interior of any inverse micelles, leading to a larger average particle size. Taken together with experiments spanning different reducing agents, surfactants, reaction concentrations, and stoichiometries, an understanding of the variability of reductions in inverse micelles was begun.

Although these synthetic questions were not at the center of the project's purpose, they were at the center of the project's path. Similarly, the problems with nanoparticle purification and specifically with product tracking by HPLC were not of primary interest, but they were and are of prime importance in the development of a silicon nanoparticle ink. Nanoparticle-based printed microelectronics depends upon high purity synthesis, intelligent ink formulation, and an understanding of device processing. While it was the ambition of the extension of this approach from CdSe to Si to address all three of these points, progress was limited to synthesis and purification. If the synthetic product can be identified during purification, there is the promise of greater understanding, and the possibility of realizing low temperature printed silicon.

## Conclusions

### Printed Inorganic Electronics

At the outset of this research *printed electronics* connotated *organic electronics*. Inorganic materials were not known to be printable, in spite of the great incentive arising from their well-known superior performance characteristics. The research described in this thesis demonstrated for the first time that inorganic semiconductors could be printed and used as the active layers in semiconductor devices and that printed inorganic materials could have device performances superior to those known for the best printed organic semiconductors.<sup>1,10</sup>

This thesis work dealt with three interrelated areas of inquiry. The first and primary area was the chemical synthesis of nanoparticles appropriate for high quality semiconductor inks. The second area was ink formulation and included purification, surface modification, and solvent selection. The final area was device fabrication and characterization.

The first semiconductor studied as a part of this work, CdSe, was chosen primarily because of its well-developed nanoparticle synthesis,<sup>131,136</sup> but also because of its successful use as the active layer in TFTs.<sup>159,160</sup> In spite of the existence of established CdSe nanoparticle syntheses, synthetic development was required to produce a nanoparticle product with a surface termination appropriate for device fabrication and a size distribution that took advantage of the considerable size-dependent melting point depression observed in nanoparticles.<sup>37,132,133</sup> Results described here found printed TFT performance to depend on the semiconductor ink solvent and the nanoparticle surface characteristics, both of which can be intimately related to the synthetic methods employed. Device quality was the ultimate metric of the success of synthesis and ink formulation. Mobilities of  $1 \text{ cm}^2\text{V}^{-1}\text{s}^{-1}$  and ON/OFF ratios in excess of  $10^4$  were obtained from printed TFTs, demonstrating for the first time that inorganic semiconductors could successfully be printed.<sup>1</sup>

The second semiconductor studied as a part of this work, Si, was chosen primarily because of its commercial dominance, but also because of it is abundant and environmentally benign. Unlike CdSe, which has very well developed nanoparticle synthetic procedures known in the chemical literature, little work has

been carried out on Si nanoparticle synthesis. Even the best synthetic procedures<sup>165,196,240,242</sup> suffer from poor and sometimes inconsistent yields, nonuniform surface termination, and chemical impurities. As a part of this thesis, the synthesis of Si nanoparticles in inverse micelles was extensively studied. The technique was found to produce a wide range of nanoparticles, networks, and tetrahedra, but for a range of reaction conditions nanoparticles were found to be the exclusive product. The synthetic method was extended and demonstrated with inert capped nonionic surfactants, enabling the synthesis of Si nanoparticles free of strong surfactant-particle interactions. While these synthetic advances were successful and necessary steps in the development of a Si ink, device fabrication was limited due to difficulties with nanoparticle purification. Si nanoparticle isolation proved to be very difficult, most likely due to low yielding reactions or the oxidation of the Si nanoparticle product during purification.

In addition to the work described in this thesis, related work at the MIT Media Lab demonstrated that inorganic nanoparticle inks can be printed at high resolution using established techniques such as ink jet printing<sup>6,15</sup> and laser writing,<sup>13</sup> as well as emerging and novel techniques such as liquid embossing<sup>2,11,12</sup> and AFM printing.<sup>14</sup> These techniques, coupled with the demonstration of printable inorganic materials described in this thesis, lay the groundwork for continued research into the printing of semiconductors and the conductors and insulators that would best compliment them.

Future research into printable II-VI semiconductors should focus on the role of morphology and chemical impurities (namely iodine) in the quality of the printed thin film. Device performance was found to be tied to both the presence of iodine and the use of pyridine as a solvent, as evidenced by the observation of gross morphological differences seen under a microscope. Exploring alternative solvents and impurities, or at least directly controlling impurities, might lead to improved device performance. Improvements might also be had with sustained research into optimized thin film deposition and processing conditions. A largely unexplored area to pursue with these films is device lifetime and the parameters relating to lifetime. Although devices were encapsulated so that they could be measured in an open laboratory atmosphere, a systematic encapsulation study or search was never undertaken. The II-VI semiconductors are ideal not only to demonstrate the feasibility of printed inorganic materials but also to serve as a test bed for research into ink optimization and the variables that are highly relevant to the improvement of printable semiconductor materials. Already, in the work

described here, the first demonstration of printed inorganic semiconductor devices has been made and simple changes in chemical impurities and ink formulation have been identified as having very important control over device properties, inducing changes of more than three orders of magnitude in both mobility and ON/OFF ratio.

Group IV nanocrystal synthesis and purification need to be more fully developed in order to address the feasibility of printing Si. Important progress was made toward this end as a part of this thesis research, although purification remains a barrier. Synthesis in inverse micelles remains a possibility, but, in contrast to published descriptions, the technique was found to be rich in complexity and subtlety. Alternative purification methods are a possibility and should be investigated, but the greatest advances to be had with this synthetic method would result from a direct collaboration with the authors of the initial studies<sup>165,263-265</sup> of the synthesis of Si in inverse micelle solutions. Coupled with the results described in this thesis – namely the extension of the synthetic method to alcohol-free capped surfactants and the mapping of the most fertile reaction stoichiometry and concentration regions – the purification knowledge and infrastructure of these researchers should lead to an identification of the feasibility of synthesis in inverse micelles as a route to demonstrating printed Si TFTs. Silicon devices themselves will require heavy characterization and comparison to commercial Si devices and printed II-VI devices. The same issues facing II-VI materials (chemical impurities and solvent selection or ink formulation) are expected to be very important to the success of printable silicon, but HPLC purification, if it is found to be a viable route to Si nanoparticle purification, should provide exquisite control over particle size, surface termination, and perhaps even chemical composition.

Future work in the development of inorganic nanocrystal inks will determine their ultimate utility. The work described in this thesis demonstrates the potential of these materials as active layers in microelectronic devices. All-printed inorganic devices were demonstrated with printing at micron-scale resolution. The possibility of realizing low temperature printed silicon is not out of reach, although to date it has been elusive. Beyond it lies work in printing high-mobility III-V semiconductors and doped semiconductors, as well as in the development of a full suite of printable materials: conductors, semiconductors, and insulators. Although the initial demonstration of the feasibility of these materials has just

been realized, it is the vision of this work that these materials enable a new means of microelectronics fabrication through high-resolution printing.



## Experimental Procedures

### CdSe Synthesis

All glassware was oven-dried and reagents were of the highest purity available except where noted.

### Pyrolysis

The pyrolysis method used was a modified procedure<sup>131,300</sup> based on published methods. Reactions were carried out under nitrogen in a fume hood. The reagents were prepared in a glove box, starting with the filtration of CdMe<sub>2</sub> (Organometallics) through a 0.2 μm Teflon filter (Millipore). A 1 M standard solution of Se in TOP was prepared by dissolving Se shot (Alfa Aesar) in TOP (Fluka) overnight. The filtered CdMe<sub>2</sub> and TOP-Se solution served as the stock for a number of reactions.

Outside of the glove box, the reaction apparatus was set up. TOPO (30 g, technical grade, Alfa Aesar) was weighed into a 250 mL round bottom flask, a stir bar added, and the flask fitted with a Vigreux column and nitrogen/vacuum inlet, a thermometer, and a wire-tied rubber septa. The flask was placed under vacuum and heated at 120 °C for 2 hours. The flask was then opened to nitrogen and the temperature increased to approximately 300 °C.

Inside the glove box, 16 mL of TOP were taken into a 20 mL polypropylene syringe (Aldrich) and half dispensed into a scintillation vial. A 250 μL syringe was then used to transfer 200 μL of CdMe<sub>2</sub> to the TOP, and the remaining TOP added to the vial. Finally 4 mL of the 1 M TOP-Se stock solution were added to the vial and the entire mixture loaded into the syringe. The syringe was outfitted with a disposable needle and removed from the glove box.

The syringe was then used to rapidly inject its contents into the hot, vigorously stirred TOPO, causing a heavy reduction in the reaction temperature. The reaction was immediately removed from heat and after cooling to ~70 °C 10 mL of butanol (Aldrich) were added to prevent the reaction mixture from solidifying.

After cooling to room temperature, the reaction mixture was transferred to an Erlenmeyer flask and the particles were isolated by metering MeOH into the reaction until the broth became cloudy. At this point an additional 2 mL of MeOH were added and the mixture was centrifuged. The supernatant was kept and an excess of MeOH added to force the majority of the remaining particles out of solution. After centrifuging, the particles were collected in butanol and the size distribution further narrowed, or the particles were taken up in pyridine for cap exchange. The supernatant was allowed to sit under N<sub>2</sub>, and the particles that precipitated onto the flask's walls were collected as a separate sample.

Cap exchange was carried out by suspending the precipitated particles in pyridine. After stirring at 60 °C for a minimum of 6 hours, the nanoparticles were precipitated out by adding hexane. The particles were collected after centrifugation and were re-suspended in pyridine and the process repeated at least twice more.

## Metathesis

Metathesis reactions were based off of a published procedure.<sup>167</sup> The nanoparticle preparation was performed under a nitrogen atmosphere in either a glove bag or a glove box. CdI<sub>2</sub> ( $7.4 \times 10^{-4}$  mol, Alfa Aesar) was dissolved in 50 mL MeOH (0.015 M, Aldrich) and cooled in a dry ice/acetone bath. Na<sub>2</sub>Se ( $7.4 \times 10^{-4}$  mol, Alfa Aesar or in-house synthesis) was similarly dissolved in 50 mL MeOH (0.015 M) and cooled. The reagents were then poured into a beaker with 30 mL chilled MeOH, reacting instantaneously to yield a red solution. The particles precipitated from the solution and were collected by centrifuging the mixture and then decanting, or by filtering the mixture. In both cases the isolated particles were repeatedly washed with MeOH to remove the soluble byproduct, NaI. Isolated particles were then taken up in pyridine (Aldrich).

A series of modified metathesis reactions were carried out in a glove box at room temperature as well as elevated temperatures. CdMe<sub>2</sub> (Alfa Aesar) and TMS<sub>2</sub>Se (Strem) were both purified by vacuum transfer and then reacted at 1-10 mM concentrations in amine solvents such as pyridine, 4-ethylpyridine, hexylamine, octylamine, nonylamine, decylamine, and dodecylamine. All of these reactions produced an agglomerated product, and most precipitated a yellow solid within minutes of the addition of the second reagent. Lower concentrations and raised

temperatures up to 115 °C were used with moderate improvement in product stability, but the product was still found to agglomerate. An alternative to these organometallic metathesis reactions was carried out by reacting CdI<sub>2</sub> and TMS<sub>2</sub>Se in pyridine or 4-ethylpyridine. The reactions were carried out at room temperature and at similar concentrations as the other metathesis reactions, using MeOH and pyridine to dissolve the CdI<sub>2</sub>. The product was soluble in pyridine and was purified by precipitation induced by the addition of an excess of MeOH or hexane.

### **Alkali Metal Selenide Synthesis**

Alkali metal mono- and diselenides were synthesized according to a published procedure.<sup>175</sup> In a nitrogen-filled glove box the elements (sodium or potassium and selenium, Aldrich and Alfa Aesar, respectively) were mixed in tetrahydrofuran (THF, 275 mL per mol Se) with catalytic naphthalene (10 mol% relative to the alkali metal). The mixture was refluxed for at least one hour and the product was allowed to settle. The solvent was removed and the product was washed with THF or hexane.

### **CdSe Film Formation and Device Fabrication**

All depositions and heat treatments were carried out in a nitrogen-filled glove box.

By evaporating the solvent from a known volume of the solution, the concentration of the pyrolysis-formed nanoparticle suspension was determined to be ~10 mg/mL. The metathesis-formed nanoparticle suspension was less concentrated, ~2 mg/mL. Pyridine-based solutions of CdSe nanoparticles were deposited by touching the tip of a micro-pipette to the surface of a glass slide or *n*-doped Si wafer. These samples were analyzed with an Olympus BX60 optical microscope, a Digital Instruments Nanoscope IIIa atomic force microscope (AFM), a Jeol JSM-6320 FV Scanning Electron Microscope (SEM), and a Tencor P10 Surface Profiler.

Cu TEM grids with amorphous carbon films were deposited onto with a single drop of CdSe nanoparticles in pyridine. The excess solution was wicked away. The grids were then used as samples for TEM and EDX.

To examine film formation, some of the coated TEM grids were placed onto hotplate at 350 or 400 °C hotplate for 30 minutes. Grids were used as samples for TEM and EDX, using a Jeol Jem-2010 Electron Microscope.

Samples for XPS were prepared on an *n*-doped Si wafer by repeatedly depositing CdSe particles synthesized by both metathesis and pyrolysis. The metathesis samples were heated at 350 °C and the pyrolysis samples heated at 400°C, both for 30 minutes. A Physical Electronics 5200 C X-ray Photoelectron Spectrometer with a Mg K<sub>α</sub> non-monochromatized source at 300 W was used.

Samples for secondary-ion mass spectrometry (SIMS) were prepared by depositing CdSe particles synthesized by metathesis onto a Si wafer with 100 nm thick thermally grown SiO<sub>2</sub> so that two films of differing thickness resulted. The films were subjected to a typical TFT fabrication process heat treatment, heating at 350 °C for 1 hour with a heating ramp rate of 80 °C/min. SIMS was performed by Charles Evans and Associates at the Evans East facility.

RBS was performed at Vanderbilt University.

Samples were prepared for Fourier transform infrared spectroscopy (FTIR) by solution depositing the material, letting it dry, and then annealing it at 400 °C. The product was scraped from the substrate and analyzed on a Nicolet Magna IR 860.

Test wafers were prepared in a clean room at the Microsystems Technology Laboratory (MTL) at MIT. Bottom-gate transistor structures were fabricated without any semiconductor in the channel. The channel length was either 3 or 8 μm and the channel width was 293 μm. The electrodes were connected to a large pad for ease of contact and consisted of 100 nm Cr with an overcoat of Au. The oxide was 80 nm thick thermally grown SiO<sub>2</sub>, and the heavily doped Si gate was common to all of the devices. Each 100 mm wafer had ~64 devices.

In a glove box, CdSe nanoparticles were deposited onto the wafer by touching a micro-pipette to the surface over the channel region of the wafer. After the solvent

evaporated, more semiconductor was deposited or the wafer was heated on a hot plate. Heat treatments at 150, 250, 300, and 350 °C were carried out. There were two general types of heat treatment, a ramp up and a thermal shock. The ramp up placed a wafer on the hot plate and gradually brought the temperature to the anneal temperature. The thermal shock program put the wafer onto the hot plate that was already at the anneal temperature. For both programs the duration of heating at the peak temperature was generally 30 minutes.

After cooling, Norland Optical Adhesive 73, a UV-curable polymer adhesive, was used to encapsulate the semiconductor area.

All devices were tested with an HP 4156A precision semiconductor parameter analyzer. Devices were probed in the dark because the CdSe films are photoconductive. Devices were not probed in the glove box. A drain-source voltage sweep of -10 to 10 V was usually used with a gate voltage sweep of -40 to 40 V.

### **Device Calculations**

TFT linear regime mobilities were extracted by equating the slope of the plot to  $(W/L)\mu C_{ox}V_D$  at  $V_D = 2.5$  V, where  $C_{ox}$  is the capacitance of the insulating gate oxide and  $W/L$  is the ratio of the channel width and length. The threshold voltage was extracted from the  $V_G$  intercept of the  $I_D$ - $V_G$  plot and the subthreshold slope was determined from the slope of a logarithmic plot of drain current versus gate voltage.

### **Si Synthesis**

All reactions and manipulations involving silicon materials were carried out in an Ar filled glove box. Reagents were of the highest purity available except where noted. All glassware was dried in an oven prior to use and silylated if it was to be exposed to silicon bearing chemicals. The silylation procedure followed a published report<sup>246</sup> and consisted of a 1-3 hour exposure of the glassware to a 2-3% solution of dichlorodimethylsilane in toluene, followed by repeated rinsing with hexane and methanol and oven drying.

## Nanoparticles from Porous Silicon

Silicon nanoparticles were prepared from porous silicon wafers that were prepared according to procedures described in the literature.<sup>138,198</sup> Silicon wafers with (100) orientation and *p*-type electrical doping and resistivity of 2-25  $\Omega\cdot\text{cm}$  were used as substrates for the formation of porous surface layers by anodization. The wafers are first sonicated in acetone for 15 minutes and dried under a stream of nitrogen. The wafers are then immersed in an electrolyte bath and optionally advanced into the bath at a rate of  $\sim 10$  mm/h. The wafers were connected to a constant current of 10, 50, or 270 mA using a platinum wire mesh immersed in the electrolyte bath as the counter electrode. The bath was agitated throughout the procedure and the temperature of the bath was kept below 15 °C with an isopropanol and dry ice bath. The composition of the bath was either HF (48% in water, doubly distilled, Aldrich) in ethanol (2:1 EtOH:HF, Aldrich) or in methanol (2:1 MeOH:HF, Aldrich) with hydrogen peroxide (32% in water, 2:1 H<sub>2</sub>O<sub>2</sub>:HF, Aldrich). After etching for 1-2 hours the wafers were removed from the electrolyte, rinsed with MeOH and sonicated for 20 minutes in an organic solvent while flushed with nitrogen. Solvents included toluene, glyme, and acetone.

## Metathesis

Silicon nanoparticle synthesis was attempted by following a procedure described in the literature.<sup>246</sup> Magnesium silicide (20 mg, Alfa Aesar) was charged into a vessel with glyme (10 mL, Aldrich) and excess silicon tetrachloride (40  $\mu\text{L}$ , Aldrich). The mixture was refluxed for 2 days, allowed to cool to room temperature, and the volatile solvent and remaining SiCl<sub>4</sub> removed *in vacuo*. Fresh glyme was introduced to the reaction product and it was further reacted at ambient temperature with the Grignard reagent butylmagnesium chloride (2 M in THF, 0.5 mL, Aldrich) for 24 hours. The solvent was again removed *in vacuo* and the product dissolved in hexane and the byproduct salts were extracted with water.

## Inverse Micellar Synthesis

Silicon nanoparticle synthesis was carried out by reductions in inverse micelles according to procedures outlined in the literature.<sup>165,267</sup> Silicon tetrachloride,

silicon tetrabromide, and silicon tetraiodide (Aldrich) were dissolved at concentrations ranging from 0.01 to 100 mM (usually 1-2 mM) overnight in surfactant solutions (10 wt% C<sub>12</sub>E<sub>5</sub> (Nikko), C<sub>12</sub>E<sub>8</sub> (Fluka), or C<sub>12</sub>E<sub>5</sub>Et surfactant in hexane or octane or 10 wt% TOAB or DDAB (Aldrich) in toluene). Reactions were usually carried out from 1-10 mL and in parallel using the same stock solution of the silicon precursor prepared the previous evening. Reducing agents were added in equimolar to fourfold excess amounts. Reducing agents (all from Aldrich) included neat anhydrous hydrazine, 1 M hydrazine in THF, 1 M LAH in THF, 1 M Superhydride in THF, and Red-Al in toluene. Reactions were allowed to proceed from 1 h to 5 days (usually 4 h). For some reactions and especially those carried out with capped surfactants and an excess of the reducing agent, octylamine was added to stabilize the product and to quench any remaining reducing agent. Product purification consisted of optional extraction with acetonitrile and preparative HPLC (Varian) using either a polymeric size exclusion column (Polymer Labs 500 or 1000 Å pore size) with THF (Aldrich, both stabilized and unstabilized) or toluene (Aldrich) as the mobile phase or a reverse phase column (Varian 100 Å pore size C18-terminated packing material) with acetonitrile (Aldrich, anhydrous) as the mobile phase.

### **Surfactant Alkylation**

The alcohol terminus of polyether surfactants was alkylated with alkyl bromides using a procedure modified from one described in the literature.<sup>289</sup> The reaction is run neat, using the surfactant as the reaction solvent, with KOH added to the surfactant (4 mol KOH per mol of surfactant) and an excess of the alkyl halide (2 mol ethyl bromide per mol surfactant). The reaction was allowed to proceed from 1-7 days and monitored by thin layer chromatography for complete conversion. The product was then purified by column chromatography, using 25% acetonitrile and 75% toluene as the mobile phase and silica gel as the stationary phase.

### **Characterization**

A Hewlett Packard (HP) 8452 Ultraviolet-Visible (UV-Vis) spectrophotometer was used for gathering UV-Vis spectra and a Jeol Jem-2010 Electron Microscope was used for TEM and energy dispersive x-ray spectroscopy (EDX). Samples for

TEM were prepared in a glove box by depositing the Si colloids onto amorphous carbon coated Cu grids (Ladd).

Samples were prepared for Fourier transform infrared spectroscopy (FTIR) by solution depositing the material onto KBr plates or by taking measurements of Si colloids in liquid cells that were loaded in an argon filled glove box. The Si nanoparticles were analyzed on a Nicolet Magna IR 860.

### **Film Formation and Device Fabrication**

Attempts at printing Si TFTs were made in a manner similar to that used to prepare CdSe TFTs, although the efforts were unsuccessful. Test wafers were prepared in a clean room at the Microsystems Technology Laboratory (MTL) at MIT. Bottom-gate transistor structures were fabricated without any semiconductor in the channel. The channel length was either 3 or 8  $\mu\text{m}$  and the channel width was 293  $\mu\text{m}$ . The Al electrodes were connected to a large pad for ease of contact. The oxide was 100 nm thick thermally grown  $\text{SiO}_2$ , and the heavily doped Si gate was common to all of the devices. Each 100 mm wafer had ~64 devices.

In an Ar filled glove box, Si nanoparticles were deposited onto the wafer by touching a micro-pipette to the surface over the channel region of the wafer. After the solvent evaporated, more semiconductor was deposited or the wafer was heated on a hot plate. Heat treatments at 350  $^{\circ}\text{C}$  were carried out for 1 hour, ramping up to that temperature at 80  $^{\circ}\text{C}/\text{min}$ .

After cooling, Norland Optical Adhesive 73, a UV-curable polymer adhesive, was used to encapsulate the semiconductor area.

All devices were tested with an HP 4156A precision semiconductor parameter analyzer. Devices were not probed in the glove box. A drain-source voltage sweep of -10 to 10 V was usually used with a gate voltage sweep of -40 to 40 V.



## Acknowledgements

I would like to thank Prof. Jacobson for his guidance with this work and for providing the vision and support for an exciting and innovative laboratory. I would also like to thank Prof. Swager and Prof. Akinwande for their help and support of this thesis. Additionally, Prof. Bawendi, Prof. Hamad-Schifferli, Prof. Antoniadis, Prof. Hammond, Prof. Gershenfeld, and Prof. Manalis all provided helpful comments or instruction at various times during this work.

I am very grateful to my colleagues in the Jacobson Group: Babak Nivi, Colin Bulthaupt, Peter Carr, Jimmy Jia, Marcin Strojwas, Dave Mosley, Eric Wilhelm, Saul Griffith, Brian Hubert, Sawyer Fuller, Danielle Smith, Brian Chow, Dave Kong, and Vikas Anant.

I would not have been able to complete this research without the assistance of Mike Frongillo (TEM and SEM), Elisabeth Shaw (XPS and AFM), Tim McClure (FTIR and profilometry), and Jason Taylor (RBS, at Vanderbilt University).

I would like to acknowledge the efforts of Linda Peterson and Pat Solakoff in helping me coordinate and finalize this thesis.

Conversations and discussions with the following people were very helpful: Doug Schulz, Chris Murray, Jess Wilcoxon, Brian Korgel, Christos Dimatrakopoulos, Zhenan Bao, Howard Katz, Ananth Dodabalapur, David Harwell, Joerg Rockenberger, and Fabio Zurcher.

As always, my family and friends deserve a great deal of thanks for their sustained support.

Most of all, I'd like to thank my wife, Savalai, for helpful comments and support.

This work made use of MRSEC Shared Facilities supported by the National Science Foundation under Award Number DMR-9400334.

## References

- 1 BA Ridley, B Nivi and JM Jacobson. "All-Inorganic Field Effect Transistors Fabricated by Printing." *Science* (286) 746-749 **1999**.
- 2 CA Bulthaupt, EJ Wilhelm, BN Hubert, BA Ridley and JM Jacobson. "All-Additive Fabrication of Inorganic Logic Elements by Liquid Embossing." *Applied Physics Letters* (79) 1525-1527 **2001**.
- 3 BA Ridley, B Nivi, BN Hubert, CA Bulthaupt, EJ Wilhelm and JM Jacobson. "Solution-Processed Inorganic Transistors and Sub-Micron Non-Lithographic Patterning Using Nanoparticle Inks." *Materials Research Society Symposium Proceedings* (581) 115-120 **2000**.
- 4 C Bulthaupt, E Wilhelm, B Hubert, B Ridley and J Jacobson. "All-Printed Inorganic Logic Elements Fabricated by Liquid Embossing." *Materials Research Society Symposium Proceedings* (624) 225-230 **2000**.
- 5 C Bulthaupt, E Wilhelm, B Hubert, B Ridley and J Jacobson. "Direct Fabrication of All-Inorganic Logic Elements and Microelectromechanical Systems from Nanoparticle Precursors." *Materials Research Society Symposium Proceedings* (636) D10.14.11-D10.14.17 **2001**.
- 6 SB Fuller, EJ Wilhelm and JM Jacobson. "Ink-Jet Printed Nanoparticle Microelectromechanical Systems." *Journal of Microelectromechanical Systems* (11) 54-60 **2002**.
- 7 S Griffith, M Mondol, DS Kong and JM Jacobson. "Nanostructure Fabrication by Direct Electron-Beam Writing of Nanoparticles." *Journal of Vacuum Science and Technology B* (20) 2768-2772 **2002**.
- 8 J Jacobson. "The Desktop Fab." *Communications of the ACM* (44) 41-43 **2001**.
- 9 J Park and JM Jacobson. "All Printed Bistable Reflective Displays: Printable Electrophoretic Ink and All Printed Metal-Insulator-Metal Diodes." *Materials Research Society Symposium Proceedings* 211-217 **1998**.

- <sup>10</sup> BA Ridley. "Inorganic Semiconductors for Printed Transistors." Master's Thesis, Massachusetts Institute of Technology **1999**.
- <sup>11</sup> CA Bulthaupt. "Liquid Embossing: A Technique for Fabricating Sub-micron Electrical, Mechanical, and Biological Structures." Master's Thesis, Massachusetts Institute of Technology **2001**.
- <sup>12</sup> EJ Wilhelm. "Design of a Liquid Embossing Machine." Master's Thesis, Massachusetts Institute of Technology **2001**.
- <sup>13</sup> S Griffith. "Towards Personal Fabrications: Tabletop Tools for Micron and Sub-Micron Scale Functional Rapid Prototyping." Master's Thesis, Massachusetts Institute of Technology **2001**.
- <sup>14</sup> BN Hubert. "Pick-and-Place Nanoassembly." Doctoral Thesis, Massachusetts Institute of Technology **2001**.
- <sup>15</sup> SB Fuller. "Ink Jet Deposition of Inorganic Nanoparticle Materials as a Route to Desktop Fabrication of Integrated Logic and Micromachinery." Bachelor's Thesis, Massachusetts Institute of Technology **2000**.
- <sup>16</sup> J Park. "All Printed Bistable Reflective Displays: Printable Electrophoretic Ink and All Printed Metal-Insulator-Metal Diodes." Bachelor's Thesis, Massachusetts Institute of Technology **1998**.
- <sup>17</sup> JY-J Jia. "Characterization of Silicon and Germanium Nanoparticles." Bachelor's Thesis, Massachusetts Institute of Technology **2002**.
- <sup>18</sup> F Garnier. "Thin-Film Transistors Based on Organic Conjugated Semiconductors." *Chemical Physics* (227) 253-262 **1998**.
- <sup>19</sup> F Garnier. "Organic-Based Electronics a la Carte." *Accounts of Chemical Research* (32) 209-215 **1999**.
- <sup>20</sup> CD Dimitrakopoulos and DJ Mascaro. "Organic Thin-Film Transistors: A Review of Recent Advances." *IBM Journal of Research and Development* (45) 11-27 **2001**.
- <sup>21</sup> CD Dimitrakopoulos and PRL Malenfant. "Organic Thin Film Transistors for Large Area Electronics." *Advanced Materials* (14) 99-117 **2002**.

- <sup>22</sup> JA Rogers and Z Bao. "Printed Plastic Electronics and Paperlike Displays." *Journal of Polymer Science A* (40) 3327-3334 **2002**.
- <sup>23</sup> CR Kagan, DB Mitzi and CD Dimitrakopoulos. "Organic-Inorganic Hybrid Materials as Semiconducting Channels in Thin-Film Field-Effect Transistors." *Science* (286) 945-947 **1999**.
- <sup>24</sup> DB Mitzi, CD Dimitrakopoulos and LL Kosbar. "Structurally Tailored Organic-Inorganic Perovskites: Optical Properties and Solution-Processed Channel Materials for Thin-Film Transistors." *Chemistry of Materials* (13) 3728-3740 **2001**.
- <sup>25</sup> DB Mitzi, K Chondroudis and CR Kagan. "Organic-Inorganic Electronics." *IBM Journal of Research and Development* (45) 29-45 **2001**.
- <sup>26</sup> DB Mitzi, CD Dimitrakopoulos, J Rosner, DR Medeiros, ZT Xu and C Noyan. "Hybrid Field-Effect Transistor Based on a Low-Temperature Melt-Processed Channel Layer." *Advanced Materials* (14) 1772-1776 **2002**.
- <sup>27</sup> FY Gan and I Shih. "Preparation of Thin-Film Transistors With Chemical Bath Deposited CdSe and CdS Thin Films." *IEEE Transactions on Electron Devices* (49) 15-18 **2002**.
- <sup>28</sup> FY Gan and I Shih. "Thin Film Transistors With Anodic Gate Dielectrics and Chemical Bath Deposited Active Layers." *Journal of Vacuum Science and Technology A* (20) 1365-1368 **2002**.
- <sup>29</sup> RS Sposili and JS Im. "Sequential Lateral Solidification of Thin Silicon Films on SiO<sub>2</sub>." *Applied Physics Letters* (69) 2864-2866 **1996**.
- <sup>30</sup> JS Im, MA Crowder, RS Sposili, JP Leonard, HJ Kim, JH Yoon, VV Gupta, H Jin Song and HS Cho. "Controlled Super-Lateral Growth of Si Films for Microstructural Manipulation and Optimization." *Physics and Statistics of Solids* (166) 603-617 **1998**.
- <sup>31</sup> J Bharathan and Y Yang. "Polymer Electroluminescent Devices Processed by Inkjet Printing: I. Polymer Light-Emitting Logo." *Applied Physics Letters* (72) 2660-2662 **1998**.

- 32 XM Zhao, YN Xia and GM Whitesides. "Soft Lithographic Methods for Nano-Fabrication." *Journal of Materials Chemistry* (7) 1069-1074 **1997**.
- 33 YN Xia and GM Whitesides. "Soft Lithography." *Annual Review of Materials Science* (28) 153-184 **1998**.
- 34 YN Xia, JA Rogers, KE Paul and GM Whitesides. "Unconventional Methods for Fabricating and Patterning Nanostructures." *Chemical Reviews* (99) 1823-1848 **1999**.
- 35 DR Lide (ed.) *Handbook of Chemistry and Physics 77th Edition* CRC Press, Boca Raton, Florida, USA, **1996**.
- 36 H Uda, H Sonomura and S Ikegami. "Screen Printed CdS/CdTe Cells for Visible-Light-Radiation Sensor." *Measurement Science & Technology* (8) 86-91 **1997**.
- 37 AN Goldstein. "The Melting of Silicon Nanocrystals: Submicron Thin-Film Structures Derived from Nanocrystal Precursors." *Applied Physics A* (A62) 33-37 **1996**.
- 38 AA Darhuber, SM Troian and S Wagner. "Physical Mechanisms Governing Pattern Fidelity in Microscale Offset Printing." *Journal of Applied Physics* (90) 3602-3609 **2001**.
- 39 JC Sturm, PI Hsu, SM Miller, H Gleskova, A Darhuber, M Huang, S Wagner, S Troian and Z Suo. "Three-Dimensional Electronic Surfaces." *Materials Research Society Symposium Proceedings* (636) D11.14.11-D11.14.12 **2001**.
- 40 PS Peercy. "The Drive to Miniaturization." *Nature* (406) 1023-1026 **2000**.
- 41 JA Rogers, Z Bao, K Baldwin, A Dodabalapur, B Crone, VR Raju, V Kuck, H Katz, K Amundson, J Ewing and P Drzaic. "Paper-Like Electronic Displays: Large-Area Rubber-Stamped Plastic Sheets of Electronics and Microencapsulated Electrophoretic Inks." *Proceedings of the National Academy of Sciences of the United States of America* (98) 4835-4840 **2001**.
- 42 JA Rogers, Z Bao, M Meier, A Dodabalapur, OJA Schueller and GM Whitesides. "Printing, Molding, and Near-Field Photolithographic

Methods for Patterning Organic Lasers, Smart Pixels and Simple Circuits." *Synthetic Metals* (115) 5-11 **2000**.

- 43 B Michel, A Bernard, A Bietsch, E Delamarche, M Geissler, D Juncker, H Kind, JP Renault, H Rothuizen, H Schmid, P Schmidt-Winkel, R Stutz and H Wolf. "Printing Meets Lithography: Soft Approaches to High-Resolution Printing." *IBM Journal of Research and Development* (45) 697-719 **2001**.
- 44 A Kumar and GM Whitesides. "Features of Gold Having Micrometer to Centimeter Dimensions Can Be Formed Through a Combination of Stamping with an Elastomeric Stamp and an Alkanethiol "Ink" Followed by Chemical Etching." *Applied Physics Letters* (63) 2002-2004 **1993**.
- 45 A Kumar, HA Biebuyck and GM Whitesides. "Patterning Self-Assembled Monolayers: Applications in Materials Science." *Langmuir* (10) 1498-1511 **1994**.
- 46 YN Xia, XM Zhao, E Kim and GM Whitesides. "A Selective Etching Solution for Use With Patterned Self-Assembled Monolayers of Alkanethiolates on Gold." *Chemistry of Materials* (7) 2332-2337 **1995**.
- 47 YN Xia and GM Whitesides. "Extending Microcontact Printing as a Microlithographic Technique." *Langmuir* (13) 2059-2067 **1997**.
- 48 YN Xia, E Kim, M Mrksich and GM Whitesides. "Microcontact Printing of Alkanethiols on Copper and its Application in Microfabrication." *Chemistry of Materials* (8) 601-603 **1996**.
- 49 Y Xia, E Kim and GM Whitesides. "Microcontact Printing of Alkanethiols on Silver and its Application in Microfabrication." *Journal of the Electrochemical Society* (143) 1070-1079 **1996**.
- 50 YN Xia, XM Zhao and GM Whitesides. "Pattern transfer: Self-assembled monolayers as ultrathin resists." *Microelectronic Engineering* (32) 255-268 **1996**.
- 51 YN Xia, M Mrksich, E Kim and GM Whitesides. "Microcontact Printing of Octadecylsiloxane on the Surface of Silicon Dioxide and Its Application in Microfabrication." *Journal of the American Chemical Society* (117) 9576-9577 **1995**.

- <sup>52</sup> TK Whidden, DK Ferry, MN Kozicki, E Kim, A Kumar, J Wilbur and GM Whitesides. "Pattern Transfer to Silicon by Microcontact Printing and RIE." *Nanotechnology* (7) 447-451 **1996**.
- <sup>53</sup> LB Goetting, T Deng and GM Whitesides. "Microcontact Printing of Alkanephosphonic Acids of Aluminum: Pattern Transfer by Wet Chemical Etching." *Langmuir* (15) 1182-1191 **1999**.
- <sup>54</sup> PM St. John and HG Craighead. "Microcontact Printing and Pattern Transfer Using Trichlorosilanes on Oxide Substrates." *Applied Physics Letters* (68) 1022-1024 **1996**.
- <sup>55</sup> YN Xia, E Kim and GM Whitesides. "Micromolding of Polymers in Capillaries: Applications in Microfabrication." *Chemistry of Materials* (8) 1558-1567 **1996**.
- <sup>56</sup> E Kim, YN Xia and GM Whitesides. "Micromolding in Capillaries: Applications in Materials Science." *Journal of the American Chemical Society* (118) 5722-5731 **1996**.
- <sup>57</sup> E Kim, YN Xia, XM Zhao and GM Whitesides. "Solvent-Assisted Microcontact Molding: A Convenient Method for Fabricating Three-Dimensional Structures on Surfaces of Polymers." *Advanced Materials* (9) 651-654 **1997**.
- <sup>58</sup> E Kim, YN Xia and GM Whitesides. "Polymer Microstructures Formed by Molding in Capillaries." *Nature* (376) 581-584 **1995**.
- <sup>59</sup> JA Rogers, ZN Bao and VR Raju. "Nonphotolithographic Fabrication of Organic Transistors with Micron Feature Sizes." *Applied Physics Letters* (72) 2716-2718 **1998**.
- <sup>60</sup> YL Loo, T Someya, KW Baldwin, ZN Bao, P Ho, A Dodabalapur, HE Katz and JA Rogers. "Soft, Conformable Electrical Contacts for Organic Semiconductors: High-Resolution Plastic Circuits by Lamination." *Proceedings of the National Academy of Sciences of the United States of America* (99) 10252-10256 **2002**.
- <sup>61</sup> J Hu, RG Beck, T Deng, RM Westervelt, KD Maranowski, AC Gossard and GM Whitesides. "Using Soft Lithography to Fabricate GaAs/AlGaAs

- Heterostructure Field Effect Transistors." *Applied Physics Letters* (71) 2020-2022 **1997**.
- 62 J Hu, RG Beck, RM Westervelt and GM Whitesides. "The Use of Soft Lithography to Fabricate Arrays of Schottky Diodes." *Advanced Materials* (10) 574-577 **1998**.
- 63 NL Jeon, J Hu, GM Whitesides, MK Erhardt and RG Nuzzo. "Fabrication of Silicon MOSFETs Using Soft Lithography." *Advanced Materials* (10) 1466-1469 **1998**.
- 64 H Junmin, D Tao, RG Beck, RM Westervelt and GM Whitesides. "Fabrication of Arrays of Schottky Diodes Using Microtransfer Molding." *Sensors and Actuators A* (A75) 65-69 **1999**.
- 65 JA Rogers, J Tate, WJ Li, Z Bao and A Dodabalapur. "Printed Organic Transistors and Molded Plastic Lasers." *Israel Journal of Chemistry* (40) 139-145 **2000**.
- 66 SY Chou, PR Krauss and PJ Renstrom. "Imprint Lithography with 25-Nanometer Resolution." *Science* (272) 85-87 **1996**.
- 67 SY Chou, PR Krauss, Z Wei, G Lingjie and Z Lei. "Sub-10 nm Imprint Lithography and Applications." *Journal of Vacuum Science and Technology B* (15) 2897-2904 **1997**.
- 68 Z Wei and SY Chou. "Multilevel Nanoimprint Lithography with Submicron Alignment over 4 in. Si Wafers." *Applied Physics Letters* (79) 845-847 **2001**.
- 69 SY Chou, C Kelmel and G Jian. "Ultrafast and Direct Imprint of Nanostructures in Silicon." *Nature* (417) 835-837 **2002**.
- 70 PR Krauss and SY Chou. "Nano-Compact Disks with 400 Gbit/in<sup>2</sup> Storage Density Fabricated Using Nanoimprint Lithography and Read with Proximal Probe." *Applied Physics Letters* (71) 3174-3176 **1997**.
- 71 Y Zheoning, SJ Schabilitsky and SY Chou. "Nanoscale GaAs Metal-Semiconductor-Metal Photodetectors Fabricated Using Nanoimprint Lithography." *Applied Physics Letters* (74) 2381-2383 **1999**.



- 72 PC Hidber, W Helbig, E Kim and GM Whitesides. "Microcontact Printing of Palladium Colloids: Micron-Scale Patterning by Electroless Deposition of Copper." *Langmuir* (12) 1375-1380 **1996**.
- 73 H Kind, M Geissler, H Schmid, B Michel, K Kern and E Delamarche. "Patterned Electroless Deposition of Copper by Microcontact Printing Palladium(II) Complexes on Titanium-Covered Surfaces." *Langmuir* (16) 6367-6373 **2000**.
- 74 W Jian, S Xiaoyun, C Lei and SY Chou. "Direct Nanoimprint of Submicron Organic Light-Emitting Structures." *Applied Physics Letters* (75) 2767-2769 **1999**.
- 75 JA Rogers, ZN Bao and L Dhar. "Fabrication of patterned electroluminescent polymers that emit in geometries with feature sizes into the submicron range." *Applied Physics Letters* (73) 294-296 **1998**.
- 76 C Marzolin, SP Smith, M Prentiss and GM Whitesides. "Fabrication of Glass Microstructures by Micro-Molding of Sol-Gel Precursors." *Advanced Materials* (10) 571-574 **1998**.
- 77 OJA Schueller, GM Whitesides, JA Rogers, M Meier and A Dodabalapur. "Fabrication of Photonic Crystal Lasers by Nanomolding of Solgel Glasses." *Applied Optics* (38) 5799-5802 **1999**.
- 78 WS Beh, IT Kim, D Qin, YN Xia and GM Whitesides. "Formation of Patterned Microstructures of Conducting Polymers by Soft Lithography, and Applications in Microelectronic Device Fabrication." *Advanced Materials* (11) 1038-1041 **1999**.
- 79 RF Service. "New Age Semiconductors Pick up the Pace." *Science* (287) 415-417 **2000**.
- 80 HE Katz and Z Bao. "The Physical Chemistry of Organic Field-Effect Transistors." *Journal of Physical Chemistry B* (104) 671-678 **2000**.
- 81 BK Crone, A Dodabalapur, R Sarpeshkar, RW Filas, YY Lin, Z Bao, JH O'Neill, W Li and HE Katz. "Design and Fabrication of Organic Complementary Circuits." *Journal of Applied Physics* (89) 5125-5132 **2001**.

- 82 ZN Bao, JA Rogers and HE Katz. "Printable Organic and Polymeric Semiconducting Materials and Devices." *Journal of Materials Chemistry* (9) 1895-1904 **1999**.
- 83 A Dodabalapur, Z Bao, A Makhija, JG Laquindanum, VR Raju, Y Feng, HE Katz and J Rogers. "Organic Smart Pixels." *Applied Physics Letters* (73) 142-144 **1998**.
- 84 ZN Bao, Y Feng, A Dodabalapur, VR Raju and AJ Lovinger. "High-Performance Plastic Transistors Fabricated by Printing Techniques." *Chemistry of Materials* (9) 1299 **1997**.
- 85 RP Zingg, N Nagel, R Bergmann, E Bauser, B Höffinger and HJ Queisser. "First MOS Transistors on Insulator by Silicon Saturated Liquid Solution Epitaxy." *IEEE Electron Device Letters* (13) 294-296 **1992**.
- 86 GK Guist, TW Sigmon, PG Carey, PS Weiss and GA Davis. "Low-Temperature Polysilicon Thin-Film Transistors Fabricated from Laser-Processed Sputtered-Silicon Films." *IEEE Electron Device Letters* (19) 343-344 **1998**.
- 87 SY Yoon, SJ Park, KH Kim and J Jang. "Metal-Induced Crystallization of Amorphous Silicon." *Thin Solid Films* (383) 34-38 **2001**.
- 88 RB Min and S Wagner. "Nanocrystalline Silicon Thin-Film Transistors with 50 nm Thick Deposited Channel Layer,  $10 \text{ cm}^2\text{V}^{-1}\text{s}^{-1}$  Electron Mobility and  $10^8$  ON/OFF Current Ratio." *Applied Physics A* (74) 541-543 **2002**.
- 89 TP Brody. "Active-Matrix TFTs Are in Trouble. Cadmium Selenide Is the Answer." *Information Display* (8) 5-9 **1992**.
- 90 WR Caseri, HD Chanzy, K Feldman, M Fontana, P Smith, TA Tervoort, JGP Goossens, EW Meijer, A Schenning, IR Dolbnya, MG Debije, MP de Haas, JM Warman, AM van de Craats, RH Friend, H Siringhaus and N Stutzmann. ""(Hot-)Water-Proof", Semiconducting, Platinum-Based Chain Structures: Processing, Products, and Properties." *Advanced Materials* (15) 125-129 **2003**.

- <sup>91</sup> M Shim, A Javey, NWS Kam and H Dai. "Polymer Functionalization for Air-Stable n-Type Carbon Nanotube Field-Effect Transistors." *Journal of the American Chemical Society* (123) 11512-11513 **2001**.
- <sup>92</sup> H Klauk, M Halik, U Zschieschang, G Schmid and W Radlik. "High-Mobility Polymer Gate Dielectric Pentacene Thin Film Transistors." *Journal of Applied Physics* (92) 5259-5263 **2002**.
- <sup>93</sup> A Afzali, CD Dimitrakopoulos and TL Breen. "High-Performance, Solution-Processed Organic Thin Film Transistors from a Novel Pentacene Precursor." *Journal of the American Chemical Society* (124) 8812-8813 **2002**.
- <sup>94</sup> BK Crone, A Dodabalapur, R Sarpeshkar, RW Filas, Y-Y Lin, Z Bao, JH O'Neill, W Li and HE Katz. "Design and Fabrication of Organic Complementary Circuits." *Journal of Applied Physics* (89) 5125-5132 **2001**.
- <sup>95</sup> H Sirringhaus, N Tessler and RH Friend. "Integrated Optoelectronic Devices Based on Conjugated Polymers." *Science* (280) 1741-1744 **1998**.
- <sup>96</sup> H Sirringhaus, PJ Brown, RH Friend, MM Nielsen, K Bechgaard, BMW Langeveld-Voss, AJH Spiering, RAJ Janssen, EW Meijer, P Herwig and DM de Leeuw. "Two-Dimensional Charge Transport in Self-Organized, High-Mobility Conjugated Polymers." *Nature* (401) 685-688 **1999**.
- <sup>97</sup> H Sirringhaus, T Kawase, RH Friend, T Shimoda, M Inbasekaran, W Wu and EP Woo. "High-Resolution Inkjet Printing of All-Polymer Transistor Circuits." *Science* (290) 2123-2126 **2000**.
- <sup>98</sup> TP Brody. "CdSe - The Ideal Semiconductor for Active Matrix Displays." *Proceedings of the SPIE* (1664) 2-13 **1992**.
- <sup>99</sup> KC Saraswat, V Subramanian and S Jurichich. "A Low Temperature Polycrystalline Si TFT Technology for Large Area AMLCD Drivers." *Materials Research Society Symposium Proceedings* (472) 439-449 **1997**.
- <sup>100</sup> HE Katz, AJ Lovinger, J Johnson, C Kloc, T Siegrist, W Li, YY Lin, A Dodabalapur, Katr and J Lovinger. "A Soluble and Air-Stable Organic Semiconductor with High Electron Mobility." *Nature* (404) 478-481 **2000**.

- <sup>101</sup> AR Brown, A Pomp, DM de-Leeuw, DBM Klaassen, EE Havinga, P Herwig and K Mullen. "Precursor Route Pentacene Metal-Insulator-Semiconductor Field-Effect Transistors." *Journal of Applied Physics* (79) 2136-2138 **1996**.
- <sup>102</sup> HE Katz. Private Communications, **1997**.
- <sup>103</sup> F Garnier. "Scope and Limits of Organic-Based Thin-Film Transistors." *Philosophical Transactions of the Royal Society of London Series A* (355) 815-827 **1997**.
- <sup>104</sup> F Garnier, R Hajlaoui and M El Kassmi. "Vertical Device Architecture by Molding of Organic-Based Thin Film Transistor." *Applied Physics Letters* (73) 1721-1723 **1998**.
- <sup>105</sup> Z Bao, AJ Lovinger and A Dodabalapur. "Organic Field-Effect Transistors with High Mobility Based on Copper Phthalocyanine." *Applied Physics Letters* (69) 3066-3068 **1996**.
- <sup>106</sup> J Jacobson, B Comiskey, C Turner, J Albert and P Tsao. "The Last Book." *IBM Systems Journal* (36) 457-463 **1997**.
- <sup>107</sup> B Comiskey, JD Albert, H Yoshizawa and J Jacobson. "An Electrophoretic Ink for All-Printed Reflective Electronic Displays." *Nature* (394) 253-255 **1998**.
- <sup>108</sup> JR Heath, PJ Kuekes, GS Snider and RS Williams. "A Defect-Tolerant Computer Architecture: Opportunities for Nanotechnology." *Science* (280) 1716-1721 **1998**.
- <sup>109</sup> CP Collier, EW Wong, M Belohradsky, FM Raymo, JF Stoddart, PJ Kuekes, RS Williams and JR Heath. "Electronically Configurable Molecular-Based Logic Gates." *Science* (285) 391-394 **1999**.
- <sup>110</sup> CP Collier, G Matterstei, EW Wong, Y Luo, K Beverly, J Sampaio, FM Raymo, JF Stoddart and JR Heath. "A [2]Catenane-Based Solid State Electronically Reconfigurable Switch." *Science* (289) 1172-1175 **2000**.
- <sup>111</sup> JR Heath. "Wires, Switches, and Wiring. A Route Toward a Chemically Assembled Electronic Nanocomputer Using Rotaxanes." *Pure and Applied Chemistry* (72) 11-20 **2000**.

- <sup>112</sup> EW Wong, CP Collier, M Behloradsky, FM Raymo, JF Stoddart and JR Heath. "Fabrication and Transport Properties of Single-Molecule-Thick Electrochemical Junctions." *Journal of the American Chemical Society* (122) 5831-5840 **2000**.
- <sup>113</sup> CP Collier, JO Jeppesen, Y Luo, J Perkins, EW Wong, JR Heath and JF Stoddart. "Molecular-Based Electronically Switchable Tunnel Junction Devices." *Journal of the American Chemical Society* (123) 12632-12641 **2001**.
- <sup>114</sup> AR Pease, JO Jeppesen, JF Stoddart, Y Luo, CP Collier and JR Heath. "Switching Devices Based on Interlocked Molecules." *Accounts of Chemical Research* (34) 433-444 **2001**.
- <sup>115</sup> Y Luo, CP Collier, JO Jeppesen, KA Nielsen, E Delonno, G Ho, J Perkins, H-R Tseng, T Yamamoto, JF Stoddart and JR Heath. "Two-Dimensional Molecular Electronics Circuits." *ChemPhysChem* (3) 519-525 **2002**.
- <sup>116</sup> MA Reed, C Zhou, CJ Muller, TP Burgin and JM Tour. "Conductance of a Molecular Junction." *Science* (278) 252-254 **1997**.
- <sup>117</sup> WA Reinert, L Jones, II, TP Burgin, Z Chong Wu, CJ Muller, MR Deshpande, MA Reed and JM Tour. "Molecular Scale Electronics: Syntheses and Testing." *Nanotechnology* (9) 246-250 **1998**.
- <sup>118</sup> J Chen, MA Reed, AM Rawlett and JM Tour. "Large On-Off Ratios and Negative Differential Resistance in a Molecular Electronic Device." *Science* (286) 1550-1552 **1999**.
- <sup>119</sup> J Chen, W Wang, MA Reed, AM Rawlett, DW Price and JM Tour. "Room-Temperature Negative Differential Resistance in Nanoscale Molecular Junctions." *Applied Physics Letters* (77) 1224-1226 **2000**.
- <sup>120</sup> MA Reed, J Chen, AM Rawlett, DW Price and JM Tour. "Molecular Random Access Memory Cell." *Applied Physics Letters* (78) 3735-3737 **2001**.
- <sup>121</sup> C Joachim. "Molecular and Intramolecular Electronics." *Superlattices and Microstructures* (28) 305-315 **2000**.

- 122 SJ Tans, RM Verschueren and C Dekker. "Room Temperature Transistor Based on a Single Carbon Nanotube." *Nature* (393) 49-52 **1998**.
- 123 A Bachtold, P Hadley, T Nakanishi and C Dekker. "Logic Circuits with Carbon Nanotube Transistors." *Science* (294) 1317-1320 **2001**.
- 124 HR Shea, R Martel, T Hertel, T Schmidt and P Avouris. "Manipulation of Carbon Nanotubes and Properties of Nanotube Field-Effect Transistors and Rings." *Microelectronic Engineering* (46) 101-104 **1999**.
- 125 V Derycke, R Martel, J Appenzeller and P Avouris. "Carbon Nanotube Inter- and Intramolecular Logic Gates." *Nano Letters* (1) 453-456 **2001**.
- 126 P Avouris. "Carbon Nanotube Electronics." *Chemical Physics* (281) 429-445 **2002**.
- 127 J Appenzeller, J Knoch, V Derycke, R Martel, S Wind and P Avouris. "Field-Modulated Carrier Transport in Carbon Nanotube Transistors." *Physical Review Letters* (89) 126801-126804 **2002**.
- 128 J Appenzeller, J Knoch, R Martel, V Derycke, SJ Wind and P Avouris. "Carbon Nanotube Electronics." *IEEE Transactions on Nanotechnology* (1) 184-189 **2002**.
- 129 A Javey, Q Wang, A Ural, Y Li and H Dai. "Carbon Nanotube Transistor Arrays for Multistage Complementary Logic and Ring Oscillators." *Nano Letters* (2) 929-932 **2002**.
- 130 A Javey, H Kim, M Brink, Q Wang, A Ural, J Gu, P McIntyre, P McEuen, M Lundstrom and H Dai. "High-Kappa Dielectrics for Advanced Carbon-Nanotube Transistors and Logic Gates." *Nature Materials* (1) 241-246 **2002**.
- 131 CB Murray, DJ Norris and MG Bawendi. "Synthesis and Characterization of Nearly Monodisperse CdE (E = Sulfur, Selenium, Tellurium) Semiconductor Nanocrystallites." *Journal of the American Chemical Society* (115) 8706-8715 **1993**.
- 132 AN Goldstein, CM Echer and AP Alivisatos. "Melting in Semiconductor Nanocrystals." *Science* (256) 1425-1427 **1992**.

- 133 P Buffat and JP Borel. "Size Effect on Melting Temperature of Gold Particles." *Physical Review A* (13) 2287-2298 **1976**.
- 134 CB Murray. "Synthesis and Characterization of II-VI Quantum Dots and Their Assembly into 3D Quantum Dot Superlattices." Doctoral Thesis, Massachusetts Institute of Technology **1995**.
- 135 AN Goldstein, VL Colvin and AP Alivisatos. "Observation of Melting in 30 Å Diameter Cadmium Sulfide Nanocrystals." *Materials Research Society Symposium Proceedings* (206) 271-274 **1991**.
- 136 L Brus. "Chemical Approaches to Semiconductor Nanocrystals." *Journal of the Physics and Chemistry of Solids* (59) 459-465 **1998**.
- 137 RW Siegel. *Scientific American* (275) 74 **1996**.
- 138 JL Heinrich, CL Curtis, GM Credo, KL Kavanagh and MJ Sailor. "Luminescent Colloidal Silicon Suspensions from Porous Silicon." *Science* (255) 66-68 **1992**.
- 139 N Herron, JC Calabrese, WE Farneth and Y Wang. "Crystal Structure and Optical Properties of  $\text{Cd}_{32}\text{S}_{14}(\text{SC}_6\text{H}_5)_{36}\cdot\text{DMF}_4$ , a Cluster with a 15-Angstrom CdS Core." *Science* (259) 1426-1428 **1993**.
- 140 WE Farneth, N Herron and Y Wang. "Bulk Semiconductors from Molecular Solids: A Mechanistic Investigation." *Chemistry of Materials* (4) 916-922 **1992**.
- 141 AP Alivisatos and AN Goldstein. "Low Temperature Thin Films Formed from Nanocrystal Precursors." *US Patent* 5,262,357 **1993**.
- 142 AN Goldstein. "Method for Depositing and Patterning Thin Films by Fusing Nanocrystalline Precursors." *US Patent* 5,559,057 **1996**.
- 143 AN Goldstein. "Group IV Semiconductor Thin Films Formed at Low Temperatures Using Nanocrystal Precursors." *US Patent* 5,576,248 **1996**.
- 144 M Pehnt, DL Schulz, CJ Curtis and DS Ginley. *US Patent* 5,711,803 **1998**.

- <sup>145</sup> DL Schulz, M Pehnt, CJ Curtis and DS Ginley. "CdTe Thin Films: Spray Deposition Using a Nanoparticle Ink Precursor." *Materials Research Society Symposium Proceedings* (426) 349-354 **1996**.
- <sup>146</sup> DL Schulz, M Pehnt, DH Rose, E Urgiles, AF Cahill, DW Niles, KM Jones, RJ Ellingson, CJ Curtis and DS Ginley. "CdTe Thin Films from Nanoparticle Precursors by Spray Deposition." *Chemistry of Materials* (9) 889-900 **1997**.
- <sup>147</sup> DL Schulz, CJ Curtis, RA Flitton, H Wiesner, J Keane, RJ Matson, PA Parilla, R Noufi and DS Ginley. "Nanoparticle Colloids as Spray Deposition Precursors to CIGS Photovoltaic Materials." *AIP Conference Proceedings* (394) 683-691 **1997**.
- <sup>148</sup> M Pehnt, DL Schulz, CJ Curtis, HR Moutinho, A Swartzlander and DS Ginley. "Nanocrystalline Solutions as Precursors to the Spray Deposition of CdTe Thin Films." *Materials Research Society Symposium Proceedings* (382) 461-467 **1995**.
- <sup>149</sup> M Pehnt, DL Schulz, CJ Curtis, KM Jones and DS Ginley. "Nanoparticle Precursor Route to Low-Temperature Spray Deposition of CdTe Thin Films." *Applied Physics Letters* (67) 2176-2178 **1995**.
- <sup>150</sup> DL Schulz, M Pehnt, CJ Curtis and DS Ginley. "Spray Deposition of CdTe Thin Films Using Nanoparticle Precursors." *Materials Science Forum* (225-227) 169-174 **1996**.
- <sup>151</sup> F Ercolessi, W Andreoni and E Tosatti. "Melting of Small Gold Particles - Mechanism and Size Effects." *Physical Review Letters* (66) 911-914 **1991**.
- <sup>152</sup> JE Martin, J Odinek, JP Wilcoxon, RA Anderson and P Provencio. "Sintering of Alkanethiol-Capped Gold and Platinum Nanoclusters." *Journal of Physical Chemistry B* (107) 430-434 **2003**.
- <sup>153</sup> D Huang, F Liao, S Molesa, D Redinger and V Subramanian. "Plastic-Compatible Low-Resistance Printable Gold Nanoparticle Conductors for Flexible Electronics." *Journal of the Electrochemical Society* (150) G412-G417 **2003**.
- <sup>154</sup> A Chemseddine, H Jungblut and S Boulmaaz. "Investigation of the Nanocluster Self-Assembly Process by Scanning Tunneling Microscopy



- and Optical Spectroscopy." *Journal of Physical Chemistry* (100) 12546-12551 **1996**.
- <sup>155</sup> DL Schulz, CJ Curtis, RA Flitton, H Wiesner, J Keane, RJ Matson, KM Jones, PA Parilla, R Noufi and DS Ginley. "Cu-In-Ga-Se Nanoparticle Colloids as Spray Deposition Precursors for Cu(In,Ga)Se<sub>2</sub> Solar Cell Materials." *Journal of Electronic Materials* (27) 433-437 **1998**.
- <sup>156</sup> JEB Katari, VL Colvin and AP Alivisatos. "X-Ray Photoelectron Spectroscopy of CdSe Nanocrystals with Applications to Studies of the Nanocrystal Surface." *Journal of Physical Chemistry* (98) 4109-4117 **1994**.
- <sup>157</sup> A Chemseddine and ML Fearheiley. "Improved Cds Buffer Window Layers for Thin Film Solar Cells." *Thin Solid Films* (247) 3-7 **1994**.
- <sup>158</sup> T Vossmeier, L Katsikas, M Giersig, IG Popovic, K Diesner, A Chemseddine, A Eychmuller and H Weller. "CdS Nanoclusters - Synthesis, Characterization, Size-Dependent Oscillator Strength, Temperature Shift of the Excitonic Transition Energy, and Reversible Absorbency Shift." *Journal of Physical Chemistry* (98) 7665-7673 **1994**.
- <sup>159</sup> TP Brody. "Birth of the Active Matrix." *Information Display* (13) 28-32 **1997**.
- <sup>160</sup> TP Brody. "The Birth and Early Childhood of Active Matrix - A Personal Memoir." *Journal of the SID* (4) 113-127 **1996**.
- <sup>161</sup> C Reita. "Why the World Is Not Rushing to Cadmium Selenide for AMLCDs." *Information Display* (9) 10-11 **1993**.
- <sup>162</sup> J Doutrelaigne, H De Smet, J De Baets, I De Rycke, A Van Calster and J Vanfleteren. "Complimentary CdSe:In/Ge:Cu TFT Circuits for Integrated Display Drivers." *Proceedings of Eurodisplay* 316-319 **1990**.
- <sup>163</sup> AM De Cubber, H De Smet, J De Vos, N Carchon and A Van Calster. "Complementary High-Voltage Technology Based on n-Type CdSe:In and p-Type Ge:Cu Thin-Film Transistors." *IEEE Electron Device Letters* (17) 581-583 **1996**.

- 164 JR Heath. "A Liquid-Solution-Phase Synthesis of Crystalline Silicon." *Science* (258) 1131-1133 **1992**.
- 165 JP Wilcoxon, GA Samara and PN Provencio. "Optical and Electronic Properties of Si Nanoclusters Synthesized in Inverse Micelles." *Physical Review B* (60) 2704-2714 **1999**.
- 166 Y Matsuki and S Ebata. "Novel Cyclosilane Compound, and Solution Composition and Process for Forming a Silicon Film." *US Patent Application* 0021760 **2001**.
- 167 RF Jarvis, M Müllenborn, BG Yacobi, NM Haegel and RB Kaner. "Solution Synthesis and Photoluminescence Studies of Small Crystallites of Cadmium Telluride." *Materials Research Society Symposium Proceedings* (272) 229-234 **1992**.
- 168 M Mullenborn, RF Jarvis, BG Yacobi, RB Kaner, CC Coleman and NM Haegel. "Characterization of Solution-Synthesized CdTe and HgTe." *Applied Physics A* (56) 317-321 **1993**.
- 169 CH Wallace, SH Kim, GA Rose, L Rao, JR Heath, M Nicol and RB Kaner. "Solid-State Metathesis Reactions Under Pressure: A Rapid Route to Crystalline Gallium Nitride." *Applied Physics Letters* (72) 596-598 **1998**.
- 170 J Wiley, P Bonneau, R Treece, R Jarvis, E Gillan, L Rao and R Kaner. "Solid-State Metathesis Routes to Layered Transition-Metal Dichalcogenides and Refractory Metals" in *Supramolecular Architecture*, 369-383 **1992**.
- 171 JP Wilcoxon. "Optical Properties of II-VI and IV Semiconductor Nanoclusters for Phosphor Applications." *Materials Research Society Fall Meeting* (E13.35) **2002**.
- 172 M Mullenborn, RF Jarvis, BG Yacobi, RB Kaner, CC Coleman and NM Haegel. "Characterization of Solution-Synthesized CdTe and HgTe." *Applied Physics A-Materials Science & Processing* (56) 317-321 **1993**.
- 173 MG Bawendi. Private Communications, **1999**.

- 174 S Behrens and D Fenske. "Cadmium Nanoclusters with Phenylselenolato- and Phenyltelluroolato Ligands: Synthesis and Structural Characterization of  $[\text{Cd}_{17}\text{Se}_4(\text{SePh})_{24}(\text{PPh}_3)_4][\text{Cd}_8\text{Se}(\text{SePh})_{12}\text{Cl}_4]$ ,  $[\text{Cd}(\text{DMF})_6][\text{Cd}_8\text{Se}(\text{SePh})_{12}\text{Cl}_4]$ ,  $[\text{Cd}_8\text{Se}(\text{SePh})_{14}(\text{PPh}_3)_2]$ ,  $[\text{Cd}_8\text{Se}(\text{SePh})_{14}(\text{DMF})_3]$  and  $[\text{Cd}_8\text{Te}(\text{TePh})_{14}(\text{PEt}_3)_3]$ ." *Physical Chemistry Chemical Physics* (101) 1588-1592 **1997**.
- 175 DP Thompson and P Boudjouk. "A Convenient Synthesis of Alkali Metal Selenides and Diselenides in Tetrahydrofuran and the Reactivity Differences Exhibited by These Salts toward Organic Bromides. Effect of Ultrasound." *Journal of Organic Chemistry* (53) 2109-2112 **1988**.
- 176 MJ Lee, SW Wright, CP Judge and PY Cheung. "High Mobility Cadmium Selenide Transistors." *Conference Record of the 1991 International Display Research Conference* 211-214 **1991**.
- 177 E Lueder. "Fabrication of CdSe-TFTs and Implementation of Integrated Drivers with Polycrystalline TFTs." *Conference Record of the 1994 International Display Research Conference* 30-38 **1994**.
- 178 E Lueder. "Fabrication of CdSe-TFTs and implementation of integrated drivers with polycrystalline TFTs." *Conference Record of the 1994 International Display Research Conference and International Workshops on Active Matrix LCDs and Display Materials* 30-38 **1994**.
- 179 TP Brody. "CdSe - The Ideal Semiconductor for Active Matrix Displays." *Proceedings of the SPIE - The International Society for Optical Engineering* (1664) 2-13 **1992**.
- 180 A Van Calster, A Vervaet, I De Rycke, J De Baets and J Vanfleteren. "Polycrystalline CdSe Films for Thin Film Transistors." *Journal of Crystal Growth* (86) 924-934 **1988**.
- 181 D Waechter, MR Westcott, F Lin and MK Hatalis. "Properties of Cadmium Selenide Thin-Films as a Function of Lateral Distance from Chromium Contacts." *Journal of the Electrochemical Society* (140) 2994-2998 **1993**.
- 182 JP Szabo and M Cocivera. "Effect of Annealing Atmosphere on the Properties of Thin-Film Cdse." *Journal of Applied Physics* (61) 4820-4828 **1987**.

- 183 MK Hatalis, F Lin and MR Westcott. "Structural and Electrical Characterization of CdSe Thin Films." *Materials Research Society Symposium Proceedings* (164) 87-92 **1990**.
- 184 A Van Calster, J Vanfleteren, I De Rycke and J De Baets. "On the Field Effect in Polycrystalline CdSe Thin-Film Transistors." *Journal of Applied Physics* (64) 3282-3286 **1988**.
- 185 MK Hatalis, F Lin and MR Westcott. "Structural and Electrical Characterization of CdSe Thin Films." *Materials Issues in Microcrystalline Semiconductors Symposium* (164) 87-92 **1990**.
- 186 GJ Scilla and JJ Wysocki. "SIMS Study of Al and Cr Metallizations on Cdse." *Journal of Vacuum Science and Technology* (18) 37-43 **1981**.
- 187 GJ Scilla and JJ Wysocki. "SIMS Study of Al and Cr Metallizations on Cdse." *Journal of Vacuum Science & Technology* (18) 37-43 **1981**.
- 188 HC De Graaff and H Koelmans. "Thin-Film Transistor." *Philips Technical Review* (27) 200-206 **1966**.
- 189 D Waechter, G Leith and S Zukotynski. "Electrical Transport Properties of Cadmium Selenide Thin-Film Transistors with Chromium Contacts." *Canadian Journal of Physics* (69) 229-235 **1991**.
- 190 S Belkouch, D Landheer, DP Masson, SR Das, T Quance, L LeBrun and SJ Rolfe. "Effects of Initial Annealing Treatments on the Electrical Characteristics and Stability of Unpassivated CdSe Thin Film Transistors." *Journal of Vacuum Science & Technology, A: Vacuum, Surfaces, and Films* (16) 860-863 **1998**.
- 191 J Hiie, M Altosaar and E Mellikov. "Comparative Study of Isothermal Grain Growth of CdS and CdTe in the Presence of Halide Fluxes." *Diffusion and Defect Data B* (67-68) 303-308 **1999**.
- 192 KA Littau, PJ Szajowski, AJ Muller, AR Kortan and LE Brus. "A Luminescent Silicon Nanocrystal Colloid via a High-Temperature Aerosol Reaction." *Journal of Physical Chemistry* (97) 1224-1230 **1993**.

- <sup>193</sup> M Hirasawa, T Seto and N Aya. "Morphological Control of Laser-Synthesized Silicon Nanoparticles." *Journal of Nanoscience and Nanotechnology* (1) 381-383 **2001**.
- <sup>194</sup> A Watanabe, M Fujitsuka, O Ito and T Miwa. "Soluble Three-Dimensional Polysilane with Organosilicon Nanocluster Structure." *Japanese Journal of Applied Physics, Letters* (36) L1265-L1267 **1997**.
- <sup>195</sup> RK Baldwin, KA Pettigrew, JC Garno, PP Power, G-y Liu and SM Kauzlarich. "Room Temperature Solution Synthesis of Alkyl-Capped Tetrahedral Shaped Silicon Nanocrystals." *Journal of the American Chemical Society* (124) 1150-1151 **2002**.
- <sup>196</sup> RK Baldwin, KA Pettigrew, E Ratai, MP Augustine and SM Kauzlarich. "Solution Reduction Synthesis of Surface Stabilized Silicon Nanoparticles." *Chemical Communications* (17) 1822-1823 **2002**.
- <sup>197</sup> G Belomoin, J Therrien, A Smith, S Rao, R Twesten, S Chaieb, MH Nayfeh, L Wagner and L Mitas. "Observation of a Magic Discrete Family of Ultrabright Si Nanoparticles." *Applied Physics Letters* (80) 841-843 **2002**.
- <sup>198</sup> JM Therrien, G Belomoin and MH Nayfeh. "Synthesis of Ultra-Small Si Nanoparticle Colloids and Thin Films - High Temperature Single Electronics." *Materials Research Society Symposium Proceedings* (Symposium H) H11.14-H11.19 **2000**.
- <sup>199</sup> Y Kitsuno, K Yano, S Tazawa, S Matsuhira and T Nakajo. "Method for Producing a Higher Silane." *US Patent* 6,027,705 **2000**.
- <sup>200</sup> P John, MJ Tricker and MJK Thomas. "Synthesising a Polysilane." *UK Patent Application* GB 2,077,710 A **1981**.
- <sup>201</sup> R West. "The Polysilane High Polymers." *Journal of Organometallic Chemistry* (300) 327-346 **1986**.
- <sup>202</sup> R West. "Polysilanes and Related Polymers" in *Inorganic Polymers*, JE Mark, HR Allcock and R West, Prentice Hall, Englewood Cliffs, New Jersey. 186-236 **1992**.

- 203 PA Bianconi, FC Schilling and TW Weidman. "Ultrasound-Mediated Reductive Condensation Synthesis of Silicon-Silicon Bonded Network Polymers." *Macromolecules* (22) 1697-1704 **1989**.
- 204 A Watanabe, T Komatsubara, O Ito and M Matsuda. "SiC/SiO<sub>2</sub> Micropatterning by Ultraviolet Irradiation and Heat Treatment of a Poly(phenylsilyne) Film." *Journal of Applied Physics* (77) 2796-2800 **1995**.
- 205 PA Bianconi and TW Weidman. "Poly(*n*-hexylsilyne): Synthesis and Properties of the First Alkyl Silicon [RSi]<sub>*n*</sub> Network Polymer." *Journal of the American Chemical Society* (110) 2342-2344 **1988**.
- 206 A Watanabe and M Matsuda. "Electrical and Optical Properties of Heat-Treated Silicon Network Polymers." *Chemistry Letters* 1101-1104 **1991**.
- 207 A Watanabe, Y Nagai, M Matsuda, M Suezawa and K Sumino. "Amorphous Silicon Structure of Heat-Treated Poly(*n*-propylsilyne) Studied by Far-Infrared Spectroscopy." *Chemical Physics Letters* (207) 132-136 **1993**.
- 208 A Watanabe, Y Nagai and M Matsuda. "Micropattern of Inorganic Film Prepared by UV-Irradiation and Heat Treatment of Polyalkylsilyne Film." *Japanese Journal of Applied Physics, Letters* (34) L452-L454 **1995**.
- 209 V Bažant and V Chvalovský. *Chemistry of Organosilicon Compounds*. Nakladatelství Československé Akademie věd Praha, Czechoslovakia, **1965**.
- 210 A Watanabe, M Fujitsuka and O Ito. "Micropatterning of SiO<sub>2</sub> Film Using Organosilicon Nanocluster as a Precursor." *Thin Solid Films* (354) 13-18 **1999**.
- 211 A Watanabe, M Unno, F Hojo and T Miwa. "Effect of Hydrogen Plasma Treatment on Formation of Amorphous Silicon Film Using Organosoluble Silicon Cluster as a Precursor." *Japanese Journal of Applied Physics, Letters* (39) L961-L963 **2000**.
- 212 A Watanabe, M Unno, F Hojo and T Miwa. "Silicon-Germanium Alloys Prepared by the Heat Treatment of Silicon Substrate Spin-Coated with Organo-Soluble Germanium Cluster." *Materials Letters* (47) 89-94 **2001**.

- 213 A Watanabe, M Unno, F Hojo and T Miwa. "Preparation of Germanium Thin Film by a Coating Technique Using a Soluble Organogermanium Cluster as a Precursor." *Journal of Materials Science Letters* (20) 491-493 **2001**.
- 214 A Watanabe, M Unno, F Hojo and T Miwa. "Electrical Properties of *tert*-Butyl-Substituted Germanium Cluster." *Chemistry Letters* 1092-1093 **2001**.
- 215 A Watanabe, M Unno, F Hojo and T Miwa. "Spatially Selective Formation of Microcrystalline Germanium by Laser-Induced Pyrolysis of Organo-Germanium Nanocluster Film." *Chemistry Letters* (87) 662-663 **2002**.
- 216 A Watanabe, F Hojo, T Miwa and M Wakagi. "Nanocrystalline Silicon Film Prepared by Laser Annealing of Organosilicon Nanocluster." *Japanese Journal of Applied Physics, Letters* (41) L378-L380 **2002**.
- 217 MM Sung, J Kluth, OW Yauw and R Maboudian. "Thermal Behavior of Alkyl Monolayers on Silicon Surfaces." *Langmuir* (13) 6164-6168 **1997**.
- 218 JM Buriak. "Organometallic Chemistry on Silicon and Germanium Surfaces." *Chemical Reviews* (102) 1271-1308 **2002**.
- 219 D Mayeri. "Synthesis and Characterization of Silicon Nanoclusters." Doctoral Thesis, University of California, Davis **2000**.
- 220 G Urry. "Systematic Synthesis in the Polysilane Series." *Accounts of Chemical Research* (3) 306-312 **1970**.
- 221 SC Gau, BR Weinberger, M Akhtar, Z Kiss and AG MacDiarmid. "Preparation of Amorphous Silicon Films by Chemical Vapor Deposition from Higher Silanes  $\text{Si}_n\text{H}_{2n+2}$  ( $n>1$ )." *Applied Physics Letters* (39) 436-438 **1981**.
- 222 PA Breddels, H Kanoh, O Sugiura and M Matsumura. "Chemical Vapor Deposition of Amorphous Silicon with Silanes for Thin Film Transistors - The Influence of the Amorphous Silicon Deposition Temperature." *Japanese Journal of Applied Physics* (30) 233-239 **1991**.

- 223 AE Delahoy. "High Rate Photochemical Deposition of Amorphous Silicon from Higher Silanes." *Journal of Non-Crystalline Solids* (77 & 78) 833-836 **1985**.
- 224 A Yoshida, S Ikeda and H Tsuchimoto. "Hydrogenated Amorphous Silicon Films Prepared from Trisilane by Windowless Hydrogen Discharge Lamp." *Journal of Non-Crystalline Solids* (164-166) 95-98 **1993**.
- 225 S Boughaba and G Auvert. "Laser Direct Writing of Micron-Size Silicon Lines from Trisilane." *Journal of Applied Physics* (78) 6791-6796 **1995**.
- 226 W Simmler. "Inorganic Silicon Compounds." *Ullmann's Encyclopedia of Industrial Chemistry* (A24) 1-19 **1993**.
- 227 K Yano, Y Kitsuno, A Sakawaki and K Kawasaki. "Formation of Silicon Membrane." *Japanese Patent Application* 07-267621 **1995**.
- 228 Y Matsuki and S Ibata. "Norbornyl-Substituted Silicon Compound, Coating Composition Containing the Compound, and Manufacture of Silicon Film." *Japanese Patent Application* 2001-058996 **2001**.
- 229 Y Matsuki and S Ibata. "Silicon Film and Formation of Its Pattern." *Japanese Patent Application* 2001-308020 **2001**.
- 230 T Shimoda, S Miyashita, S Seki, M Furusawa, I Yudasaka, Y Takeuchi and Y Matsuki. "Method for Forming Silicon Film." *International Patent Application* WO 00/59015 **2000**.
- 231 S Seki, T Shimoda, S Miyashita, M Furusawa, I Yudasaka, Y Matsuki and Y Takeuchi. "Method for Forming Silicon Film and Ink Composition for Ink Jet." *International Patent Application* WO 00/59014 **2000**.
- 232 M Furusawa, S Seki, S Miyashita, T Shimoda, I Yudasaka, Y Matsuki and Y Takeuchi. "Manufacture of Solar Cell Containing Semiconductor Thin Layers." *International Patent Application* WO 00/59044 **2000**.
- 233 Y Matsuki. "Silane Compound-Based Coating Composition for Providing Silicon Coating Film." *International Patent Application* WO 00/58409 **2000**.



- 234 JP Wilcoxon, PP Provencio and GA Samara. "Synthesis and Optical Properties of Colloidal Germanium Nanocrystals." *Physical Review B* (64) 035417/035411-035417/035419 **2001**.
- 235 JR Heath and PF Seidler. "Separation of Nucleation and Crystallization in the Solution-Phase Synthesis of Group IV Quantum Structures." *Materials Research Society Symposium Proceedings* (298) 91-98 **1993**.
- 236 JR Heath, JJ Shiang and AP Alivisatos. "Germanium Quantum Dots: Optical Properties and Synthesis." *Journal of Chemical Physics* (101) 1607-1615 **1994**.
- 237 A Watanabe, M Fujitsuka, O Ito and T Miwa. "Control of Silicon Dimensionality of Polysilanes and Their Optical Properties." *Molecular Crystals and Liquid Crystals Science and Technology, Section A: Molecular Crystals and Liquid Crystals* (316) 363-366 **1998**.
- 238 A Watanabe, T Sato and M Matsuda. "Origin of Broad Visible Emission from Branched Polysilane and Polygermane Chains." *Japanese Journal of Applied Physics* (40) 6457-6463 **2001**.
- 239 JD Holmes, KJ Ziegler, KP Johnston, RC Doty and BA Korgel. "Artificial Atoms of Silicon." *Materials Research Society Symposium Proceedings* (582) H2.5.1-H2.5.5 **2001**.
- 240 JD Holmes, KJ Ziegler, RC Doty, LE Pell, KP Johnston and BA Korgel. "Highly Luminescent Silicon Nanocrystals with Discrete Optical Transitions." *Journal of the American Chemical Society* (123) 3743-3748 **2001**.
- 241 JD Holmes, KP Johnston, RC Doty and BA Korgel. "Control of Thickness and Orientation of Solution-Grown Silicon Nanowires." *Science* (287) 1471-1473 **2000**.
- 242 RA Bley and SM Kauzlarich. "A Low-Temperature Solution Phase Route for the Synthesis of Silicon Nanoclusters." *Journal of the American Chemical Society* (118) 12461-12462 **1996**.
- 243 BR Taylor, SM Kauzlarich, HWH Lee and GR Delgado. "Solution Synthesis of Germanium Nanocrystals Demonstrating Quantum Confinement." *Chemistry of Materials* (10) 22-24 **1998**.

- 244 BR Taylor, SM Kauzlarich, GR Delgado and HWH Lee. "Solution Synthesis and Characterization of Quantum Confined Ge Nanoparticles." *Chemistry of Materials* (11) 2493-2500 **1999**.
- 245 C-S Yang, SM Kauzlarich and YC Wang. "Synthesis and Characterization of Germanium/Si-Alkyl and Germanium/Silica Core-Shell Quantum Dots." *Chemistry of Materials* (11) 3666-3670 **1999**.
- 246 C-S Yang, RA Bley, SM Kauzlarich, HWH Lee and GR Delgado. "Synthesis of Alkyl-Terminated Silicon Nanoclusters by a Solution Route." *Journal of the American Chemical Society* (121) 5191-5195 **1999**.
- 247 SM Kauzlarich, Q Liu, S-C Yin, HWH Lee and B Taylor. "The Novel Synthesis of Silicon and Germanium Nanocrystallites." *Materials Research Society Symposium Proceedings* (638) F6.5.1-F6.5.6 **2001**.
- 248 BR Taylor, GA Fox, LJ Hope-Weeks, RS Maxwell, SM Kauzlarich and HWH Lee. "Solution Preparation of Ge Nanoparticles with Chemically Tailored Surfaces." *Materials Science and Engineering B* (B96) 90-93 **2002**.
- 249 Q Liu and SM Kauzlarich. "A New Synthetic Route for the Synthesis of Hydrogen Terminated Silicon Nanoparticles." *Materials Science and Engineering B* (B96) 72-75 **2002**.
- 250 AN Goldstein. "Method for Photolytic Liquid Phase Synthesis of Silicon and Germanium Nanocrystalline Materials." *US Patent* 5,850,064 **1998**.
- 251 A Kornowski, M Giersig, R Vogel, A Chemseddine and H Weller. "Nanometer-Sized Colloidal Germanium Particles - Wet-Chemical Synthesis, Laser-Induced Crystallization and Particle Growth." *Advanced Materials* (5) 634-636 **1993**.
- 252 NA Dhas, CP Raj and A Gedanken. "Preparation of Luminescent Silicon Nanoparticles: A Novel Sonochemical Approach." *Chemistry of Materials* (10) 3278-3281 **1998**.
- 253 D Harwell. "Synthesis of Silicon Nanoparticles and Metal-Centered Silicon Nanoparticles and Applications Thereof." *International Patent Application* WO 01/14250 **2001**.

- 254 C-S Yang, SM Kauzlarich, YC Wang and HWH Lee. "Photoluminescence as a Function of Aggregated Size from *n*-Butyl-Terminated Silicon Nanoclusters." *Journal of Cluster Science* (11) 423-431 **2000**.
- 255 JR Heath and FK LeGoues. "A Liquid Solution Synthesis of Single Crystal Germanium Quantum Wires." *Chemical Physics Letters* (208) 263-268 **1993**.
- 256 A Kurtz and H Park. "Synthesis and Characterization of Aluminum Nanocrystals." *The Nucleus* (79) 10-12 **2001**.
- 257 T Hanrath and BA Korgel. "Nucleation and Growth of Germanium Nanowires Seeded by Organic Monolayer-Coated Gold Nanocrystals." *Journal of the American Chemical Society* (124) 1424-1429 **2002**.
- 258 PS Shah, JD Holmes, KP Johnston and BA Korgel. "Size-Selective Dispersion of Dodecanethiol-Coated Nanocrystals in Liquid and Supercritical Ethane by Density Tuning." *Journal of Physical Chemistry B* (106) 2545-2551 **2002**.
- 259 KJ Ziegler, RC Doty, KP Johnston and BA Korgel. "Synthesis of Organic Monolayer-Stabilized Copper Nanocrystals in Supercritical Water." *Journal of the American Chemical Society* (123) 7797-7803 **2001**.
- 260 LE Pell, T Hanrath and BA Korgel. "High Temperature Solution-Phase Synthesis of Silicon and Germanium Nanocrystals and Nanowires." *Materials Research Society Fall Meeting* (F6.1) **2002**.
- 261 RK Baldwin, KA Pettigrew, E Ratai, SM Kauzlarich and MP Augustine. "Solution Reduction Synthesis and Characterization of Passivated Silicon Nanoparticles." *Materials Research Society Fall Meeting* (F8.41) **2002**.
- 262 KA Pettigrew, PP Power and SM Kauzlarich. "A New Synthetic Route to Alkyl Terminated Silicon Nanoparticles." *Materials Research Society Symposium Proceedings* (737) F1.8.1-F1.8.6 **2003**.
- 263 JP Wilcoxon and GA Samara. "Tailorable, Visible Light Emission from Silicon Nanocrystals." *Applied Physics Letters* (74) 3164-3166 **1999**.

- 264 JP Wilcoxon, GA Samara and PP Provencio. "Absorbance and Photoluminescence of Si, Ge, and MoS<sub>2</sub> Nanoparticles Studied by Liquid Chromatography." *Proceedings of the Electrochemical Society* (99-22) 225-239 **1999**.
- 265 JP Wilcoxon and SA Craft. "Liquid Chromatographic Analysis and Characterization of Inorganic Nanoclusters." *Nanostructured Materials* (9) 85-88 **1997**.
- 266 JP Wilcoxon and RL Williamson. "Formation of Metal Colloids in Inverse Micelles and Microemulsions." *Materials Research Society Symposium Proceedings* (177) 269-274 **1990**.
- 267 JP Wilcoxon. "Method for the Preparation of Metal Colloids in Inverse Micelles and Product Prepared by the Method." *US Patent* 5,147,841 **1992**.
- 268 JP Wilcoxon, RL Williamson and R Baughman. "Optical Properties of Gold Colloids Formed in Inverse Micelles." *Journal of Chemical Physics* (98) 9933-9950 **1993**.
- 269 JP Wilcoxon, A Martino, RL Baughmann, E Klavetter and AP Sylwester. "Synthesis of Transition Metal Clusters and Their Catalytic and Optical Properties." *Materials Research Society Symposium Proceedings* (286) 131-136 **1993**.
- 270 JE Martin, JP Wilcoxon, J Odinek and P Provencio. "Control of the Interparticle Spacing in Gold Nanoparticle Superlattices." *Journal of Physical Chemistry B* (104) 9475-9486 **2000**.
- 271 JP Wilcoxon, JE Martin and P Provencio. "Size Distributions of Gold Nanoclusters Studied by Liquid Chromatography." *Langmuir* (16) 9912-9920 **2000**.
- 272 JP Wilcoxon, JE Martin and P Provencio. "Optical Properties of Gold and Silver Nanoclusters Investigated by Liquid Chromatography." *Journal of Chemical Physics* (115) 998-1008 **2001**.
- 273 JE Martin, JP Wilcoxon, J Odinek and P Provencio. "Superlattices of Platinum and Palladium Nanoparticles." *Journal of Physical Chemistry B* (106) 971-978 **2002**.

- 274 JP Wilcoxon and PP Provencio. "Use of Surfactant Micelles to Control the Structural Phase of Nanosize Iron Clusters." *Journal of Physical Chemistry B* (103) 9809-9812 **1999**.
- 275 JP Wilcoxon and GA Samara. "Strong Quantum-Size Effects in a Layered Semiconductor: MoS<sub>2</sub> Nanoclusters." *Physical Review B* (51) 7299-7302 **1995**.
- 276 JP Wilcoxon, PP Newcomer and GA Samara. "Strong Quantum Confinement Effects in Semiconductors: FeS<sub>2</sub> Nanoclusters." *Solid State Communications* (98) 581-585 **1996**.
- 277 DV Leff, L Brandt and JR Heath. "Synthesis and Characterization of Hydrophobic, Organically Soluble Gold Nanocrystals Functionalized with Primary Amines." *Langmuir* (12) 4723-4730 **1996**.
- 278 AG Cullis, LT Canham and PDJ Calcott. "The Structural and Luminescence Properties of Porous Silicon." *Applied Physics Reviews* (82) 909-965 **1997**.
- 279 S Berhane, SM Kauzlarich, K Nishimura, RL Smith, JE Davis, HWH Lee, MLS Olsen and LL Chase. "Investigation of Colloidal Si Prepared from Porous Silicon." *Materials Research Society Symposium Proceedings* (298) 99-102 **1993**.
- 280 RA Bley, SM Kauzlarich, HW Lee and JE Davis. "Characterization of Silicon Nanoparticles Prepared from Porous Silicon." *Materials Research Society Symposium Proceedings* (351) 275-280 **1994**.
- 281 RA Bley, SM Kauzlarich, JE Davis and HWH Lee. "Characterization of Silicon Nanoparticles Prepared from Porous Silicon." *Chemistry of Materials* (8) 1881-1888 **1996**.
- 282 KH Jung, S Shih, TY Hsieh, DL Kwong and TL Lin. "Intense Photoluminescence from Laterally Anodized Porous Si." *Applied Physics Letters* (59) 3264-3266 **1991**.
- 283 Z Yamani, WH Thompson, L AbuHassan and MH Nayfeh. "Ideal Anodization of Silicon." *Applied Physics Letters* (70) 3404-3406 **1997**.

- 284 L Mitas, J Therrien, R Twesten, G Belomoin and MH Nayfeh. "Effect of Surface Reconstruction on the Structural Prototypes of Ultrasmall Si<sub>29</sub> Nanoparticles." *Applied Physics Letters* (78) 1918-1920 **2001**.
- 285 G Belomoin, J Therrien and MH Nayfeh. "Oxide and Hydrogen Capped Ultrasmall Blue Luminescent Si Nanoparticles." *Applied Physics Letters* (77) 779-781 **2000**.
- 286 P Rittmeyer. "Hydrides." *Ullmann's Encyclopedia of Industrial Chemistry* (A13) 199-226 **1993**.
- 287 R Boukherroub, S Morin, P Sharpe and DDM Wayner. "Insights into the Formation Mechanisms of Si-OR Monolayers from the Thermal Reactions of Alcohols and Aldehydes with Si(111)-H." *Langmuir* 7429-7434 **2000**.
- 288 NY Kim and PE Laibinis. "Thermal Derivatization of Porous Silicon with Alcohols." *Journal of the American Chemical Society* (119) 2297-2298 **1997**.
- 289 RAW Johnstone and ME Rose. "A Rapid, Simple, and Mild Procedure for Alkylation of Phenols, Alcohols, Amides, and Acids." *Tetrahedron* (35) 2169-2173 **1979**.
- 290 B Rubin, GH Moates and JR Weiner. "Transistor-Grade Silicon." *Journal of the Electrochemical Society* (104) 656-660 **1957**.
- 291 AF Holleman and E Wiberg. *Lehrbuch der Anorganischen Chemie*. Walter de Gruyter, Berlin, **1995**.
- 292 JP Wilcoxon. Private Communications, **2002**.
- 293 U Wannagat and W Liehr. "Hydrazin-Silicium-Verbindungen." *Angewandte Chemie* (69) 783 **1957**.
- 294 U Wannagat and H Niederprüm. "Umsetzungen des Diphenyl-Dichlorsilans mit Hydrazinen." *Angewandte Chemie* (70) 745 **1958**.
- 295 M Brust, M Walker, D Bethell, DJ Schiffrin and R Whyman. "Synthesis of Thiol-Derivatized Gold Nanoparticles in a 2-Phase Liquid-Liquid System." *Chemical Communications* (7) 801-802 **1994**.

- 296 NR Subbaratnam and AK Bhattacharya. "The Influence of Triiodide Ions on Nonadditive Light Absorption of Iodine and Organic Salts." (1) 5-11 **1955**.
- 297 MR Linford, P Fenter, PM Eisenberger and CED Chidsey. "Alkyl Monolayers on Silicon Prepared from 1-Alkenes and Hydrogen-Terminated Silicon." *Journal of the American Chemical Society* (117) 3145-3155 **1995**.
- 298 S Sun and CB Murray. "Synthesis of Monodisperse Cobalt Nanocrystals and Their Assembly into Magnetic Superlattices." *Journal of Applied Physics* (85) 4325-4330 **1999**.
- 299 MK Weldon, BB Stefanov, K Raghavachari and YJ Chabal. "Initial H<sub>2</sub>O-induced Oxidation of Si(100)-(2x1)." *Physical Review Letters* (79) 2851-2854 **1997**.
- 300 CA Leatherdale. Private Communications, **1998-1999**.